MULTIPURPOSE INFRARED SYSTEMS (MIRS III)

Texas Instruments, Incorporated

Prepared for:

Advanced Research Projects Agency
Air Force Avionics Laboratory

28 June 1974

TEXAS INSTRUMENTS
INCORPORATED

ARPA

FINAL TECHNICAL REPORT

MULTIPURPOSE INFRARED SYSTEMS

(MIRS III)

28 June 1974

Prepared by:

Equipment Group
Electro-Optics Division
FSCM 96214

Sponsored by:

Advanced Research Projects Agency
ARPA Order No.: Project No. 2476

This research was supported by the Advanced Research Project Agency of the Department of Defense and was monitored by the Air Force Avionics Laboratory under Contract Number F33615-73-C-1328

TEXAS INSTRUMENTS
INCORPORATED

TABLE OF CONTENTS

TABLE OF CONTENTS (CONT'D)

TABLE OF CONTENTS (CONT'D)

LIST OF ILLUSTRATIONS

LIST OF ILLUSTRATIONS (CONT'D)

LIST OF ILLUSTRATIONS (CONT'D)

LIST OF ILLUSTRATIONS (CONT'D)

LIST OF TABLES

ABSTRACT

This report covers the effort under Air Force contract number F33615-73-C-1328 entitled Multipurpose Infrared Systems (MIRS III) Project No. 2476. The stated objective of this program was to advance the state-of-the-art technology for low cost; low weight; thermal imaging systems for remote piloted vehicles. The principle areas of study are in automatic focus compensation, structures, optic system designs and electronic multiplexing methods.

The report covers preliminary designs for three types of FLIR systems and predicts quantity cost of production for quantities of 100 and 500.

This report also includes design data that allows the application of technology to the reduction of piece part costs by using plastic parts. In this manner, temperature compensation of refractive optical systems, and compensated reflective optical systems, can be fabricated with improved performance and reduced weight.

Valuable fall-out of this study includes; techniques that can be used in manned aircraft systems to improve performance, make them simpler to operate, and reduce system power and weight requirements.

I. INTRODUCTION

The feasibility of small Lightweight Sensor Packages for mini-RPV Systems has been established by ARPA through the PRAERIE and CALERE RPV programs. This program was established to accomplish design studies and enhance the capabilities of suppliers of sensor packages that reduce weight and power requirements while improving system performance capabilities.

The design study program addressed system design and fabrication techniques encountered in lightweight design through passive focus, structures, optics, and electronics. Section II covers the effort of passive focus through structures, plastics, mechanisms for passive athermalization, and electronic automatic focus. Section III presents data on lightweight optics using reflecting elements along with refractive components. Section IV addresses the present state of electronic multiplexing used in CALERE II and CCD research being accomplished under other contracts at Texas Instruments.

The information presented in some of the appendicies are available in other literature; however, its inclusion here will allow the reader to maintain continuity.

II. AUTOMATIC FOCUS COMPENSATION

A. PASSIVE ATHERMALIZATION

The objective of passive athermalization is to design a lens system which passively compensates for changes in focus position due to temperature variations in the operating environment.

The principal causes of temperature dependent focus variations are these:

- Thermal deformation of lens housing material
- Lens thickness and radii change
- Change in optical material index of refraction

There are several practical advantages to be realized from using a passive compensation technique. First, it is a less expensive, simpler, and more reliable approach than using a servo motor and temperature sensor to obtain the required lens movement. Secondly, the concept requires a minimum of volume, thus, it lends itself to compact mechanical packaging situations. Thirdly, for systems with no active focus control, it lessens the restriction on controlling the ambient air temperature around the optics. From the system standpoint, the relaxed constraints on environmentally controlled air are reflected in reduced system weight and cost.

A possible passive athermalization design approach is the use of several different types of lens materials in the optical design. The number of required materials is equal to the number of degrees of freedom for which compensation is desired - e.g., primary color, secondary color, temperature, etc. This approach appears complex in comparison to a mechanical system that compensates by mechanically moving a single lens.

The most practical methods of obtaining linear mechanical motion of a lens assembly are these:

- Plastics with a high thermal expansion
- Fluid filled bellows
- Bi-metallic material approaches

Each of these methods will be discussed in detail with considerations and test results illustrated where applicable. However, before examining the methods of compensating for a defocus condition, a brief description of "depth of focus" is considered.

There is more than one meaning to "depth of focus". For the purpose of this analysis, it will be defined as the range of acceptable blur circle degradation, measured in radians.

Consider first the rate of increase of blur circle measured in inches:

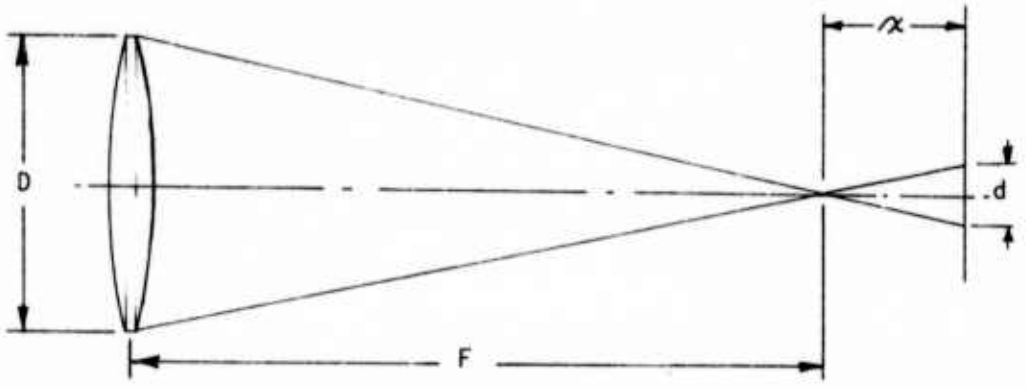

The blur circle diameter, d, at the detector is given by simple geometry as:

$$d = \frac{Dx}{f} ,$$

where
- x = amount of defocus
- D = optics diameter
- F = optics focal length

Thus, The angle blur size at the defocus position is:

$$\delta = \frac{d}{F} = \frac{Dx}{F^2}$$

Object position

If the defocus condition is due to object position; that is, if the system is focussed at infinity and the object is really at a distance S, then the focus error x is given by $x = \frac{F^2}{S.}$ When this is substituted into the angular blur equation, the result is $\delta = \frac{D}{S}$, indicating that angular blur size is not a function of focal length, but only a optics diameter and object distance.

Temperature

If the defocus condition is due to temperature, a different situation exists. The defocus error is simply the difference between the lens focal length change and the lens housing length change:

$$\alpha = F \beta \Delta T - F' \alpha \Delta T$$

where

F	=	optics focal length
F'	=	mechanical lens housing length
α	=	housing material linear coefficient of thermal expansion
ΔT	=	temperature change
β	=	effective temperature coefficient of focal length

In the simplest case, $F = F'$, and $\varkappa$ is the difference in the index of refraction thermal coefficient (divided by n-1) and the linear coefficient of thermal expansion of the lens material. Since germanium is the primary lens material of 8-14 micron lens systems, it suffices to analyze the lens as if it were a single germanium lens. For this case:

$$\beta = -\left[\frac{300 \times 10^{-6}}{(4-1)}\right] - 6 \times 10^{-6} = -94 \times 10^{-6}/^{o}C$$

is negative because the lens focal length decreases with increasing index of refraction. If the housing is aluminum, then

$$\alpha = 22 \times 10^{-6}/^{o}C.$$

Thus, for a single germanium lens,

$$\varkappa_T = F \Delta T (-94 \times 10^{-6} - 22 \times 10^{-6})$$

$$\varkappa_T = -116 \times 10^{-6} F T$$

Again, applying the angular blur calculation gives

$$\delta_T = \frac{D\varkappa_T}{F^2}$$

$$\delta_T = \frac{-116 \times 10^{-6} D \Delta T}{F}$$

$$\delta_T = \frac{-116 \times 10^{-6} \Delta T}{f/no.}$$

Thus, it is seen that f/no. and temperature difference determine the angular blur size, and that small f/no. are worse than large f/no. optics.

The temperature effects on the MTF of a typical two element, uncompensated lens system are shown in Figure 1.

During the search for a feasible design, various approaches were considered. The simplest method of course would be to make an actuator out of a material whose thermal expansion characteristics were fitted to the required air space movement. In addition, the material must have the mechancial strength necessary to hold the optical elements in proper alignment during environmental

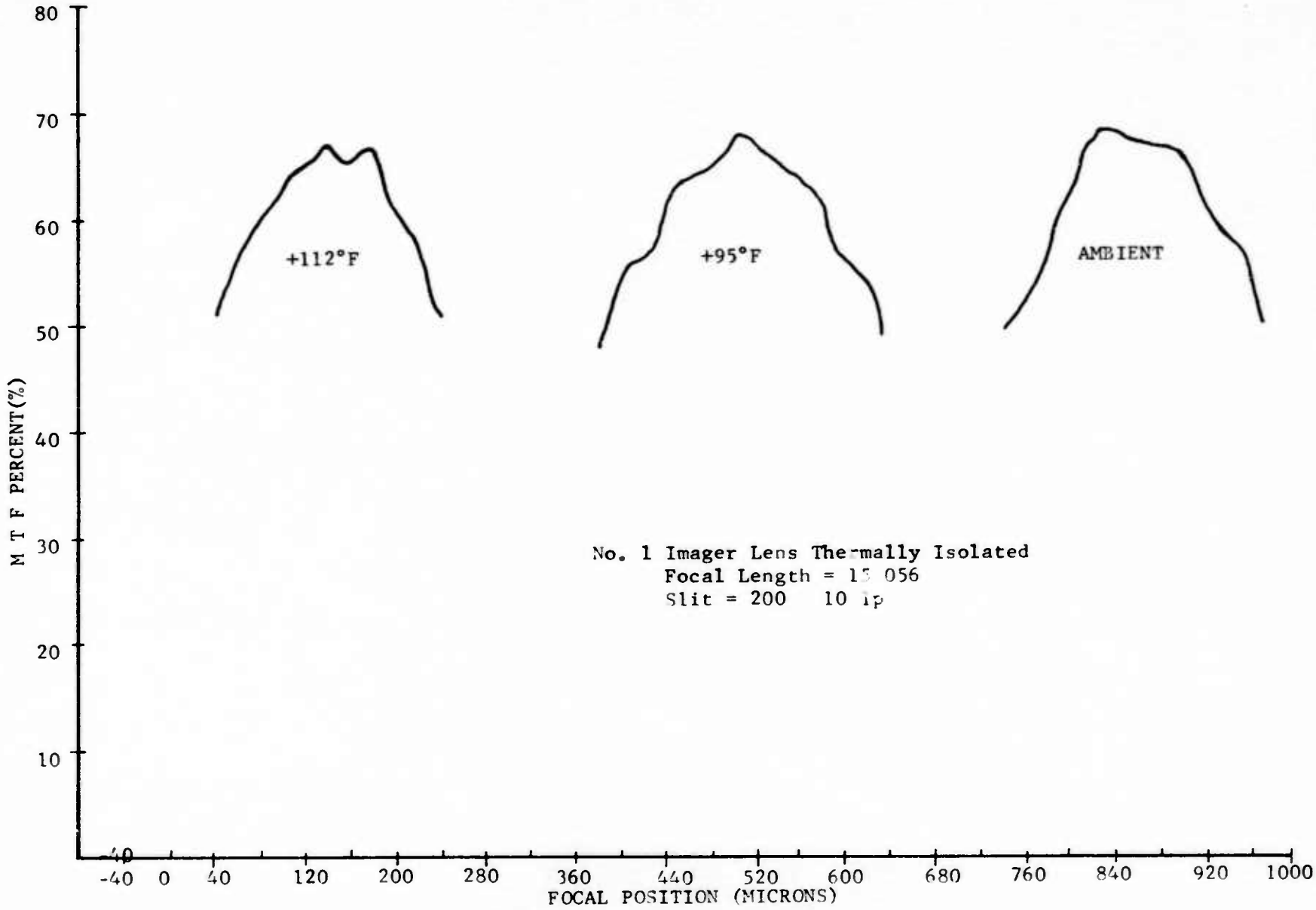

Figure 1. SAST A-thermalization Using Aluminium Rods (No Compensation)

shock and vibration. The material selected must possess other properties as well. These are: 1) linear expansion over the temperature range likely to be encountered in service operation 2) repeatability of expansion characteristics during both increases and decreases in temperature 3) reaction times that match the dn/dt effects of temperature change on the optical elements. The required thermal expansion coefficient of the actuator material is a function of both the dn/dt effect and the length of the actuators. The higher the material's expansion rate, the shorter the actuators needed.

1. Use of Plastics

It is understood that complicated plastic structures can be molded to replace heavier aluminum parts. Along with the substantial weight savings to be realized by using plastic structures, a cost savings can be realized due to simplified fabrication techniques. These advantages are made possible by the outstanding mechanical properties of the engineering family of plastics. One such property to be exploited for FLIR design is the coefficient of thermal expansion. These are of such great value as to prescribe their use as prime movers for temperature - related optical focus compensation.

When considering the use of plastics for structural applications properties other than thermal expansion must be considered. Cast or machined aluminum has been the predominate material of construction of FLIRs for years. Only recently have plastics been recognized as serious competitors where strength to weight ratio turnaround time and part cost are considerations. The high performance of the engineering plastics have begun to overshadow the memories of low grade plastic toys and novelties of the past. Appendix A is a compilation of major physical properties, including raw material cost, comparing a variety of plastics to aluminum and steel. To summarize that comparison:

	THERM/EXP (IN/IN/^{0}F)	STRENGTH/WT TENSILE / S.G.	$/lb.	$/in^3	oz/ in^3 part
ALUMINUM	1.3 X 10^{-5}	11,194	.51	.049	14.2
STAINLESS STEEL	.5 X 10^{-5}	10,336	.5	.140	41.0
POLYCARBONATE 40% GLASS FIBER	1.2 X 10^{-5}	13,907	1.51	.081	8.0
ABS 40% GLASS FIBER	1.6 X 10^{-5}	11,760	.84	.041	7.2

Being viscoelastic in nature, plastics' mechanical properties are temperature and rate dependent. A portion of this study period was devoted to accumulating available information and data showing the property variation with temperature of many plastics. The results of that effort are attached in graphical form as Appendix B. In selecting a plastic for use as a FLIR component material, these graphs provide an excellent reference given the operating temperature range of the system.

Briefly, with increasing temperature, plastics in general exhibit a decreased tensile strength, tensile modulus, flexural modulus and an increased impact strength and thermal expansion coefficent. Most desirable are those plastics which show an independence of temperature with regard to their properties. The engineering family plastics come close to providing this degree of mechanical stability. Such plastics are polycarbonate, nylon, acetal, polysulfone, polyester, phenylene sulfide, epoxy and phenolic.

Engineering plastics are priced higher than aluminum and steel, especially in the fiberglass reinforced form. However, their strength to weight ratio is greater than the metals, the price per unit volume is competitive, the manufacturing techniques are more economical, and the overall cost/part is therefore less. Finished part weight is far lighter than when fabricated from metal, and large quantities of parts may be rapidly molded to consistent dimensions after an eight week average period of tool design and build.

Thermal expansion has been the key property in providing suitable athermalization for a FLIR optics system. Plastics offer a wide range of thermal expansion coefficients depending on the type of resin, type and amount of reinforcement and an isotropic behavior resulting from nonsymetric gating of a molded plastic part. Coefficients as low as aluminum can be obtained with 40% reinforced ploycarbonate (1.2×10^{-5} in/in/^{0}F) and expansion as high as 45×10^{-5} in/in/^{0}F is found in the rubber family. Only a limited number of plastics exhibit linearity of thermal expansion. These are the polycarbonates and silicon rubbers. That linearity lends itself well to athermalization design since the expansion and contraction of lens spacings may be accurately predicted for a specified temperature range. Included in Appendix B are thermal expansion test results as interpreted from a Thermal Mechanical Device Analysis.

A particularly undesirable characteristic of many plastics is fungus suspectibility. Plastics are categorized as inert to fungus attack or fungi-susceptible according to MIL-STD-454C, Requirement 4. Those plastics earmarked as fungi-susceptible must be tested for fungus-resistance even when modified with a biocide under Method 508 of MIL-STD-810, before its use is permitted in a military component. Table 1 lists the common plastics according to their fungus classification. The test method for fungus resistance is incorporated in this report as Appendix C.

Early efforts to impart fungus resistance to a plastic involved the surface treatment of the finished part by a solution or emulsion coating process. This afforded only superficial protection and still left the plastic vulnerable to attack once the surface was scratched or marred. Today most biocides are compounded into the ploymer during processing (molding, extruding, etc.) for in-depth protection.

Typical of deleterious effects of fungus on plastics are:

1. Weight gain or loss.
2. Change in mechanical properties (tensile strength, stiffness, elastic modulus, etc.).
3. Changes in permiability to moisture, gases and solvents.
4. Changes in electrical properties.
5. Production of unwanted color and/or odor.

TABLE I - Fungi-susceptibility of Materials

GROUP I

(Fungus-inert in all modified states and grades)

Acrylics
Acronitrile-styrene
Acrylonotrile-vinyl, chloride copolymer
Asbestos
Ceramics
Chlorinated polyether
Glass
Metals
Mica
Plastic Laminates:
    Silicone-glass fiber
    Phenolic-nylon fiber
Diallyl phthalate
Polyacrylonitrile
**Polyamide
Polycarbonate
Polyester-glass fiber laminates
Polyethylene, high density above 0.940
Polyethylene terephthalate
Polyimide
Polymonochlorotrifluorethylene
Polypropylene
Polystyrene
Polysulfone
Polytetrafluoroethylene
Polytetrafluoroethylenepropylene
Polyvinylidene Chloride
Silicone resin
Siloxane-polyolefin polymer
Siloxand-polystyrene

**Literature shows that under certain conditions Polyamides may be attacked by selective micro-organisms. However, for military applications they are considered Group I.

TABLE I - Fungi-susceptibility of Materials (Cont'd)

GROUP II

(Not fungus-resistant in all grades, fungus-resistance shall be established by test)

ABS (acrylonitrile-butadiene styrene)
Acetal resins
Cellulose acetate
Cellulose acetate butyrate
Epoxy-glass fiber laminates
Epoxy-resin
Lubricants
Melamine-formaldehyde
Organic polysulphides
Phenol-formaldehyde
Polydichlorostyrene
Polyethylene, low and medium density, 0.940 and below
Polymethyl methacrylate
Polyurethanes (the ester types are particularly susceptible)
Polyphenylene oxide
Polyrecinoleates
Polyvinyl chloride
Polyvinyl chloride-acetate
Polyvinyl fluoride
Rubbers, natural and synthetic
Urea-formaldehyde

TABLE 1 (Continued)

The families and members of the biocides used frequently in fungus-susceptible plastics are organotins, bromated salicylanilides, carbamates, quaternary ammonium compounds, arsenic compounds, mercaptans and mercury compounds. The organotins and brominated salicylanilides alone offer the desired characteristics of:

1. Effectiveness at very low concentration levels.
2. Minimal volatility loss and retention of effectiveness after exposure to plastics processing temperatures.
3. Chemical stability to resist color changes in finished part.
4. Low toxicity to humans.

Another adverse characteristic of plastics in their ability to support combustion. Knowledge of a particular plastic's degree of flammability has been misleading and confusing due to the established manner of testing over the years. Until the acceptance of the oxygen index test is more widespread, a numerical measure for flammability comparison of plastics is lacking in the industry. Still prevelent today and under attack by the Federal Trade Commission is the UL and ASTM manner of loosely classifying plastics as self-extinguishing, non-burning, burning, or slow burning. The self-extinguishing category is further broken down into SE-0, SE-1 and SE-2. This customary flammability test is conducted according to ASTM D-568 and ASTM D-635 and UL bulletin 94 wherein an open flame is applied to the plastic specimen in air for 30 seconds, removed, and the results observed.

UL Burning Rating Code

Self-Extinguishing
- 0 - Extinguishment in vertical bar in 5 seconds or less.
- 1 - Extinguishment in vertical bar in 25 seconds or less with no flaming dripping.
- 2 - Same as SE-1 except that flaming dripping occurs.

Slow-Burning

Burning at a rate less than 1.5 in./min. UL currently has no code for materials burning faster than 1.5 in./minute.

ASTM Burning Rating Code

Non-burning

Failure of a horizontal bar to ignite or burn over more than 1" of length after two 30 second exposures to Bunsen Burner flame. This is not to say that the plastic is not combustible or ignitible under other test conditions. The use of this term is misleading since virtually all organic materials can be made to burn.

Self-Extinguishing

Failure of a horizontal bar to burn continuously over a 4" length but burns beyond the first 1".

Burning

Burns continuously for at least 4". A burning rate of in./min is recorded via stop watch.

Oxygen Index

The numerical percentage of minimum oxygen concentration to support combustion after vertical specimen is ignited by an external flame.

These flammability tests are described in detail under Appendix D. The reliability of the UL 94 and ASTM D568 and D635 ratings is doubtful since the test procedure is subject to non-statistical averaging, human judgement and bunsen burner flame variations.

Another fallacy of these flammability tests is that they do not yield information about smoke content or toxicity due to burning. A plastic can be rated ASTM self-extinguishing but it may give off enough smoke or toxic fumes as it smolders to be dangerous.

Figure 2 illustrates ratings of plastics according to UL, ASTM, oxygen index and smoke production. Testing for smoke output, toxicity and oxygen index has just recently gained significance and data is presently scarce.

Flame retardants and smoke suppressants are commercially available usually as halogenated additives or antimony oxides for compounding into plastic resins. The use of them is dictated by cost, intended use and environment of the final part, as well as by the plastic resin flammability characteristics.

Two independent studies were initiated to determine the feasibility of using plastic materials as the prime movers of passively athermalized optical systems. One investigation used the existing optical system designed for the SASI FLIR, and one used the TOW FLIR optics as a base line.

a. Optics Group Study of SASI

First, a search was conducted to find a material that would meet the necessary requirements for use in athermalization of the SASI FLIR. The high thermal expansion requirement eliminated many materials from consideration. Only plastics appeared to come close to the required expansion level. After reviewing these performance requirements with several resin manufacturers it was decided that high density polyethylene had the most promising properties.

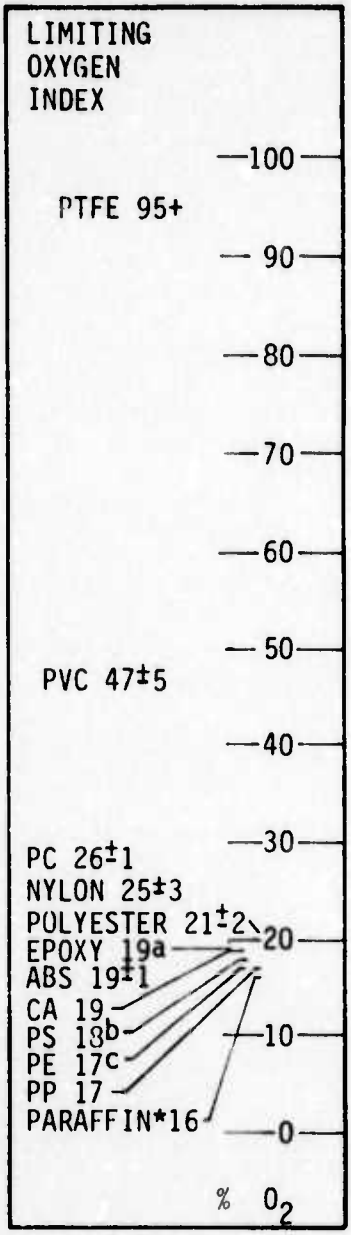

A S T M D-2863 (Fenimore-Martin Technique). Sample is Burned in a Measured Mixture of O_2 and N_2 in which the Percentage of Oxygen is Decreased to Determine Minimum Amount Necessary to Support Combustion. Normal Atmosphere at Sea Level is 21% O_2

Source, Modern Plastics Encyclopedia, 1973-1974
I.N. Einhorn, Proceedings 1973 Polymer Conference

*From "Flammability Handbook for Plastics"

a-Up to 45; b-Up to 28; c-Up to 27

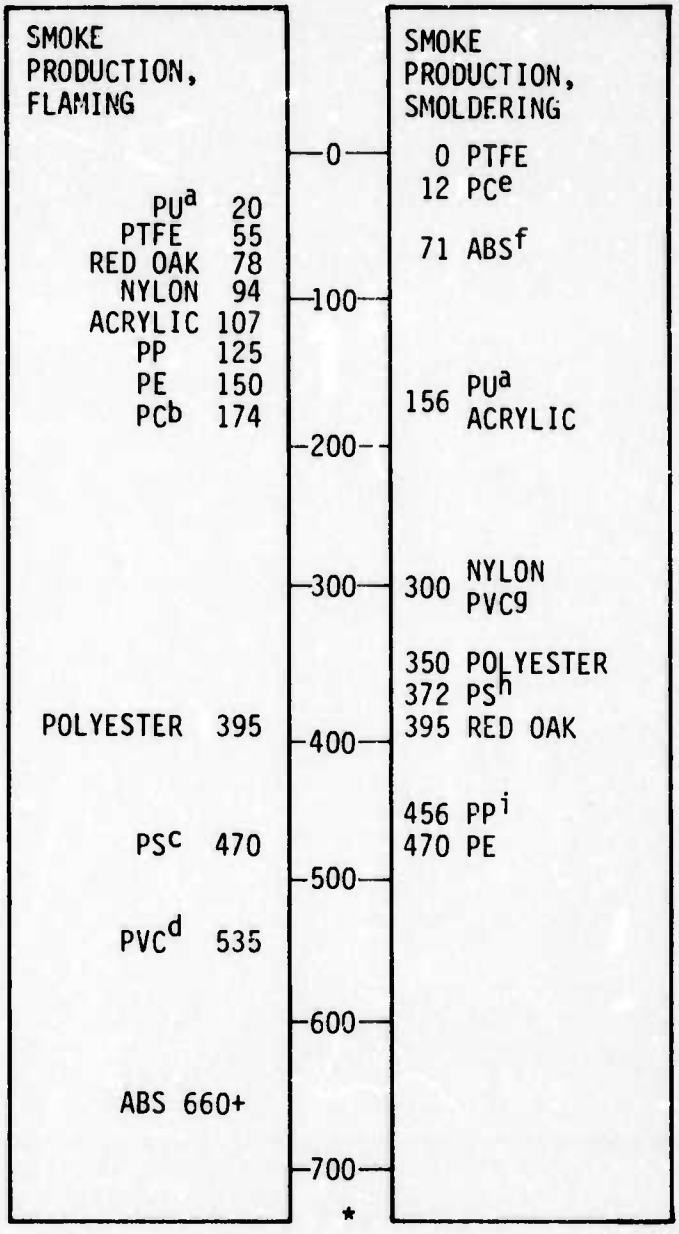

NSB Smoke Chamber. Sample is placed in a closed cabinet and exposed to radiant heat while flaming or smoldering. Smoke production is expressed as specific optical density, measured by a photocell across a light path within the chamber.

Source Journal of Fire & Flammability, July 1970, "Flammability Handbook for Plastics".

a-Flexible PU foam
b-Also tested at 325
c-Also tested at 660+
d-Also tested at 660+
e-Also tested at 50
f-Also tested at 660+
g-Also tested at 470
h-Also tested at 345,395
i-Also tested at 660+

*Specific optical density, maximum

Figure 2. Burn and Smoke Testing (Continued Next Page)

FLAME SPREAD RATING

	UL 94				ASTM D-635		
							BURNING RATE, IN./MIN.
ABS	●		●	●	●	●	09-2.0
ACETAL				●		●	1.1
ACRYLIC	●	●	●	●	●	●	0.6-1.6
ALKYD	●	●			●		
CA	●	●		●	●	●	<1.5
EPOXY	●				●		
NYLON	●	●	●	●	●	●	0.5-0.8
PHENOLIC	●	●		●	●		
PC	●	●	●	●	●		
POLYESTER	●		●	●	●	●	0.8-1.3
POLYESTER	●	●		●	●	●	1.0
PE			●			●	1.0-1.1
PP			●	●		●	<1.5
PS	●	●	●	●	●	●	1.2-1.5
PVC	●				●		
PU				●	●	●	<1.5
PTFE	●				●		

UL 94. Sample is held horizontally or vertically and twice exposed to flame for 30 seconds. Cotton is placed under sample to catch flaming drippings. Ratings, vertical test: SE-0, self-extinguishes in 5 seconds (average) and no flaming drippings ignite cotton; SE-1, self-extinguishes in 25 seconds (average) and no flaming drippings; SE-2, same as SE-1, buj with flaming drippings. Rating, horizontal: SB, slow burning at less than 1.5 in./min. for samples 1/8 in. thick.

ASTM D-635. Sample is held horizontally and exposed to flame for 30 seconds. Ratings: B, burning by this test if two or more of 10 specimens burn 4 in., with the burning rate in in./min. given; SE, self-extinguishing by this test if none of 10 or one of 20 samples burns 4 in., with average time to extinguishment reported as a superscript and average extent of burning in in. given as subscript.

Source: Modern Plastics Encyclopedia, 1973-74.

Figure 2. Burn and Smoke Testing (Continued From Previous Page)

The precise movements required for the optical elements precluded reliance on published thermal expansion data. Instead, thermal expansion characteristics of the polyethylene were measured in-house over the expected operating temperatures range of the system. Similar tests were conducted on other actuator materials under investigation. Samples of high density polyethylene were procured from local vendors and the thermal expansion coefficient was measured by the Analytical Services Lab of Texas Instruments. The tests were performed using a djalatometer with measurements being made over a temperature range from $-50^{o}C$ to $+50^{o}C$. Several samples were measured in an attempt tc obtain the most accurate figure possible; however, there was not sufficient time to conduct a full scale ASTM measurement program. Typical test results are shown in Figure 3. As can be seen from the graph, the thermal expansion varied considerably with temperature. At low temperatures, relatively low expansion coefficients of $12 \times 10^{-5}/^{o}C$ were measured while at elevated temperatures this figure increased to around $25 \times 10^{-5}/^{o}C$. (Figure 4). This non-linearity was found to be a characteristic of other plastic materials as well. Two notable exceptions were found in polycarbonates and silicone rubbers. Figure 4 shows a comparison between the thermal expansion coefficients of high density polyethylene and optical grade polycarbonate. It can be seen that the expansion coefficient of polycarbonate is almost constant over a wide temperature range. In addition to this, the material possesses excellent machining and mechanical properties. Unfortunately, its expansion coefficient of $6 \times 10^{-5}/^{o}C$ is too low for use as a mechanical actuator. On the other hand, silicone rubber has a high expansion coefficient of about $22 \times 10^{-6}/^{o}C$. This value is linear over the $+50^{o}C$ to $-50^{o}C$. However, this temperature range, except for a small low temperature region, has poor mechanical properties and could not serve as a structural member in a lens housing. It was decided, therefore, that high density polythylene would be used to test the basic athermalization concept.

The thermal expansion rates of polyethylene, as with other plastics, can be expected to vary considerably from sample to sample. This is due to a variety of factors inherent in their manufacturing process; fortunately, steps can be taken to minimize these effects. Sheet polyethylene, for example, has expansion coefficient variations of greater than 10 percent from the center to the edge of the sheet. High density polyethylene rods display greater thermal expansion in the axis in which they are cast. This is less true of low and medium density types. Other factors to be considered are void inclusions within the material and variations in formulation from batch to batch. Another possible characteristic of pressure cast polyethylene is instability of the material's thermal expansion property. According to one foundry, unannealed polyethylene often exhibits a high α value when heat is first applied to it, but in subsequent temperature cycling the thermal expansion rates are greatly reduced. However, testing under laboratory conditions failed to support this claim.

Problems such as these can be minimized if proper precautions are taken when ordering the polyethylene. Consistent physical properties can only be obtained by using polyethylene that has been formulated from the same resin type. Therefore, polyethylene should always be specified by resin number. Homogeneity of the material can be assured by specifying the polyethylene to be "void free" with verification by x-ray examination. Finally, the polyethelene should be purchased in an annealed form. The precautions listed above are not normally taken during plastic casting; however, some foundries will produce the material in this manner when requested to do so.

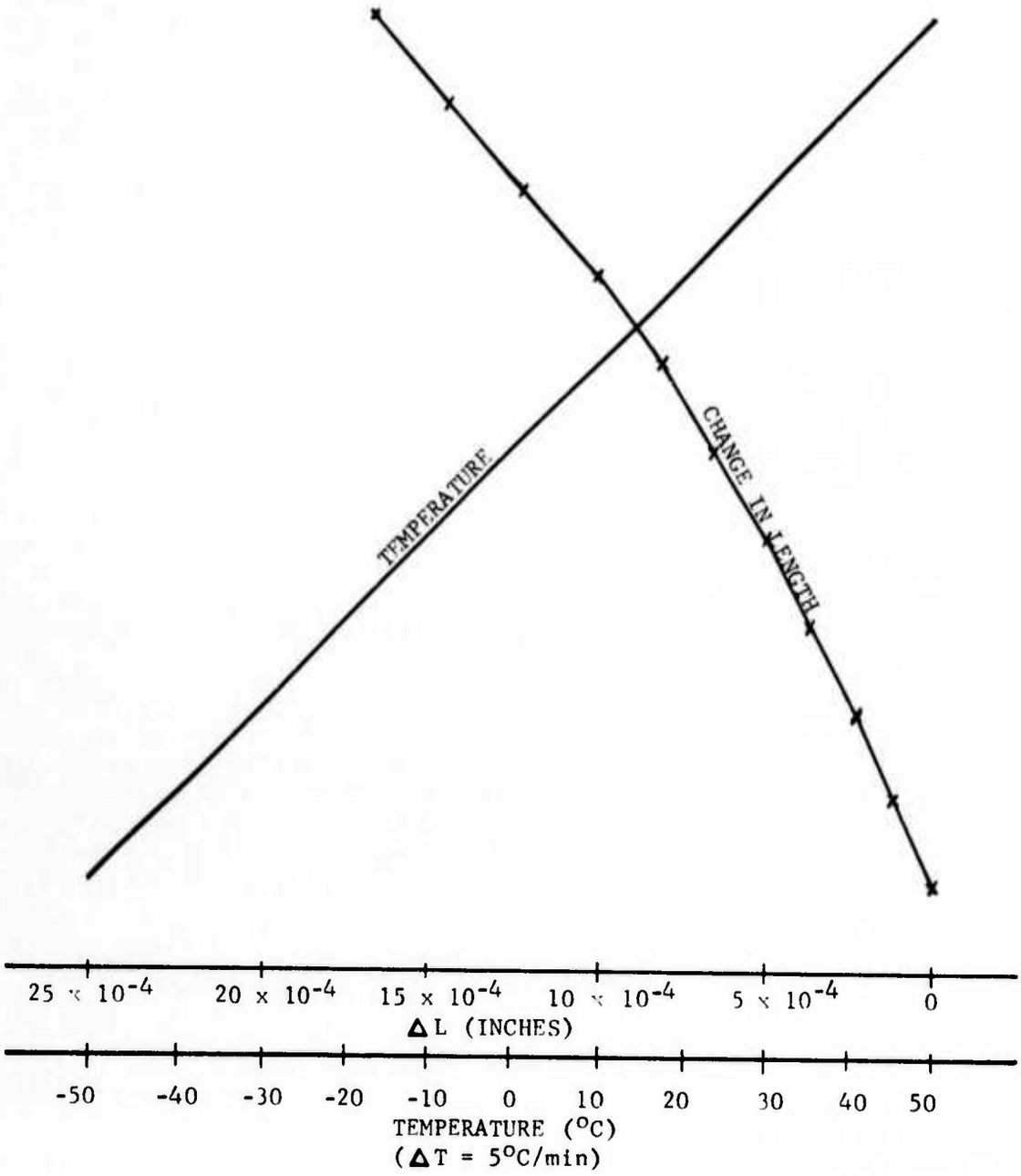

Figure 3. Thermal Expansion Measurement (High Density Polyethylene).

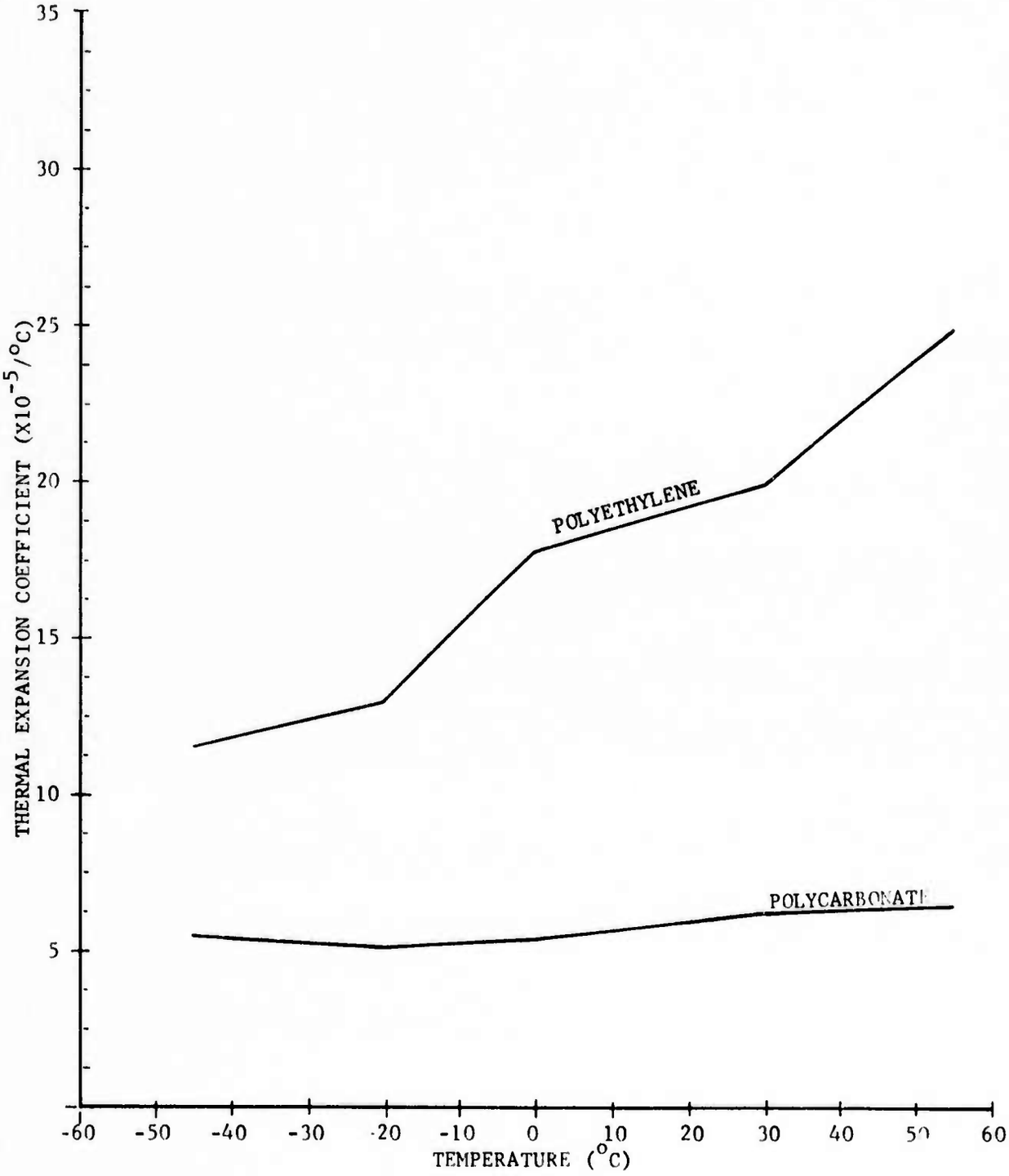

Figure 4. Thermal Expansion Coefficients.

Test evaluation was made of a composite design approach using high density polyethylene and aluminum. The purpose of this approach was to tailor the athermalization movement to the optical requirement.

The optical requirement for compensation was a lens movement of 0.4 mils/°C ($= \frac{\Delta L}{\Delta T}$). To obtain this movement, two rods parallel to each other were used. Rod dimensions are shown in Figure 5.

Design considerations dictated the rod length, L, of 2.25 inches. Thus, the required thermal expansion coefficient (α) is by definition:

$$\alpha_{reqd} = \frac{(\Delta L)}{(L)\ (\Delta T)} = \frac{0.0004^{in.}}{(2.25\ in)\ 1^{o}C} = \frac{(0.0004)}{(2.25)\ (1.8)^{o}F}$$

$$\alpha_{reqd} = 9.87 \times 10^{-5}\ \ 1/^{o}F$$

Six thermal expansion test measurements were made on the plastic used. It was ascertained that the thermal expansion coefficient (α) of the plastic was approximately

$$\alpha_{poly} = 13.7 \times 10^{-5}\ \ in/in/^{o}F$$

Literature data indicated for the aluminum

$$\alpha_{Al} = 1.3 \times 10^{-5}\ in/in/^{o}F$$

Theoretical value for the rod assembly was, then,

$$\alpha_{ROD} = \frac{2}{9}(\alpha_{Al}) + \frac{7}{9}(\alpha_{poly}) = \alpha_{ROD} = 10.9 \times 10^{-5}\ in/in/^{o}F$$

The higher than required α was to compensate for the rod being inclined to the lens, i.e., a component of the total movement is not utilized.

The test bed was a two element a-focal section placed in front of an imaging cell. The athermalization movement devices to be evaluated connected the two a-focal elements. The a-focal section was subsequently enclosed in a box. Forced airflow was directed thru the box across the lens elements and athermalization device. Inlet temperature of the air was varied above room ambient by use of a variable power heater placed in the airstream. Schematically, this set up is as shown in Figure 6.

During testing the back focal length (BFL) of the lens system was monitored. The athermalization device being evaluated was considered satisfactory if the BFL did not change due to increased afocal temperature. It was determined from these tests and computer analyses that lens movement repeatability must be held to $\leq$10 percent deviation.

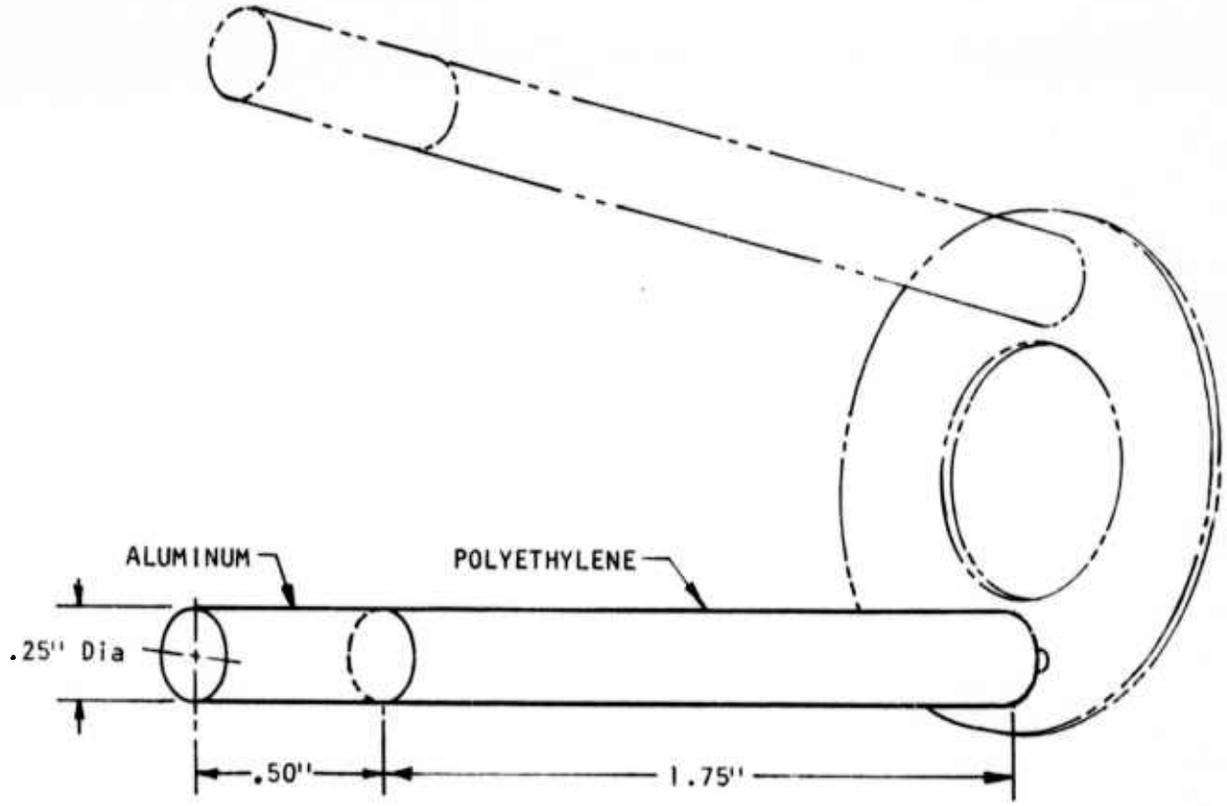

Figure 5. Two Material Athermalization Compensation Rod.

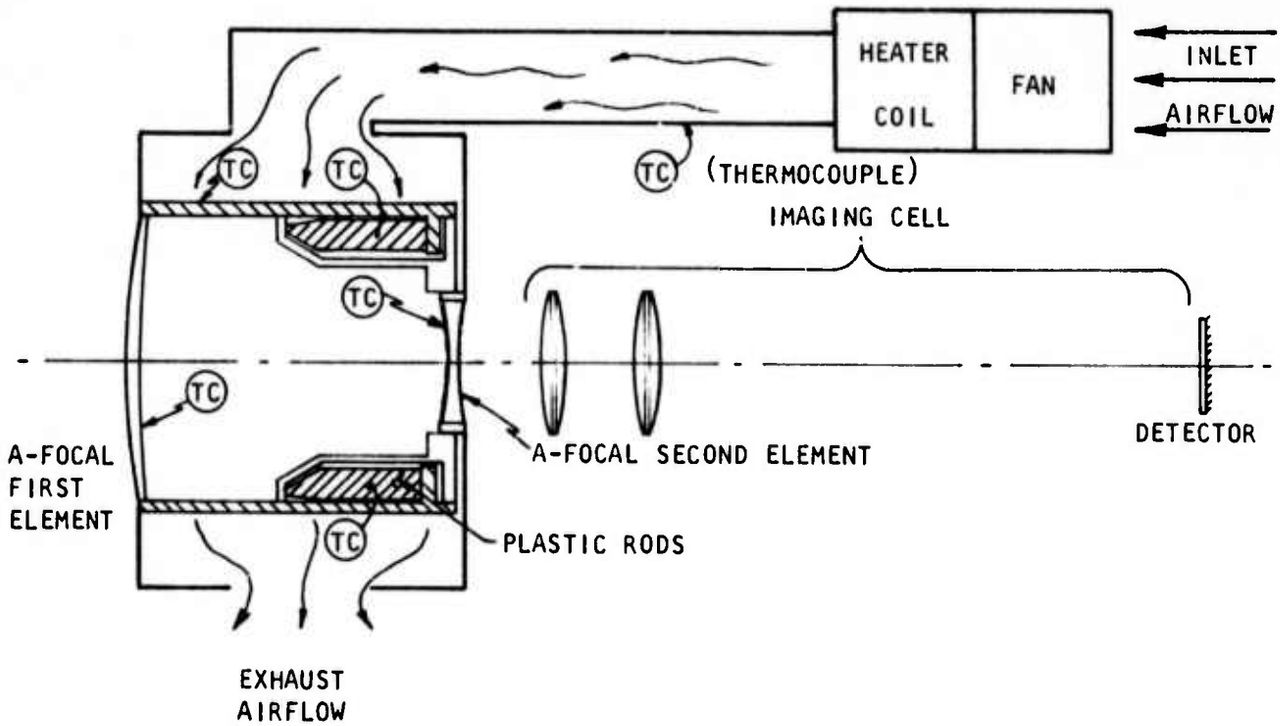

Figure 6. "Passive" Athermalization Thermal Test Set Up.

From test data of the compensated imaging cell it was found that the lens moved 0.0088 inches (ΔL) during a $40^{o}F$ temperature increase (ΔT). The effective α value demonstrated here is

$$\alpha = \frac{(\Delta L)}{(L)\ (\Delta T)} = \frac{(0.0088)}{(2.25)\ (40)^{o}F} = 9.77 \times 10^{-5}\ in/^{o}F$$

MTF and focal position change data from the testing are in Figure 7 for inspection. As shown, the total image shift was approximately 50 microns. Total MTF change was 4.6 percent. If uncompensated, the lens system peak MTF change with temperature as shown in Figure 8 would be considerably greater.

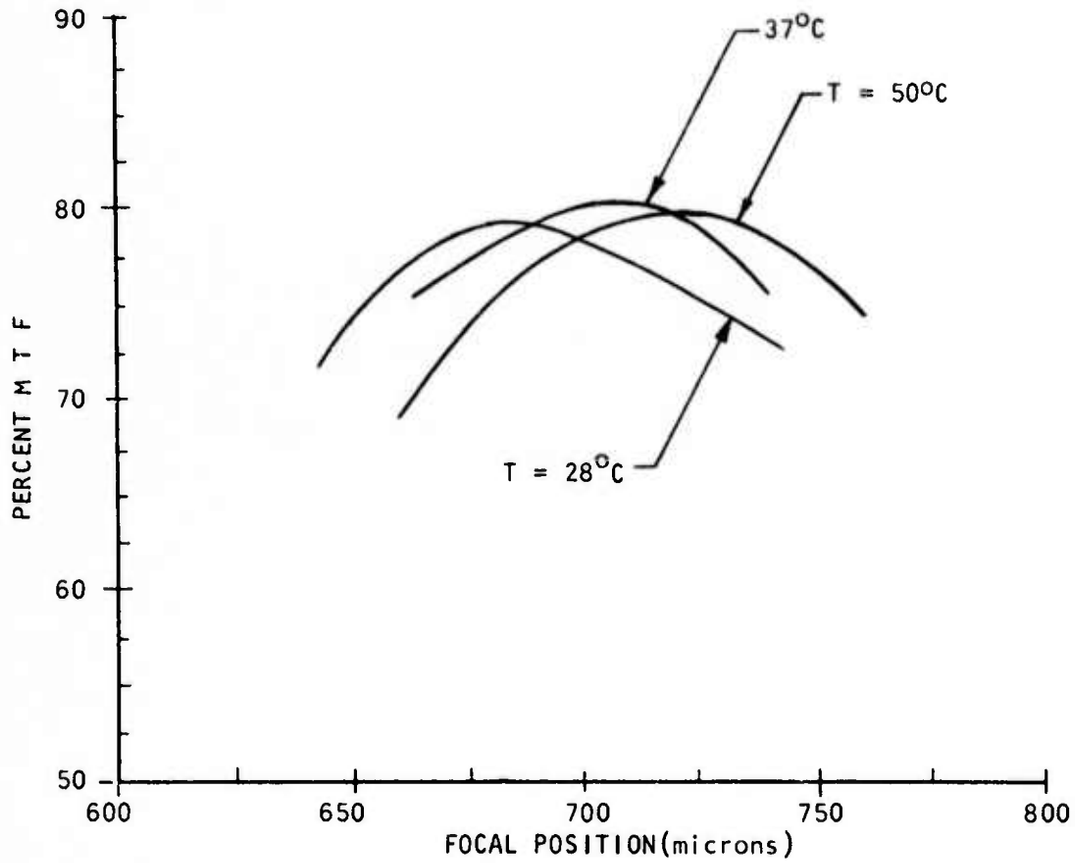

Figure 7.

Focal Position Change Data

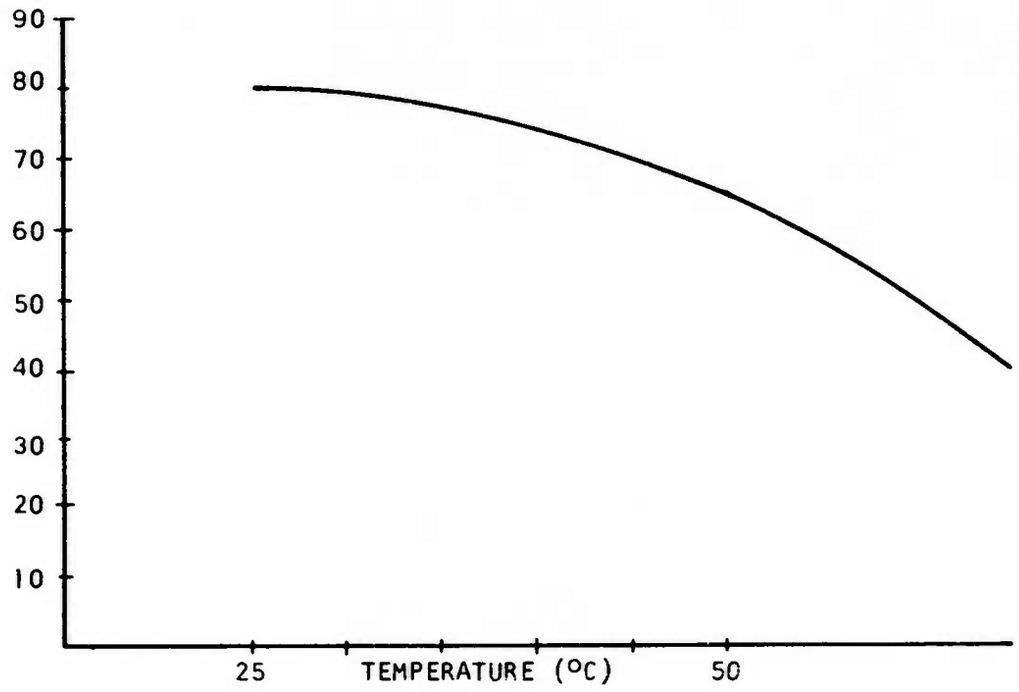

Figure 8. Peak MTF Change with Temperature, with no Athermalization Compensation.

b. Plastics Group Study of TOW

Passive athermalizations for the Preliminary TOW optical system was initiated to determine feasibility for passive structural plastic designs. The TOW optic system has seven IR lens ahead of the BFL (see Figure 9). Each of these lens and each spacing between lens has an effect on the BFL if they are changed from their in-focus dimensions, positions and indices.

By varying the temperature from $20^{o}C$ to $100^{o}C$ the focal position moves linearly- .0018 inches/^{o}C in the NFOV (i.e., as the temperature is increased, the image is moved closer to the lens). Compensation for focal shift is obtained by changing the position of the detector with respect to the lens, or changing the spacings between the lens elements to maintain a constant image plane. The same generalization is true for the WFOV where the focal position moves linearily .00023 inches/^{o}C. Each of the lens spacings has a different effect on the BFL change. Thickness #1 has the greatest effect and can be assumed linear in the range of BFL motion to be encountered. The variations of BFL with lens spacing are as follows:

			Len spacing/inches
1.	$.001\Delta T_1$	NFOV= $-.00175\ \Delta$BFL	5.1108
2.	$.001\Delta T_1$	WFOV= $-.00036\ \Delta$BFL	$\approx$2.150
3.	$.001\Delta T_2$	= $-.0008\ \Delta$BFL	.04066
4.	$.001\Delta T_3$	= No effect on BFL	3.000
5.	$.001\Delta T_4$	= $-.0004\ \Delta$BFL	.3104
6.	$.001\Delta T_5$	= $-.0002\ \Delta$BFL	2.400
7.	$.001\Delta T_6$	= No effect on BFL	.300
	BFL		.6220

Therefore, as the temperature increases one or more of the lens spacings must decrease. Changing T_2 is impractical because of the limited travel available. Obviously, athermalizing the BFL via T_1 motion is the logical approach since it would require the least motion of all lens spacings to achieve the desired BFL compensation

Athermalization must be designed for a temperature range of $-20^{o}C$ to $+40^{o}C$. Over this range, the BFL will shift as follows:

$$-.0018 \frac{\text{NFOV}}{\text{in}/^{o}C} \times 60^{o}C = -.108 \text{ in. BFL}$$

$$-.00023 \frac{\text{WFOV}}{\text{in}/^{o}C} \times 60^{o}C = -.0138 \text{ in. BFL}$$

Using a decreasing T_1 spacing as temperature increases to properly athermalize this BFL shift would require the T_1 dimension to move

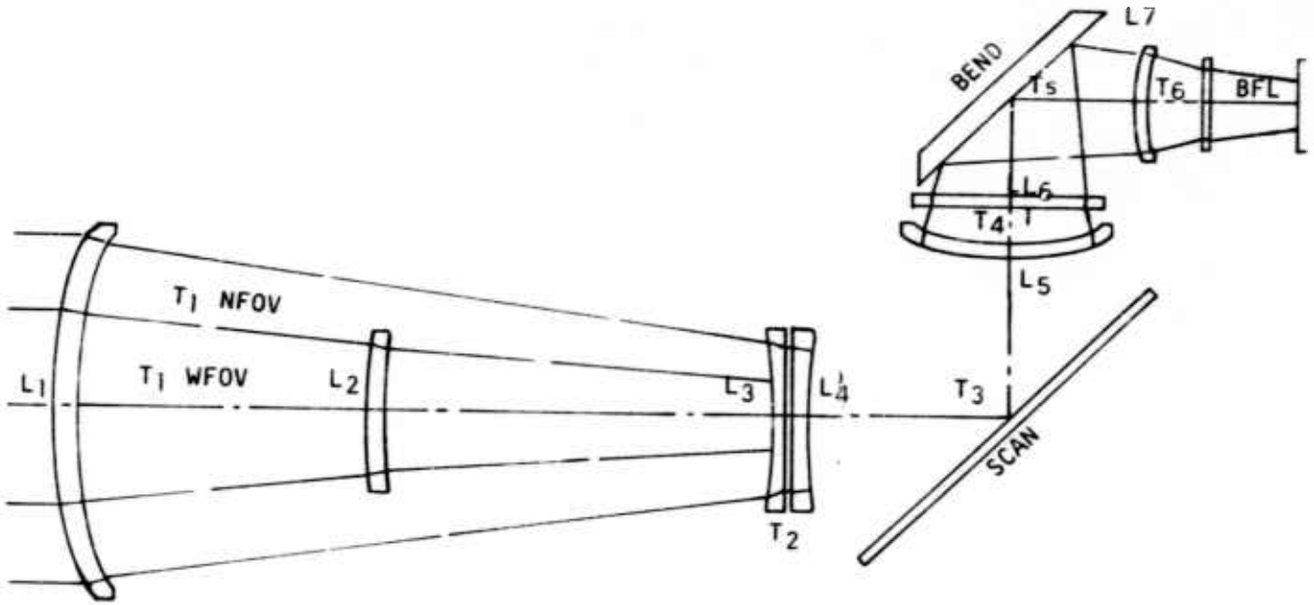

Figure 9. TOW FLIR Lens Arrangement.

$$\frac{.001 \text{ in } \frac{\text{NFOV}}{T_1}}{.00175 \text{ in}_{BFL}} \times -.108 \text{ in}_{BFL} = -.0617 \text{ in. } T_1$$

$$\frac{.001 \text{ in } \frac{\text{WFOV}}{T_1}}{.00036 \text{ in}_{BFL}} \times -.0138 \text{ in}_{BFL} = -.0383 \text{ in. } T_1$$

The T_1 movement can be designed to either the NFOV or WFOV requirement. If the T_1 space is contracted -.0617 in, then the WFOV is overcompensated by 0.0234 in. This excess .0234 in. to T_1 contraction for the WFOV has a reduced effect on the BFL of

$$-10234 \text{ in}_{T_1} \times \frac{.00036 \text{ in BFL}}{.001 \text{ in}_{T_1}} = -.0084 \text{ in. BFL}$$

When multiplied by the .00036 factor. The -.0084 in. error over 60°C for the WFOV must be adjusted for in secondary athermalization of the field-of-view switching mechanism. The same would hold true if the T_1 movement were designed to the .0383 in. required by the WFOV. However, the BFL error before secondary athermalization would be much greater than -.0084. Instead it would be

$$-.0234 \text{ in}_{T_1} \times \frac{.00175 \text{ in}_{BFL}}{.001 \text{ in. } T_1} = -.0410 \text{ in. BFL}$$

For this reason, the T_1 movement was matched to the NFOV. Then, the secondary athermalization is not as critical to the IOW optical performance. In fact, the -.0084 in. error is close to being in the ±.003 in. BFL tolerance, particularly if the system were calibrated at the mid-range temperature (10°C) so as to split the .0084 in. into a ± .0042 tolerance.

The design for athermalization was broken down into two parts. First, all seven lenses must be held in place securely and second, the lenses must then be moved to yield the T_1 space dimension needed. The approach was to mount each lens in a lens retainer and then attach the retainer and lens to the optics housing or to the athermalizing element. Only the #1 and #2 WFOV lenses would be moved with temperature; the #1 lens being the primary athermalizing element and the WFOV lens correcting for the .0234 in. #1 lens over-travel that exists when the WFOV is switched into optics system in place of the NFOV doublet.

Figure 10 illustrates a plastic lens retainer designed to hold a lens snuggly across the 60°C temperature range with constant pressure. The lens is supported in three places along the circumference on one side and along the full circumference on the opposite side. An RTV silicone potting compound may be used to guarantee uniform retention of the lens in this cylindrical holder. In the case of increasing temperature, if the X dimensions are held in the retainer design, the thermal expansion tending to loosen the

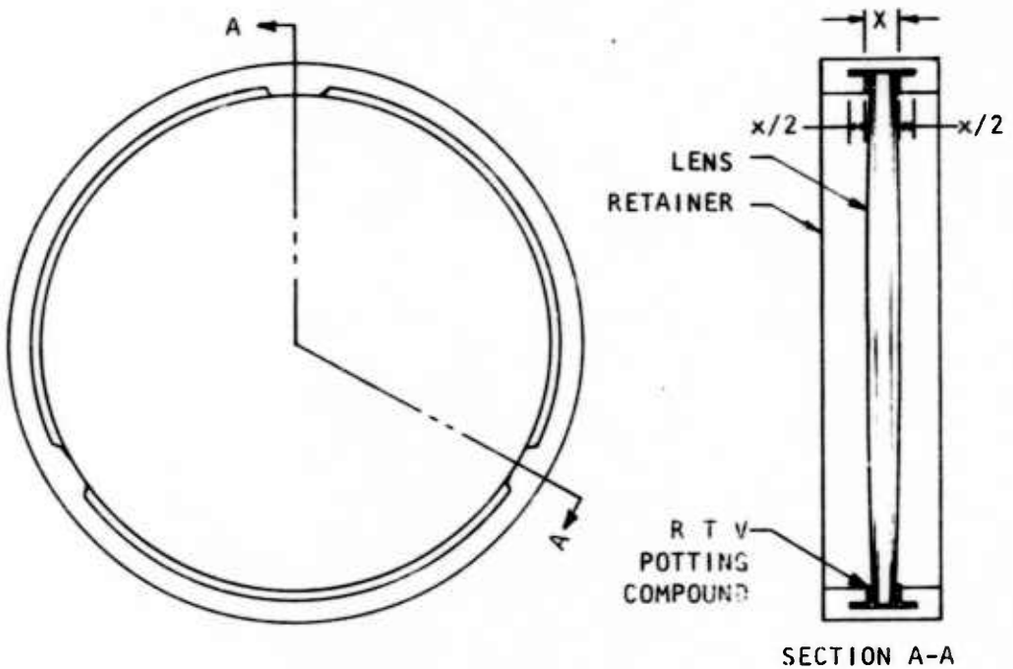

Figure 10. Plastic Lens Retainer-60°C Temperature Range.

lens would be counteracted by the X/2 dimensions expanding in such a way as to tighten the lens within the retainer. The result is reversible and yields a constant pressure on the lens to reduce distortion or slippage.

In Figure 11 the lenses are shown within their retainers which in turn are attached to the optics housing in either a press-fit tongue and groove or ultrasonic welded manner. The optics housing is designed in 40% glass reinforced polycarbonate for minimum thermal expansion of 2.1×10^{-5} in/in^{o}C matches that of aluminum and enables close control of lens spacings since it is a linear as well as a minimum expansion coefficient. The expansion can be tailored to any higher expansion up to 5.8×10^{-5} in/in/^{o}C by reducing the glass content from 40% or by orienting the fibers of glass from parallel to transverse to critical part axis. This orientation is controlled by plastic molding gate position and flow characteristics. Data summarizing the thermal expansion testing of numerous plastics along three axes is incorporated in Appendix E.

Attempts to decrease the expansion coefficient further by means of higher glass reinforcement concentration (above 40%) have been documented by commercial suppliers of reinforced plastics. The results were quite negative as no appreciable change in coefficient occurred while tensile strength, impact resistance and all other physical properties with the exception of flexural modulus dropped off rapidly. There simply is not enough plastic resin available to bind the glass fibers adequately. Three different approaches were explored using plastic devices. These were the following:

- Polycarbonate strip stacking
- Polycarbonate gear/lever
- Silicon rubber element

Polycarbonate Stacking

Figure 11 depicts the use of Polycarbonate stacks to retract the #1 lens .0617 in. over 60^{o}C. Each stack is composed of layers of polycarbonate. The layers alternate from 40% glass reinforced to unreinforced polycarbonate. The outer layer is the optics housing itself and the inner layer is the #1 lens retainer. The operating principle depends on the difference of thermal expansion coefficients of reinforced and non-reinforced polycarbonate.

$$\begin{array}{ll} \text{Polycarbonate 40\% glass} & 2.1 \times 10^{-5} \text{ in/in/}^{o}\text{C} \\ \text{Polycarbonate} & \underline{-6.5 \qquad\quad -5 \text{ in/in/}^{o}\text{C}} \\ & = -4.4 \times 10^{-5} \text{ in/in/}^{o}\text{C} \end{array}$$

The glass reinforced layers expand the T_1 spacing, but the unreinforced layers contract the spacing at three times the expansion rate. The number of layers

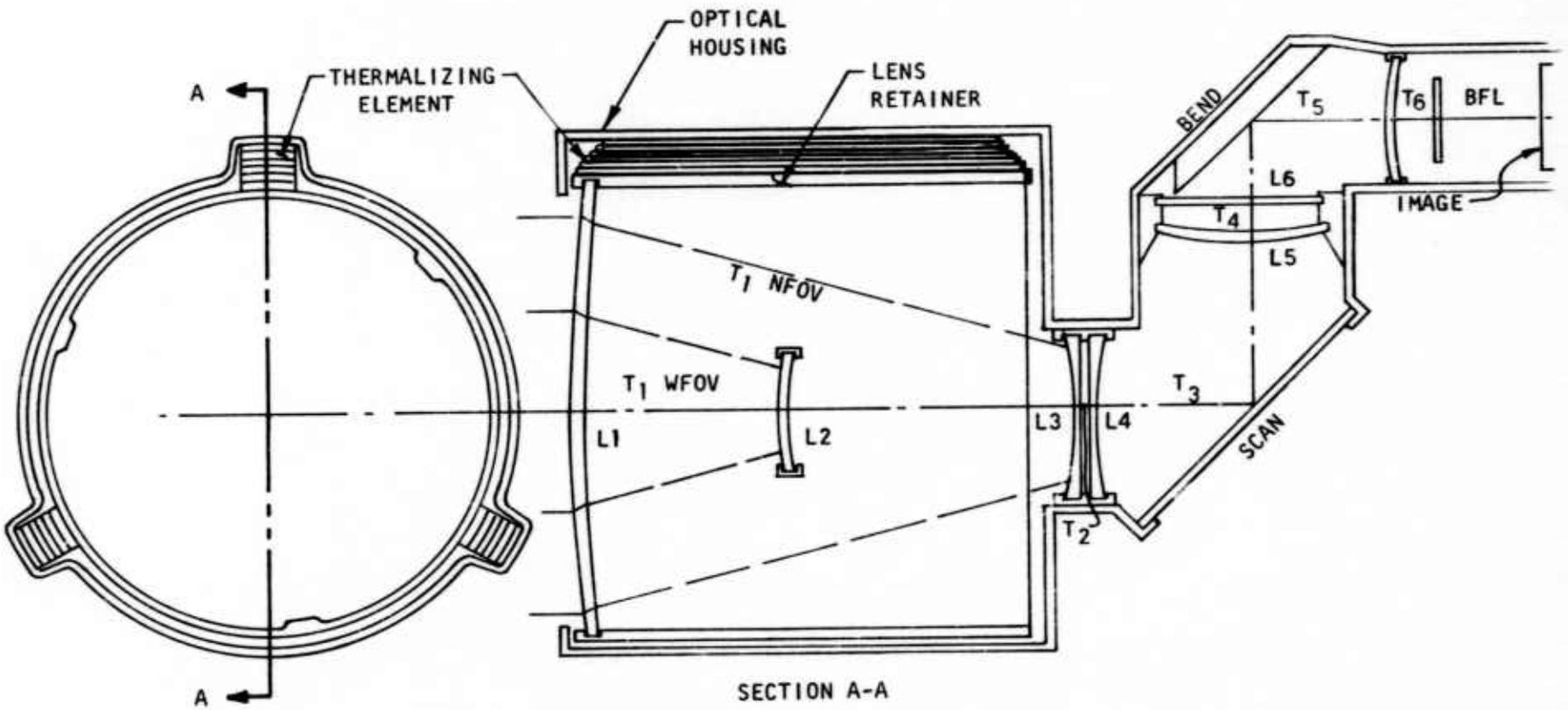

Figure 11. Lens Retention; Press Fit, Tongue and Groove or Ultrasonic Welding.

is determined by the overall contraction desired. In this case, the 15 layers needed, become quite bulky compared to previous TOW FLIR systems. A prototype of such a mechanism was built and tested to prove the concept would work and to correlate TMA expansion data to prototype behavior. The results showed a net dimensional contraction with heating accurate to within 5% of the calculated predicted contraction derived from the TMA coefficients. See Figure 12. Polycarbonate has a linear, predictable expansion from -55°C to +85°C.

If greater movement or less space is required of the passive athermalization system, two approaches remain. These are: (1) Use a material in the stack with no thermal expansion to increase the net movement or (2) use movement amplification techniques.

Two materials which exhibit thermal expansion coefficients of zero are the cermet family and Kelvar 49.

Cermet

A cermet is a material containing both ceramic and metal. Cermets have been made using a wide range of ceramics (oxides and carbides) and metals (iron, chromium, molybdenum, etc.) in an attempt to combine the refractory and oxidation-resistant properties of ceramics with the thermal-shock resistance and tensile strength of metals.

Promising cermets are TiC/Alloy (the alloy containing Ni, Co, Mo, W, Cr in various proportions), Al_2O_3/Cr and Al_2O_3/Fe.

Other attempts to define cermets have been suggested: Cermets are a heterogeneous combination of metal(s) or alloys with one or more cermatic phases in which the latter constitutes approximately fifteen to eighty-five percent by volume and in which there is relatively little solubility between metallic and ceramic phases at the preparation.

There are two basic types of cermets:

Oxide Based Cermets

- Alumina-metal cermets
  - Alumina-alloy cermets
  - Chromium-alumina cermets

Carbide-Based Cermets

- Titanium carbide-metal composition
- Titanium carbide-metal infiltrated cermets
- Titanium carbide-steel cermets

Cermets were developed during WWII in Germany and the U.S. to satisfy the need for a high-temperature, stress resistant material for use in jet engine development.

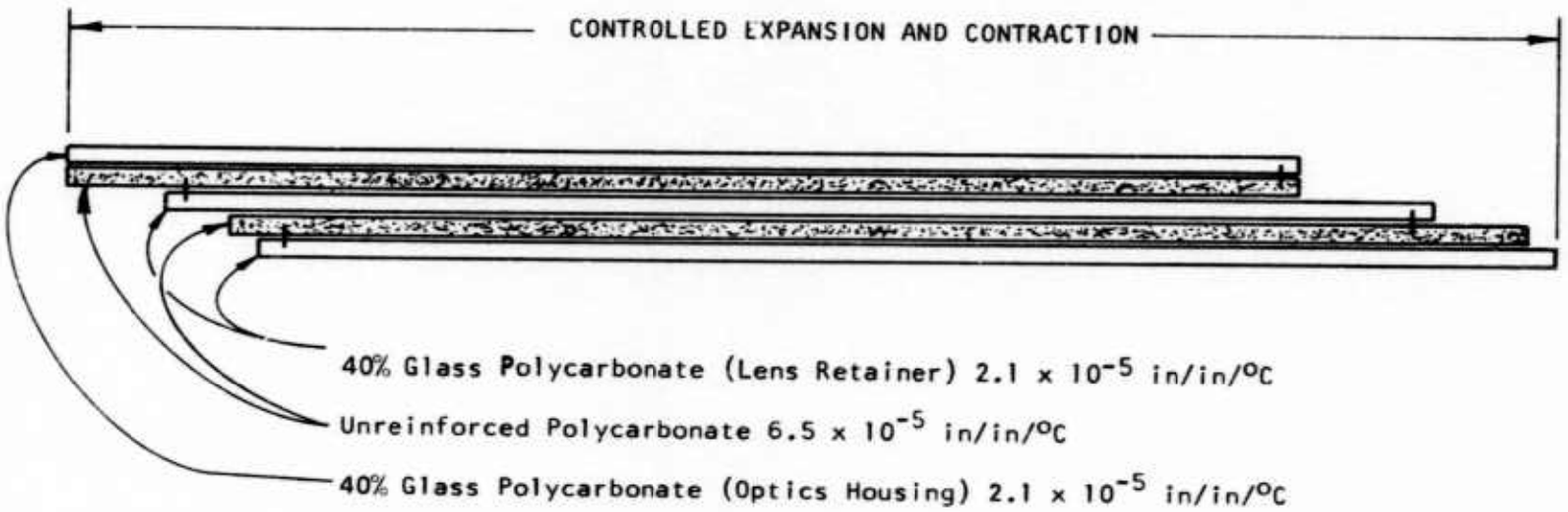

2.1×10^{-5} in/in/°C (100°)(22.7 in) = +.4767 in.
6.5×10^{-5} in/in/°C (100°)(-13.2 in) = -.8580
NET -.3813 in. Contraction with 100°C Heating

Figure 12. Prototype Polycarbonate Stack.

The combination of materials to use in the development of the first cermets was not looked upon as being particularly difficult, it was thought that it was simply a matter of "time" before scientists hit upon the correct combination.

It was well known that alloys had nearly all of the desired features, such as ductility, high strength, and high thermal conductivity and were nearly good enough. The high-temperature applications desired was a bit beyond the best known metal or alloy of the day. This led to the combination of the higher melting point and greater chemical stability, (oxidation resistance) of the ceramic with the nearly good enough metals so as to create a new material, cermet. Such names as "ceremetallic", "Ceramul", and "ceremet" were also used to define this new material but the U.S. Air Force, the main sponsor in this field, finally insisted that one term, "cermet" be used by its research contractors. This term was subsequently accepted almost completely in the United States.

Cermets can be formed by all the processes normally used in forming ceramics:

- Slip casting
- Plastic forming (extrusion)
- Powder pressing (hot and cold)
- Infiltration

A summarized grouping of cermet forming methods for producibility trade-off studies can be found in Table II.

A slip casting requires a slurry (slip) of Al_2O_3 plus Cr suspended in water. A pH of about 4 resulting from HCL added as an electrolyte is desirable to maintain the particles in suspension. The specific gravity of the suspension depends, in part, upon the Al_2O_3-Cr ratio, and therefore is not meaningful, but total solids to water ratio should be 1 to 2 or lower on a volume basis. Casting in plaster molds is accomplished in the usual way. The acid attack on the plaster mold is severe compared to the normal attrition of ceramic practice.

Operations employed with Al_2O_3-Cr cermets include extrusion and forming against plaster die surfaces. In either case it is necessary to use an organic plasticizer in addition to water in order to render the mass workable. Alginates and water soluble, high molecular-weight hydrocarbons have been used, but cannot be regarded as being completely satisfactory plasticizing additives from the standpoint of either workability or ease of complete elimination.

Cold pressing is the most common method employed in connection with cermets, and specifically Al_2O_3-Cr cermets.

Pressing is done at room temperature utilizing steel die pressing methods or hydrostatic pressing in rubber container or a combination of both methods.

TABLE II CERMET FORMING METHODS

	SLIP CAST	COLD PRESS	HOT PRESS	EXTRUDED
SIZE CAPABLITY	LIMITED BY GREEN STRENGTH	LIMITED BY PRESS CAPACITY	LIMITED BY PRESS CAPACITY	WIDE RANGE
SHAPE CAPABILITY	INTRICATE SHAPES, UNDERCUTS, ECT.	STRAIGHT SIDED, FEW DETAILS	STRAIGHT SIDED, LITTLE DETAIL	STRAIGHT DIMENSIONS
MOLD OR DIE REQUIREMENTS	WOOD OR METAL PATTERNS, PLASTER MOLDS	HARDENED DIES	GRAPHITE DIES	ABRASION RESISTANT DIES
PRODUCTION RATE	SLOW	RAPID	MODERATE	RAPID
LABOR PRODUCTION COST	HIGH	LOW TO MODERATE	MODERATE TO HIGH	LOW

- Steel Die Pressing - utilizes a charge of finely ground Al_2O_3-Cr (for example) which can usually be pressed at 10,000 to 12,000 psi without the addition of a binder lubricant.

- Hydrostatic Pressing - Preparation may consist of charging granulated powers directly into rubber molds or encasing a previously pressed cermet in a thin-walled rubber or plastic envelope.

Hot pressing is as simple as the name implies, both heat and pressure are applied to the cermet charge simultaneously.

The mechanism of the infiltration process is governed by the relationship and possible interaction between the high-melting solid phase (skeleton) and the liquid metal phase (infiltrant).

Four different conditions can be distinguished:

- Neither wetting of the solid surfaces by liquid nor solubility of either component in the other

- Wetting but not solubility.

- Wetting connected with limited solution of the solid in the liquid component.

- Wetting connected with the complete solubility of either component in the other.

This process is typically used with copper and brass infiltrated iron parts; silver-infiltrated molybdenum and tungsten contact metals; and nickel, cobalt and iron-infiltrated tungsten and tungsten carbide tools and dies.

The "formed" cermet charge must be "sintered" to bond the cermet particles.

Firing or sintering of Al_2O_3-Cr cermets, for example, is accomplished in a high purity H_2 atmosphere with some provision being made for a limited amount of oxidation of the surface of the Cr particles.

The method of bond formation between Cr and Al_2O_3 is believed to be one in which Cr_2O_3 tightly adheres to Cr, in one instance, and is dissolved (solid solution) in Al_2O_3, in the other instance. While no detectable film of Cr_2O_3 remains in many specimen of Al_2O_3-Cr cermets, it consistently is a measure of specimen quality as indicated by strength, porosity, and modulus of elasticity.

In making cermets of other metals and Al_2O_3, a workable procedure for bond formation consists of forming solid solution of approximately 10% Cr_2O_3. This solid solution is ground and mixed with a metal such as iron, and forming follows as with Al_2O_3-Cr compositions. In sintering at 2700°F in He plus a small percentage of H_2, the exsolution and reduction of Cr_2O_3 and the alloying of chromium with iron are reactions which, taken together, permit bond formation

between the depleted solid solution phase of Al_2O_3-Cr_2O_3 and the Fe or Fe-Cr alloy phase which forms. This solution of the exsolved and reduced Cr in Fe facilitates the reaction which would not proceed perceptibly in the purest H_2 if the Fe solvent metal were not present.

By similar techniques Al_2O_3 plus a small amount of other oxide can be combined with metals -e.g., iron, nickel, and cobalt-to form a cermet of low porosity and generally good quality.

The basic requirements necessary to cermet fabrication are these:

Raw materials

- Metals
- Ceramics
- Acids
- He environment
- H_2 environment

Tools

- Dies, Molds } Steel/Rubber

Equipment

- Sintering oven (to 4000°F)

The use of "cermets" in the application of lens mounts in FLIR systems is a possibility. The cermets offer excellent thermal properties necessary to the focus mechanism. Cermet data are located in Appendix F.

The main disadvantages are these:

- The technology involved in the production of cermets having a particular "balance of properties" is limited. Cermets have found their major use as coatings.

- The fabrication techniques that would be required to form intricately shaped lens housings would have to be developed.

- The close tolerances, which must be held, would require post-forming machine operation, since such dimensional accuracy is not possible with cermets.

Considerable developmental work would have to be successfully accomplished before cermets could be used as the material in mass produced parts and housings.

Kelvar 49

Kelvar 49 is DuPont's trademark for a DP-01 fiber. The fiber was developed in 1971-1972 and is presently in the last stages of development and first stages of marketing. The fiber is organic and a superior substitute for asbestos. It has high tensile strength and excellent characteristics. (See Appendix G.)

Kelvar-49 may be used in similar applications as any other reinforcement utilizing the same basic equipment. Some examples of processes would be these:

- Wet lay-up or prepregging of fabrics and tapes.
- Filament winding.
- Chopped fiber and sheet molding compound.

All the development work has been in the area of reinforcing thermosets plastics (epoxy and polyester). Development has just begun with thermo-plastics (polycarbonate and nylon) and the use of injection molding of Kelvar 49.

Present applications are large interior/exterior panels for aerospace, helicopter blades, and other structural parts. With the advent of new development, intricate cross section should be possible.

At present Kelvar 49 exists as a "potential" for use in FLIR systems. It offers the mechanical and thermal properties (when in an epoxy matrix) required of the housings and lens mounts.

Its main advantage is its relatively low cost and its relative ease of processing with respect to cermets.

Again, as previously mentioned, this reinforcing fiber is in its developmental stages and still requires considerable technological advances for high volume production of intricate parts.

Polycarbonate Gear-Lever

Figure 13 shows a technique devised to utilize the physical properties of polycarbonates yet reduce the bulkiness of 15 polycarbonate layers. The net linear motion of two unreinforced layers is applied to the #1 lens retainer through a gear-lever to multiply the motion linearly. The pivot point of the lever is determined according to the motion required. The gear teeth mesh with racks in both the second polycarbonate layer and the lens retainer. The disadvantage of such a design lies in its questionable reliability. The proper meshing of the gear teeth is susceptible to shock and vibration as the lens retainer could rotate or shift off center with respect to the optics housing.

Silicone Rubber Element

Of the various designs developed for #1 lens movement, the use of silicone rubber providing the right motion and rigidly supported between the optics housing and the lens retainer appears most promising. With a hardness of Shore A 80, a compression molded silicone rubber (not to be confused with "RTV" silicone) exhibits a linear thermal expansion in the direction of mold flow of

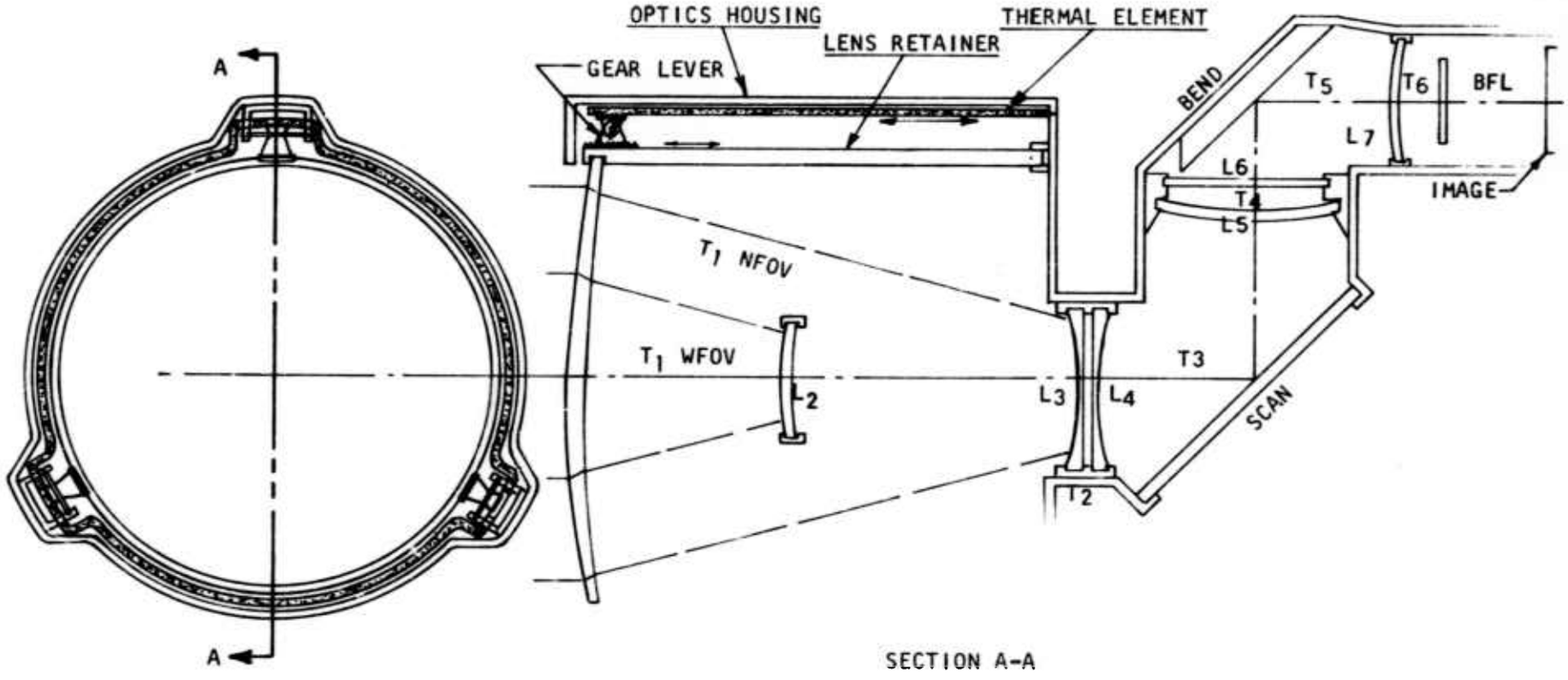

Figure 13. Gear - Lever Heat Compensation.

24.9×10^{-5} in/in/^{o}C. Over the 60^{o}C range, only 4.89 in. of silicone length is required to provide housing and retainer of glass reinforced polycarbonate. Thus 4.89 in. can be accommodated between the #1 lens and the NFOV doublet without resorting to the stack-up approach previously discussed. (See Figure 14.)

The silicone must be supported rigidly to prevent its sagging or bending which would change the T_1 athermalization motion. The FOV secondary athermalization would lend itself best to this design due to the limited space available. A simple, reliable design of light weight and low cost is achieved. Silicone exhibits a glass transition temperature of -35^{o}C which limits its linear behavior and use in athermalization to that lower limit.

2. Use of Bellows - Optics Group

In addition to laminated plastics the concept of using a fluid filled bellows for obtaining movement was considered. Typical construction of a liquid filled bellows is shown in Figure 15. The bellows evaluated in the athermalization program were manufactured by the Robertshaw Company, which is a subsidiary of the Fulton Sylphon Division.

Due to bellows construction, the thermal movement is essentially axial, while the amount of movement is determined by the bellows fluid reservoir size and type of fluid used. The selection of fluid type is important since fluids with a high coefficient of volumetric expansion minimize size and weight. With the dimensions shown in Figure 15, and MS-9036 fluid, a movement of .063 to .077 in. between -67^{o}F and +131^{o}F was obtained.

Examination of the bellows found them to be quite flexible, structurally. Consequently, for supporting the lens while in motion, it was necessary to enclose the bellows in an outer cylinder. Design details are shown in Figure 16.

An improvement over the fluid filled bellows was the use of an annular bellows. Annulus size being sufficiently large to allow for mounting of the thermal compensation lens. Figure 17 shows a typical size for this approach.

3. Use of Bi-Metallic Components, Optical Group

Highly flexive bi-metallic thermostat material was evaluated as a lens movement concept. A 0.50 inch thick sample was obtained from the Metals and Control Division of Texas Instruments at Attleboro, Massachusetts. The material is constructed of three elements metallurgically bonded together in layers. It is produced commercially under the trade name, "TRUFLEX".®

Some positive recommendations that can be made about this material are these:

- Certain designs can be stiffened to minimize vibrations.
- It is relatively easy to machine.
- Raw stock is inexpensive.
- It is readily available in several sizes.
- Published temperature deflection equations allow for a variety of design concepts.

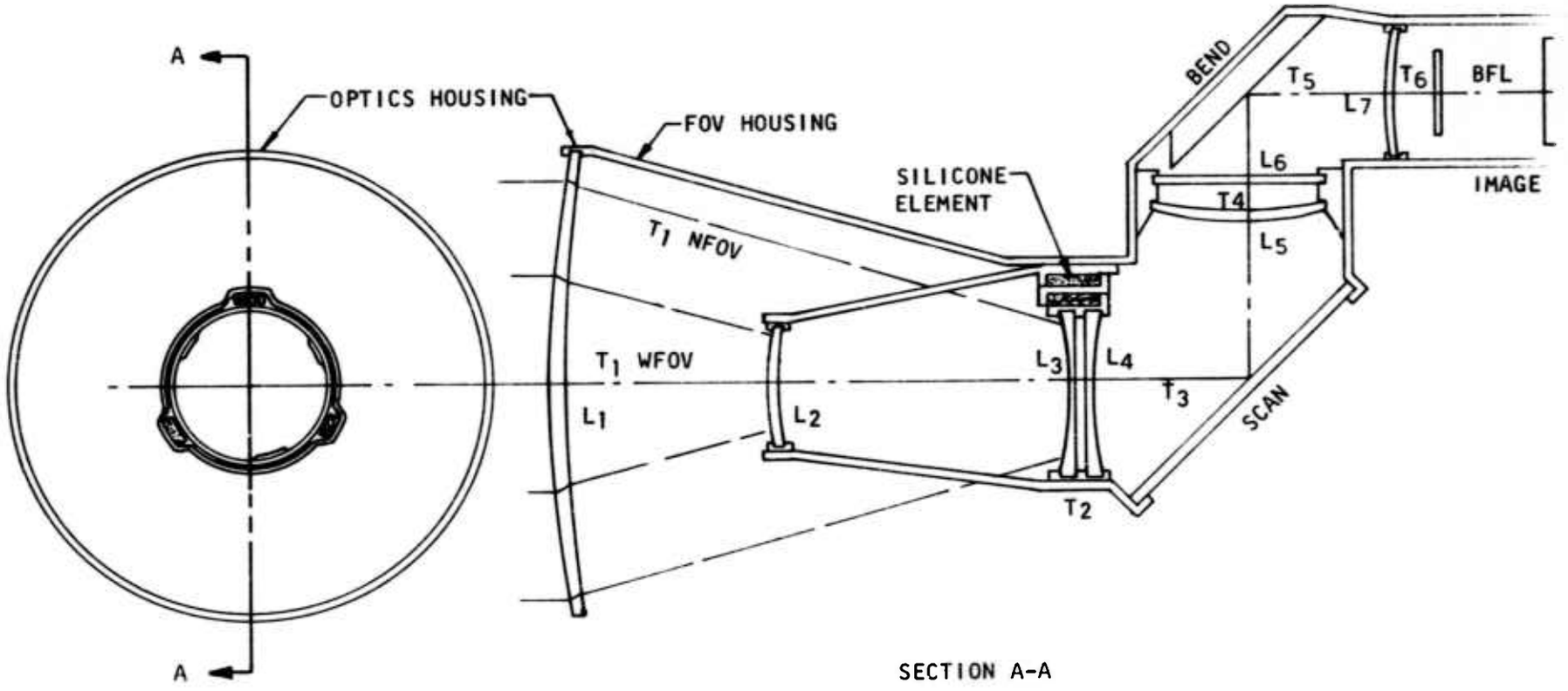

Figure 14. Silicone Element, Temperature Compensation over 60°C.

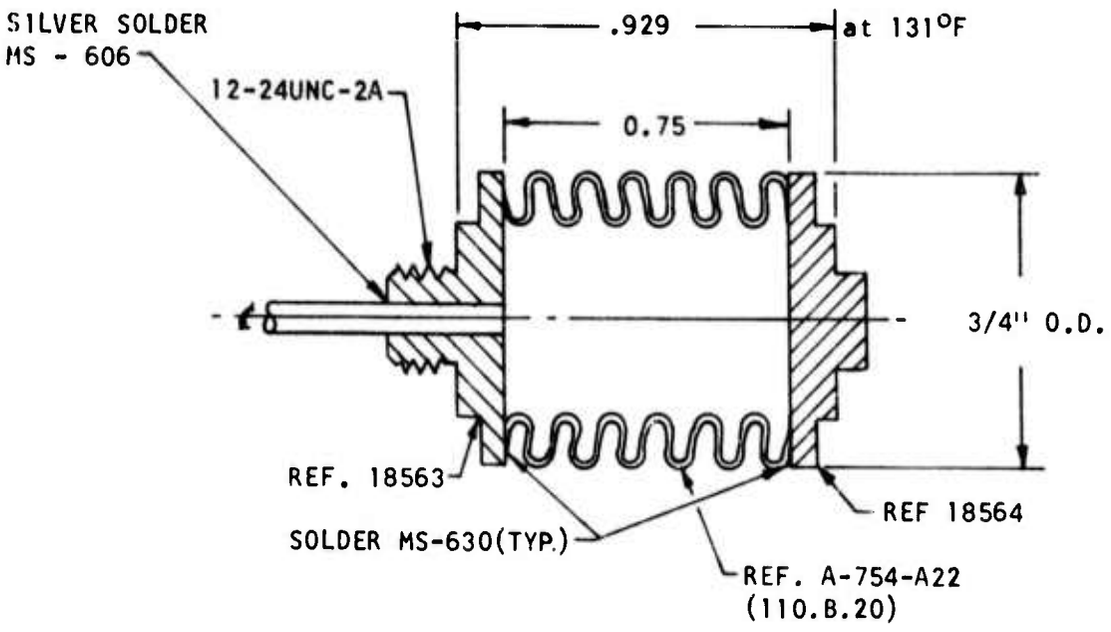

Figure 15. Typical Bellows Size.

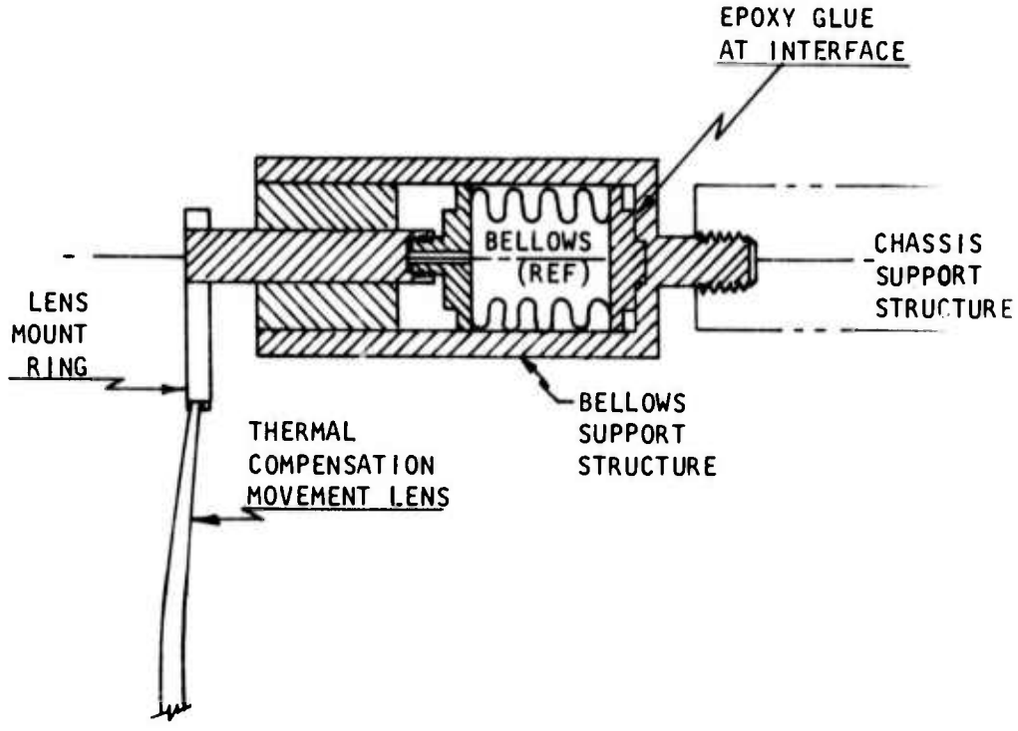

Figure 16. Bellows and Support Structure Assembly.

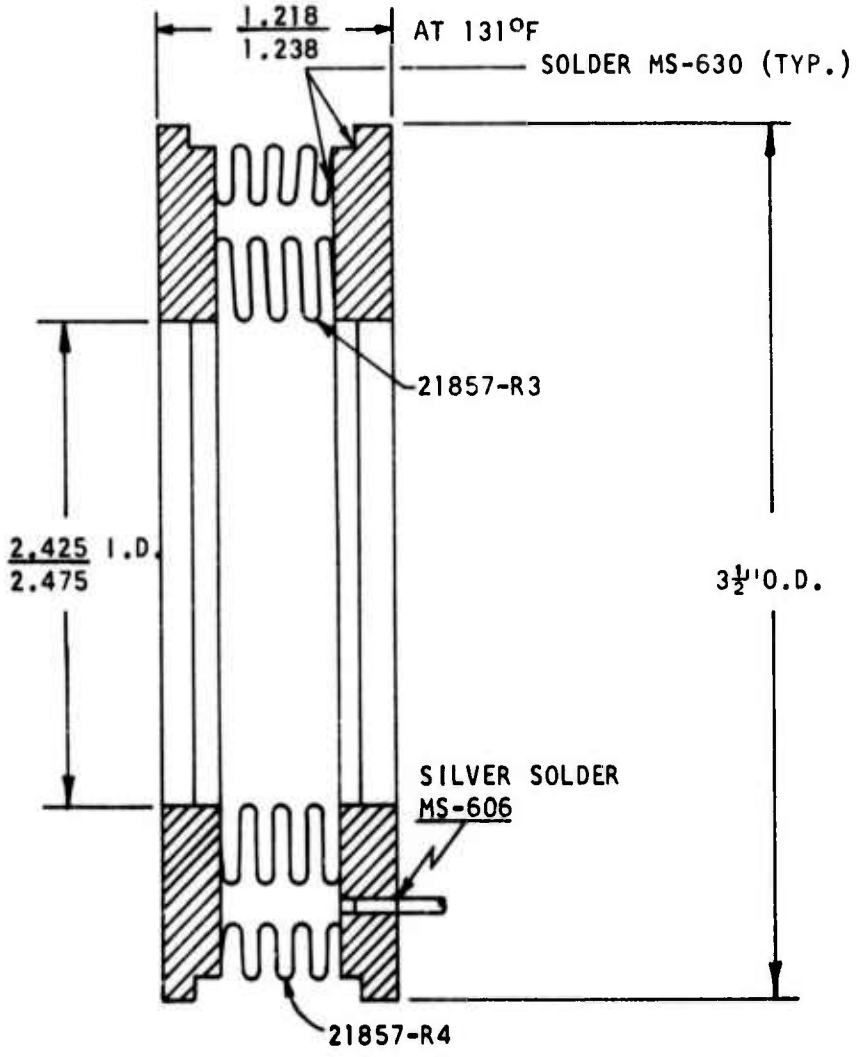

Figure 17. Annular Bellows.

Figure 18 is the thermal deflection data published by Metals and Controls. Nomenclature is as identified in the brochure the data were taken from.

The configuration selected for evaluation was the disc. The size of the disc was sufficient for the compensating lens to be potted in the annule. The outer edge of the disc was then bonded with potting compound to a mounting ring. This is as shown in Figure 19. A "dual disc" design is shown in Figure 20. This design would allow for twice the movement obtained from the single disc.

Limited testing of the disc alone tended to confirm predicted temperature deflections. However, on assembly, it was found that the potting compound restrained the edges of the disc. This, in turn, restricted the deflection by as much as 50 percent. Consequently, it was concluded that to use this concept it would be necessary to oversize the outer diameter of the disc. The exact amount of oversizing would have to be determined by testing.

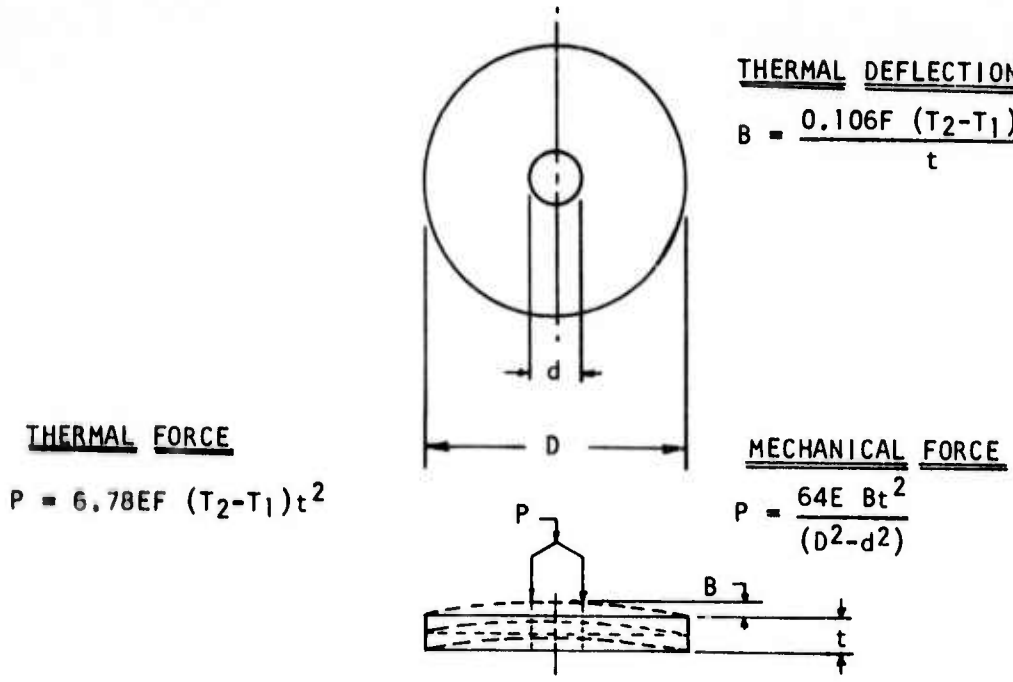

Figure 18. Disc, Thermal Deflection.

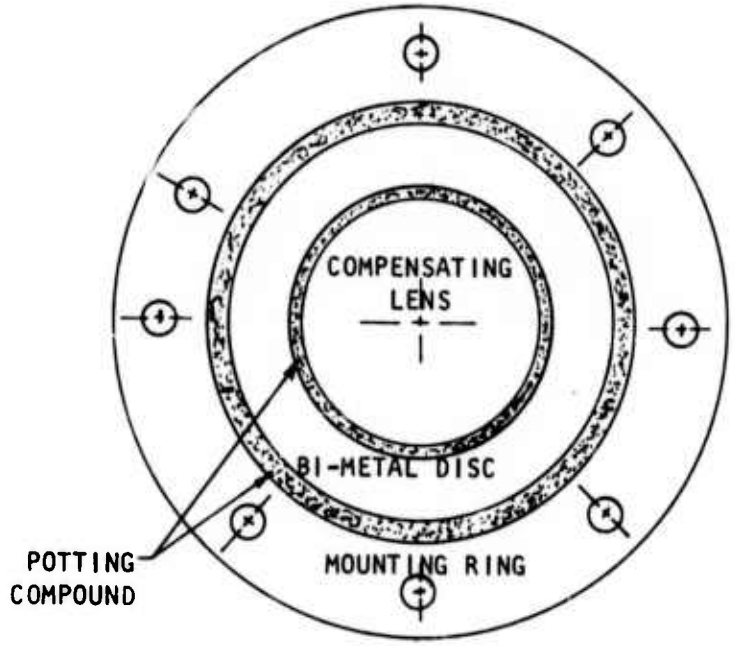

Figure 19. Bi-Metal Disc Design for Thermal Compensation.

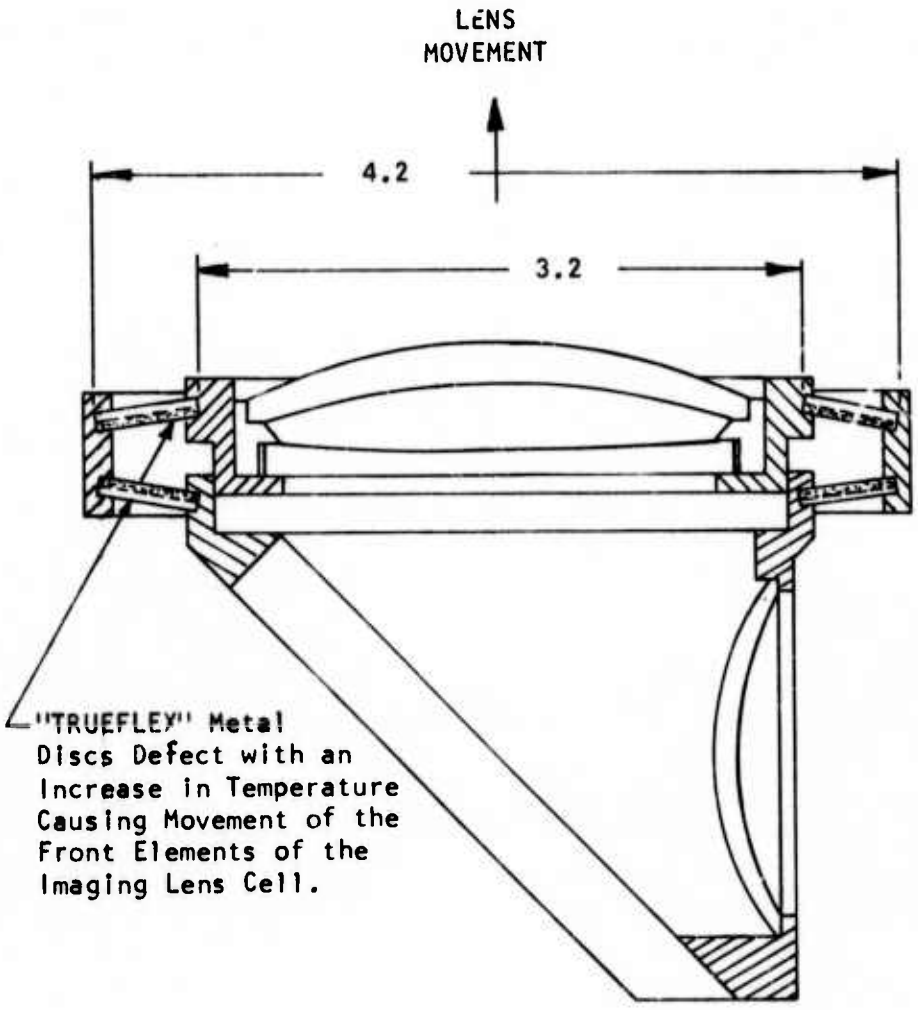

Figure 20. "Dual Disc" Bi-Metal Design Concept.

4. Automatic Focus Conclusions

Several conclusions can be drawn regarding passive athermalization design approaches. Among these is that the thermal transient "time constant" of the device must match up reasonably well with that of the lens system it compensates. This is to say that as the lens temperature changes, so must that of the compensating device. Depending on optical element packaging, it may not always be possible to accurately predict the time constant. Then, a limited amount of thermal testing is necessary. From heat transfer theory it can be shown that the time constant is dependent, in part, on the thermal capacitance of the device; i.e., the product of weight and specific heat. Consequently, should testing show that the device time constant is not compatible, then the size or thickness might be changed accordingly. For example, if plastic rods are used, then they could be hollowed to reduce the thermal mass.

Also important are structural and vibration considerations. Military equipment is typically subject to broad ranges of vibrations and shock loads. For meeting these requirements a device must be strong enough to withstand the required shock loading. The natural frequency of the device should be high enough such that deflections at resonant dwell do not degrade the optical signal. Again, due to possible internal vibration amplification thru the package, testing may be necessary to evaluate vibration design.

To conclude, it does appear feasible to successfully incorporate a passive athermalization design into an optics system. The design approach used will vary with packaging restrictions. From experience, it is suggested the design should have some amount of over-compensation initially allowed for. This will allow for any uncertainty in either optical movement requirement or mechanical movement.

B. FREQUENCY FOCUS COMPENSATION

In an optical system, an optical focus capability is necessary if the otpics are sensitive to range and temperature differences. The optics associated with most FLIR systems are very sensitive to focus in both the infrared and visible spectrum.

An observer if viewing a FLIR display finds the information content on the screen a direct function of the sensitivity, or the minimum resolvable temperature (MRT), capabilities of the system. The MRT is associated inversely by the modulation transfer function (MTF) of the system. Therefore, if the system is defocused, the information content of the viewed scene will decrease.

Much effort and money has been expended to achieve FLIR's that are very thermally sensitive. It is therefore imperative that the maximum sensitivity of a FLIR be maintained throughout a mission. Therefore, MTF must be optimized at all times.

One of the major contributions to the lack of focus in a FLIR is the infrared optics. As the resolution increases, the depth of the field decreases for range focus. Figure 21 shows the change in focus as a function of range for a 0.1 milliradian FLIR focused at infinity, 8000 feet, and 1000 feet. Note that the original MTF will degrade by 10% at 9000 feet if the system was originally focused at infinity. On the other hand, if the FLIR were focused at 1000 feet, the 10% degradation occurs at 1100 and 900 feet demonstrating a very small depth of field. Figure 22 illustrates the range focus for a 0.55 milliradian FLIR. These curves show the depth of focus is not nearly as critical for 0.55 mr as 0.1 mr FLIR optical systems.

Range focus is not the only contributor to MTF loss due to optical system defocus. Other contributors are the changing refractive index for infrared glasses, the expansion of structure, and the changes of curvature of the lenses over temperature differences. If a change of temperature does occur, the lenses in an optical system must be refocused in order to compensate for the changes in image position of the optics. Figure 23 shows the MTF change as a function of temperature for the above mentioned optical system. Note that for the 0.1 mr system the 10% MTF degradation occurs at $\pm 1.1^{o}C$ about the nominal setting while for the 0.55 mr FLIR the MTF 10% degradation point occurs at $\pm 2.6^{o}C$.

Range and temperature focus in infrared optical systems has become more critical. Currently, independent manually operated optical movements are required for each FOV, along with a remote closed-loop servo or athermalization system, required for temperature focus. Any other scheme may be a compromise of the situation. Therefore, elaborate mechanical movement mechanisms are required, and this adds weight and consumes power from the aircraft.

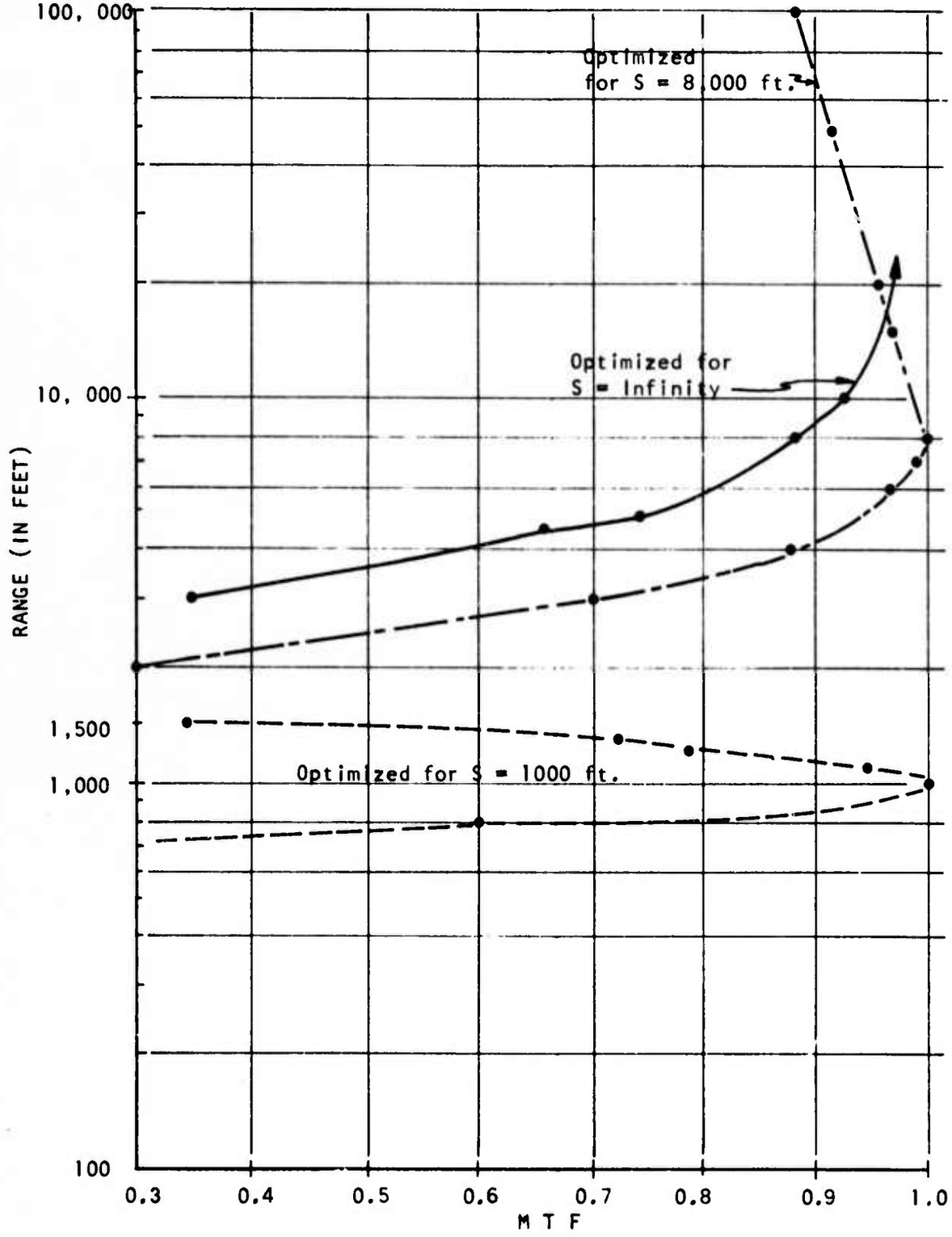

Figure 21. Range vs M T F

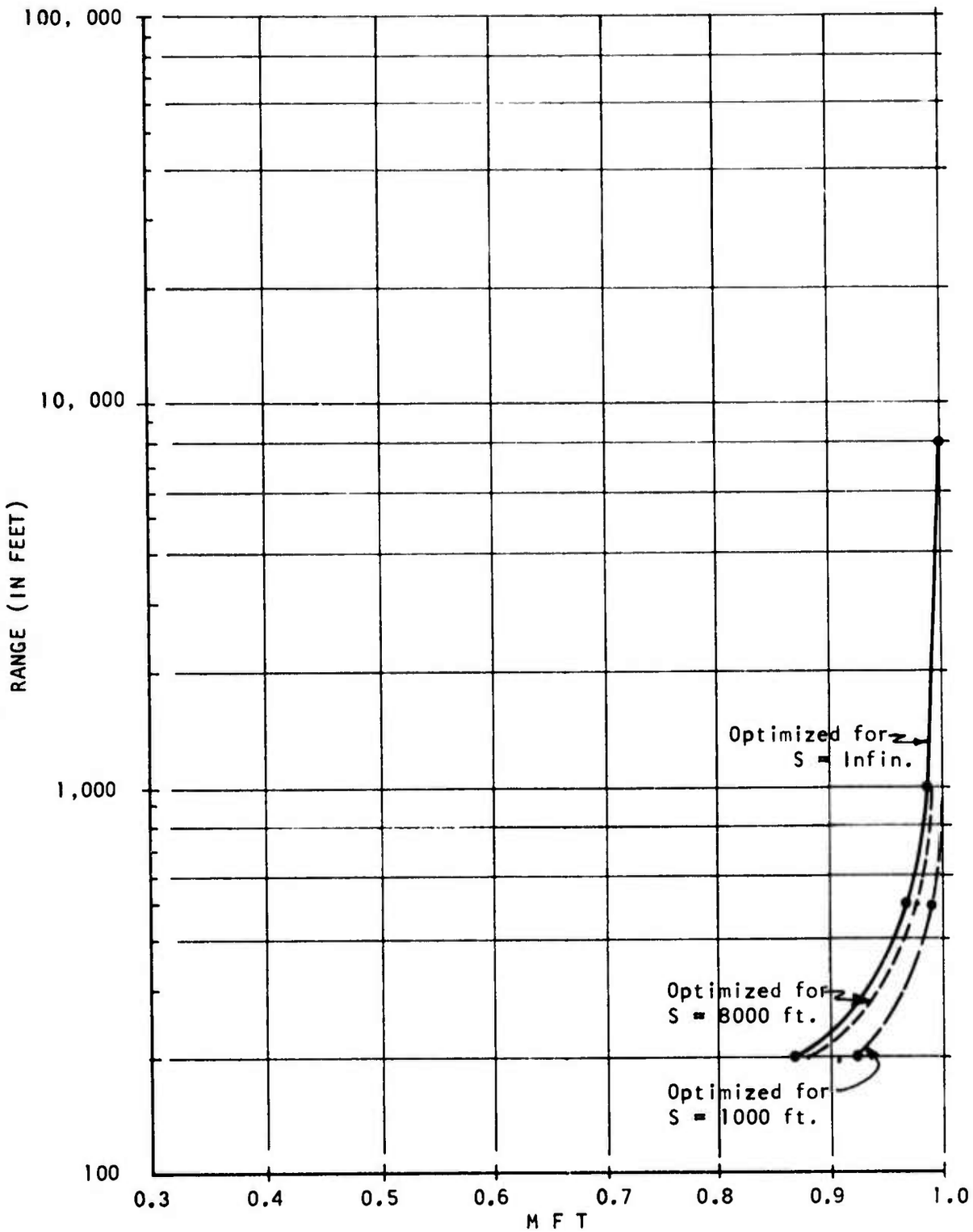

Figure 22. Range vs M T F.

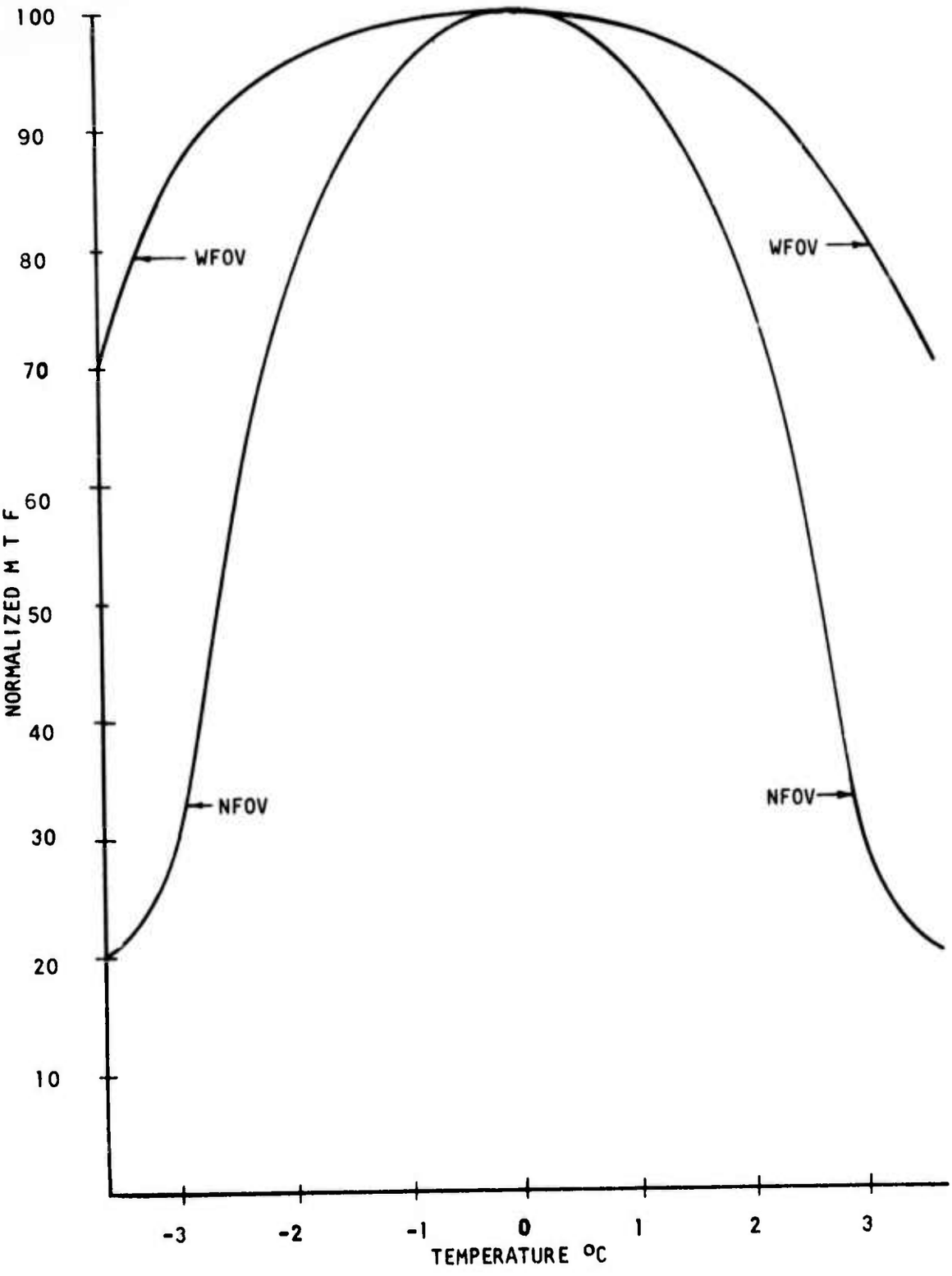

Figure 23. MTF Degradation as a Function of Temperature.

A manual focus requires the FLIR operator to spend time refocusing which can decrease the probability of target detection. From the above discussion, a more desirable choice is some automatic means of focus such that the operator is not concerned. This is the basis for this part of the study: Investiagte the possibility of automatic focus from both the feasibility and manipulation standpoint. It should also be noted that the automatic focus should be independent of defocus caused by temperature or range change.

1. Program Plan

In this study, the direction taken was to examine the video after the initial amplification of the detecotr signal. This helped to determine if there was a decrease of high frequency information as the system went out of focus, and /or a decrease in the AC video amplitude as the IR optics were defocused. Both of these conditions were expected to exist. After data were taken regarding frequency and amplitude of scanned scenes, a breadboard circuit was designed and tested on a FLIR optical system.

2. Optical System Testing

A test was performed to determine if there was enough decrease in high frequency information with defocus to be used in an automatic system. A FLIR sensor with a remote focus capability was used for this test. The plan was to record the IR video out of the preamplifiers on magnetic tape. The scene was recorded with the FLIR in both stationary and moving modes. The scenes were put in good focus and recorded, then defocused and recorded. Due to hardware limitations only the NFOV could be defocused. Figure 24 is the test setup used to measure the decrease in high frequency video information as a function of IR focus.

The video information recorded on the tape was then run through a spectrum analyzer to monitor the frequency content of the information. A model (UA-15A) spectrum analyzer from Federal Scientific Company was used. Figure 25 shows a sample plot of the frequency data and Appendix J has additional reduced data.

Figrues 26, 27, and 28 show condensed data of the type shown in Figure 25. Figure 26 is a plot of small targets in a stationary scene where Curve (1) is a wide FOV in a focused condition, Curve (2) is a narrow FOV in a focused condition, Curve (3) is a NFOV in a defocused condition. Note the decrease in high frequency information for the defocused condition Curve (3). Figure 27 and 28 show corresponding data for large target stationary scene and a moving scene.

3. Results

From these data, taken for automatic focus, several conclusions were drawn;

(1) The amount of high frequency information depended on the target background.

(2) The frequency range indicating highest deviation of information with defocus condition is about one half the system resolution frequency, 30 KC.

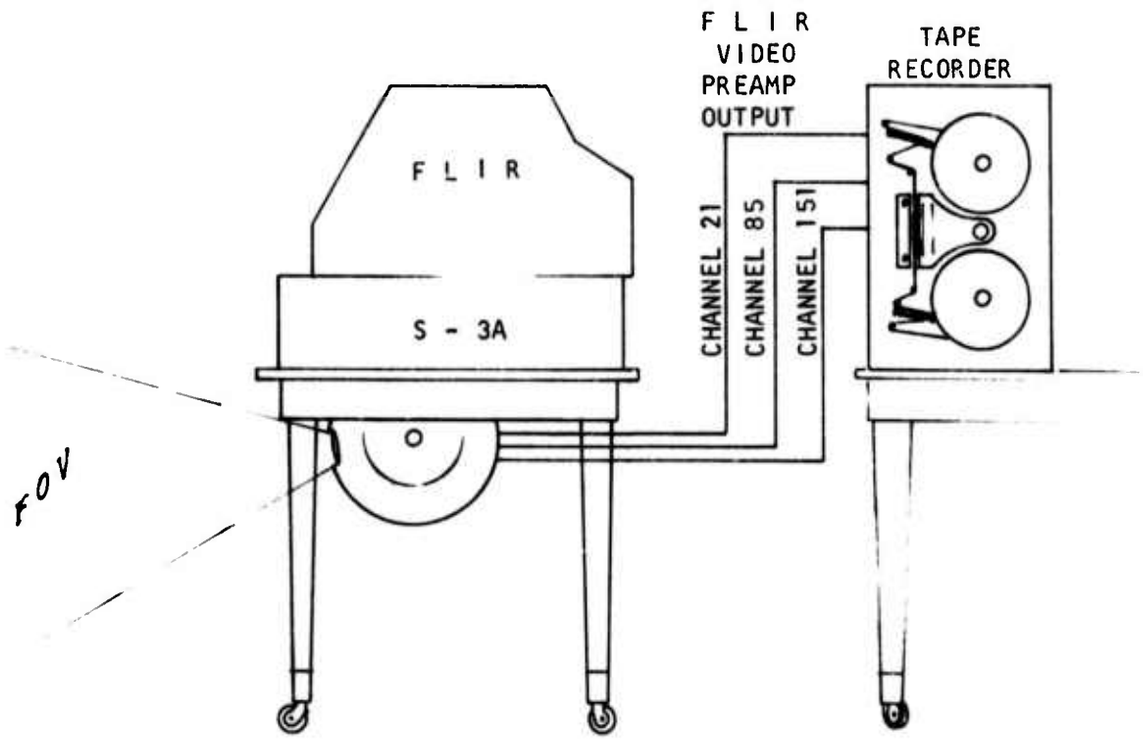

Figure 24. FLIR Video Recording Setup.

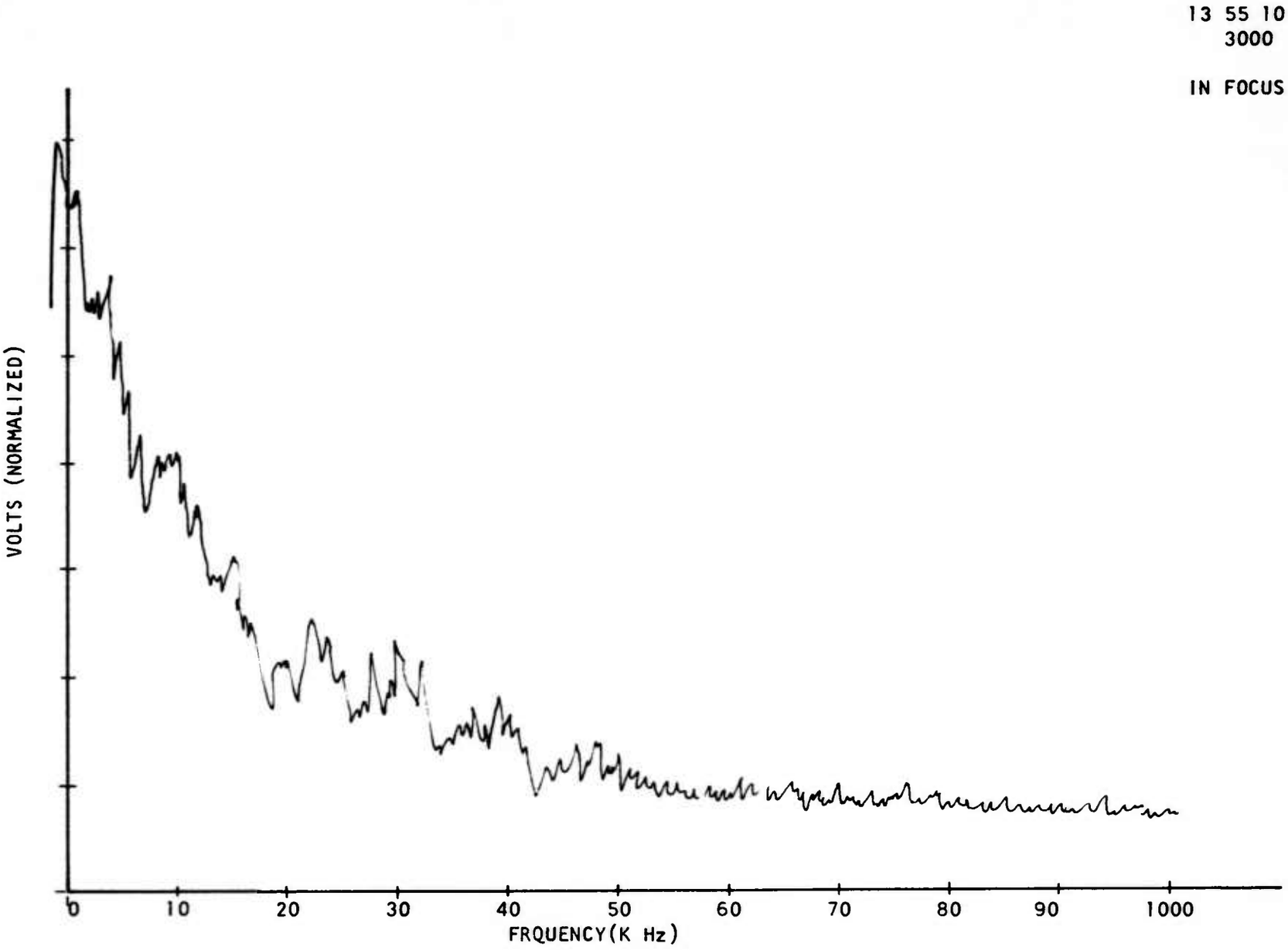

Figure 25. Sample Frequency of S - 3A FLIR Preamp Output.

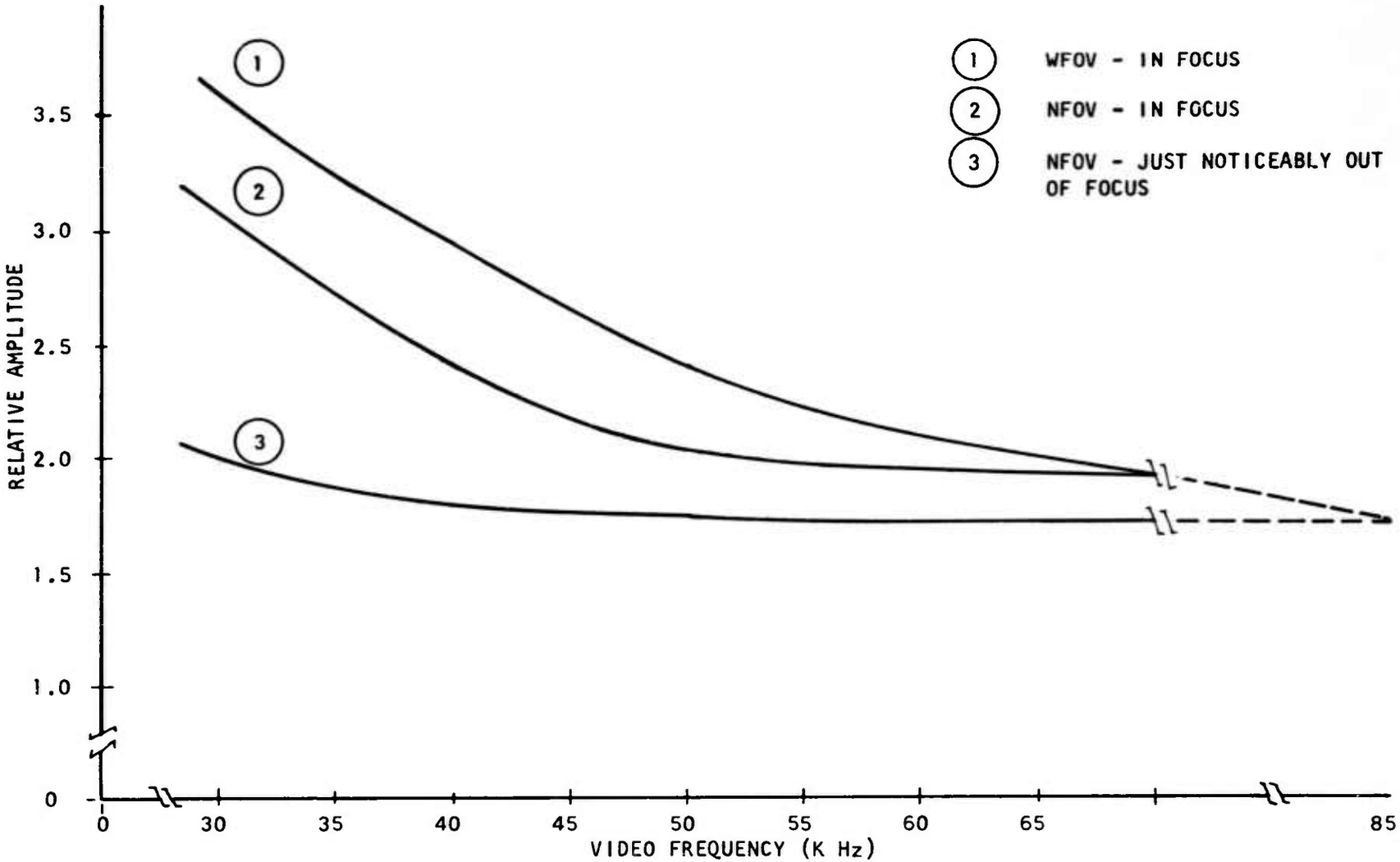

Figure 26. Small Targets - Stationary Scene.

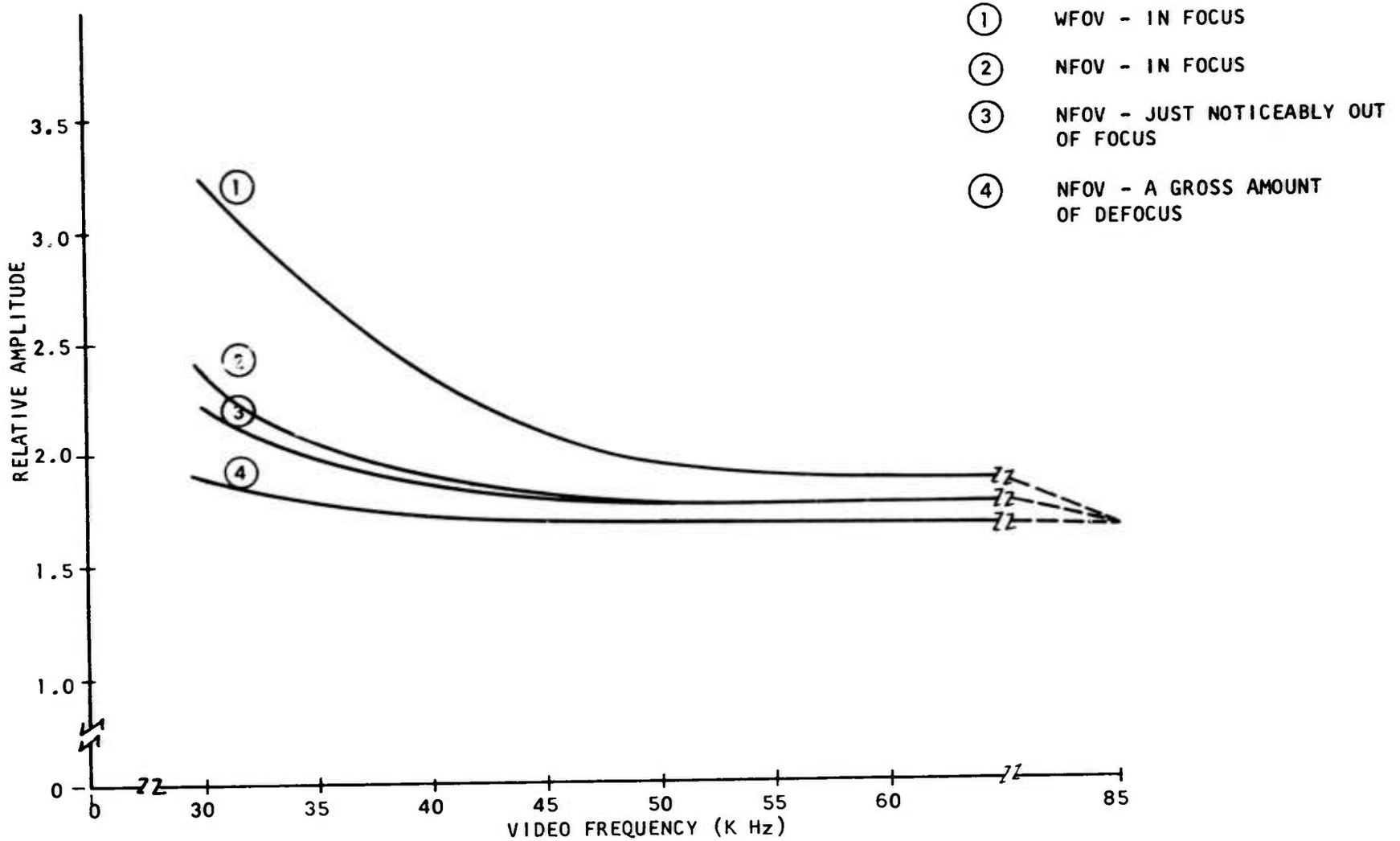

Figure 27. Large Target - Stationary Scene.

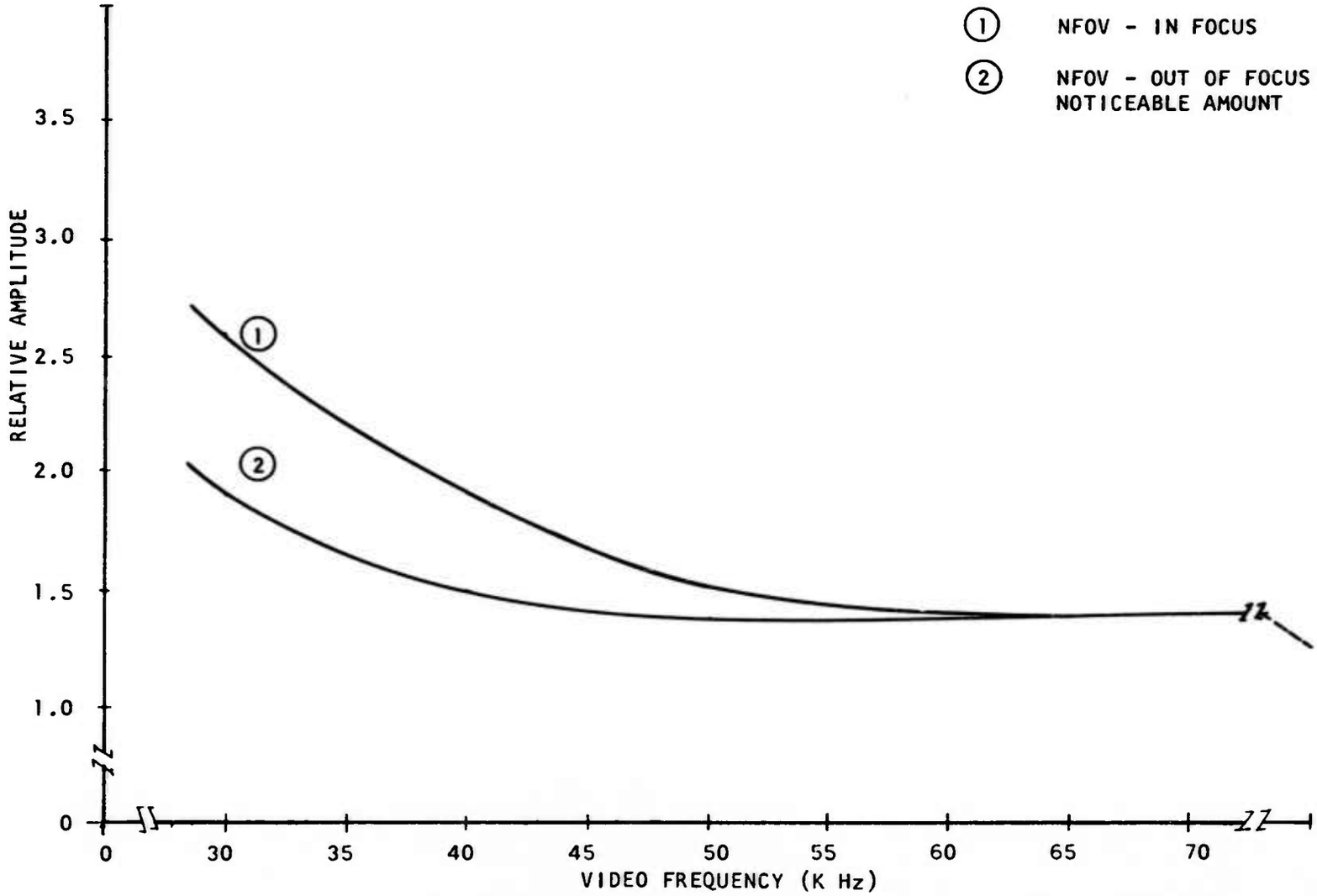

Figure 28. Channel 85, Moving Scene.

(3) A moving scene did not appreciably alter the effect of defocus, or results were unaltered.

(4) High frequency information decreased as the IR optics were defocused.

From the data gathered in the frequency content portion of the test, it was decided to pass the infrared video information through a variable bandpass filter and note the changes in signal level as a function of focus. A RMS voltmeter was connected across the output of the video information. The test set-up is shown in Figure 29.

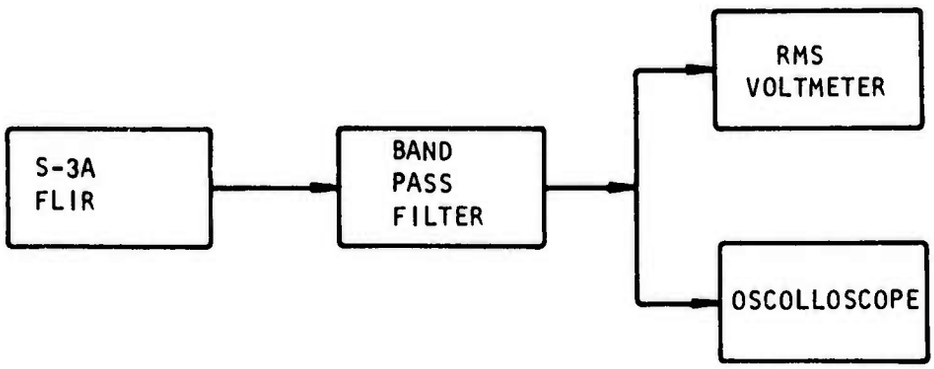

Figure 29 Video Signal Level Change as a Function of Focus Test Set-Up

The FLIR was positioned and several scenes were recorded. The filtered information ranged from 40 KHz bands down to 5 KHz bands, and varied from one third the FLIR IR resolution frequency to the IR resolution frequency of the system. A typical oscilloscope output is shown in Figure 30.

Figure 30. In Focus & Out of Focus Oscilloscope Trace of Filtered IR Video Information

During the tests, the greatest change in amplitude was observed over a bandwidth between one third the resolution frequency and the resolution frequency of the FLIR. In general, 20 KHz to 40 KHz or 60 KHz seemed to have the greatest change. The spatial frequency bandwidth of the S-3A FLIR is 58 KHz.

The tests on focus indicate that it is indeed true that the frequency content and amplitude for IR scenes in and out of focus can be measured. One of the foreseeable problems is that scenes with limited information, or IR spatial frequency content, would be more difficult to measure due to small signal levels in the IR at resolution spatial frequencies. It should be also noted that single channel outputs change as targets are moved through the scene, causing peaking of the data. Summing channels together would be one method of compensating for the above problem areas.

See Appendix J for raw data of test mode.

4. System Test Results

Using data collected in previous tests as a guide, a means of automatic IR focus was conceived and a preliminary design breadboarded. A functional diagram of the breadboard is shown in Figure 31.

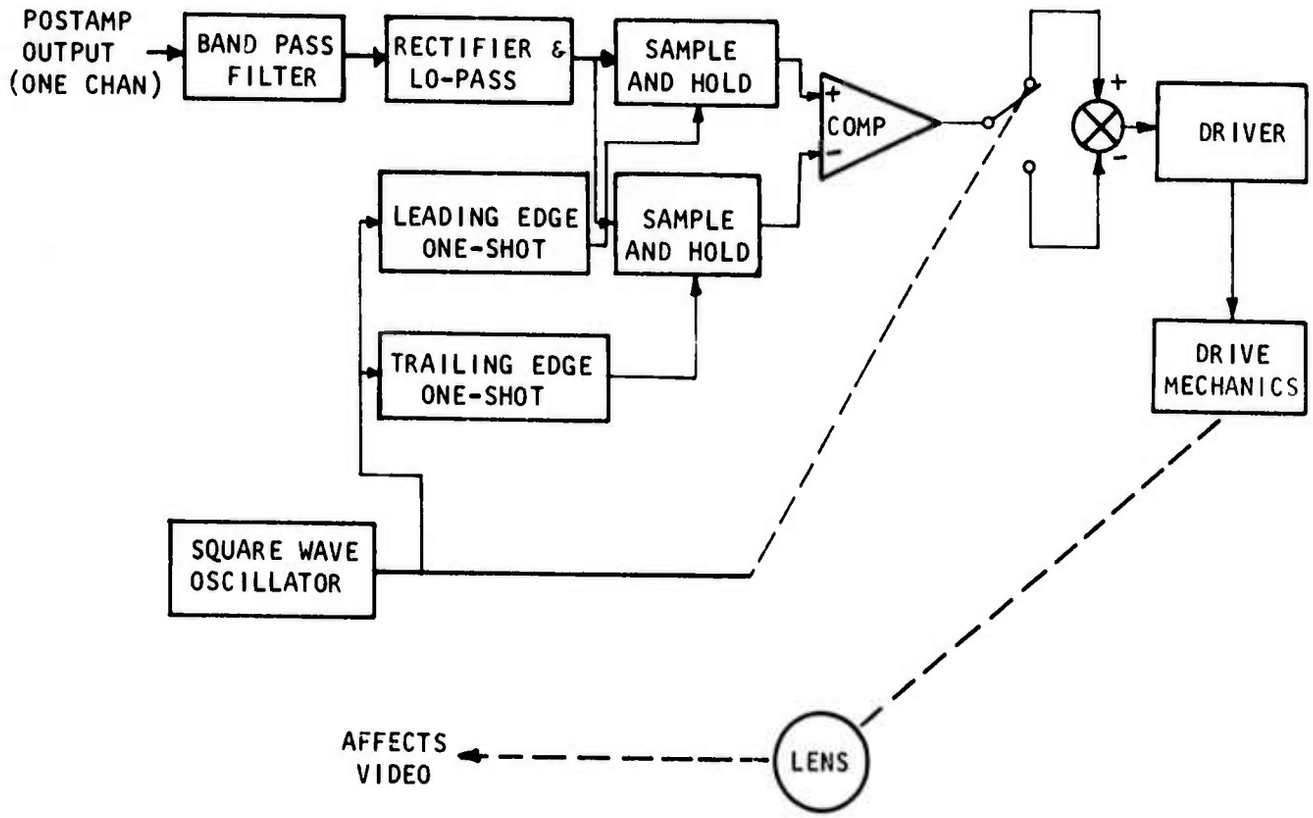

Figure 31. Breadboard Functional Diagram

The tests performed were of an empirical nature. The bandpass filter and oscillator were commerical test equipment to allow various adjustments. An S-3A FLIR receiver with zoom assembly was set up on the bench and then in the tower for "real" video. The bench tests consisted of moving the target plate in and out of its normal focus position and visually observing the image on a monitor. Also, the focus system was disabled, the FLIR moved out of focus, and the focus system enabled while monitoring the displayed image. The same type of tests were performed with "real" video in the tower. Various focus requirements were achieved by pointing at near targets (100 feet) and far targets (10,000 feet).

The bench tests were considered inconclusive due to the low duty cycle and amplitude of the video; however, the tower tests showed encouragement. Additional loop gain was required to obtain a usable video amplitude change. The system achieved hands-off focus with various changes in range, but would occasionally lose optimum focus and would hunt. It was particular as to the video content and level, and would focus much better, and consistently, with many small targets in the frame than with a few large targets in the frame. The amount of lens movement per step was variable and on one occasion the focus gear train seized and required realignment.

5. Frequency Focus Conclusions

Although the simplified system did not work consistently well, its short comings can be attributed to several minor problems that can be solved. An existing, unmodified zoom assembly was used having a DC motor driven by a voltage source. Inconsistencies in the gear train caused loading of a motor as a function of lens position thus preventing a constant lens movement per step. This contributed to eratic loss of focus. The sample and hold circuits had excessive drift for this application (100 mv/sec). This required a minimum change rate of video amplitude of greater than 100 mv/sec between samples thus limiting the dynamic range. The single video channel monitored showed almost as much level difference due to IR energy content as that due to focus. As a result, slewing the FLIR would momentarily confuse the focus system.

The drive mechanism should consist of a stepper motor or equivalent with a drive train designed for this oscillating application. A constant scale factor for the mechanics would eliminate an uncontrollable variable.

More stable sample and hold circuits should be used to increase the dynamic range. LH0023 sample and hold IC can provide drift rates of 1 mv/sec or less. Several video channels should be averaged to prevent IR level dominance with one channel. Perhaps the LED power supply current could be monitored to provide a summation of all the video channels. Further improvement may be gained by incorporating a slow AGC amplifier after the bandpass filter. If the time constant on the AGC is long enough, the focus loop will be unaffected, but will allow much more static level range.

III. SYSTEM OPTICS DESIGN

A. OPTICS

One of the primary objectives of this study was to develop a multipurpose FLIR which can be used for a wide range of RPV applications. The use of Texas Instruments common module flir optical system lends itself well to this goal. Various systems can be tailored by simply changing the infrared afocal sections to yield the required resolution and performance.

The afocal sections can be of three basic forms: refractive, reflective or catadioptric (See Figures 32 and 33). Each of these optical configurations were studied and compared during the course of this contract resulting in a choice of refractive optics for low resolution systems and catadioptric optics for high resolution FLIRS. These choices were based on complexity, transmission, ease of manufacture and assembly and performance.

1. Refractive Optical Afocals

Two refractive afocal designs which have proven to be successful for FLIR systems are the Galilean and Inverting telescope. Direct imaging systems have also been used, but these must be completely redesigned for each application which removes them from the multipurpose field. Therefore, the direct imaging type was eliminated from this evaluation.

Table III is a comparison between Galilean and Inverting types of refractive afocals. A Galilean typically has between three and five elements in each field of view while the inverting generally consists of between five and nine elements. Therefore, the Galilean has better transmission and weight characteristics, and is less expensive to manufacture. However, the inverting can be better color corrected, is not plagued by vignetting, and is easier to adapt to alternate fields of view (different resolutions). The exit pupil of the Galilean is between the front and rear groups, and cannot be moved outside in any practical instance, resulting in the designer having to make elements oversize in order to avoid vignetting.

The inverting afocal readily overcomes the vignetting problem because the exit pupil naturally falls behind the eyepiece when the optical stop is placed at the front lens.

Table III shows that each of the two types of afocal have certain advantages and disadvantages. Secondary color abberation can be more readily reduced with the inverting afocal than with the Galilean. This limits the Galilean to an afocal ratio of about 3X, and the inverting to a ratio of about 5 1/2X. Therefore, a best compromise is to use the Galilean for systems to 1/4 milliradian resolution, and an inverting afocal for systems between 1/4 and 1/7 milliradian resolution.

Obviously, these guidelines are not binding. One consideration which might be decisive is the length of the afocal section. Assuming all other parameters equivalent, the inverting afocal is longer than the Galilean

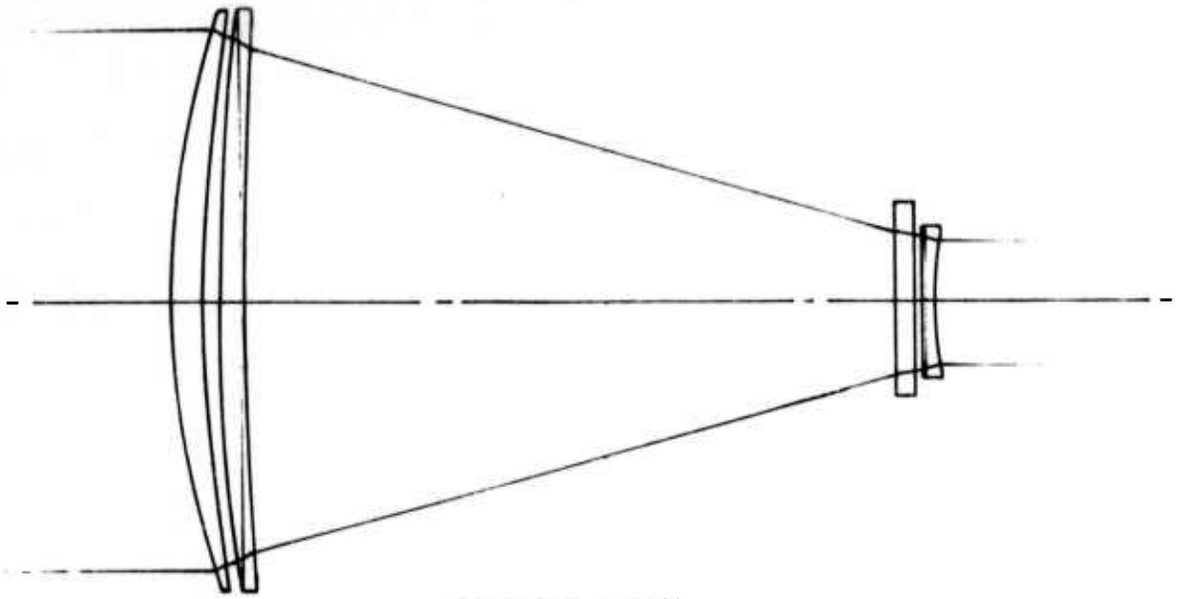

GALILEAN AFOCAL

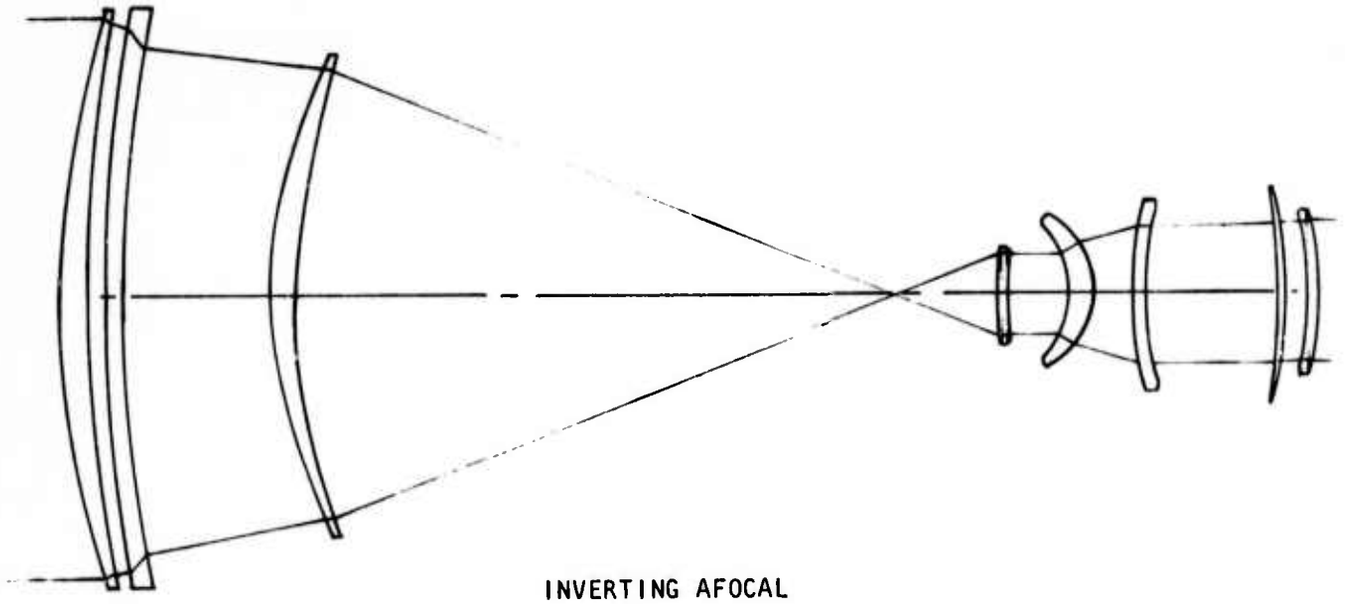

INVERTING AFOCAL

Figure 32. Afocal Types

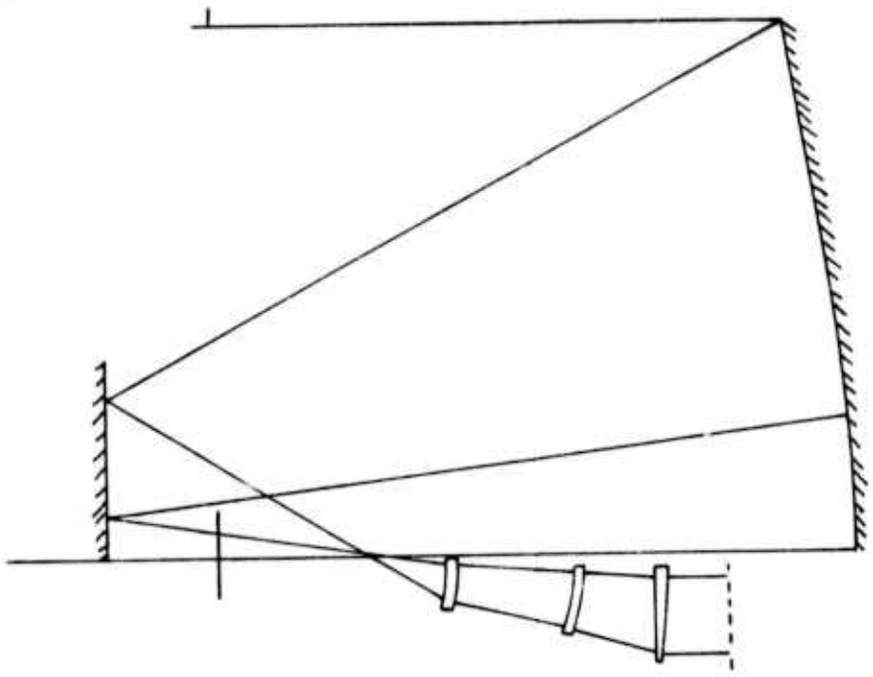

Figure 33. Catadioptric Afocal

GALILEAN	INVERTING
ADVANTAGES	
● Simplicity	● Resolution
● Weight	● Exit Pupil Location
● Transmission	● Folding
● Length	● Color Correction
LIMITATIONS	
● Color Correction	● Number of Elements
● Exit Pupil Location	● Manufacture Costs
● FOV Change	● Weight
● Vignetting	● Length
● Hump	● Cold Spike

Table III. Comparison of Galilean and Inverting Afocal Systems

by the following ratio: (See Figure 34)

$$K = \frac{AR + 1}{AR - 1}$$

where

K = ratio of the lengths
AR = afocal magnification ratio

2. Catadioptric Afocal

The limitations of refractive optical systems required a new approach to extend FLIR system resolutions, increase MTF performance, and maintain weight and size within current vehicle capabilities. These considerations resulted in the choice of a Catadioptric afocal system.

A Cassegrainian system with corrector lenses was attempted but abandoned for several reasons: the obscuration produced by the secondary mirror was close to 50% whenever the overall length was held to 1.5 times the focal length. Also, the energy is further obstructed by the eyepiece elements after it leaves the secondary mirror. (See Figure 35)

A suitable solution was obtained by changing the configuration to an off axis inverting catadioptric (cat) afocal. (See Figure 33) This necessitated making the primary mirror both parabolic and aspheric, all other surfaces being spherical. The performance of the Cat system is superior to the refractive afocals. It has been computed to be about 1% less than the diffraction limit for the systems designed to date, see Table IV. These designs have included resolutions from 1/4 to 1/16 milliradians. The Catadioptric is slightly shorter than a comparable refractive afocal, but it must take up more width to accomodate the secondary mirror. The weight of a Cat system is dependent on the technique for fabrication of the primary mirror. A glass mirror substrate should not be thinner than 1/8 of its diameter for mechanical stability during manufacture and use. Therefore, a glass mirror would weigh approximately 20 pounds for 12" aperature. By lightweight mirror technology this could be reduced to about 10 pounds. A third method is replication of the mirror. This technique would result in a 12 inch mirror weighing about three tenths (0.3) of a pound. Thus, a typical off-axis two field of view afocal would weigh about 1.34 pounds for the optical elements (based on a 1/12 mr. f/2 system). Secondary color does not appear to be a problem with the Cat system. A 1/15 mr. system was designed which had less than six microradians of secondary color.

A change of resolution with an accompanying change of field-of-view can be accomplished merely by switching eyepieces. This method is limited to a ratio of about 4 to 1. If a greater power change is required, the Cat system can be by-passed with a simple refractive afocal.

A significant technical breakthrough was achieved during the development of the Catadioptric afocal system. This consisted of removing the deformation of the primary mirror surface and transferring the aspheric

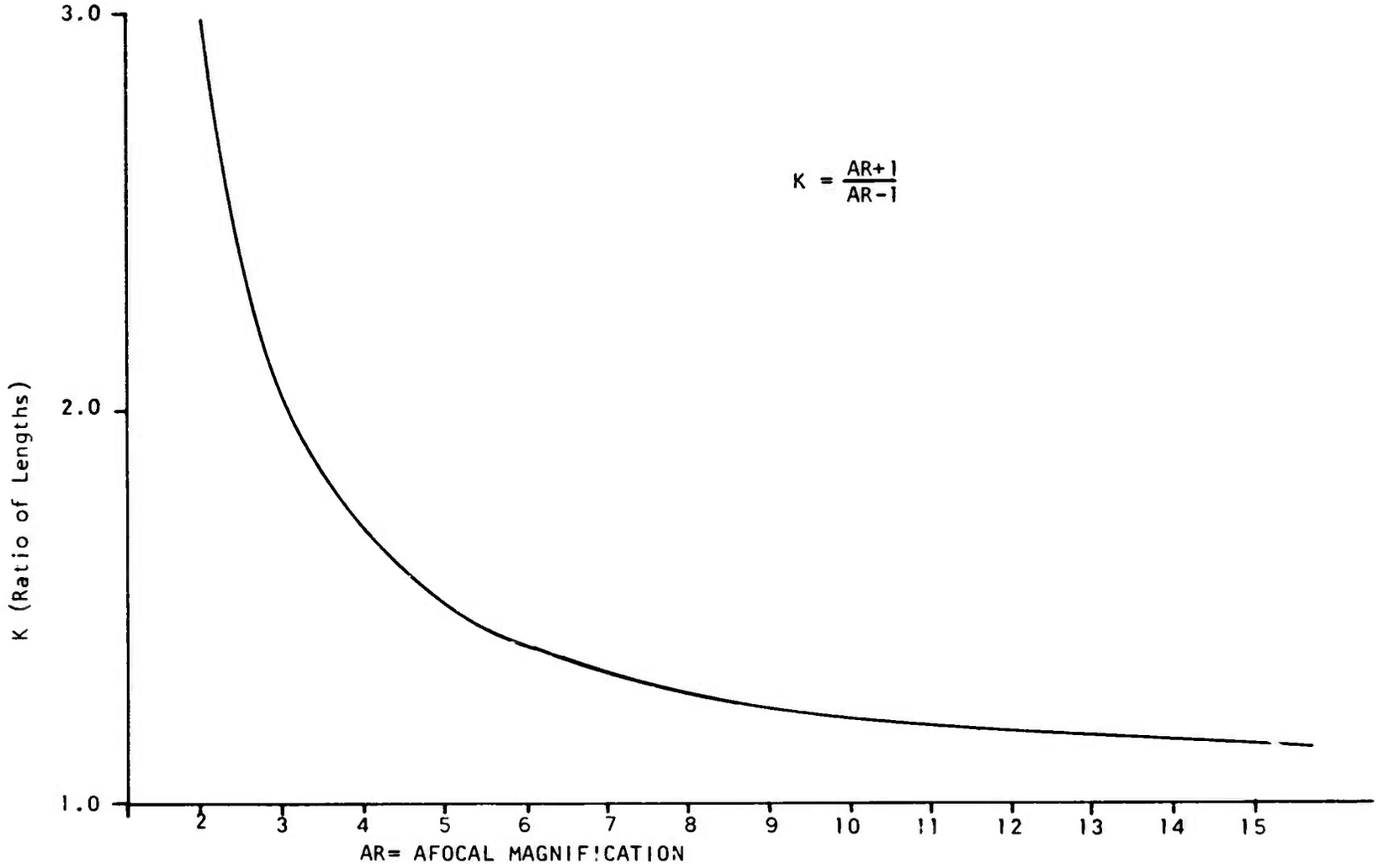

Figure 34. Ratio of Lengths of Inverting Afocal vs Length of Galilean Afocal

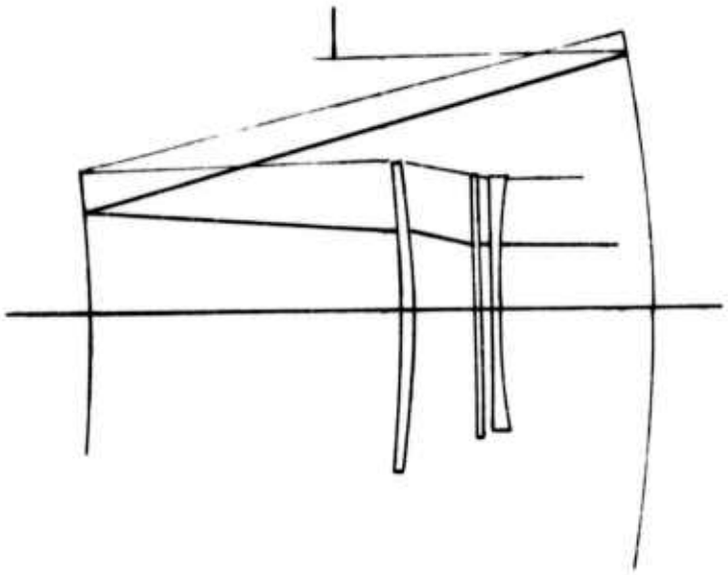

Figure 35. Cassegrain Catadioptric Afocal

TABLE IV

	1/8 MILLIRADIAN				1/16 MILLIRADIAN			
	GEOMETRIC MFT		DIFF * GEOM[1]		GEOMETRIC MTF		GEOM * DIFF[2]	
	Tangential	Sagittal	Tangential	Sagittal	Tangential	Sagittal	Tangential	Sagittal
A	98.70	99.20	74.03	81.34	98.06	99.07	51.00	63.40
B	94.10	95.77	70.58	78.53	94.27	96.91	49.02	62.02
C	99.17	98.59	74.38	80.84	96.28	96.54	50.07	61.79
D	94.00	93.27	70.50	76.48	94.64	96.68	49.21	61.88

A = Axis; B = Elevation; C = Azimuth; D = Azimuth and Elevation

1. Tangential Diffraction Limit = 75%
   Sagittal Diffraction Limit = 82%
2. Tangential Diffraction Limit = 52%
   Sagittal Diffraction Limit = 64%

Performance of a Typical Catadioptric Afocal with Texas Instruments Common Module Components.

deformation constants to the exit pupil of the system. This allows the primary mirror to be made spherical, and thus, easier and less expensive to manufacture. A penalty arises from having to add an element at the exit pupil position for aspherization (See Figure 36). Also, when the field of view is changed, a different aspheric element must be used with that eyepiece. This requires an aspheric element for each field of view, however, it would still be less expensive to make two small aspheric elements than it would be to make a large off-axis aspheric parabola.

3. Optical Design Conclusions

The optimum afocal configuration is dependent on a multitude of factors. Therefore, a specific recommendation must be viewed as a guideline. With this reservation, it is recommended that Galilean refraction afocals be used for systems of 1/4 mr resolution or less, that inverting refractive afocals be used for systems between 1/4 mr and 1/8 mr, and that the catadioptric afocal be used for systems of 1/8 mr or greater.

A well corrected, 1/4 mr Galilean system can achieve from 90% geometrical MTF on axis to 85% at 1.5° off axis. It is simple and lightweight, and the overall length is a minimum. It generally has no more than four elements and thus the transmission is about 88% through the Galilean afocal.

Typical 1/8 mr inverting refractive afocal system performance varies from 90% geometrical MTF on axis to 85% at 1.5° off axis. This type afocal will normally have six (or more) elements resulting in a transmission of about 82% or less. It is inherently longer than a Galilean, and often must be made abnormally longer in order to eliminate non optical problems such as cold spike or hump. As an example, an existing 1/10 mr Galilean afocal system has an overall length of 10.3 inches and an MTF spread of from 81% geometrical on axis to 66% over 1.5°. A 1/10 mr inverting afocal is 19 inches long and has an MTF spread of 87% geometrical on axis to 84% over 1.5°. The Galilean has 4 elements and the inverting has 7 elements.

A Catadioptric 1/10 mr afocal system has two mirrors and five refractive elements which might be reduced to four elements. Since one of the refractive elements is included in order to remove the aspheric terms from the primary mirror and transfer them to the exit pupil of the afocal. It has 70% transmission and its performance covers 99% geometrical MTF on axis to 90% at 1.5° off axis.

B. SYSTEM DESIGN AND PERFORMANCE CALCULATIONS

Three FLIR systems have been designed using each of the three optical systems discussed in Section III A optical design. System number 1 is a two field-of-view (FOV) high resolution system. The instantaneous field of view in the narrow field is 1/15 milliradian, and the wide field of view is 1/8 milliradian. The system is designed to meet the large reconnaissance RPV problem. This design utilizes two spherical mirrors and five compensating lenses in the afocal for each FOV. The Texas Instruments common module IR imager

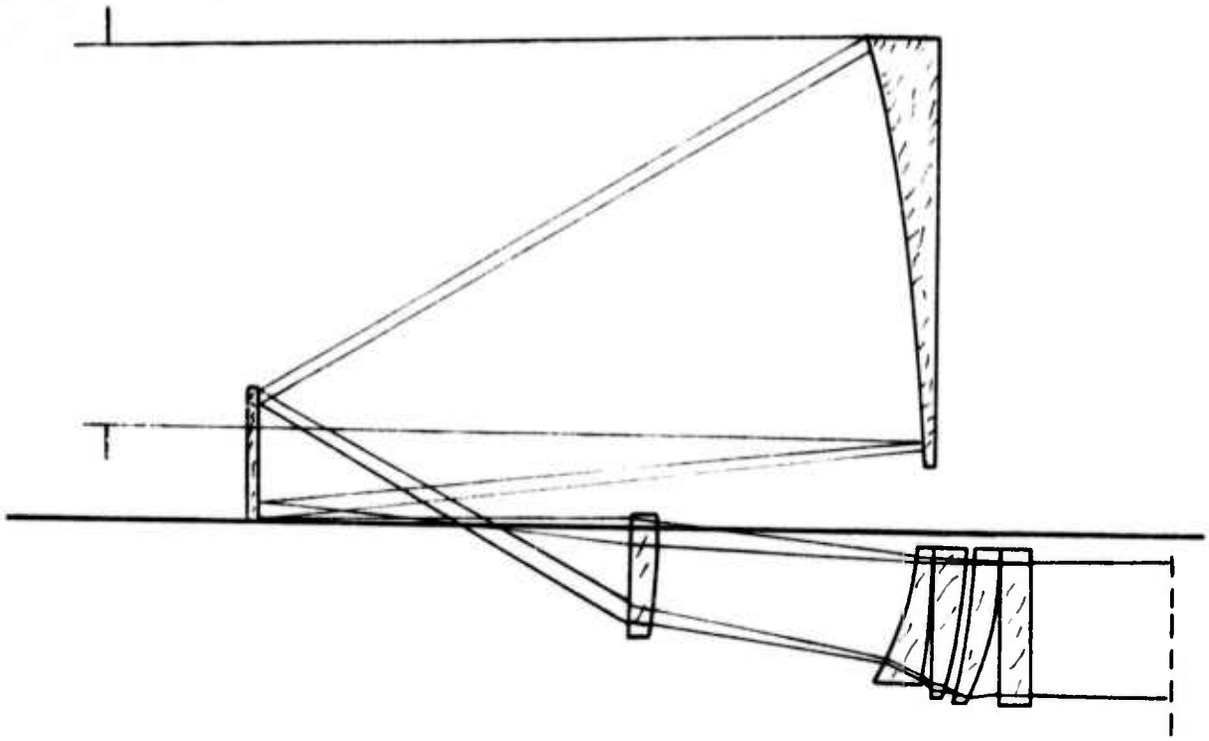

Figure 36. Inverting Off-Axis Catadioptric Afocal with Aspheric Exit Pupil

is used as the imaging lens. The system is electro-optical multiplexed utilizing Texas Instruments common modular components. However other types of multiplexing can be used, see Section IV.

The second design is a small system with three fields of view. The high resolution mode is a reflective 1/4 milliradian afocal. The wide FOV's used refractive optics to achieve one and two milliradian middle and wide field of view. As the system is configured any of the three FOV's can be used independently. The second system is electronically multiplexed to save weight, volume and power.

The third system is a mini-2 FOV Galilean system. The optical package uses two elements in the afocal to give 1/4 and one milliradian resolutions. The fields of view are changed by rotating the afocal section 180 degrees.

1. System MTF

The MTF of FLIR systems are dependent on several components. The MTF equations are dependent on several components. The MTF equations for Electronic and Electro-Optical Multiplexer are:

$$MTF_{\text{syst electronic multiplexed}} = (MTF_{\text{IR Diffraction}})(MTF_{\text{IR Geometric Blur}})(MTF_{\text{Amplifier \& Multiplexer}})$$

$$(MTF_{\text{Display}})\quad(MTF_{\text{Detector Scan}})$$

and

$$MTF_{\text{System Electro-Optical multiplexed}} = (MTF_{\text{IR Diffraction}})(MTF_{\text{IR Geometric Blur}})(MTF_{\text{Detector Scan}})$$

$$(MTF_{\text{Amplifier}})(MTF_{\text{LEDS}})(MTF_{\text{Camera Optics}})(MTF_{\text{Display}})$$

where

$$MTF_{\text{IR Diffraction}} = \left[1 - \left\{\frac{\pi}{2}\quad\frac{\lambda}{\Delta^2\ \theta_o\ D_o}\quad\frac{f}{f_o}\right\}\right]$$

λ = wavelength (microns)

$\Delta\theta_o$ = system resolution

D_o = stop aperture in cm

f/f_o = spatial frequency

Figure 37 is a plot of $MTF_{IR\ Diffraction}$ for optical systems with f-numbers of 1.5 to 3.0.

The MTF associated with the IR optics geometric blur data is given by the equation:

$$MTF = e^{-(\pi \sigma_r f)^2}$$

where

σ_r = radius of optical blue

f = spatial frequency of systems

A typical MTF plot is given in Figure 38 for this curve a σ_r of 0.0004 in was used.

The MTF of the detector scan is associated with the physical dimensions of the detector elements. The equation for the detector scan MTF is:

$$MTF = \frac{\text{Sin}\ fd}{fd}$$

where f = spatial frequency

d = detector size

A typical plot fo an 0.002- X 0.002- inch detector is shown in Figure 39.

2. Video Electronics MTF

The system video electronics has an MTF associated with it that is the normalized gain-versus-frequency characteristics of the amplifiers. Bandwidth out to 30 kHz and slightly beyond the MTF is greater than 90% at resolution spatial frequencies for electro-optical multiplexed systems.

Electronic multiplexed systems must have spatial frequency roll off in order to alleviate aliasing and noise. Appendix H is a detailed analysis of pre-sampling filters on multiplexer performance.

3. Light Emitting Diode

Light emitting diodes have an associated MTF due to the rectangular shape of the emitter. The equation for the emitter MTF is:

$$MTF\ emitter = \frac{\text{Sin}\ \pi\ fd}{\pi fd}$$

where f = spatial frequency scan direction

d = emitter dimension

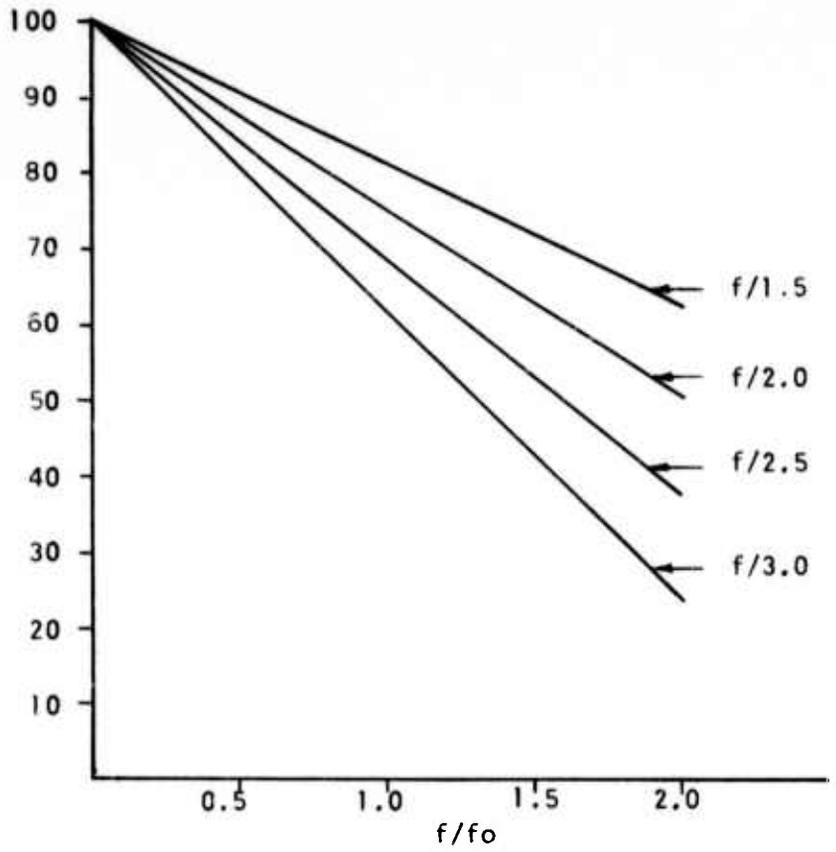

Figure 37. MTF IR Diffraction Plots

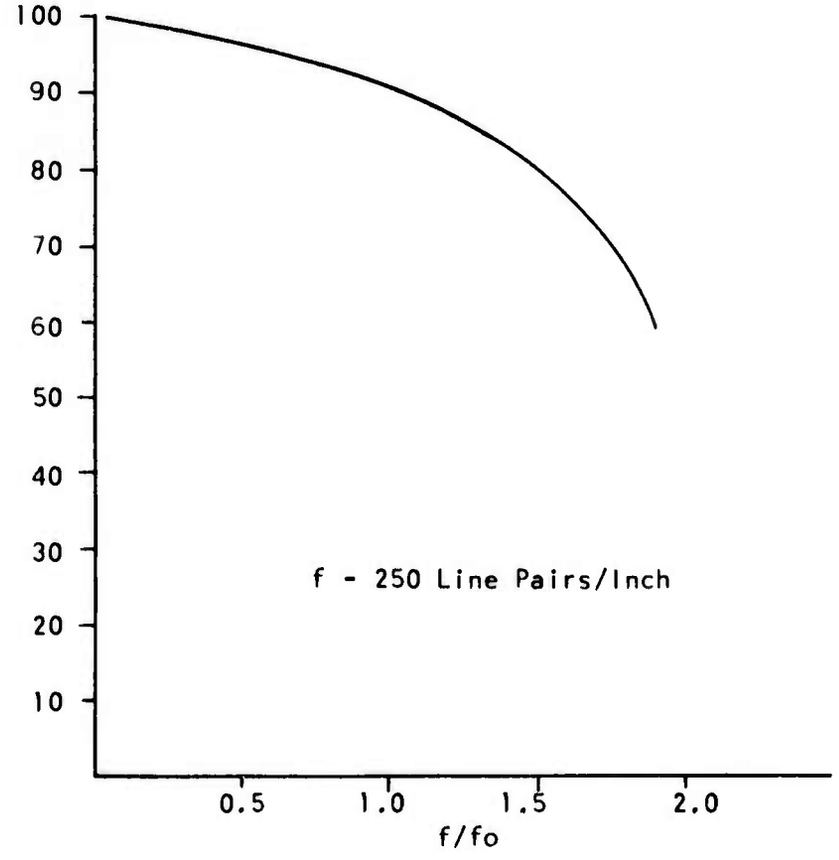

Figure 38. MTF IR Geometric Blur Radius 0.0004 Inch

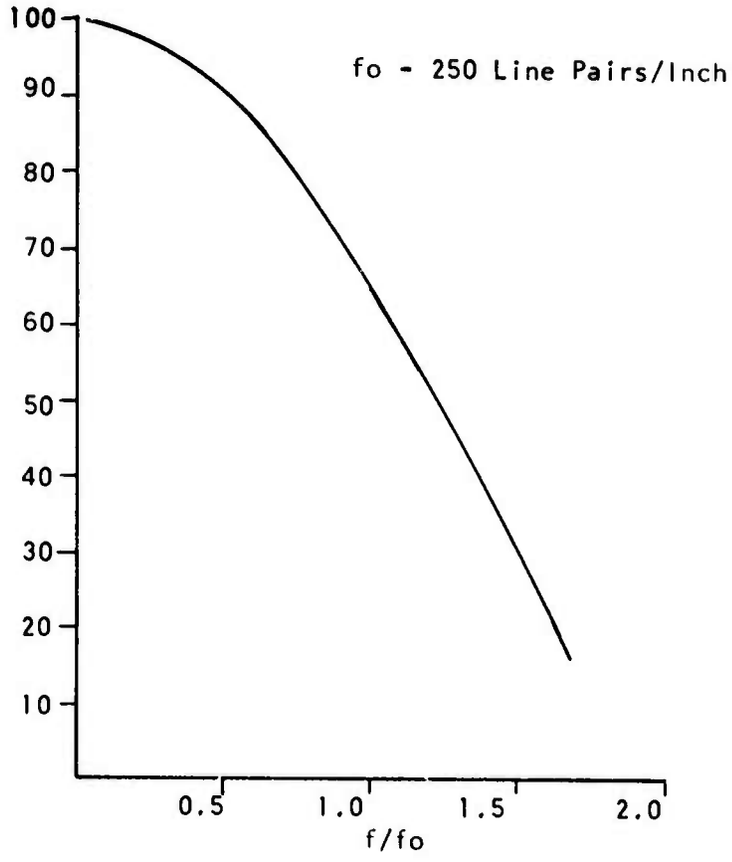

Figure 39. MTF Detector Scan for a
0.002 X 0.002-Inch Detector

Figure 40 is a plot of an 0.001- inch emitter in the horizontal scan plane.

4. Camera Optics

The equation for the MTF associated with camera optics is identical to that of the IR optics MTF. Visible optics are designed with multiple lenses and materials to minimize abberations. The diffraction and geometric visible optics MTF exceed 90% in most cases. The camera optics MTF are included in the electro-optical system equation.

5. Camera and Display

The camera electronics are designed for optimum MTF and at resolution frequencies exceeding 80% MTF. The primary element in the camera MTF is the vidicon response and varies for each system.

6. Thermal Sensitivity (NET)

An important measure of infrared system performance is noise equivalent temperature (NET). This is the required temperature difference between a blackbody radiation source and its background for the system to produce a signal of equal strength to the noise level.

$$NET = \frac{F^2}{\sigma T_o^3 \ \tau_o \tau_a \ D^*(T_o)} \sqrt{\frac{\pi}{4 t_o \ A_d}}$$

where

F = f-number of system IR optics

σ = Stefan-Boltzmann constant, watts cm^{-2} deg^{-4}

T_o = background temperature, ^oK

τ_o = IR optics transmission

τ_a = atmospheric transmission

$D^*(T_o)$ = detector detectivity of radiation from a target at background temperature, cm $Hz^{\frac{1}{2}}$ $watts^{-1}$

t_o = detector dwell time, seconds

A_d = detector area, cm^2.

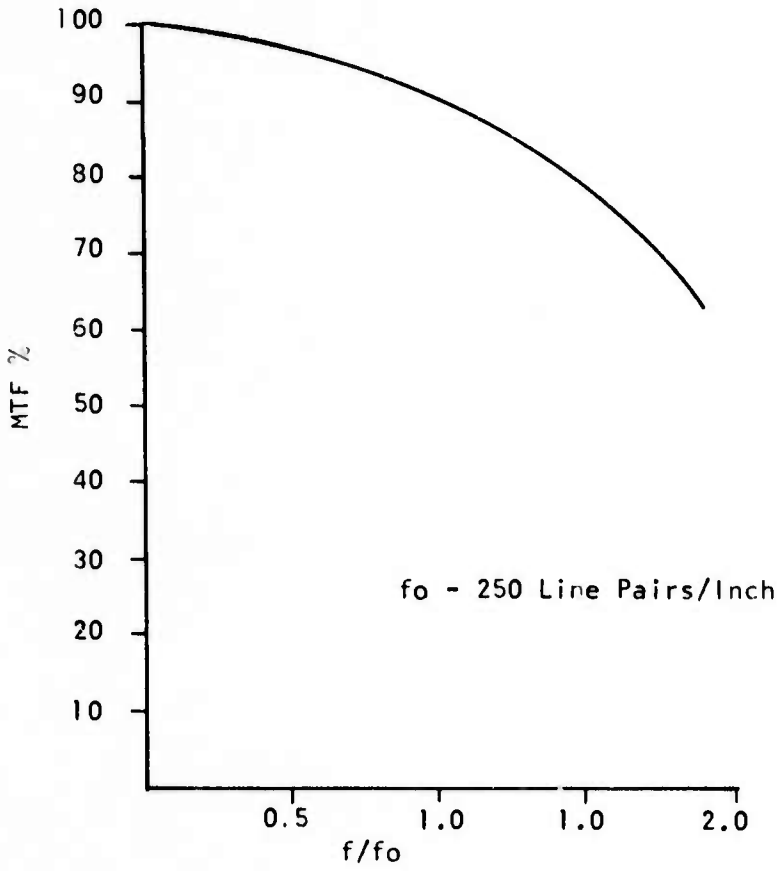

Figure 40. Emitter Scan MTF Plot for 0.001 Emitter

The tradeoffs in designing a FLIR system with optimized NET basically involve the parameters in the above equation. The f-number of the IR optics must be as small as possible to provide the desired low NET. On the other hand, to optimize detector D*, cold shielding to as small a collecting solid angle as possible is desirable. This is governed to some extent by the optics f-number, and is a tradeoff consideration. Detector area (A_d) should be large for low NETs, yet should be small for good spatial resolution ($\triangle\theta$) and minimum overall system size and weight. In general, for application in systems where long-range recognition of small targets is required, the detector area is selected as small as can be practically produced. This results in a smaller package size for the system optics. Where both aperture and overall package size limitations exist, it is important that all design parameters are optimized to provide adequate thermal sensitivity.

7. Minimum Resolvable Temperature (MRT)

The following expression for MRT is developed from SNRD equations relating MRT, NET, and MTF:

$$MRT = 0.75\ (f/fo)\ \frac{NET}{MTF_{(f)}}$$

A value of 0.6 is used when the noise bandwidth of the video electronics is used in the NET calculations.

The development of the MRT equation is included in Appendix I. In the specific calculations of system performance for the three systems, the a factor of 0.6 was used since NET was calculated using noise bandwidth of the IR video.

Another important consideration for an RPV FLIR system is the weight of the optical elements and structure. The weight of structures is covered in Section II. Therefore the following section will address the optics weight.

Weight savings can be realized by designing optical systems using reflective catadioptric techniques for the large optical elements. Weight reduction is a result of using less of the infrared materials such as Ge and TI 1173. Table V below shows the density of the materials used in FLIR optics.

Material	Density or Area
Aluminum Mirror	0.1 lb/in^3
Replicated Mirror	0.04 lb/ft^2
Ge	0.1925 lb/in^3
TI 1173	0.1687 lb/in^3

Table V. Materials and Densities

Figure 41 shows the differences in weight between one-field-of-view reflective Casegrain afocals and Galilean afocals as a function of the front element apertures.

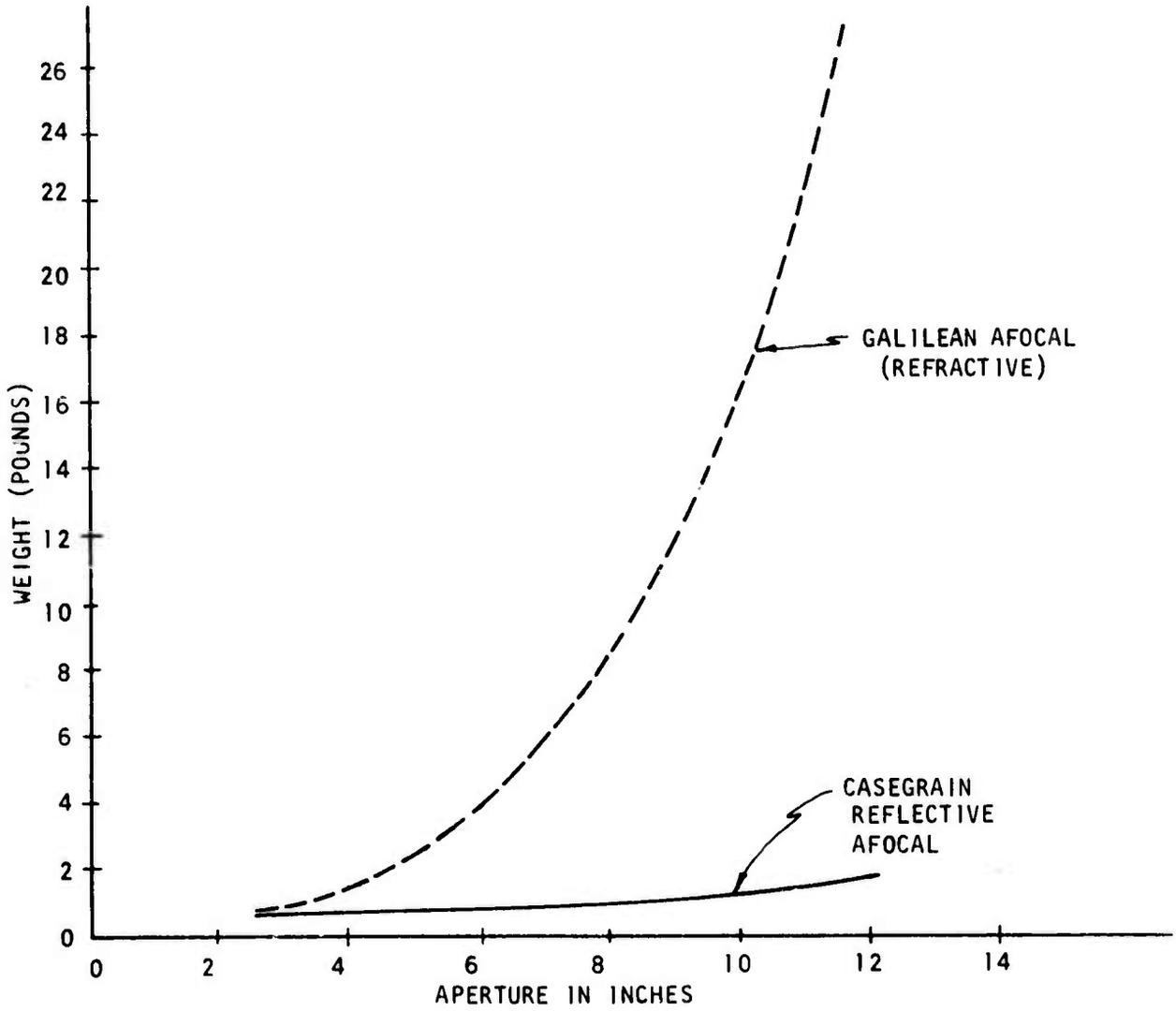

Figure 41. Weight Approximation for Galilean Afocal and Casegrain Reflective Afocal

IV. FLIR SYSTEM DESIGN

The following designs demonstrate the types of FLIR systems that can be designed using the technique discussed in Section III.

A. SYSTEM NUMBER ONE, HIGH RESOLUTION

System one, Figure 42, has two fields of view using a catadioptric afocal and Texas Instruments common modular components as building blocks for the remainder of the system. The resolutions selected for this design are 1/15 mr NFOV and 1/8 mr WFOV. A 10" stop was selected resulting in a f/3 for the 1/15 mr system and up to f/1.6 for the 1/8 mr FOV. The afocal magnification corresponds to 11:25x for the NFOV and 6X for the WFOV where:

$$\text{Afocal magnification} = \frac{\text{optical focal length}}{\text{focal length imager}}$$

The optical system afocal utilizes reflective spherical mirrors as common primary and secondary optical elements. The five compensating lenses change with each FOV. The FOV change can be accomplished with a rotating barrel or with lateral movement of the compensating lens.

The largest MTF degradation for system one is associated with the diffraction limit of the IR optics in both fields of view. The current design for the 1/15 mr system has an optical f-number of 3.0 corresponding to an $MTF_{diffraction}$ limit of 62% at resolution frequencies. The 1/8 mr or WFOV is running at an f/2.0 therefore, the diffraction MTF associated with this f/no is 75% at resolution frequencies.

The geometric MTF's of the IR optics are shown in Figure 43 for the NFOV and Figure 44 for the WFOV. At resolution frequencies the ($MTF_{IR\ Geometric}$) is 96% or greater in both fields of view. This corresponds to an IR optical MTF of 60% for the NFOV and 72% for the WFOV.

There is degradation in the elevation direction of the reflective system. A study determined that the MTF begins to degrade at the 80% off axis field point in the elevation direction.

System one is electro-optical multiplexed using common modular light emitting diodes and visible collimator optics. A camera imaging lens is required to display the LED array onto the vidicon face. The magnification of the camera imaging lens is 0.59X.

The MTF of the electro-optical multiplexer is at least 90% for the LED, and 90% for the camera lens on axis, with only a slight (10%) degradation off axis, and a camera system electronically peaked to have an MTF of 100%.

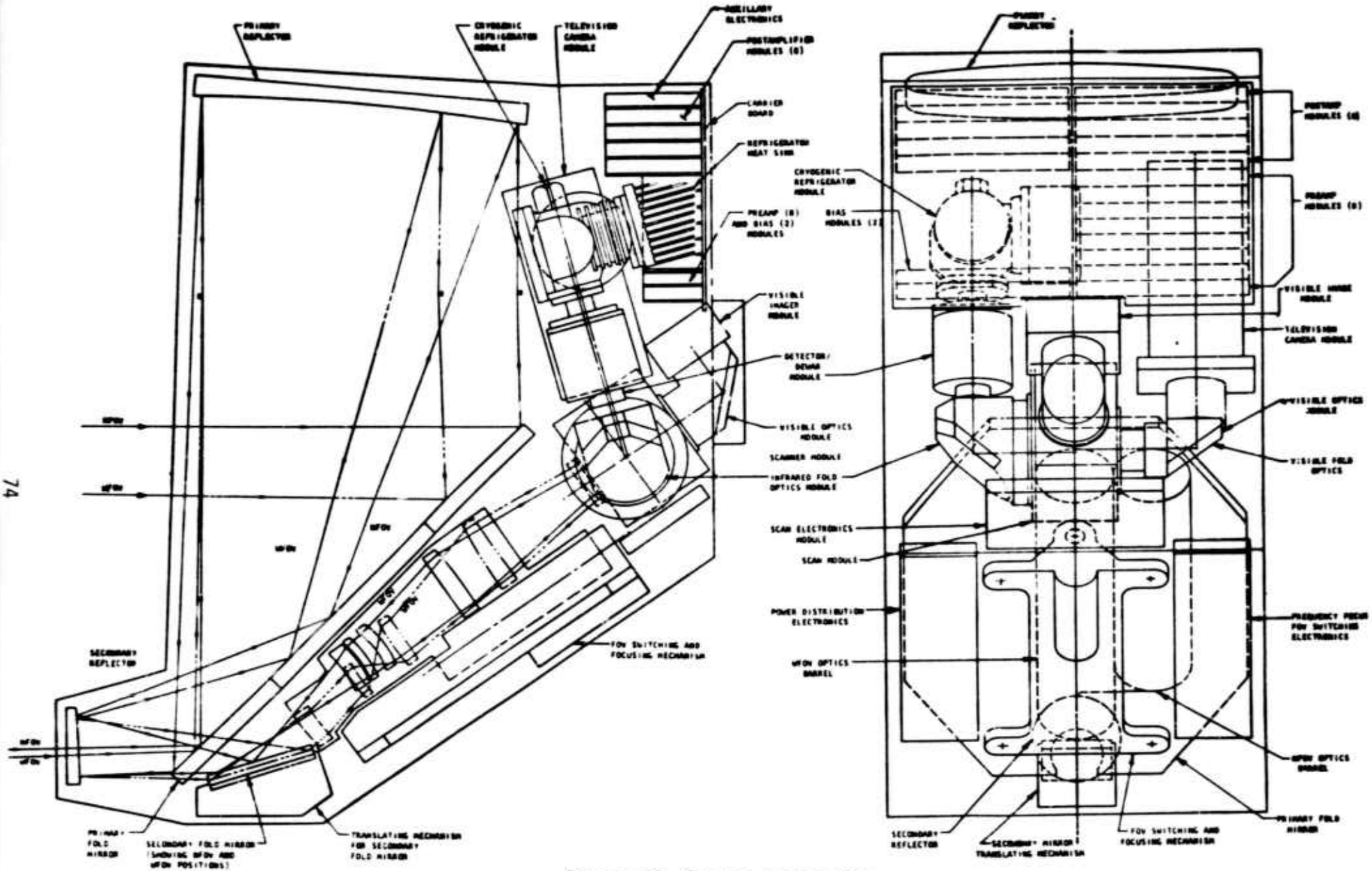

Figure 42. System Number One

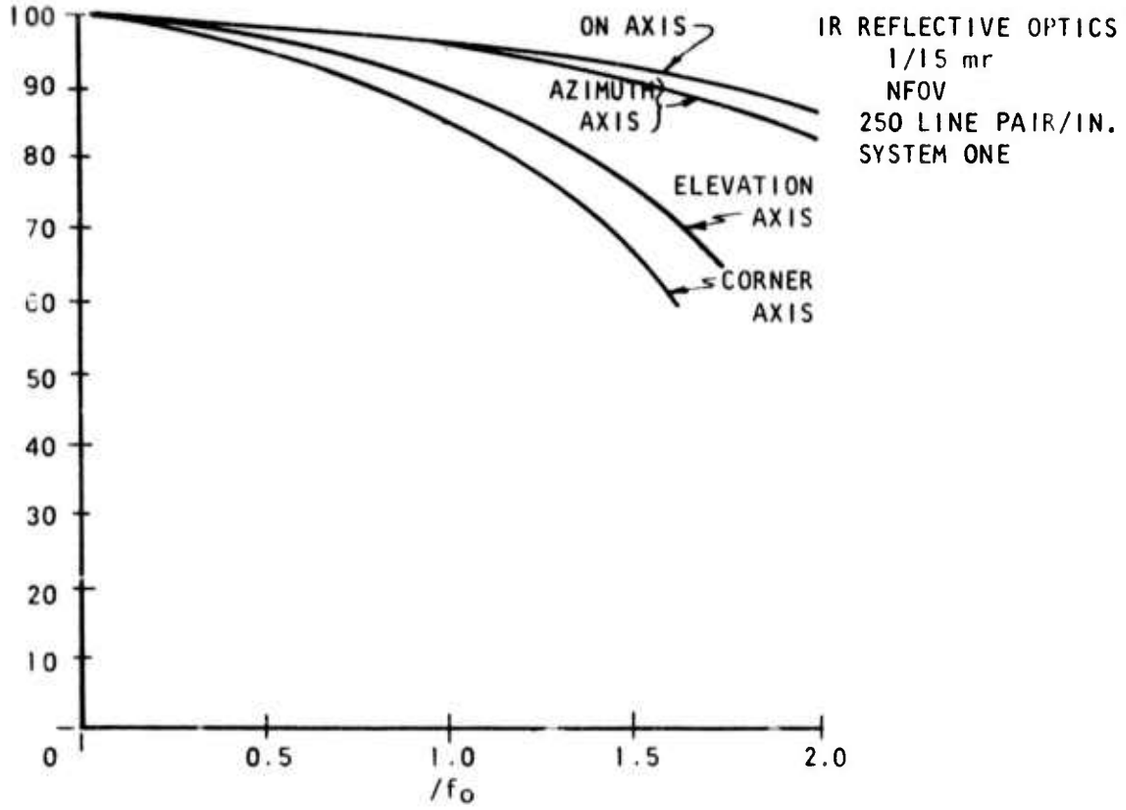

Figure 43. Geometric MTF NFOV.

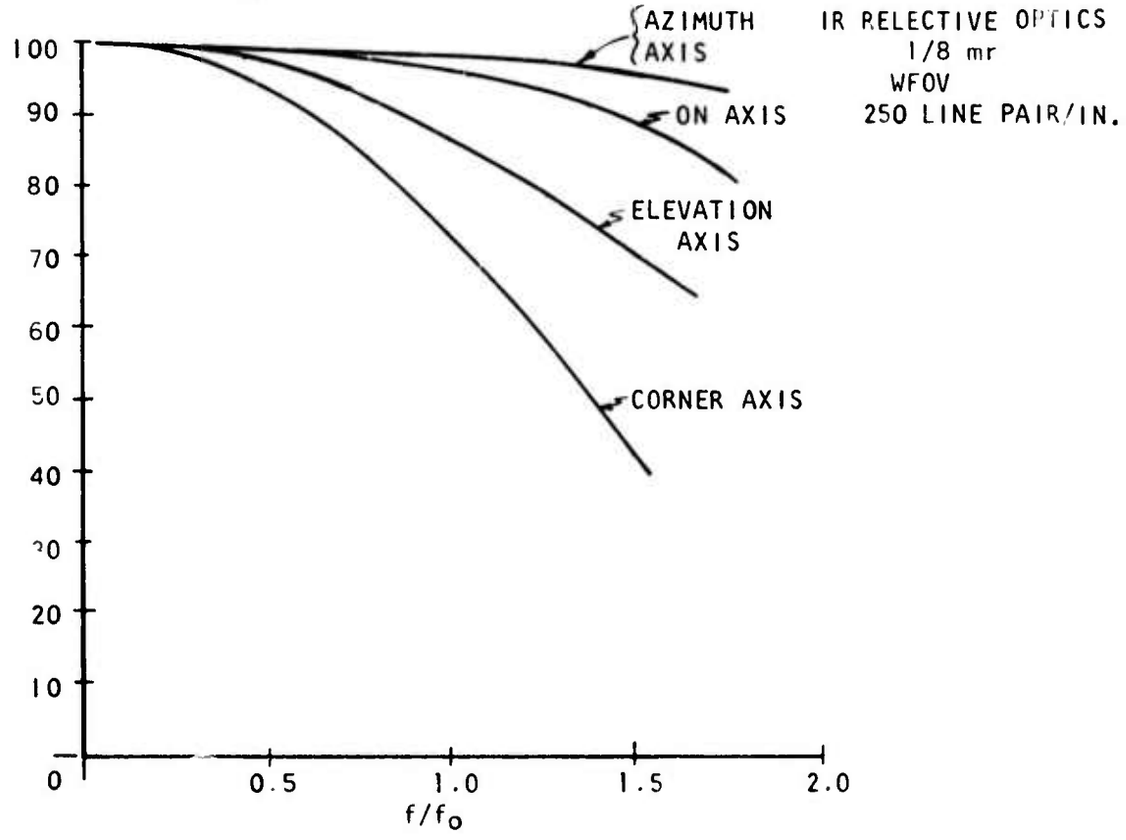

Figure 44. Geometric MTF WFOV.

The common modular video electronics have an MTF of greater than 90% at resolution frequencies. A value of 0.9 therefore is used in MTF calculations for the video electronics.

Figure 39 shows the MTF associated with the detector scan. At resolution frequencies the MTF of the detector is 64%.

The MTF equation for system number one is:

$$MTF_{System\ one} = (MTF_{IR\ Geometric})\ (MTF_{IR\ Diffraction})\ (MTF_{Detector\ Scan})\ (MTF_{Electronics})\ (MTF_{LED's})\ (MTF_{Visible\ Optics})\ (MTF_{Camera})\ (MTF_{Display})$$

Substituting

$$MTF_{NFOV} = (0.96)\ (0.62)\ (0.64)\ (0.9)\ (0.9)\ (0.9)\ (1.0)\ (0.8)$$

On Axis = 22% at the display in the WFOV

Therefore, the MTF at f/fo on the display is 22% in the NFOV and 27% in the WFOV. This difference is associated with the diffraction limit of the optics.

The NET of system number one is given by:

$$NET = \frac{f^{\#2}\ \sqrt{BWn}}{\sigma T^3\ \sqrt{A_d}\ D^*_{300}\ \gamma_o}$$

where

f = system f number

BW_n = system noise

A_d = detector area

D^*_{300} = D* detectivity at 300°C

γ_o = optical transmission

when

$f^{\#}$ = 2.0 WFOV and 3.0 NFOV

$$BW_n = \frac{\frac{\pi}{2}(\text{Azimuth IR lines})(\text{TV Frame Rate})}{\text{Scanner Duty Cycle}}$$

$$= \frac{\frac{\pi}{2}(450 \text{ lines})(30 \text{ frames/sec})}{0.7}$$

$$= 30.3 \text{ kHz}$$

$$A_d = [(0.002)(2.54)]^2 = 25.8 \times 10^{-6} \text{ cm}^2$$

$$\tau_o = 0.452$$

$$D^*_{300} = 1.25\, D^*_{500} = (1.25)(6 \times 10^9) = 7.5 \times 10^9$$

Substituting

$$NET = \frac{(9)(174)(6.53 \times 10^3)}{5.08 \times 10^{-3})(7.5 \times 10^9)(0.452)}$$

$$= 0.59^oC \text{ in the NFOV}$$

The optics transmission value is derived from the following optical elements:

8 Refractive elements

2 Spherical mirrors

1 Scan mirror

4 Folding mirrors

$$NET = \frac{(4)(174)(6.53) \times 10^3)}{(5.08 \times 10^{-3})(7.5 \times 10^9)(0.452)}$$

$$= 0.26^oC \text{ in the WFOV.}$$

The NET is 0.59^o in the NFOV and 0.26^oC in the WFOV. The difference due primarily to the optical f number of the 2 systems .

MRT is calculated from

$$MRT = K \frac{NET}{MTF} \frac{f}{fo}$$

$$= (0.6) \frac{(0.59)}{(0.22)} (1)$$

$$= 1.61^oC \text{ in the NFOV for 1/15 system}$$

$$MRT = 0.58^oC \text{ in the WFOV for 1/8 mr system}$$

The overall performance of system one will be 1.61°C MRT in the NFOV and 0.58°C in the WFOV.

Table VI is a comparison between a classical Galilean Afocal and the Reflective Catadioptic Afocal described above. In the reflective optical design, there are 10 optical elements and four mirrors in both the wide and narrow fields of view. The Galilean has only 11 optical elements in the WFOV and 10 in the NFOV. This difference results in transmission differences of 0.452 in the reflective system compared to 0.513 and 0.534 in the refractive optical system.

The overall system performance of the two systems is almost the same. At f/fo = 1.0 MTF in the reflective system is 0.58°C in the wide field and 1.61°C in the narrow field of view. The high MRT in the NFOV is primarily due to the slow f-number of the optical systems. The MTF's of the reflective system do exceed those of the Galilean afocal system as shown in the table.

The highest advantage of the reflective optic system over the refractive system is optical weight. The total weight of all the optical elements including the folding mirror is estimated to be 1.91 lbs for the reflective system and 16.8 lbs for the Galilean optics system. These weights include structure to hold the two sets of optics.

An intermediate system was designed with reflective optics incorporating several changes from system one mentioned above. The difference between the system one and the intermediate system are shown in Table VII. The resolution of system one in the NFOV is 1/15 mr and the intermediate reflective system NFOV resolution is 1/16 mr. The 10-inch aperture was kept constant in both designs. The biggest change was the detector size. The detector size was 0.0015 inches for the intermediate system and 0.002 inches for system one. This detector size change allowed the effective focal length of the intermediate optical system to be 24 inches compared to 30 inches for system one, see Figure 45.

The NET of the intermediate system is calculated form the equation

$$NET = \frac{f^{\#2}\sqrt{BWn}}{\sigma T^3 \sqrt{A_d}\, D^*_{300}\, \gamma_o}$$

as mentioned earlier.

where

$f^{\#}$ = 2.0 WFOV and 2.4 NFOV

$BWn = \frac{1}{2}\frac{(450)(30)}{.7} = 30.3$ kHz

$A_d = (0.0015)(2.54)^2 = 14.5 \times 10^{-6}$ cm^2

$\gamma_o = 0.51$

$D^*_{300} = 7.5 \times 10^9$

	REFLECTIVE		GALILEAN	
	WFOV	NFOV	WFOV	NFOV
τ_o	.452	.452	.513	.534
Res θ	@.125 mr	0.0667 mr	0.125 mr	0.0667 mr
Number of Optical Elements	1.6 to 3.0	3.0	1.6 to 3.0	3.0
f#	1.6 to 3.0	3.0	1.2 to 2.4	2.4
Weight of Optical Elements	1.644 lbs	1.644 lbs	16.669 lbs	16.669 lbs
Geometric MTF				
On Axis	96	96	94	81
El Axis	86	89	96	80
Az Axis	98	96	72	68
Corner Axis	73	85	60	54
NET_{Avg}	.26	.59	.233°C	.503
$MRT_{f/fo}$	.58°C	1.61°C	.532°C	1.61°C
FOV $\frac{el}{az}$	$\frac{2.3}{3.06}$	$\frac{1.22}{1.63}$	$\frac{2.3}{3.06}$	$\frac{1.22}{1.63}$
Aperture	7.5"	10"	7.5"	10"

TABLE VI. COMPARISON OF REFLECTIVE AND GALILEAN OPTICAL SYSTEMS

TABLE VII. SYSTEM ONE AND INTERMEDIATE SYSTEM DIFFERENCES

	REFLECTIVE #1 SYSTEM		INTERMEDIATE #1 SYSTEM	
	WFOV	NFOV	WFOV	NFOV
τ	0.452	0.452	0.51	0.51
Resolution θ	0.125 mr	0.0667 mr	0.125 mr	0.0625 mr
Number of Optical Elements	14	14	12	12
f-Number	1.6 to 3.0	3.0	1.2 to 2.4	2 - 4
Weight of Optical Elements	1.644 lbs	1.644 lbs	1.59 lbs	1.59 lbs
Geometric MTF On Axis	96	96	99	99
El Axis	86	89	95	96
Az Axis	98	96	98	96
Corner Axis	73	85	93	96
NET	0.26°C	0.59°C	0.31°C	0.45°C
$MRT_{f/fo = 1}$	0.58°C	1.61°C	0.69°C	1.08°C
FOV $\frac{el}{az}$	$\frac{2.3}{3.06}$	$\frac{1.22}{1.63}$	$\frac{2.57}{3.43}$	$\frac{1.29}{1.71}$
Aperture	7.5"	10"	6"	10"
Number of Afocal Compensating Lenses	5	5	3	3
Reflective mirrors	spherical	spherical	aspheric parabola	aspheric parabola

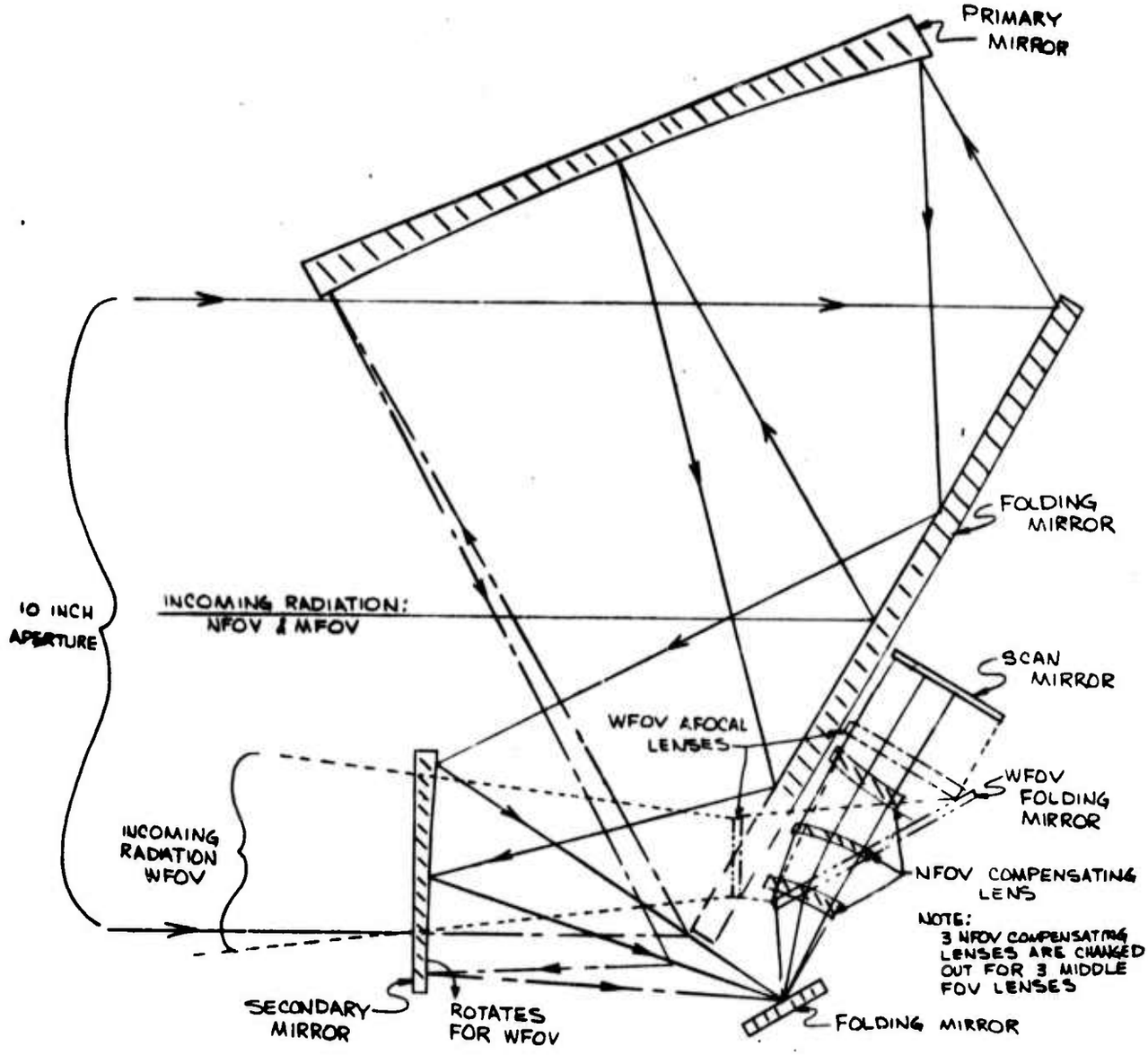

Figure 45. Intermediate System Number 1.

Substituting

$$NET_{NFOV} = \frac{(5.76)\ (174)\ (6.53 \times 10^{3})}{(3.81 \times 10^{-3})\ (7.5 \times 10^{9})\ (5.1)} = 0.45^{o}C$$

$$NET_{WFOV} = \frac{(4)\ (174)\ (6.53 \times 10^{3})}{(3.81 \times 10^{-3})\ (7.5 \times 10^{9})\ (.51)} = 0.31^{o}C$$

The sensitivity is 0.45°C in the NFOV and 0.31°C in the WFOV for the intermediate system. This corresponds to 0.59°C NET in the NFOV and 0.26° in the WFOV for system one.

MRT's are calculated from

$$MRT = (K)\frac{(NET)}{(MTF)}\ \frac{f}{f_o}$$

$$MRT_{NFOV} = (0.6)\ \frac{(.45)}{(.25)} = 1.08^{o}C \text{ in the NFOV}$$

$$MRT_{WFOV} = (0.6)\frac{(.31)}{(.27)} = 0.69^{o}C \text{ in the WFOV}$$

The overall performance of the intermediate system exceeds that of system one mentioned above. The NFOV sensitivity (MRT) goes from 1.61°C in system one to 1.08°C in the intermediate system. The WFOV sensitivity is 0.69° C in the intermediate system and 0.58°C in system one. The f/no can be decreased easily in all systems for more system sensitivity in the WFOV.

1. System One Mechanical Design

System one is a reflective two-field-of-view system utilizing lightweight replicated optics for the primary, secondary, and folding mirrors in the design. The afocal includes two common spherical mirrors for each FOV and five individual refractive lenses. The refractive optics are switched between the NFOV and WFOV in the zoom assembly as shown in Figure 42.

The remainder of system one is made up of Texas Instruments common modular components. These common modules, include the scan module, IR imager, Dewar/detector-cooler, video processing module, LED, and visible collimator. The following subsections describe each of the common modules used in system one design.

The remaining receiver components of system one include the zoom switch mechanism, focus control mechanism and mechanical assembly. The fields of view are changed by rotating the zoom switch barrel about a common axis. The common pivot is threaded in order to focus the barrel, for either manual focus, frequency focus or athermalization techniques as discussed in Sections I and V. The zoom technique lends itself to a single focus mechanism utilizing any of the three possibilities mentioned above.

An external power supply will contain the video regulators and TV electronics required for the FLIR operation.

The system weight and power is shown in Table VIII. The individual components are broken out to indicate distribution.

The main structure is an integrated optical bench which supports and aligns the refractive optics, folding mirrors, FOV switching mechanism, scanner module, detector/dewar module, cryogenic refrigerator module, visible imager module, visible optics, and television camera module. This bench is a composite aluminum and fiberglass structure designed for optimum strength and rigidity while adding minimum weight to the assembly. Electronic modules are enclosed in shielded containers and are attached through brackets to the optical bench.

System one is large but by utilizing reflective optics the overall weight of the system can be minimized. An estimate of 20 pounds of optics and structure can be eliminated by using reflective optics over a comparable Galilean afocal.

Many components can be built of plastics, see Section II. Housings for electronics, optics barrels, and brackets could be made of plastic materials.

The overall performance as described is not ideal, but by increasing the aperture of the optics better system performance could be realized.

Generally the approach taken for system one established the feasibility of large reflective optics, and that good MTF can be realized with such optics. The current design indicates a lack of thermal sensitivity; however, with different size apertures, FOV and transmission, higher performance can be realized.

2. Scan Module

The diagram of the scan technique (Figure 46) shows the scan module function. One side of the scan mirror directs incoming infrared energy through the IR imaging lens onto the detector array. The opposite side of the same mirror simultaneously directs visible light output from the LED array through the visible collimating lens for viewing by a TV camera.

The scan module consists of the scan mechanism as shown in Figure 47. Figure 48 shows the scanner assembled in its housing.

FUNCTION	WEIGHT (LBS)	POWER (WATTS)
AFOCAL OPTICS	1.91	-
ZOOM MECHANISM & STRUCTURE	3.5	-
SCANNER	1.3	3.0
SCANNER PWB	0.31	INCLUDED IN SCANNER
CAMERA	2.0	24.0
CAMERA LENS	2.7	-
DETECTOR/DEWAR	1.0	-
VISIBLE COLLIMATING LENS	1.1	-
EMITTER	0.4	14.0
IR IMAGER	1.2	-
PREAMP PWB (8)	1.36	3.9
POSTAMP PWB (8)	2.48	7.2
DETECTOR BIAS REGULATOR (2)	0.14	4.5
AUXILIARY CONTROL PWB	0.31	3.3
MISCELLANEOUS PWB'S (6) & WIRING	1.5	20.0
POWER SUPPLY (EXTERNAL)	28.0	100.0
COOLER	6.0	40.0
STRUCTURE	8.0	-
TOTAL	63.21	219.9

TABLE VIII. SYSTEM ONE WEIGHT AND POWER REQUIREMENTS

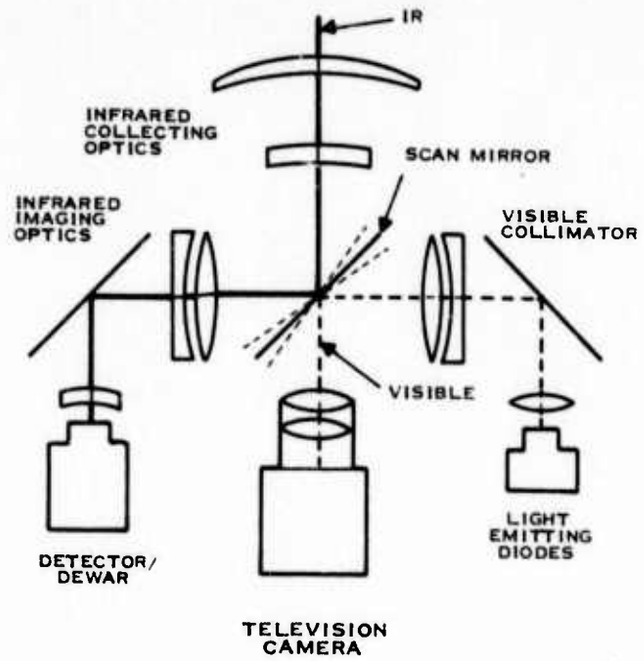

Figure 46. Scanning Diagram

The scan mechanism consists of a double-sided flat scan mirror, an interlace gimbal, and associated drive circuitry. A flat mirror is mounted in the gimbal on the scan axis. Flex pivots are used in this application because they are compatible with the oscillatory motion of the gimbal and the scan mirror. They require no lubrication and have extremely low friction within the rotational limits of the mirror.

Use of this type scan mechanism with the electro-optical multiplexer eliminates scan-to-scan target displacement. There is no chance of mirror misalignment, and precision mechanical synchronization of the moving scan mirror mass is not required. A point in the image plane of the LED array will not change with respect to the same point in the IR image plane. Since there is only one mirror, each point in the IR image is simultaneously regenerated in the LED image plane.

Horizontal scanning is achieved by pivoting the scan mirror about the scan axis located in the gimbal. This is accomplished by moving the scan mirror and mirror frame which are coupled directly to the torque motors on both ends of the scan axis.

Figure 47. Scanner Mechanism

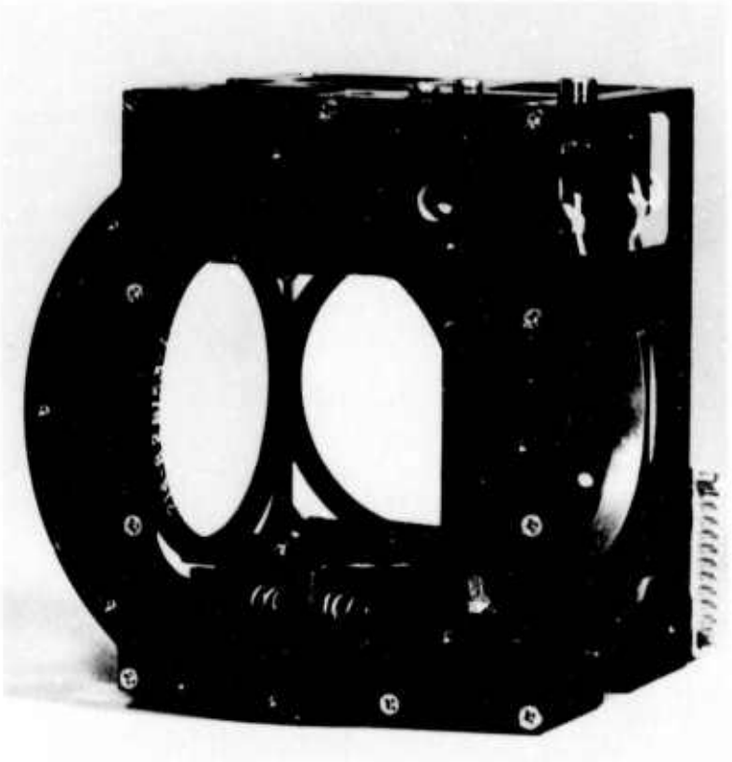

Figure 48. Scanner Module

An extension of the scan mirror frame contacts the return springs at each end of the active scan. The return springs act as energy-conserving elements for the scan axis, storing kinetic energy of motion in one direction and restoring that energy to the scan axis as motion in the opposite direction.

During operation, the main scan mirror oscillation occurs about the scan axis, and the other oscillation occurs about the interlace axis at the end of each scan to effect a 2:1 interlace. Two solenoids attached rigidly to the sensor frame drive the gimbal about the interlace axis. The solenoid plungers are mounted integrally with the gimbal. The position of two adjustable mechanical stops located next to the solenoids determines the total angular movement of the gimbal about the interlace axis.

By tuning the system to oscillate at the desired frame rate, scan power can be reduced to the amount needed to overcome the losses in the return springs and the flex pivots, requiring minimum power for the scan torque motor.

A block diagram of the scan drive and control system is given in Figure 49. A magnetorestive transducer provides a dc voltage level proportional to the scan mirror position. The scan drive uses this signal in a closed-loop servo system to provide a linear scan that can be synchronized with an external signal.

The interlace motion is sensed with a magnetic pickup device which is identical to the one used for scan position detection. This provides contactless position sensing of a small metal projection on the gimbal frame. The device differentially compares the magnetic field distribution over the sensitive face of the pickup. An input voltage is required, and, when the metal piece is displaced with respect to the centerline, the symmetry of the field distribution will be altered, resulting in a positive or negative output. The interlace circuitry develops a waveform which supplies proper accelerating and decelerating signals to a set of solenoids. Two solenoids are used, one for each interlace position. Part of the scan drive position feedback is used in the interlace signal generation to energize the interlace solenoids at the end of each scan.

A summary of the scan module characteristics is given in Table IX.

3. Infrared Imager Module

The infrared imager module (IR imager) mounts to the scan module and focuses the scanned infrared energy collected by the afocal lenses onto the detector array. The IR imager consists of three lenses, two germanium and one TI 1173 Glass, and a folding mirror providing an effective focal length of 2.67 inches.

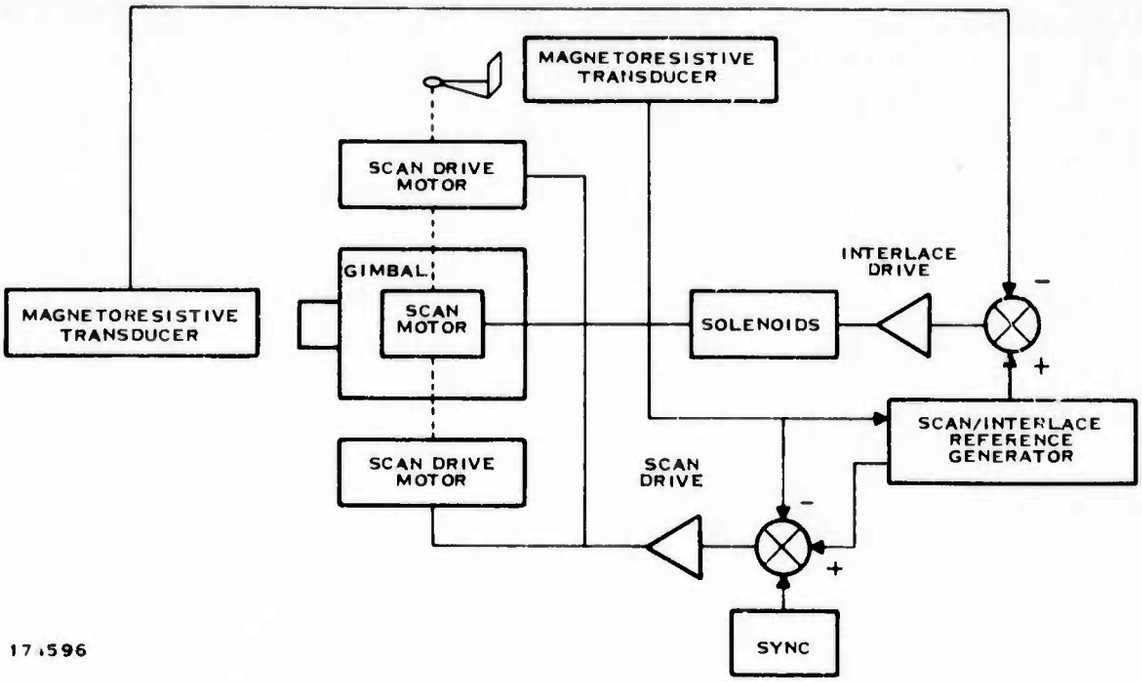

Figure 49. Scan Drive and Control System Block Diagram

Antireflection coatings of MLAR-306 and MLAR-204 on the germanium and TI 1173 Glass lenses reduce narcissus effects and Fresnel losses, and improve transmission over the desired spectral region.

The IR imager is shown in Figures 50 and 51. The imager graduations seen in Figure 51 allow the imager to be mounted to the scan module at any desired angle consistent with emitter and detector orientation.

TABLE IX. SCAN MODULE CHARACTERISTICS

Electrical power requirements	7.5 watts
Weight	1.45 pounds
Optical characteristics	
IR aperture	1.80 inches high by 3.04 inches wide
Visible aperture	1.50 inches high by 1.80 inches wide
Coating peak transmission	8- to 12.5 um IR side
Mirror flatness	One fringe per 2-inch-diameter aperture
Mirror surface finish	80 - 50
Interlace activation	Each Scan
Scan rate	120 fields/second, 60 frames/second
Usable duty cycle	65 percent

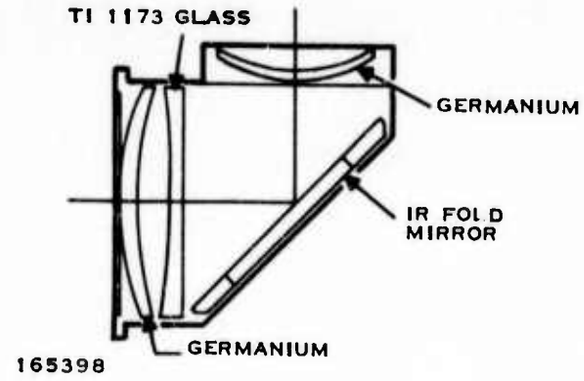

Figure 50. Imager Module Schematic

4. Detector/Refrigerator Modules

The detector/refrigerator package is composed of two independent modules: the Dewar/detector and the cryogenic refrigerator. The design of these modules allows assembly and disassembly for maintenance without disturbing either the vacuum in the Dewar, which contains the detector, or the gas used in the refrigerator.

The detector module is optimized for low heat loss and long vacuum life. It slip-fits over the cooler coldfinger with a small gap between the respective coldfingers of the cooler and the detector-vacuum module. This fit allows a positive thermal and mechanical junction to be formed at the cold end of the coldfinger. The cooler has enough capacity to cool the detector-vacuum module and to cryopump the interspace formed between the two respective coldfingers. A vacuum seal is formed at the Dewar base and cooler flange. The primary advantage of this approach is maintainability. As independent modules, the Dewar/detector and cooler can be separated and reassembled without helium or vacuum loss and the time required to replace a refrigerator is reduced.

a. Dewar/Detector Module

The infrared detectors are factory-mounted in a self-contained vacuum assembly called a Dewar. This unit (Figure 52) contains the HgCdTe detector array and an interconnecting lead pattern to feedthrough pins which are used for enternal connection to the video preamplifiers. Included in the Dewar module is an internal cold shield and the detector bias resistors.

The Dewar/detector is an independent module that is adaptable to various types of refrigerators. The Dewar contains 180 detector elements, allowing this module to meed the requirements of high-performance systems; yet it is compact enough to fit the envelopes of the miniature units. A grounding scheme and a connector pattern were established to allow the user the freedom to use any number of detectors up to a limit of 180 elements.

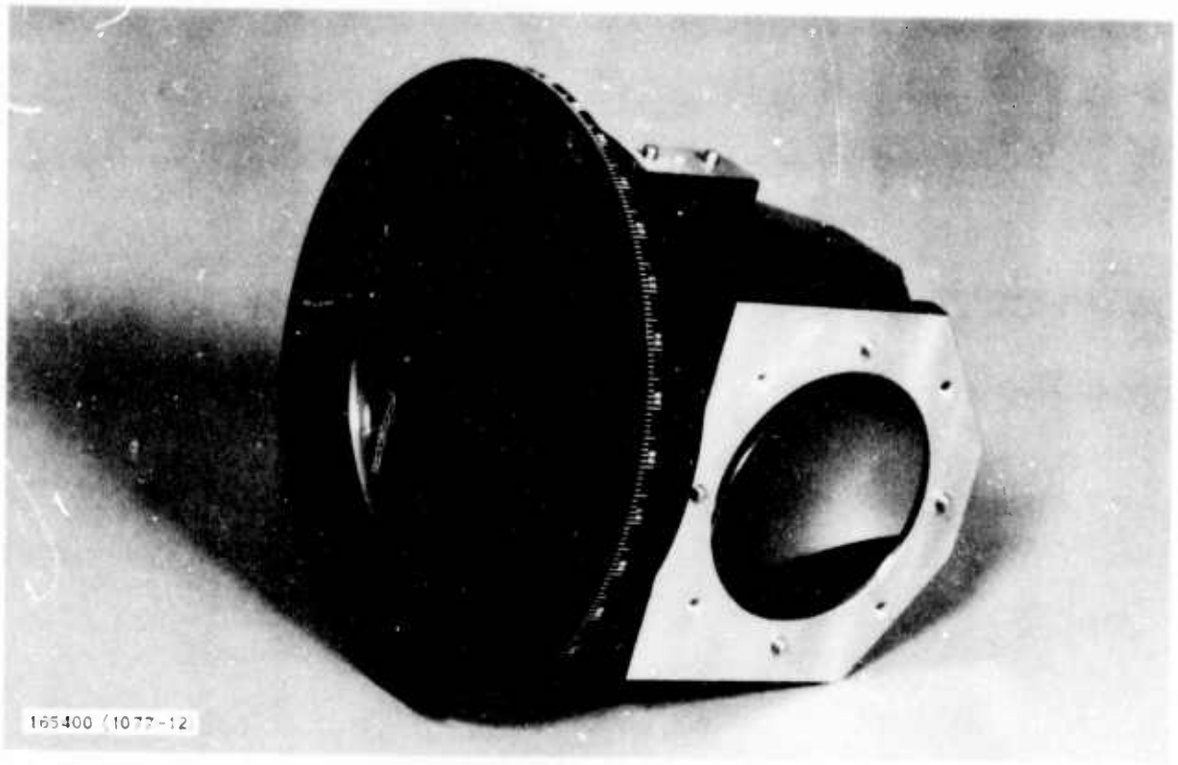

Figure 51. Imager Module

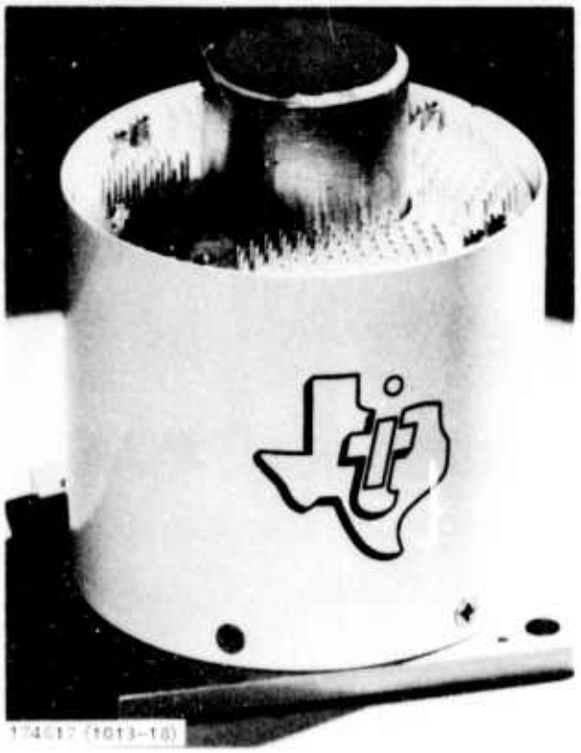

Figure 52. Detector/Dewar Module

In the past, the most frequent detector-module failure mode was the loss of the vacuum insulation required for cryogenic cooling. Several techniques have been used in the past, including VacIon pumps and CO_2 purging, but none have proved as effective as getter pumps.

Standard module vacuum maintenance has been simplified by using recently developed getter elements that exhibit high pumping speeds at room temperature (unpowered). The only service required is periodic reactivation of the getter surfaces. Reactivation is required at approximately 1-year intervals. The reactivation sequence lasts 15 minutes, and requires an automatic firing box to be attached to the external getter leads.

Two diodes are installed within the Dewar to permit measuring the temperature achieved at the detector. Since the forward voltage across a diode varies with temperature, a simple voltage measurement and a calibration chart yield the temperature.

TABLE X. DETECTOR CHARACTERISTICS

Detector material	HgCdTe
Detector size	0.002 by 0.002 inch on 0.004-inch centers
Cutoff wavelength	7.6 to 11.75 um
Primary operating temperature	$77^{o}K$
Number of elements	180
Detector FOV	75 degree effective (Restricted by internal cold shield)
Peak detectivity	D 2.4×10^{10} cm $Hz^{\frac{1}{2}} W^{-1}$ (90 percent of elements)
Peak responsivity	R 2.5×10^{4} V/W (90 percent of elements)

The detector array is fabricated from a single piece of HgCdTe material, using the latest monolithic fabrication techniques. These techniques permit a linear array to be manufactured to precise geometrical uniformity. This geometric uniformity of elements within the array eliminates detecting area variations that affect instantaneous FOV. Uniformity also presents a low cross-sectional area to adjacent detectors, resulting in very low optical and electrical crosstalk. Detector uniformity from channel to channel is ensured by single-piece construction.

b. Cryogenic Refrigerator Module

The refrigerator module (Figure 53) is a Stirling-cycle unit designed to cool HgCdTe detectors to 77 ^{o}K. Stirling-cycle units operating around $77^{o}K$ require very little power, less than 50 watts. (See Table XI for cooler parameters). Bearing loads and wear on sealing surfaces are minimized, enhancing reliability and reducing heat dissipation into the FLIR.

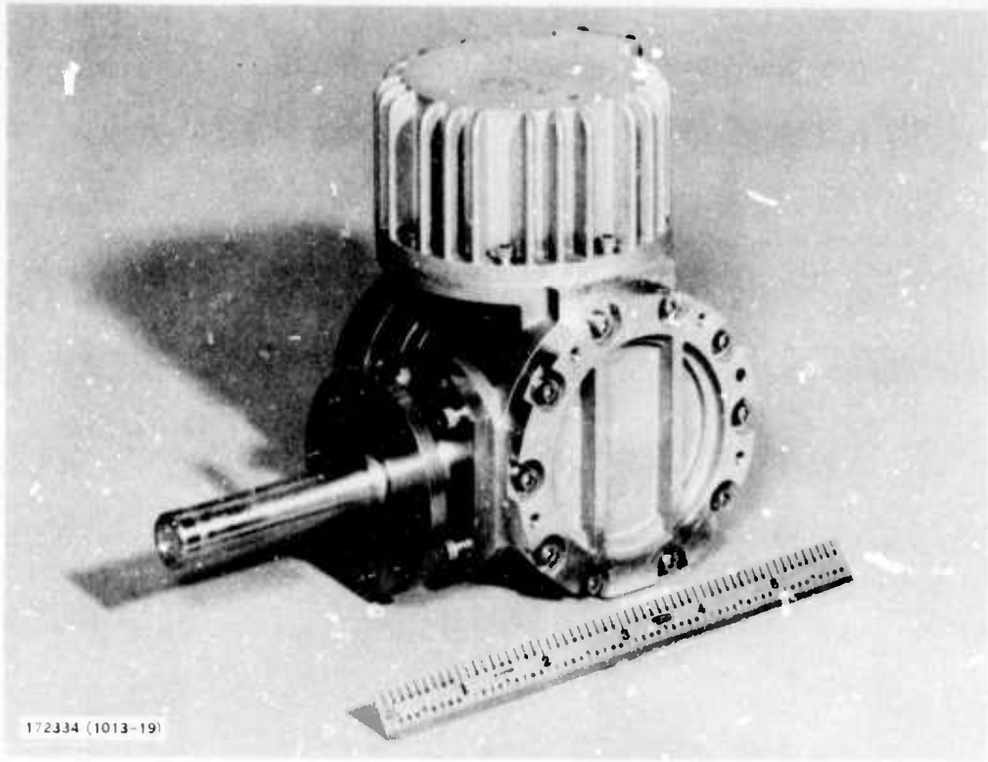

Figure 53. Modular Stirling-Cycle Cooler

TABLE XI. CRYOGENIC COOLER PARAMETERS

Cooldown time	within 15 minutes to $77^{o}K$
Input power	50 VA, 115 Vac, 400 Hz, 1 phase
Weight	4 pounds
MTBF	1,000 hours minimum

Protective devices for the cooler are incorporated in the power supply design to prevent inputs of improper phase relation from the ac power.

The proposed cooler/Dewar combination is capable of reaching temperature stability within 20 minutes of turn-on when operating in a $+65^{o}C$ ambient temperature environment. The real interest lies in the time required for the cooler/detector package to provide an adequate signal to produce usable video. Present systems require between 3 and 8 minutes. HgCdTe detectors have a

very wide temperature operating range and, although the best results are achieved at approximately 77°K, usable operation is available to the system after 100°K is reached in the cooldown. This feature allows the system to operate several minutes before reaching the optimum operating temperature.

5. Electronic Video-Processing Modules

a. Function

The function of the video electronics (Figure 54) is to amplify the extremely low-level signals present at the detector to a useful level and to perform signal processing such as gain and level control to enable the reconstruction of the infrared scene with a scanned array of light-emitting diodes. Figure 55 is a block diagram which shows the typical functions performed as part of this processing. Processing is repeated on each individual detector channel.

The video electronics are divided into several functional groups: low-noise stages which include the preamplifiers, gain/control stages which include the postamplifiers, emitter normalization modules, and auxiliary electronics modules. It is advantageous to physically and electrically separate these functions to eliminate electrical crosstalk and other electrical grounding problems. Each preamplifier printed circuit board contains 20 parallel-channel preamplifier stages. The postamplifier printed circuit boards also contain 20 parallel-channel stages. This conserves packaging space and mimizes interconnecting wires by supplying power and control commands to groups of 20 channels (one printed circuit board.)

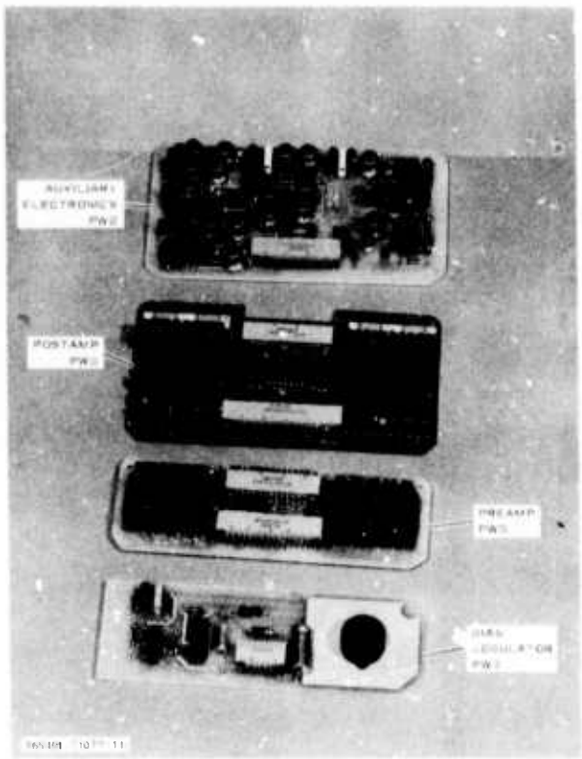

Figure 54 Typical Video Electronics Modules

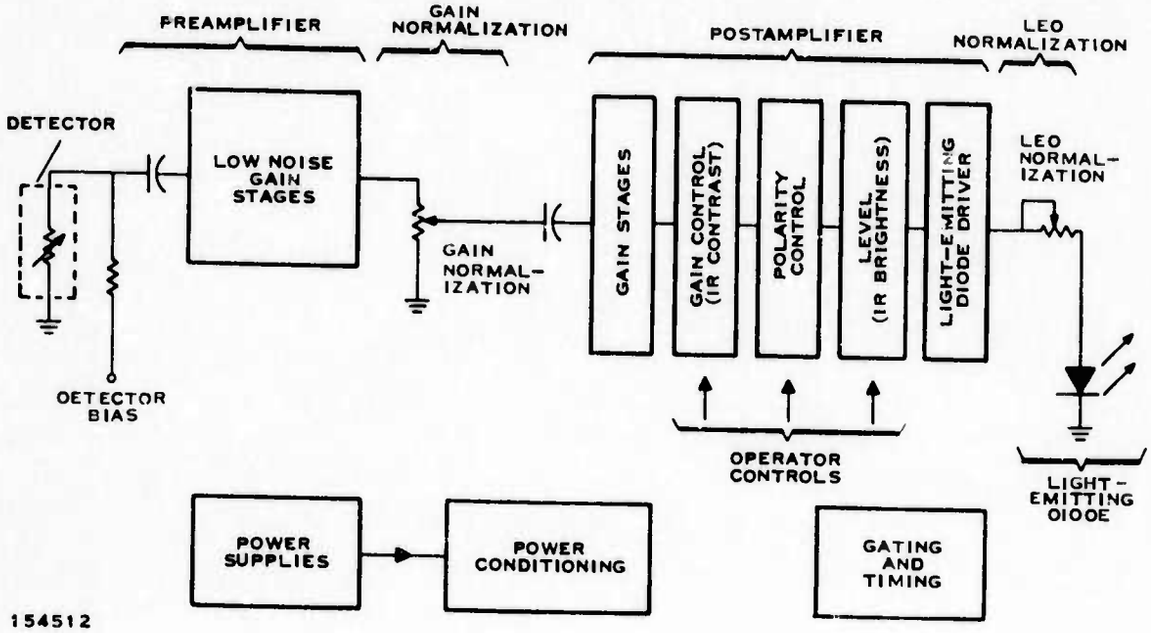

Figure 55. Typical Video Chain Functions

The preamplifier and postamplifier modules are based on monolithic integrated circuits (ICs) developed and manufactured specifically for FLIR applications by Texas Instruments. The ICs are highly reliable ceramic dual in-line packages. Each IC contains five channels of its particular function. The preamplifier uses an SN25900 IC, the characteristics of which are listed in Table XII. The postamplifier module is made up of two postamplifier ICs (SN25903) and an LED driver IC (SN25906). These integrated circuits are characterized in Tables XIII and XIV.

TABLE XII. PREAMPLIFIER CHARACTERISTICS (S/N 25900)

Power	11 mA at 4V total for five channels
Input impedance	5,000 ohms
Output impedance	500 ohms
Gain	75 volts/volt
Gain tracking	$\pm$ 0.5 dB
Noise	1.5 nV/Hz$^{\frac{1}{2}}$ at 1 kHz maximum
Package	14-pin ceramic dual in-line

TABLE XIII. POSTAMPLIFIER CHARACTERISTICS (S/N 25903)

Power	±3V at 5 mA/package
Input impedance	10 kilohms
Output impedance	200 ohms
Gain	5 to 100 volts/volt
Features	Adjustable gain
Package	16-pin ceramic dual in-line

TABLE XIV. LED DRIVER CHARACTERISTICS (S/N 25906)

Power	±6 volts at 5 mA/package
Input impedance	8 kilohms
Gain	6 volts/volt
DC tracking	±0.5 percent
Package	16-pin ceramic dual in-line
Features	Separate supply input for emitter supply voltage

In addition to the preamplifiers and postamplifiers, the video chain contains an emitter normalization module which equalizes the output brightness-versus-signal characteristic of each emitter, an auxiliary electronics module for interface between the control electronics and the amplifiers, and a bias regulator module which provides the power for the bias resistors located in the Dewar/detector module. Figure 56 is a block diagram of the video electronics.

b. General Characteristics

The electronics are such that the system will operate with target temperatures from -50° to +3,000°C and with background temperatures from -50° to +60°C (assuming emissivity of 1). No blooming, overshoot, or saturation will occur for targets in the -50°C to +50°C temperature range. The video electronics and other system elements (LEDs and television camera) allow the processing of a 10-gray-shade range.

Overshoot is minimized in the electronics design. If the video electronics is ac-coupled and does not have dc response, the electrical signal of a large target will "droop" as the target is scanned. When the trailing edge of a large target is scanned, the signal will overshoot by an amount equal to the droop. Droop, and hence overshoot, are minimized by lowering the low-frequency response in the video chain. Decreasing the low-frequency response has

the adverse effect of increasing the saturation recovery time (because of gun flash, for example.) A tradeoff must be made to optimize the droop and flash recovery time. Test results obtained from TINTS and PINDTS were used to determine the optimum low-frequency response for the common module video chain. Video chain saturation caused by gun flash will not cause the system to latch up or become inoperative.

c. Detector Preamplifier Interface

HgCdTe detectors have an impedance of approximately 50 ohms, and the preamplifiers designed for those detectors are optimized for this source impedance. Detectors of the size proposed for this system have peak responsivities of 25,000 volts/watt, nominal, resulting in a detector noise voltage, e_d, of

$$e_d = \frac{R\lambda_p \sqrt{A_d}}{D^*\lambda_p} = \frac{(25{,}000) \times (5 \times 10^{-3})}{2.4 \times 10^{10}} \quad \frac{\text{volts}}{\sqrt{\text{Hz}}}$$

$$e_d = 5.2 \times 10^{-9} \text{ volts/Hz}^{\frac{1}{2}}$$

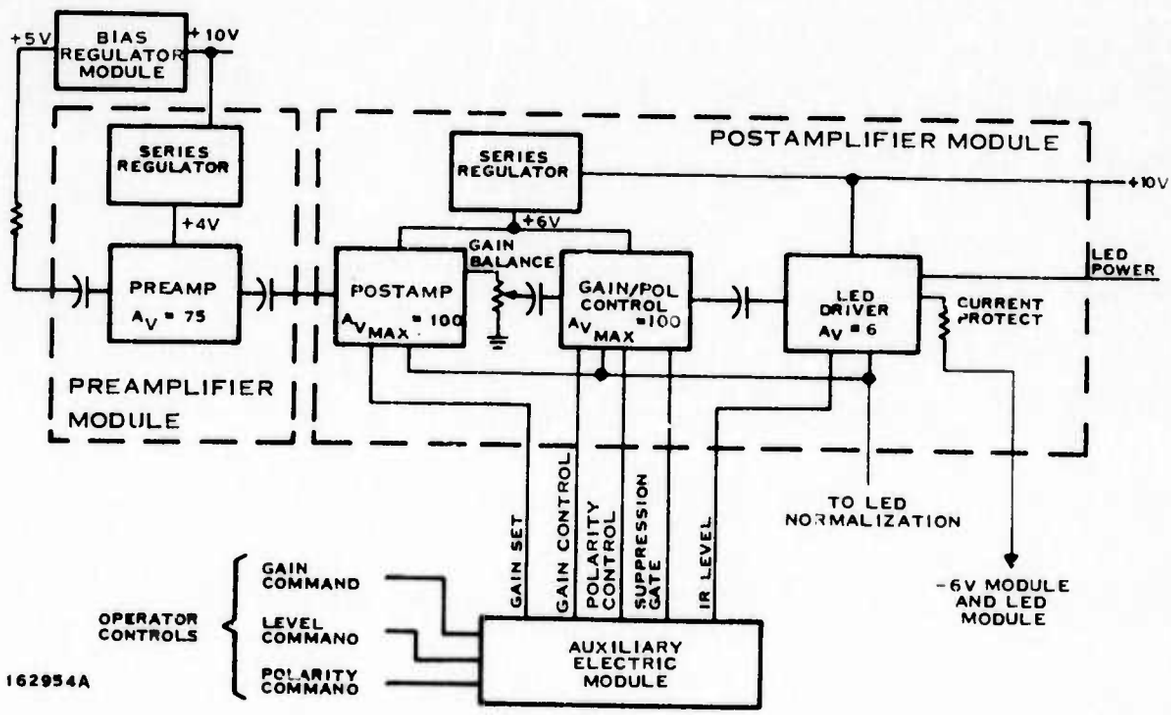

Figure 56. Infrared Video Electronics Block Diagram

where

$R_{\lambda p}$ = peak responsivity (25,000 volts/watt)

A_d = detector area in cm^2

$D^*_{\lambda p}$ = peak detectivity in cm $Hz^{\frac{1}{2}} W^{-1}$ ($\cong$ 2.4×10^{10})

The amount of additional noise produced by the preamplifier is kept to a minimum. The preamplifiers have a typical equivalent input noise equivalent input noise voltage of approximately 1.3×10^{-9} volts/$Hz^{\frac{1}{2}}$, and the resultant signal-to-noise degradation is only 3 percent.

$$\text{Degradation factor} = \frac{\sqrt{(5.2 \times 10^{-9})^2 + (1.3 \times 10^{-9})^2}}{5.2 \times 10^{-9}} = 1.03$$

d. Grounding and Electromagnetic Interference

Proper ground techniques become extremely important in FLIR systems, because the signals at the detector are of such low levels. The signal on each detector is amplified by approximately 100 dB (100,000) before it modulates the light-emitting diodes. Signal routing and power conditioning must be controlled very carefully to minimize electrical crosstalk between channels, feedback effects, and oscillation problems.

6. Electro-Optical Multiplexer

a. Features and Functions

The electro-optical multiplexer is a unique feature of Texas Instruments FLIR systems. It simultaneously accomplishes multiplexing and scan conversion of multiple-channel IR video information into standard single-channel composite TV format (4 X 3 aspect ratio and 30 frames per second). The video output of Texas Instruments FLIR systems can be displayed on multiple standard 875-line CRT TV displays, can be tape-recorded, data-link transmitted, or used with standard TV automatic target contrast trackers.

The concept of this electro-optical multiplexer scheme is simple. First, the detector scan is recreated with a geometrically equivalent array of LEDs. Then the system contains a visible image of the infrared scene of interest. This scene is viewed by a standard television camera using a mass-produced, ruggedized vidicon (Model RCA 4503A). This simple scheme accomplishes the difficult tasks of multiplexing and scan conversion in one single operation. Figure 57 illustrates the concept.

In the modular FLIR, the electro-optical multiplexer consists of three standard modules: LED array, visible collimating lens, and TV camera.

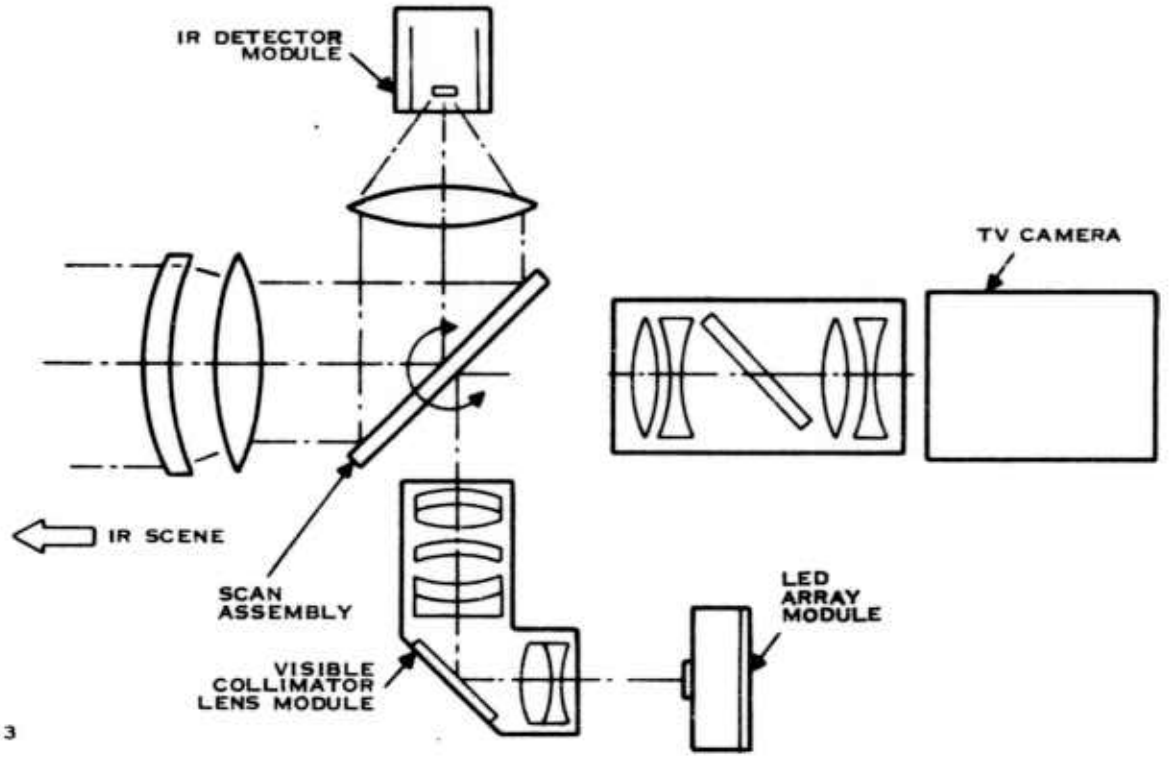

FIGURE 57. ELECTRO-OPTICAL MULTIPLEXER SCHEMATIC

b. Main Elements

The electro-optical multiplexer comprises three main elements: the visible collimator lens module, the LED array module, and the camera module

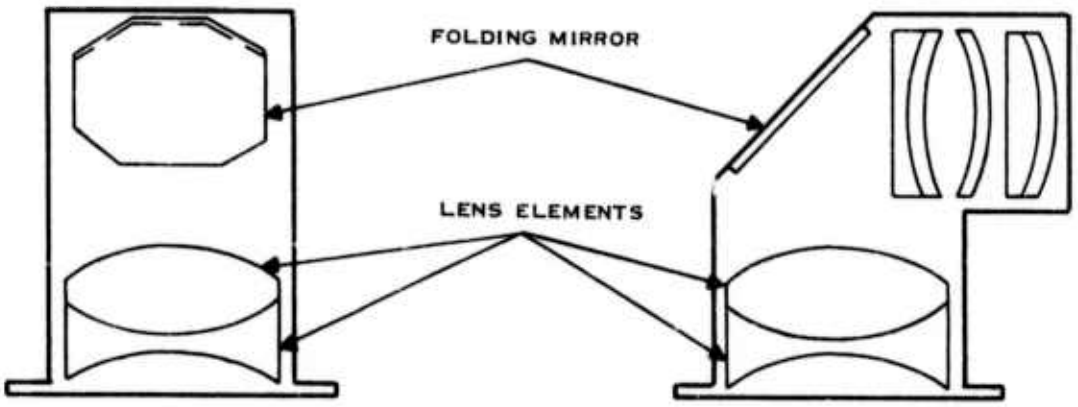

Figure 58. Visible Lens Module Collimator

(1) Visible Collimator Lens Module

The visible collimator lens module (Figure 58) is positioned directly behind the scan mirror of the scan mechanism subassembly. This lens collimates the light from the LEDs, which are located at the focal point of the lens. The energy beam from the diodes passes through the collimating lens, is reflected from the scan mirror, and subsequently, is imaged onto the vidicon by the camera lens.

The visible collimator lens module is a self-contained unit which will interface with the scanner module in a number of orientations. A photograph of this module is shown in Figure 59.

(2) LED Module

The array of 180 0.001- by 0.002-inch gallium arsenide phosphide (GaAsP) LEDs is fabricated in-line, identical to the detector format. The LEDs emit red light at approximately 6.600 Å or 0.66 um. The array is capable of radiant emittance of 200 watts per square foot. This affords a brightness of more than 3 footlamberts.

The LEDs are mounted to a heatsink and sealed under an optical window. Electrical connections to each diode are made using flexible printed cabling to standard connectors. Figures 60 and 61 show the LED module.

(3) Television Camera Module and Lens

The television camera is not a common module part; however, it is included in this section for descriptive purposes. A high-resolution, 1-inch, vidicon TV camera is used to reproduce the LED-scanned imagery.

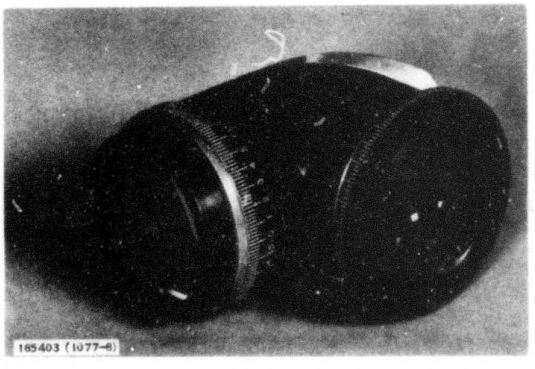

Figure 59. Visible Collimator Lens Module

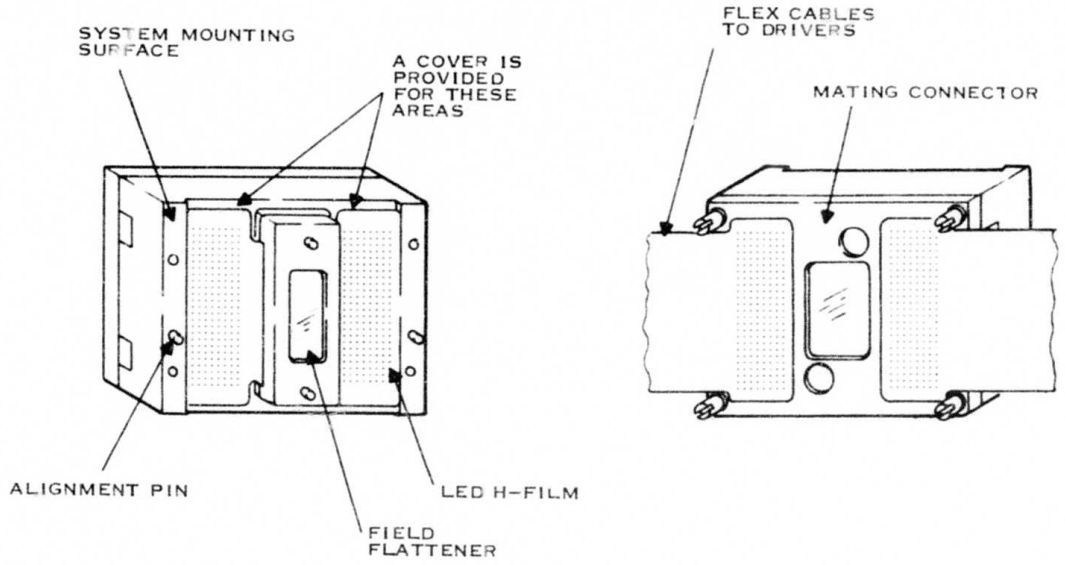

Figure 60. LED Module

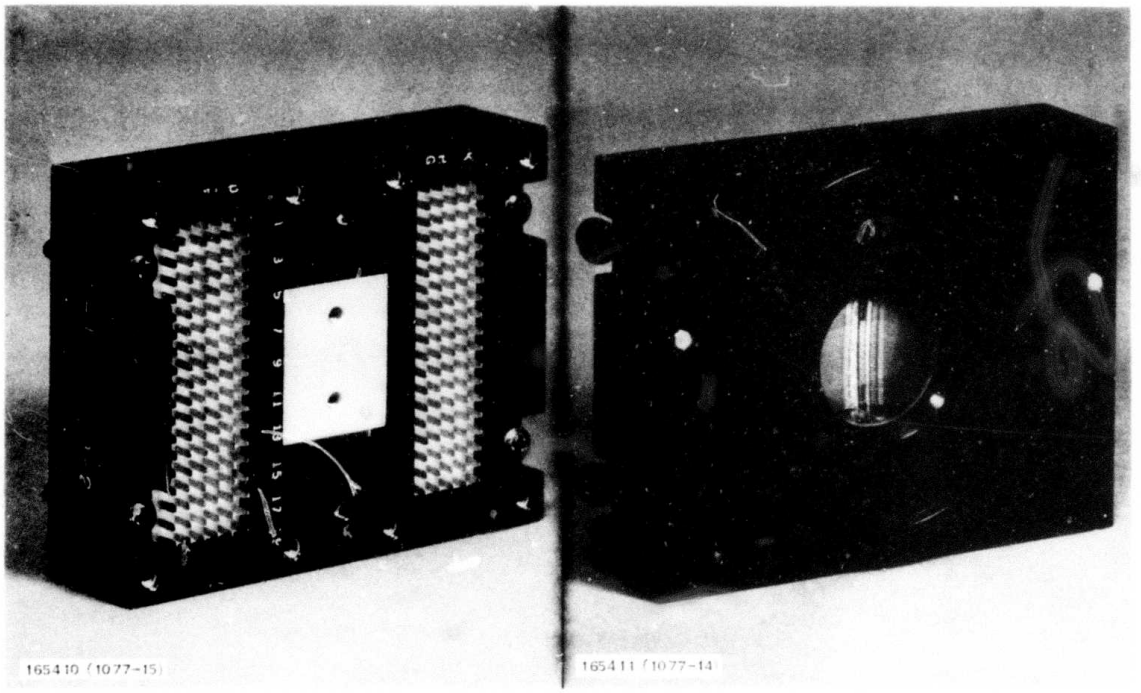

Figure 61. LED Module Photographs

To minimize the physical size and heat dissipation of the TV camera head module, the television system is separated into two assemblies, the camera head and the control unit. The camera head consists of the vidicon and lens system, video preamplifier, and deflection circuits (Figure 62). The camera control unit consists of the television signal-processing electronics and power supply and is located in the electronics box. Figure 63 is a block diagram of the camera. Camera characteristics are listed in Table XV.

The camera operates at 875 TV lines per picture height. This particular line rate was chosen after extensive studies at Texas Instruments which considered signal-to-noise ratio, bandwidth, resolution, and moire effects.

The displayed video appearance and usefulness are enhanced by adding gamma correction, aperture correction, temperature compensation, and a selectable gray-shade generator. Circuitry is provided in the camera electronics to gamma-correct the system (at the camera output) to a value of 1. The gamma-correction circuitry uses nonlinear circuit techniques which produce a correction factor that is a function of the LED element and associated camera system characteristics. Aperture correction compensates for MTF roll-off in the vidicon by using a delay line aperture circuit, resulting in an improved system MTF without detrimental effects such as video ringing or overshoot.

The camera uses a vidicon target voltage temperature control that greatly reduces the effects of vidicon gain changes over temperature. Thus the video output level is constant.

A 10-step gray-shade waveform is generated within the camera electronics. This feature allows the operator to optimize the sensor display according to ambient light conditions. Since the gray scale presents both minimum and maximum video level content information in 10 discrete steps, the sensor display is optimized within a given set of ambient lighting conditions. The full dynamic range of the display is then available to the operator.

The TV camera deflection circuitry is synchronized by a crystal-controlled sync generator which maintains the timing relationships in the deflection circuitry to $\pm$0.0005-percent accuracy. Short-term jitter, or frame-to-frame instability, in the TV camera is thus negligible.

The horizontal and vertical deflections that determine picture size and linearity are accomplished with analog circuitry. The deflections are not subject to frame-to-frame jitter.

The TV camera uses high reliability, precision, burned-in components throughout. Typical values of drift experienced in other Texas Instruments FLIR systems are ±2 percent in size and centering over time and temperature. Linearity remains within 2 percent peak-to-peak.

The TV system electronics are designed to accommodate tube currents in excess of 300 nA. The sensor used in the TV camera is an RCA 4503A vidicon which was selected because of its high sensitivity, log lag, and wide dynamic range.

The collimated light from the scan mirror is focused on the vidicon tube by the vidicon imaging lens. Its focal length and magnification are designed so that the LED image size matches the vidicon format. Optical distortion is less than 1 percent over the full field.

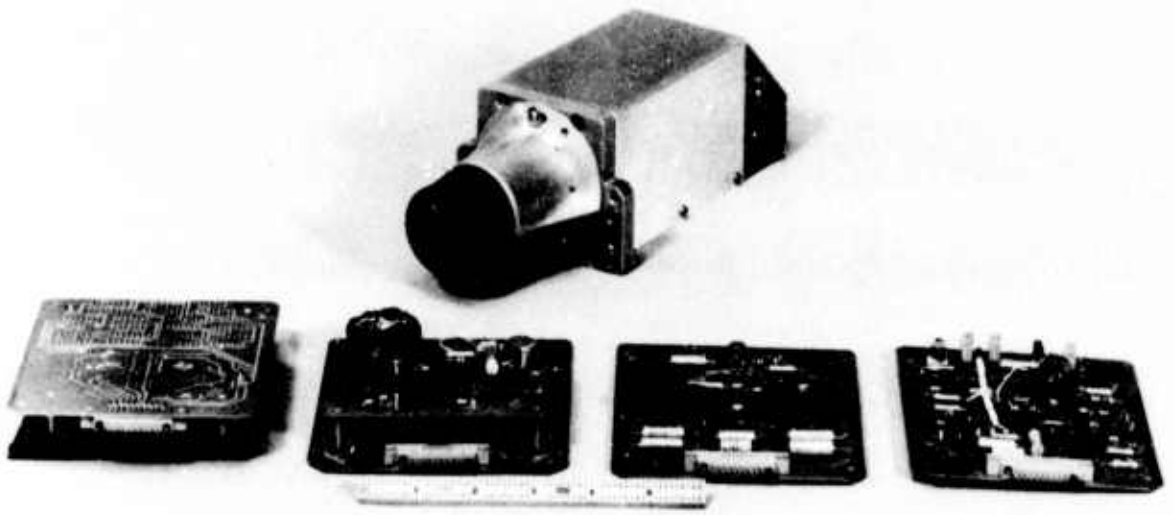

Figure 62. Television Camera Module and Electronics

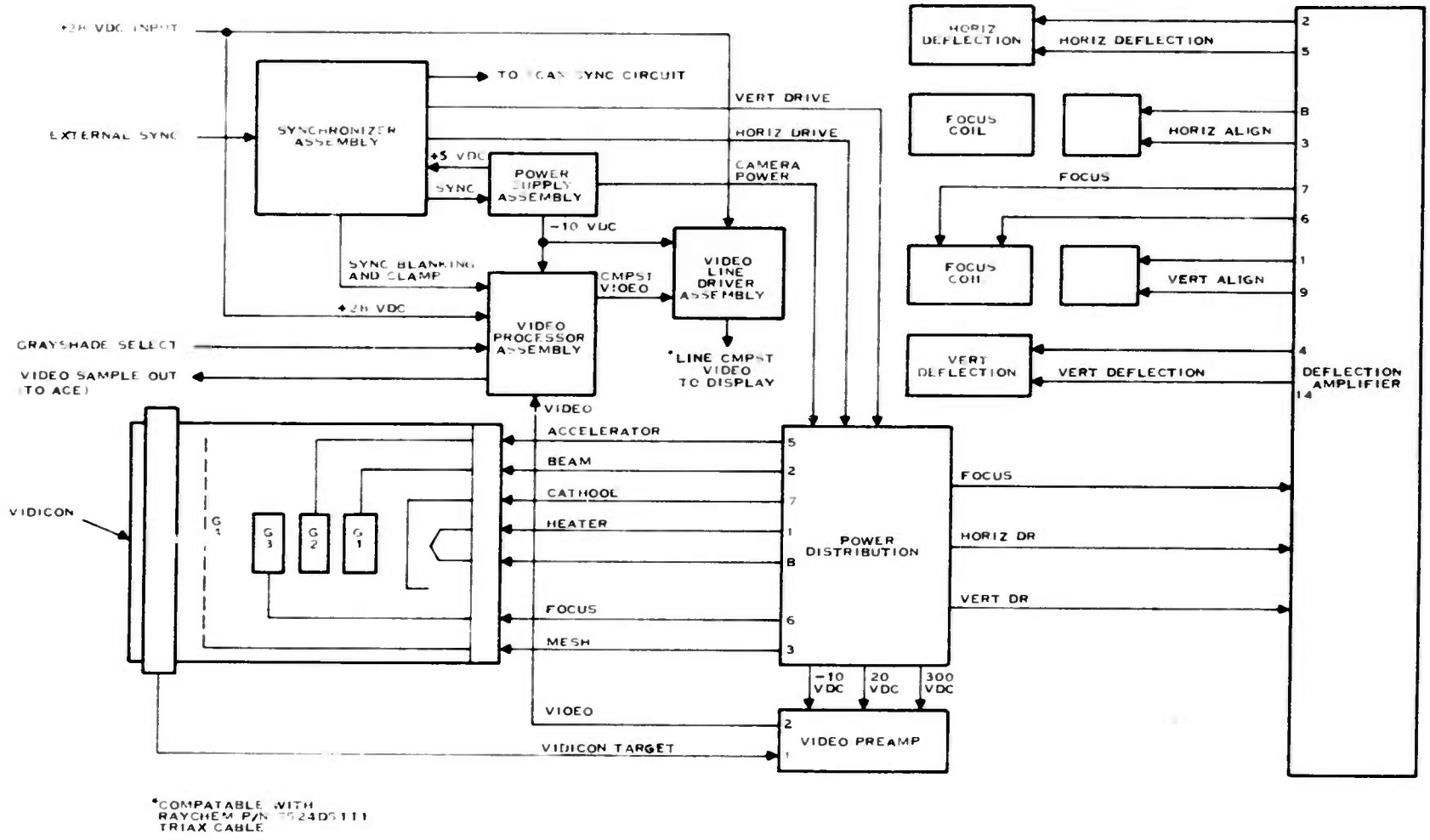

Figure 63. Camera System Functional Block Diagram

TABLE XV. TV CAMERA CHARACTERISTICS

Parameter	1-inch Vidicon Camera
Module size	
Head (including lens)	3-inch diameter X 10.5 inches
Electronics	5 X 5 X 6 inches
Module weight	
Head	4.01 pounds
Electronics	3.25 pounds
Synchronization	Internal modified RS-343A 875 lines; 60 fields per second 2:1 interlace or external
Video output	1.4 volts peak to peak 1-volt video 0.3-volt sync 0.1-volt blanking
Video polarity	Black negative
Signal-to-noise ratio	40 dB with 300 nA I_s
Sweep linearity	$\pm$ 1 percent
Geometric distortion	$\pm$ 2 percent
Gray scale	10 shades of gray
Aperture correction	Yes
Gamma correction	Yes
Bandwidth	7.5 MHz $\pm$2 dB
MTF performance	Aperture correction compensates for MTF of vidicon to produce an MTF = 1 $\pm$ 0.5 to 350 lines, with linear degradation to 0 at 700 lines.

B. SYSTEM NUMBER TWO, THREE FIELD-OF-VIEW CATADIOPTIC SYSTEM

System two is a three field-of-view system, using both a Catadiopic reflective afocal design for the 1/4 mr NFOV and refractive optics for one and two mr wide fields of view. The Texas Instruments common modular imager is used to focus the radiation onto the detector array. The afocal magnifications consist of a 3X magnification for the narrow FOV, and a 0.75X and 0.375X magnification for the middle and wide fields of view respectively. All FOV's are f/2.0.

The system layout utilizes the same aperture for all fields of view by inserting mirrors in the proper location. This allows the rays of the wide fields of view to use the available aperture. System two is comprised of the Texas Instruments common modular scanner, IR imager, detector dewar and video electronics. System two uses the electronic multiplexer discussed in Section V.

The geometric blur MTF for the IR optics is optimized across the FOV. The on-axis MTF is 96% for the three fields of view. The diffraction limit of f/2.0 optics is 75% (Figure 64) resulting in IR optical MTF of 72%. The geometric MTF's for the three fields of view are shown in Figures 64, 65, and 66 for the NFOV, MFOV, and WFOV respectively.

System two is electronic multiplexed. A video rolloff of type g mentioned in the multiplexed system rolloff section yields about 80% MTF at resolution frequencies.

Figure 39 shows the MTF associated with the detector scan at resolution frequencies. The value at f/fo is 64%.

The final MTF at f/fo = 1.0 of system two is given by:

$$MTF_{\text{System \#2}} = (MTF_{\text{IR Geometric}})\,(MTF_{\text{IR Diffraction}})\,(MTF_{\text{Detector Scan}})\,(MTF_{\text{Electronic Multiplexer}})\,(MTF_{\text{Display}})$$

$$= (0.96)\,(0.75)\,(0.64)\,(0.8)\,(0.8)$$

$$= 30\% \text{ at } f/fo = 1.0$$

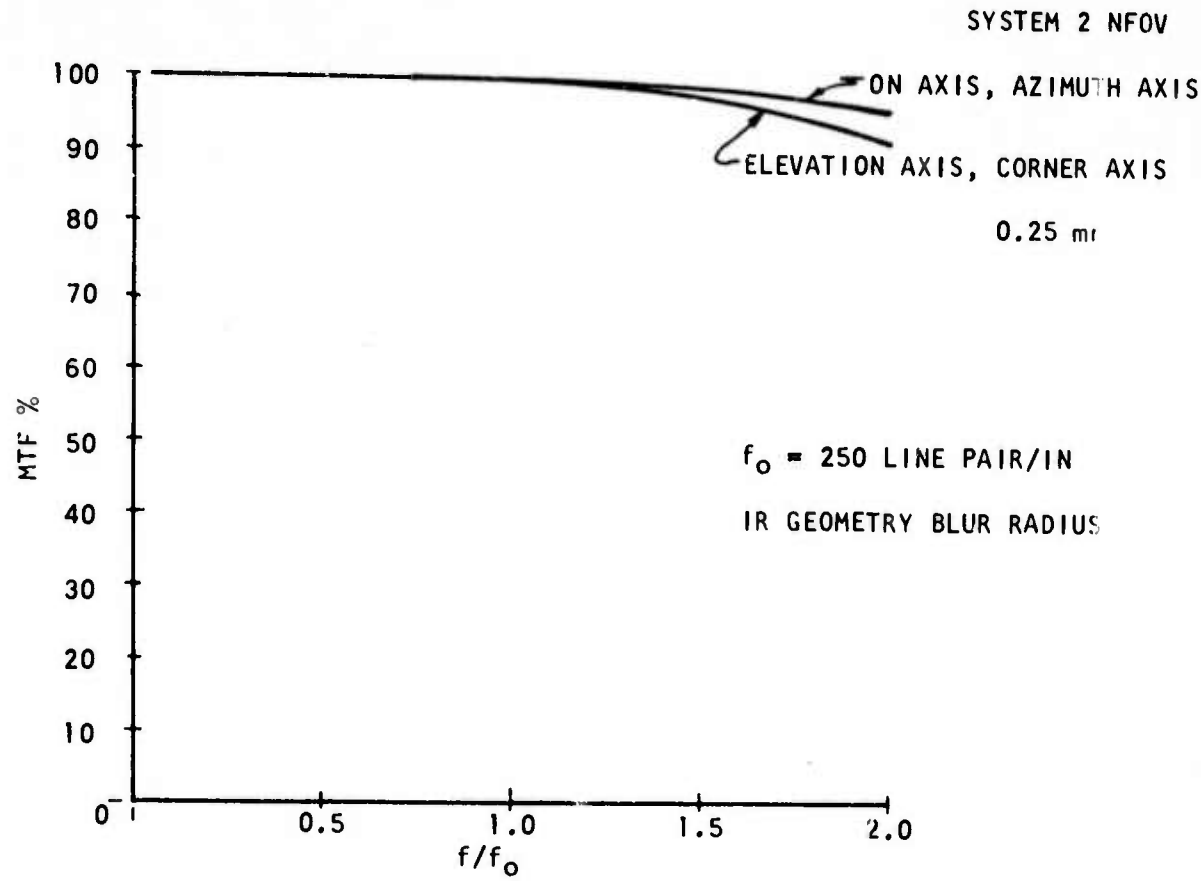

Figure 64. System Two NFOV Geometric MTF.

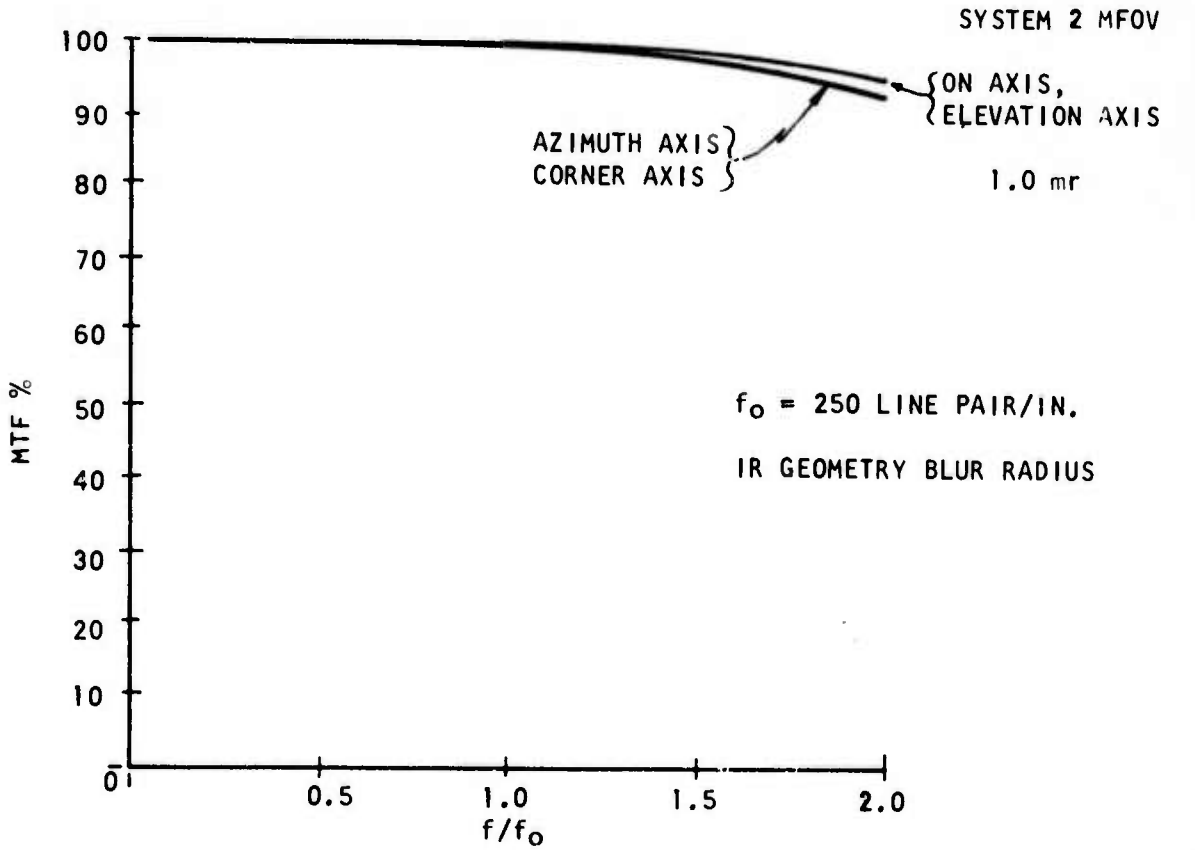

Figure 65. System Two MFOV Geometric MTF.

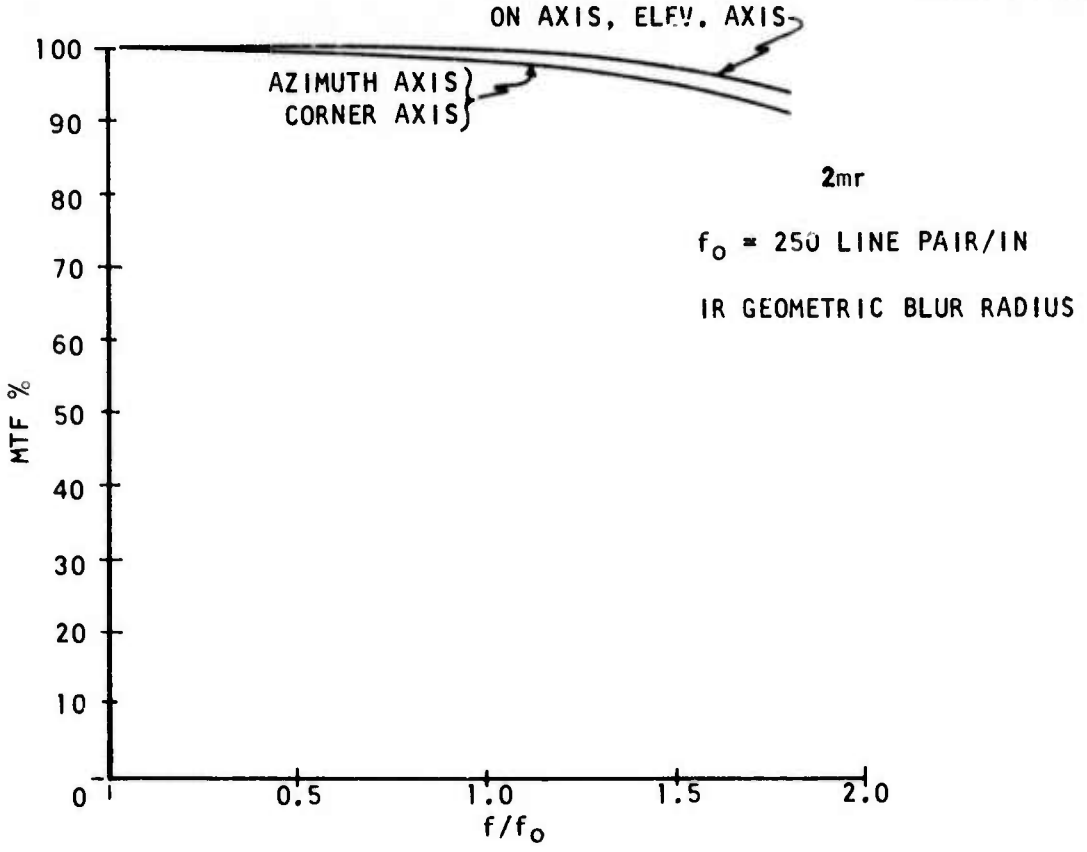

Figure 66. System Two WFOV Geometric MTF.

The NET of system two is given by the equation

$$NET = \frac{(f^{\#})^2 \sqrt{BWn}}{\sigma T^3 \sqrt{A_d}\ D^*_{300}\ \tau_o}$$

where

$f^{\#}$ = system f number

BWn = system noise bandwidth

A_d = detector area

D^*_{300} = D* detectively at 300°C

τ_o = optical transmission

where

f = 2.0 for all FOV

$$BWn = \frac{\pi}{2}\ \frac{(\text{Azmiuth IR lines})(\text{TV Frame Rate})}{\text{Scanner Duty Cycle}}$$

$$= \frac{\pi}{2}\ \frac{(160)(30)}{0.7}$$

= 10.7 KHz

A_d = 25.8×10^{-6} cm^2

τ_o = 0.51 NFOV and 0.63 WFOV and MFOV

D^*_{300} = $1.25\ D^*_{300} = 7.5 \times 10^9$

Substituting for the NFOV

$$NET_{NFOV} = \frac{(4)\ (103)\ (6.53 \times 10^3)}{(5.08 \times 10^{-3})(7.5 \times 10^9)(0.51)}$$

NET_{NFOV} = 0.14^oC

and for the WFOV and MFOV:

$$NET = \frac{(4)\ (103)(6.5 \times 10^3)}{(5.08 \times 10^3)(7.5 \times 10^9)(.63)}$$

and

NET = 0.12^oC

The calculated NET for the narrow FOV in the designed system will be $0.14^{o}C$. The middle and wide fields of view will have NET's of $0.12^{o}C$.

MRT is calculated from

$$MRT = K \frac{NET}{MTF} \frac{f}{fo}$$

and for the NFOV

$$MRT = \frac{(0.6)(0.14)}{0.3} = 0.28^{o}C$$

and for the MFOV, WFOV

$$MRT = \frac{(0.6)(0.12)}{0.3} = 0.24^{o}C$$

The overall performance of system two will be $0.28^{o}C$ MRT in the NFOV and $0.24^{o}C$ MRT in the wider fields of view. The sensitivity differences are due to the optical transmission difference between the narrow and wider fields of view.

A comparison between system two and the current ANVS system is shown in Table XVI. In the calculations, the ANVS system does not have simultaneous fields of view as do the systems in the field at present. The number of optical elements in the systems is approximately the same; therefore, the transmission will be compatible. The ANVS system has 61% optical transmission while that of system two varies from 51% in the NFOV to 63% for the wide fields of view.

An advantage of system two over the present ANVS system is that the MRT of system two is $0.24^{o}C$ in the wider FOV and $0.28^{o}C$ in the NFOV. The ANVS system has $0.32^{o}C$ across all FOV's. This difference is due primarily to the optical f-number of the IR optics.

The overall weight of system two optics is slightly less than that of the ANVS system or 0.17 pounds.

1. System Two Mechanical Design

System two has three fields of view to be called narrow (NFOV) medium (MFOV), and wide (WFOV). The NFOV uses the catadioptic afocal while the MFOV and WFOV use refractive optics.

When the system is to be used in either the MFOV or WFOV, a folding mirror must be inserted at 45^{o} to the optical axis and in front of the primary spherical mirror. See Figure 67. This motion is accomplished by a motor-driven ball screw and linkage system.

TABLE XVI.

COMPARISON OF SYSTEM TWO AND ANVS FLIR

	SYSTEM TWO			ANVS FLIR		
	NFOV	MFOV	WFOV	NFOV	MFOV	WFOV
Number of Optical Elements	12	9	9	10	10	10
τ_o	.51	.63	.63	.61	.61	.61
Resolution mr	.25	1.0	2.0	.25	1.0	2.0
f-Number	2.0	2.0	2.0	2.5	2.5	2.5
FOV $\frac{El}{Az}$	$\frac{1.7}{2.3}$	$\frac{6.87}{9.17}$	$\frac{13.7}{18.4}$	$\frac{2.25}{3.0}$	$\frac{9.0}{12.0}$	$\frac{18.0}{24.0}$
Aspect Ratio	4/3	4/3	4/3	4/3	4/3	4/3
Number of Detectors	60	60	60	80	80	80
MTF IR						
On Axis	99	99	99	93	96.3	77
El Axis	98	98	99	82	71	37
Az Axis	99	99	98	30	47	72
Corner Axis	98	99	98	51	49	60
NET ^oC	.14	.12	.12	.2	.2	.2
MRT ^oC	.28	.24	.24	.32	.32	.32
Weight of Optics System	1.23 lbs.			1.4 lbs		

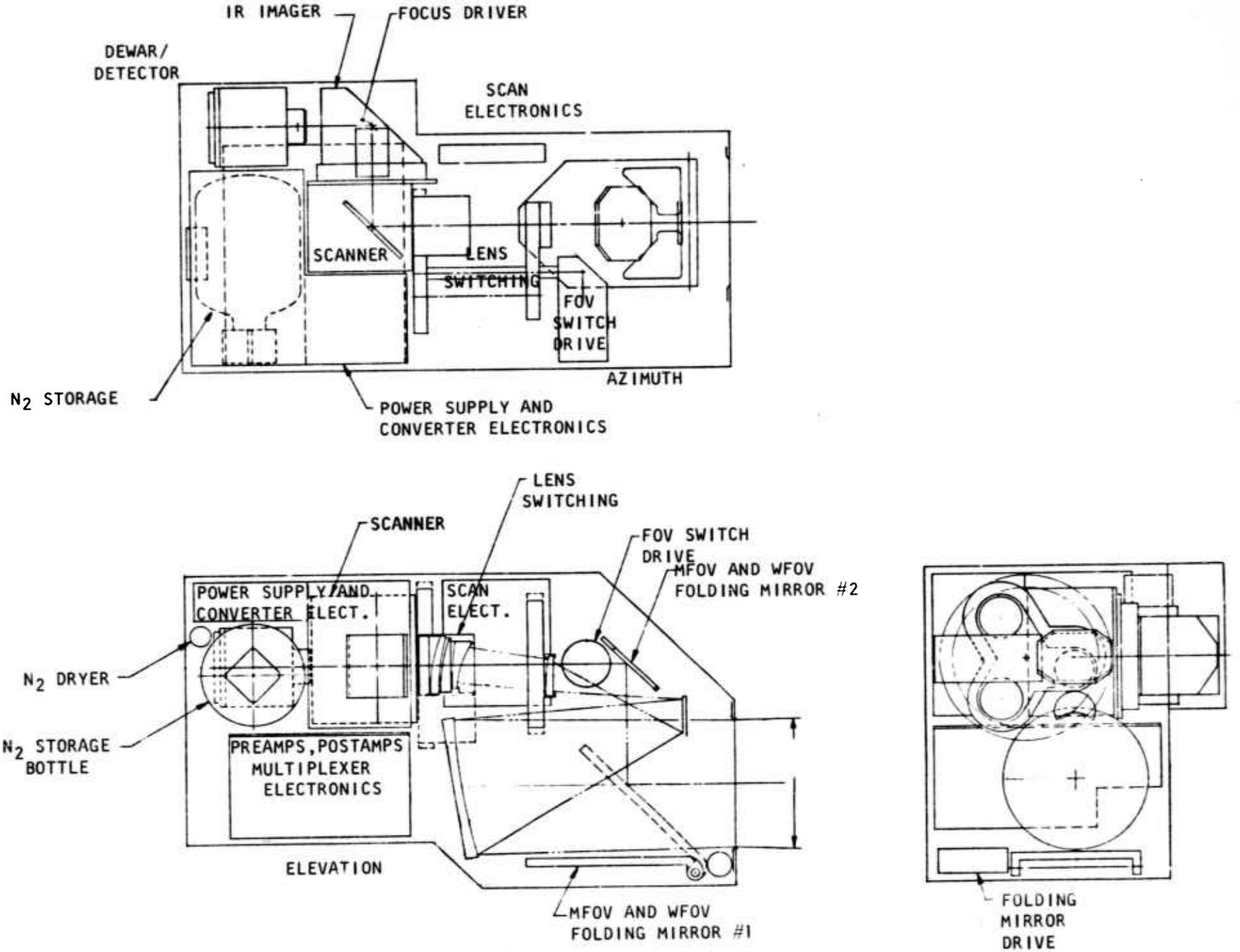

Figure 67. System Number Two

The energy radiation from the three fields of view exit from the afocal into the Texas Instruments Common Module Scan Mirror.

The common module imager is used to focus the radiation onto the detectors. All focus compensation takes place in the infrared imager by a DC motor. Passive athermalization may be linked to the imager through techniques discussed in Section II.

The Texas Instruments common module detector/dewar assembly is used in the system design. The dewar/detector assembly has 180 detectors available; however in this design only 60 are required.

A Joule-Thompson cryostate is used to cool the detector array to $77^{o}K$. The dry nitrogen required can be stored in a small lightweight bottle at 6000 psi. Typically, a 25 cubic inch bottle will provide a hold time of approximately two hours of continuous operation.

Three common module preamps and three modified common module postamps are used in the video amplifier chain of the system prior to multiplexing. Video filters are used to minimize aliasing and signal to noise ratio degradation as mentioned in Appendix H.

Table XVII shows the calculated weight and power requirements for system two. System two requires a single DC power input. All associated voltages are regulated in the DC Power Supply and converter electronics. If regulated voltages are available from other sources a power savings of 6.5 watts and a weight reduction of 0.75 pounds can be realized.

System two, as designed, is completely self-sustaining, thereby requiring only external DC power to operate. If items starred (*) in Table XVII are determined unnecessary, or available from other sources aboard the aircraft, a weight savings of 6.22 pounds and power savings of 6.5 watts is possible.

System two will be assembled with one main U-shaped aluminum sheet metal structure. All system components will mount to this structure with a result of stiffening the housing. The housing will be made of sheet aluminum, i.e., 0.40 thickness with dimples stamped into it at strategic locations for stiffening.

Folding mirror number one will mount directly to the main structure housing. A plastic afocal optics structure will be molded to mount all afocal optics and the zoom mechanism. The primary, secondary and MFOV and WFOV mirror number two will be mounted directly to the plastic structure on three point adjustable pads for alignment purposes. The rotating zoom mechanism will mount directly to the afocal housing on a common shaft. The afocal housing will be a removable module to facilitate alignment and assembly. This afocal housing will be the main stiffening member for the outer sheet metal structure.

The scanner will hold the IR imager and detector/dewar in the proper location. The detector/dewar will be attached to the imager to eliminate imager focus problems due to vibration along the optical axis. The imager and detector/dewar scanner will then be hard mounted to the main structure.

TABLE XVII. SYSTEM TWO WEIGHT AND POWER REQUIREMENTS

	WEIGHT (POUNDS)	POWER (WATTS)
OPTICS	1.5	-
DETECTOR/DEWAR	0.94	-
SCANNER	1.3	2.8
PREAMPS PWB (3)	0.5	1.08
POSTAMPS PWB (3)	0.9	3.23
MULTIPLEXER/TIMING PWB	0.2	0.92
SYNC GENERATOR WPB	0.16	0.53
BIAS PWB	0.07	1.62
VIDEO FILTER PWB	0.05	-
SCAN DRIVER PWB	0.30	INCLUDED IN SCANNER
VIDEO PROCESSOR PWB	0.20	0.75
*NITROGEN BOTTLE	1.83	-
*N_2 DRYER	0.14	-
IMAGER	1.2	-
FOLDING MIRROR DRIVE	1.0	
LENS SWITCHING DRIVE	1.5	5.6 INTERMITTANT
*FOCUS DRIVE	0.5	
*SHROUD	2.0	-
*POWER SUPPLY	1.75	6.5
ALUMINUM AND PLASTIC STRUCTURE & MISCELLANEOUS WIRING	3.0	-
TOTAL	18.74 LBS	17.44 CONSTANT 5.6 INTERMITTANT

Support for the nitrogen bottle and electronics will be from the sheet metal outer structure. A copper coated plastic electronics box will contain all the system electronics.

Weight reduction techniques and lightweight materials will be used throughout the structure of this system to provide high strength and rigidity with minimum weight.

2. System Two Conclusions

System two is an intermediate lightweight FLIR with three fields of view. The design effort on this system has resulted in a high quality FLIR with good MRT and MTF while maintaining low weight and power.

C. SYSTEM THREE, LIGHTWEIGHT TWO FOV SYSTEM

System three IR optics consists of a Galilean afocal and IR imaging lens. The complete IR lens system utilizes five optical elements for two fields of view. The resolution selected for the FOV's are ¼mr and 1.0 mr. This optic design could be expanded to several other FOV's if desired. The afocal was designed with a 2X afocal magnification in the NFOV and 0.5X magnification in the WFOV. With the 4-inch effective focal length of the IR imager, the system design has 8-inch and 2-inch focal length systems.

Focal length is calculated from:

Focal Length = Afocal Magnification X Focal Length Imager

The original system was designed to be an f/2.0 However, system layout indicated that an f/2.5 system was required in order to make use of the Texas Instruments common modular scanner. This was required because the optical ray bundle size of an f/2.0 optical system at the exit of the afocal is too large for the newly designed modular scan mirror.

The MTF loss of system number three IR optics was primarily due to diffraction limit of the optics. The IR geometric MTF is plotted in Figure 68a for the NFOV and Figure 68b for the WFOV. The IR geometric MTF at f/fo = 1.0 is 94% - the NFOV. and 96% in the WFOV. The optical performance exceeds 64% at the on-axis position of the scan.

System number three is designed using electronic multiplexing. A double RC filter was selected with 80% MTF at resolution frequency to reduce aliasing and signal to noise ratio. Figure g (in Appendix H) shows the modulation associated with the electronic multiplexer.

The largest contributor to resolution degradation is the detector scan (see Figure 39).

The last area analyzed for MTF degradation included the data link and display. In this analysis, the MTF associated with the display and data link is assumed to be 80% for the display and 100% for the data link.

The overall equation for system three MTF can be written:

$$MTF = (MTF_{IR\ Geometric})(MTF_{IR\ Diffraction})(MTF\ detector\ scan)$$

$$(MTF\ electronic\ multiplexer)\ (MTF_{data\ link\ \&\ display})$$

Therefore

$$MTF = (0.94)(0.68)(0.64)(0.80)(0.80)$$

$$= 0.26 \quad or \quad 26\%$$

The NET of system three is given by the equation

$$NET = \frac{(f^{\#})^2\sqrt{BWn}}{\sigma T^3\ \sqrt{A_d}\quad D^*_{300}\ \tau_o}$$

$f^{\#}$ = system f number

BWn = noise electronic bandwidth

A_d = detector area

D^*_{300} = D^*_{300} detector @ 300°K

τ_o = optical transmission

where

$f^\#$ = 2.5

and

$$BWn = \frac{\pi}{2} \frac{(\text{Azimuth IR Lines})(\text{TV Frame Rate})}{\text{Scanner Duty Cycle}}$$

$$= \frac{(160 \text{ lines})\ (30 \text{ frames/second})}{0.7} \quad \frac{(3.14)}{2}$$

= 10.8 KHz

$$Ad = \left[(0.002)(2.54)\right]^2 = 25.8 \times 10^{-6}$$

τ_o = 0.75 for five lenses

τ_o = 0.72 for five lenses two mirrors

$$D^*_{300} = 1.25\ D^*_{500} = (1.25)(6 \times 10^9) = 7.5 \times 10^9$$

Therefore,

$$NET = \frac{(6.25)(104) - (6.53 \times 10^3)}{(5.08 \times 10^{-3})(7.5 \times 10^9)(.72)}$$

$NET = 0.155^oC$

and MRT is calculated from

$$MRT = (K)\left(\frac{NET}{MTF}\right) \frac{f}{fo}$$

$$MRT = (.6) \frac{(.155)}{(.26)} (1)$$

$MRT = 0.36^oC$ MRT

The overall performance of system three will be 0.37°C at resolution frequencies. Figure 68c shows the overall MRT as a function of f/fo for values out of f/fo = 1.5.

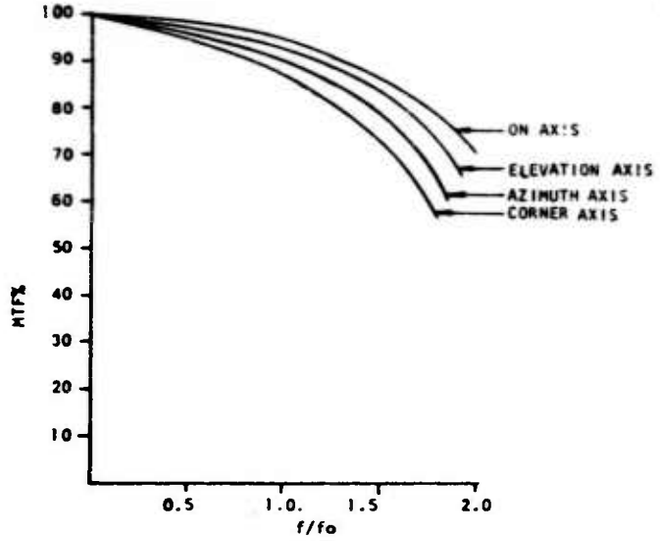

Figure 68a. System Three NFOV MTF vs. f/fo

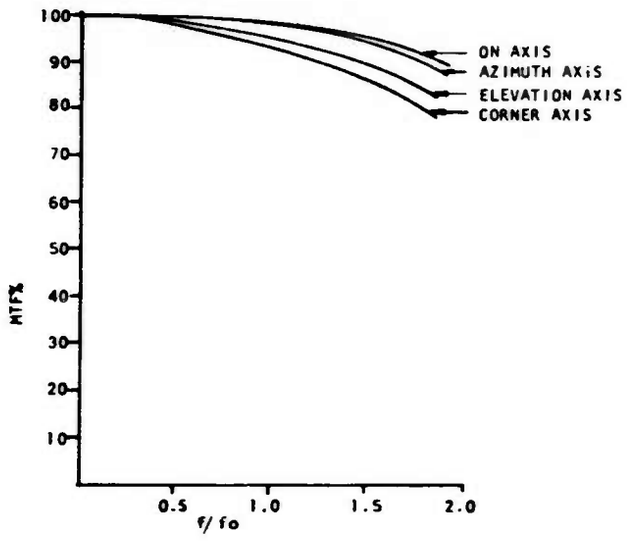

Figure 68b. System Three WFOV MTF vs. f/fo

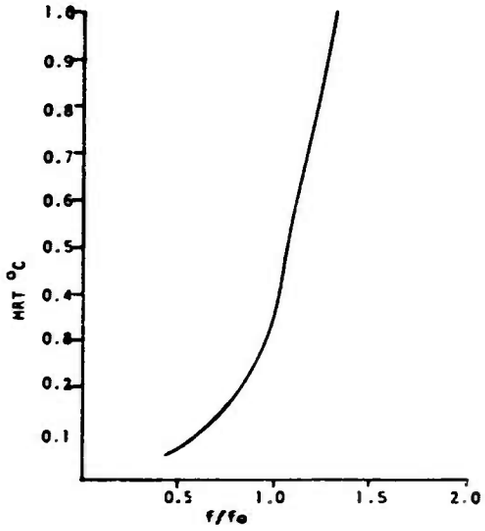

Figure 68c. System Three NFOV MRT vs. f/fo

A comparible Galilean afocal with a common modular IR imaging lens uses nine opitcal elements for both fields of view. Optical MTF performance for such a lens system is comparible to the performance of the five-element system mentioned above. Transmission losses in the four-element Galilean afocal is greater than the two-element afocal mentioned above. Table XVIII compares the performance parameters of the two systems.

The calculated weight of the five-element system is less than that of the nine-element IR optical system by 0.15 pounds.

This amounts to an 11% weight reduction. It is believed, however, that the weight of the optics in system three can be further reduced, since the present design was not optimized for minimum lens thickness.

The overall performance of system three is better than the classical Galilean afocal system, and the primary reason for the increase in sensitivity is due to optical transmission.

1. System Three Mechanical Design

The afocal optics system is made up of two elements which when packaged with a 90^0 folding mirror make up the FOV switching module. A unique feature of the design allows the FOV to be changed simply by exchanging the positions of the two afocal lenses while maintaining the same air space between them. The housing would be rotated 180^0 about the axis perpendicular to the folding mirror and intersecting the optical center line. Motion and position are accomplished by means of a gear motor and four-point Geneva mechanism. (See Figure 69 for system layout.)

The Texas Instruments common module scanner is used for scanning the FOV in the horizontal plane. System one analysis shows the Texas Instruments common module scanner in more detail.

The infrared imager is unique to the design of the optical system used in system three. This special three element imager is used, and consists of two germanium elements and one TI 1173 optical element. The imager is packaged in a straight line configuration but if necessary could be folded.

IR focus takes place in the first lens of the imager. Range focus is accomplished manually and preset to a predetermined range. Athermalization should be used for temperature focus. Using the scanner as a fixed reference, a mechanical linkage can be fastened to the focus mechanism to yield the proper lens translation with temperature. Different types of mechanical linkages are discussed in Section I.

The common module detector/dewar assembly is used in the system design. Sixty detectors out of the 180 available detectors are used. More explicite discussion of the detector/dewar module is explained in system one discussion.

TABLE XVIII

SYSTEM THREE PARAMETERS COMPARED TO CLASSICAL GALILEAN AFOCAL

	SYSTEM THREE		GALILEAN AFOCAL	
	WFOV	NFOV	WFOV	NFOV
Number Optical Elements	9	9	6	6
	0.72	0.72	0.66	0.66
Resolution mr	1.0	0.25	1.0	0.25
f-number	2.0	2.0	2.0	2.0
FOV $\frac{EL^o}{AZ^o}$	$\frac{6.87}{9.17}$	$\frac{1.7}{2.3}$	$\frac{6.87}{9.17}$	$\frac{1.7}{2.3}$
ASPECT RATIO	4:3	4:3	4:3	4:3
DETECTORS	60	60	60	60
MTF IR On Axis	98	94	98	94
El Axis	96	92	96	92
Az Axis	97	89	95	89
Corner Axis	93	87	93	87
NET ^oC	0.155^oC	0.155^oC	0.17^oC	0.17^oC
MRT	0.36^oC	0.36^oC	0.39^oC	0.39^oC
WEIGHT	1.35 lbs		1.5 lbs	

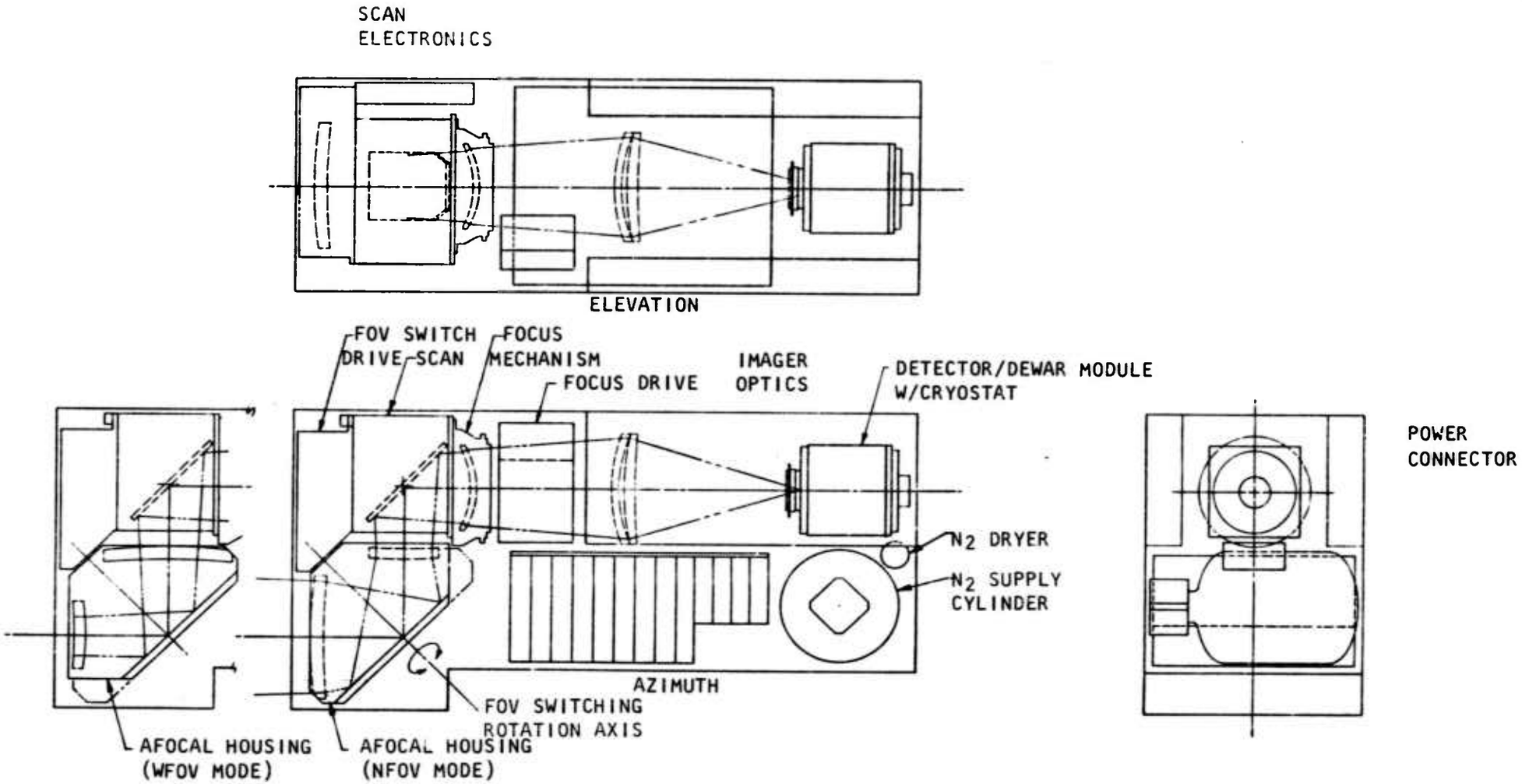

Figure 69. System Number 3.

A Joule-Thompson cryostate is used to cool the detectors to 77°C. Dry nitrogen at 6000 psi is stored in a 25 cubic inch bottle. Initial cool-down uses approximately 1500 psi of nitrogen and takes from 30 to 60 seconds. The remaining nitrogen in the storage bottle lasts between one and two hours of continuous operation.

Three common module preamps and modified common module postamps are used in the video amplifier chain of the system prior to multiplexing. Video chain filters are used to minimize aliasing and signal to noise ratio degradation as mentioned in Appendix H.

Tables XIX and XX show the predicted system weight and power requirements of the FLIR system. Table XIX is the minimum system weight and power requirements necessary for good system performance. The predicted system weight is 7.32 pounds and power requirements of 10.975 watts. The regulated voltages to run the FLIR system are assumed available from the aircraft.

The primary FLIR structure is cylindrical in shape with primary location and mounting achieved from the scanner assembly. Included in the structure assembly are the Infrared imager and detector/dewar assemblies. This structure could be made of plastics, Fiberglass, honeycomb and/or aluminum. Light weight techniques are utilized throughout the mechanical design.

The zoom switch mechanism mounts directly to the front side of the scanner assembly. The folding mirror is a replicated mirror.

The electronics mount alongside the main structure, close to the detector/dewar. This was done to minimize wiring and wire length. The electronics are enclosed in a copper coated plastic box.

Table XX lists optional features with weights and power requirements of such.

2. System Number Three Conclusions

System three is a very simple system with minimal weight. Overall performance is exceedingly good with MRT's less than 0.3°C in both fields of view. The weight of the basic system has been calculated to be 7.32 pounds, and a system ready for RPV flight with all options would be 12.49 pounds. The power required for system operation is 10.975 watts as shown in Table XIX.

TABLE XIX

SYSTEM THREE
WEIGHT & POWER REQUIREMENTS

	WEIGHT (lbs)	POWER (Watts)
Video Processor	0.2	.750
Optics	0.7	-
Detector/Dewar	0.94	-
Scanner	1.30	2.84
Preamps PWB (3)	0.50	1.08
Post amps PWB (3)	0.90	3.23
Multiplexer/Timing PWB	0.20	0.924
Sync Generator	0.16	0.53
Bias	0.07	1.62
Video Filter	0.05	-
Scan Drive PWB	0.30	Included in Scanner
Aluminum and Plastic Structure and Miscellaneous	2.0	-
Total	7.32 lbs	10.975

TABLE XX

MISCELLANEOUS OPTIONS

	WEIGHT (lbs)	POWER (Watts)
25 in^3 N_2 Bottle	1.83	-
N_2 Dryer	0.14	-
Focus Drive	0.40	5.6 Watt intermediate
Shroud	1.80	-
Lens Switch	1.00	5.6 Watt intermediate
Total	5.17	

V. SYSTEM ELECTRONICS

A. IMAGE BUFFER MODULES FOR FLIR SYSTEM (CCD)

The image buffer module in a modular FLIR will simultaneously store the parallel output of many infrared detectors as they are scanned across a scene. The stored information will then be read out sequentially from the buffer in a TV-compatible format. The successful application of an image buffer to the modular FLIR should produce advantages relative to the electro-optically multiplexed FLIR. These include:

- Controlled electronic multiplexing for compatibility with TV or data link
- Improved modulation transfer function at the system resolution frequency
- Lower cost
- Lower power consumption
- Smaller volume
- Improved line-to-line uniformity.

They will be considered in more detail in this section, along with performance differences and potential problem areas.

1. Function of an Image Buffer

The implementation of the image buffer concept in a FLIR system is shown schematically in Figure 70. The signal from each detector is ac-coupled to a preamplifier and filter. The signals are then loaded simultaneously into the memory units of either bank A or bank B during one scan of the mirror (1/60th second). During the next scan the memory units of the other bank are loaded in a similar fashion while the first bank units are read out sequentially into a video amplifier for immediate display. The sequential readout occurs in about the time of the simultaneous readin; therefore, each memory unit is read at a much higher rate than that at which it is loaded. The shortest storage time occurs for the last information bit in the first image line, and the longest time occurs in the first bit of the last image line, which is in storage during most of the 1/60th-second mirror scan and most of 1/60th-second write time of one interlaced video field. Note that a Texas Instruments FLIR typically has only about 3/4 as many lines in the FLIR system as in a standard TV display; however, the frame rates and data rates will be compatible with TV.

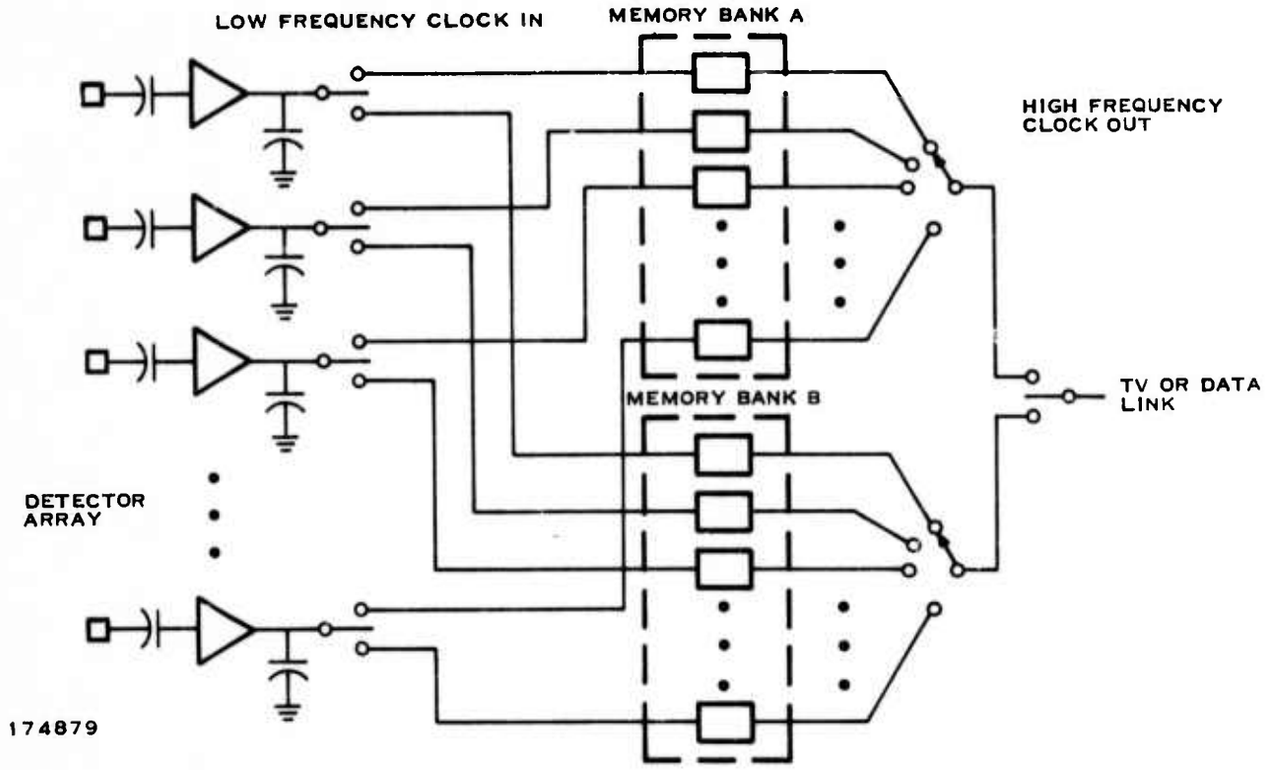

Figure 70 . Functional Layout of Image Buffer

In the present modular FLIR concept the function of the image buffer is performed by the electro-optic multiplexer. A display is created by modulating a light-emitting diode (LED) array with the video from the infrared detector array. The elements of the LED array are connected to those of the detector array in a one-to-one fashion. A visible scene is painted with the LEDs, using the back surface of the receiver scan mirror as shown in Figure 71 . To drive the LED array, an electronic video chain, as shown in Figure 72 , is required for each detector. The impact of a CCD image buffer upon the modular FLIR will be measured by the number of elements of the electro-optic multiplexer chain that can be replaced effectively. The requirements placed on the image buffer are:

60 fields/second (30 frames/second: 2/1 interlace)

60 to 180 detector lines

180 lines/field: 360 lines/frame

480 resolution elements/line

1.8 to 2.8 samples/resolution element

900 to 1,320 storage locations/line

Line storage time 0 to 33 milliseconds

Output data rate 17.3 to 16 MHz.

Note that by covering the span of 60 to 180 detectors, all classes of FLIR systems are included.

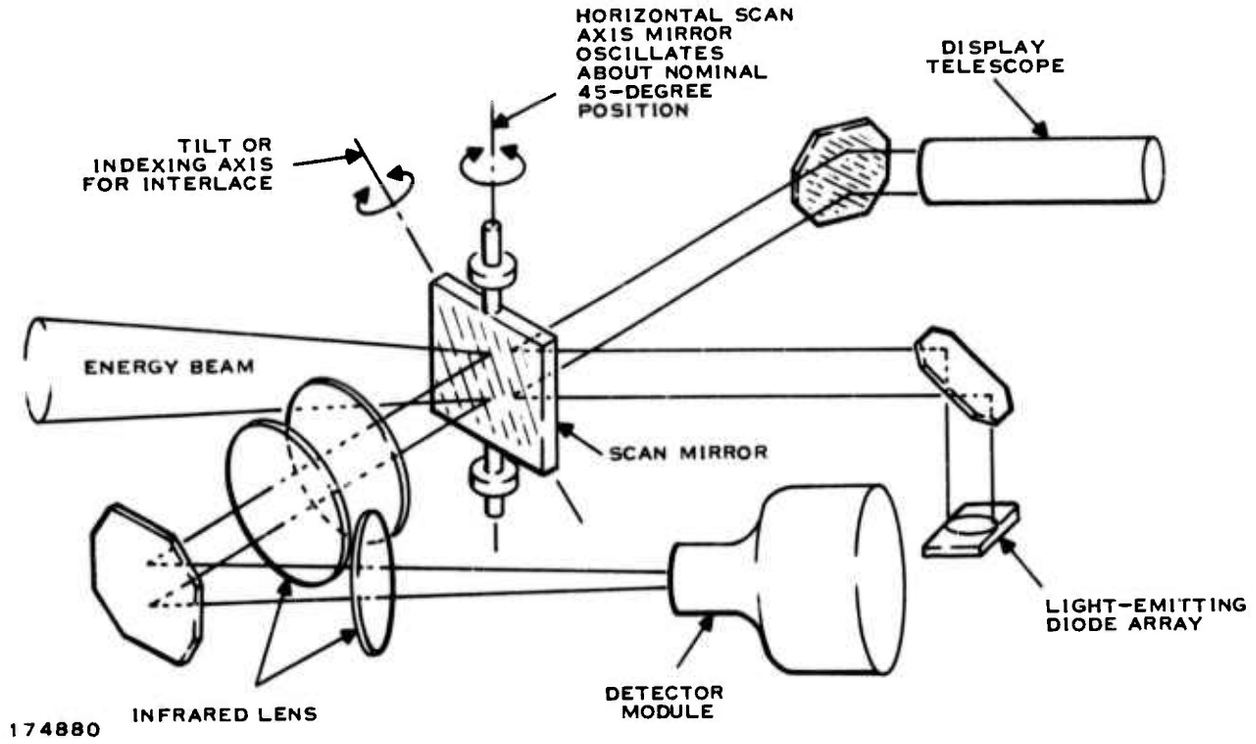

Figure 71. Schematic of Modular FLIR Scan Concept

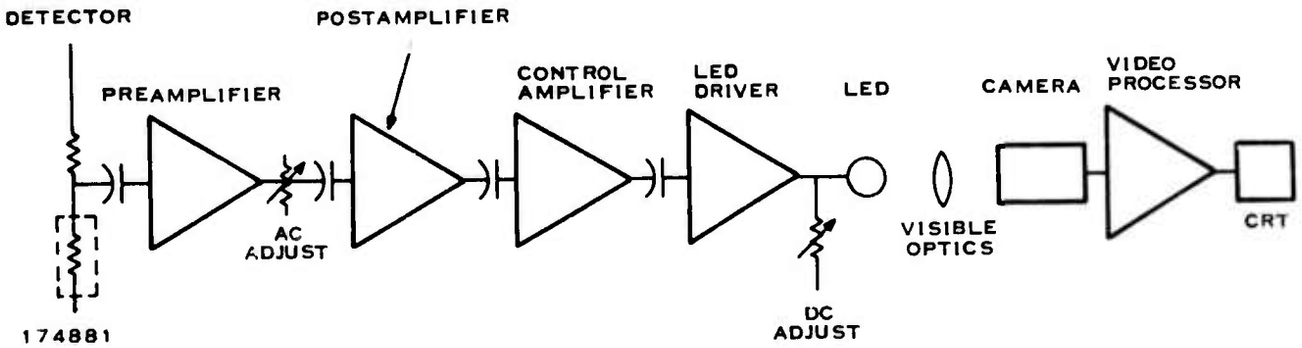

Figure 72. Block Diagram of Video Chain for EO Multiplexer

As defined, the image buffer should be a module that is line replaceable and that can be used with different CRTs and with systems using different numbers of detectors. To achieve this the module must be split into several submodules or units, just as the present modular FLIR video chain is split into preamplifiers, postamplifiers, control amplifiers, and LED drivers.

A preliminary concept of the CCD image buffer module has been defined. The units of the conceptual module, as shown in Figure 73 , are control, memory, and post conditioner. The control unit provides the timing trains for clocking the samples of analog imagery data in and out of the buffer as follows:

OUTPUT

Timing Trains

Bank selection for parallel channel read
Sample read
Memory selection for serial write
Sample write

CRT Sync Signals

INPUT

Infrared scanner sync pulses

This control unit must interface with both the infrared scanner and CRT to maintain proper synchronism in the read/write cycle. The limits of the counting logic within the unit will have to be set according to the number of infrared detectors.

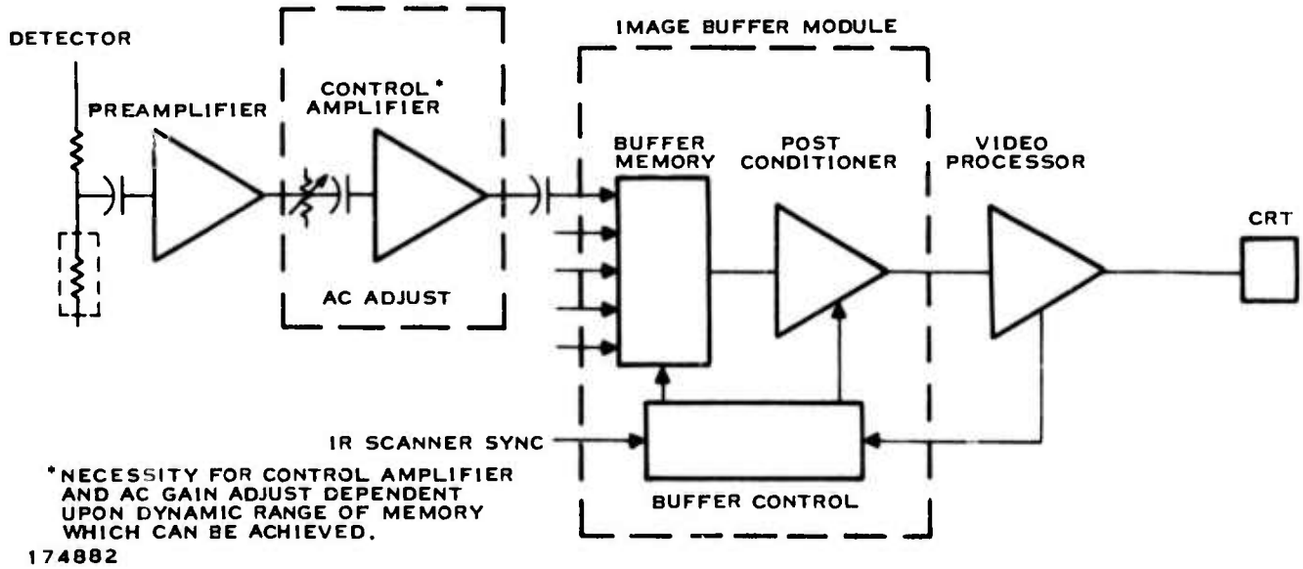

Figure 73 . Block Diagram of CCD Image Buffer Module and Video Chain

The second unit in the buffer is the memory unit, consisting of PCBs which contain the CCD memories, their drive buffers, and signal routing logic. These high-density boards will be identical; the number of detector channels will determine only the number of units required, since all routing before the PCBs is done by the control unit.

The third unit in the buffer is the postconditioner, which conditions the sampled signal prior to the final conditioning for CRT display. The CCD memory units will have different ac and dc operating characteristics, just as do the detectors and LEDs. Hence, variations between elements of the memory unit must be compensated to present a uniform display response. The advantage in the case of the image buffer over the present technique of adjustments for each channel is that the uniformity can be obtained in a single high-bandwidth amplifier. The gain and offset introduced by this amplifier will be controlled from a small digital storage unit which is addressed by the control unit.

A comparison between an electro-optically multiplexed FLIR and a CCD image buffer is given in Table XVIII.

2. Characteristics of a CCD Image Buffer

For a favorable impact on future FLIRs, the CCD image buffer module should show all the benefits itemized in the beginning of this section, with particular emphasis on improved MTF, lower power consumption, and smaller volume. These quantities are tightly interrelated in what might be termed a "design volume." For example:

> A high-density memory element package would mean smaller volume.
>
> If the highest possible MTF were desired, the power consumption would increase and the volume would possibly increase, also.

To optimize the total "design volume", there is a reasonable set of device architectures, drivers, and packages to consider.

The three basic CCD geometries, as shown in Figure 74 , are linear, serial-parallel-serial (SPS), and demultiplex-linear-multiplex (DLM). In present and future FLIR systems a large number of storage cells are required for each memory unit. Since the MTF of the device depends upon the total number of storage cells that a sample must move through, the linear geometry gives very poor performance. Examination of Figure 74 shows that in the SPS geometry a sample moves through the fewest number of cells. As expected, this device gives the highest performance. On the other hand, the DLM geometry has a simple drive circuit and requires less power for device operation than does the SPS. Initially, while the device technology was still low and individual cell characteristics were poor, the performance requirements demanded that SPS geometries be used. However, as device technology has improved, the MTF for the DLM geometry appears to be satisfactory, so that using this geometry conserves cost and power.

TABLE XXI. COMPARISON OF EO MULTIPLEXER AND CCD IMAGE BUFFER*

EO Multiplexer	Preamplifier	Postamplifier	Control Amplifier	LED Driver	LED	Visible Optics	Camera	Video Processor	CRT	Total
Signal gain	75	25 to 200	25 to 200	6						
Dynamic range (volts)	80	60	60	60			40	40	30	
Bit resolution required	14	10	10	10			6	6	5	
Power (watts)	1.6	4.8	2.2	2.2	2.7		30			43.5
Size (cubic inches)	52		140		6.5		224	17		440
Weight (pounds)	1.4		2.7		0.5		7.25			12
CCD Image Buffer				**Image Buffer**						
Signal gain	75		25 to 200	0.03						
Dynamic range (volts)	80		60	40				40	30	
Bit resolution required	14		10	6				6	5	
Power (watts)	1.6		2.2	7.7						11.5
Size (cubic inches)	52		50	284				17		403
Weight (pounds)	1.4		1.4	4.0						6.8

*Based upon a 360 IR line modular FLIR system.

- CHARACTERISTICS
  - SIMPLE DRIVE
  - LOW MTF: $\approx N_S(1-\alpha)$ WHERE N_S IS THE NUMBER OF ELEMENTS AND α IS THE CHARGE TRANSFER EFFICIENCY*
  - HIGH POWER CONSUMPTION: $\approx CV^2f$ WHERE C IS CAPACITANCE, V IS CLOCK VOLTAGE, f IS CLOCK FREQUENCY

*CTE DEGRADES WITH FREQUENCY

(A) LINEAR GEOMETRY

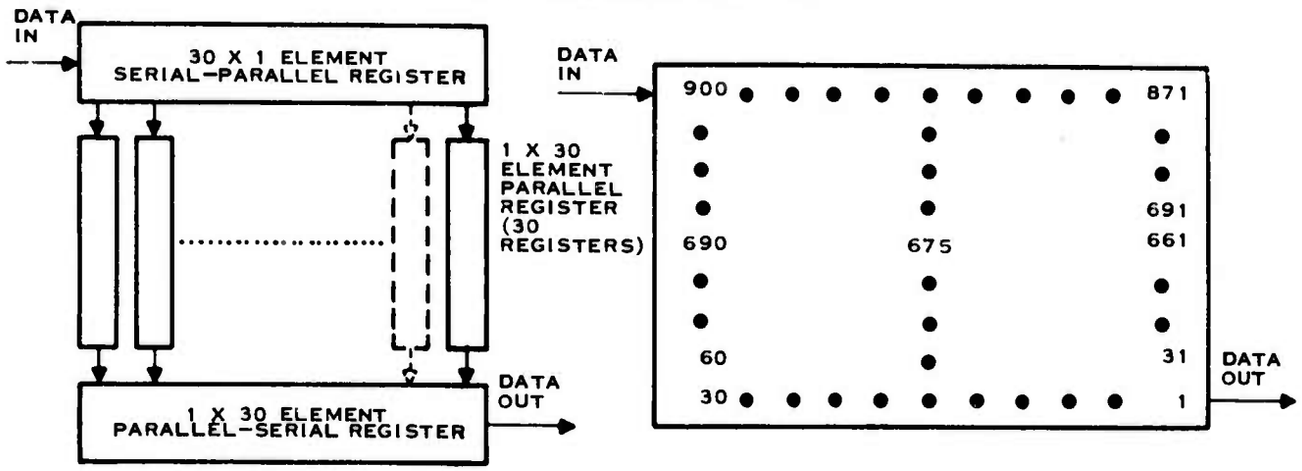

- CHARACTERISTICS
  - COMPLEX DRIVE
  - EXCELLENT MTF
  - MODERATE POWER CONSUMPTION

(B) SERIAL-PARALLEL-SERIAL (SPS) GEOMETRY

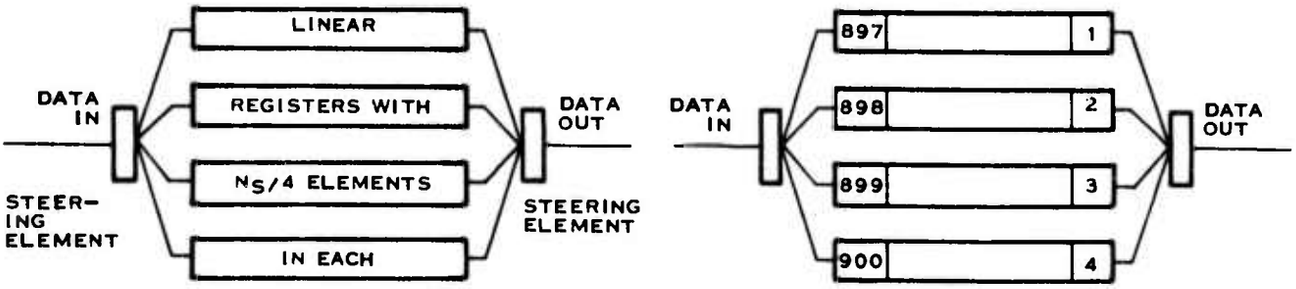

- CHARACTERISTICS
  - SIMPLE DRIVE
  - GOOD MTF
  - LOW POWER CONSUMPTION

174883 (C) DEMULTIPLEX-LINEAR-MULTIPLEX (DLM) GEOMETRY

Figure 74 . Basic CCD Geometries

Packaging is the other key element which affects the "design volume". At the present time, each CCD is in a separate package, resulting in the need for as many packages as there are infrared lines. This first possible packaging option is shown in Figure 75. The options are given in terms of the DLM geometry and CMOS drivers. The first two options involve increasing the number of CCDs per package. This will have relatively little impact. The greatest system impact will be felt in options III and IV which are hybrid packages; here the CMOS buffers, channel logic, and CCDs are on separate chips but in the same package. The actual impact of these and other characteristics of CCD image buffers will be discussed in the remainder of this section.

a. Performance

A standard measure of FLIR system performance is the modulation transfer function (MTF) which is related to the attenuation of signal frequency components. The system MTF is the product of all component MTFs. The CCD image buffer replaces the LEDs and the TV vidicon. In general, the image buffer will have a higher MTF than the replaced components. Figure 76 shows this for one possible system in which all other MTFs are assumed unchanged. However, before this and other potential benefits can be realized, solutions must be found to some problems that arise in connection with the use of CCDs. The effect on performance will be considered here. The present status and progress made on eliminating the sources of these effects is treated later.

(1) Ghosts

A single line of imagery from a detector can be stored by CCDs in parallel channels instead of a single linear shift register. When this is done, the charge transfer inefficiency (the small amount of charge left behind on each transfer) causes ghosts to appear. The separation between an object and its ghost is inversely proportional to the number of parallel channels, and the strength is proportional to the charge transfer inefficiency. The waviness of the MTF curve in Figure 76 corresponds to a ghost appearing about 15 resolution elements from the source, but with an amplitude less than 2 percent of the source. As will be discussed in Subsection II.C., the device technology is developing to the point that ghosting has ceased to be a major consideration in module design.

(2) Shading

Dark current in CCDs causes a buildup of charge in each storage bin. The magnitude of this false signal depends upon the storage time. Since storage time in the CCD buffer depends on the location of the particular resolution element in the TV display, brightness will vary from left to right and from top to bottom, with the brightest area in the upper righthand corner. If dark current can be reduced below about 10 nA/cm^2, it should no longer be a problem. As discussed in Subsection II.C., results from other programs indicate that this will be achieved by mid-1974. The uniform variation across the display should also lend itself to compensation or cancellation techniques.

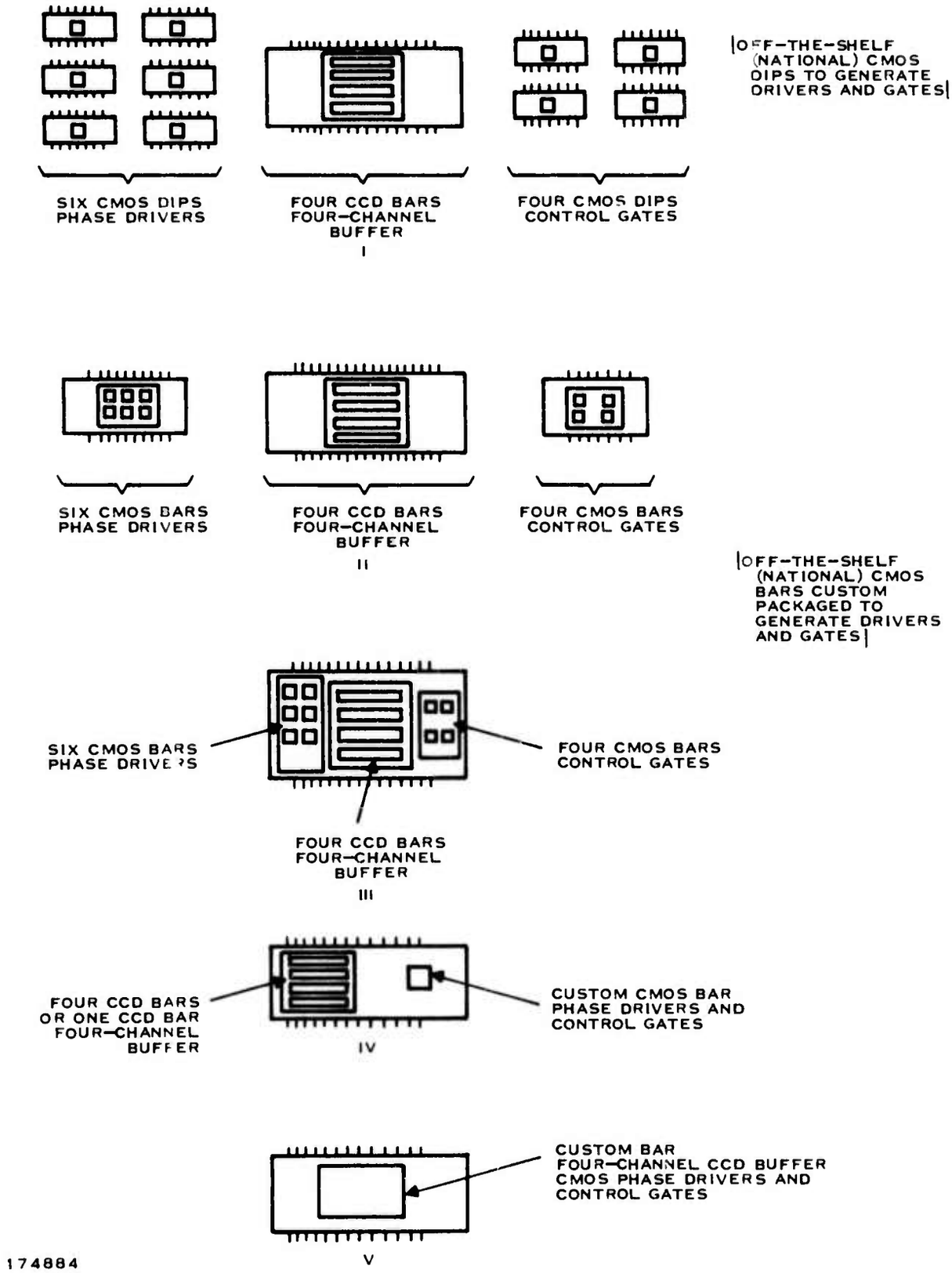

Figure 75. Packaging Configurations

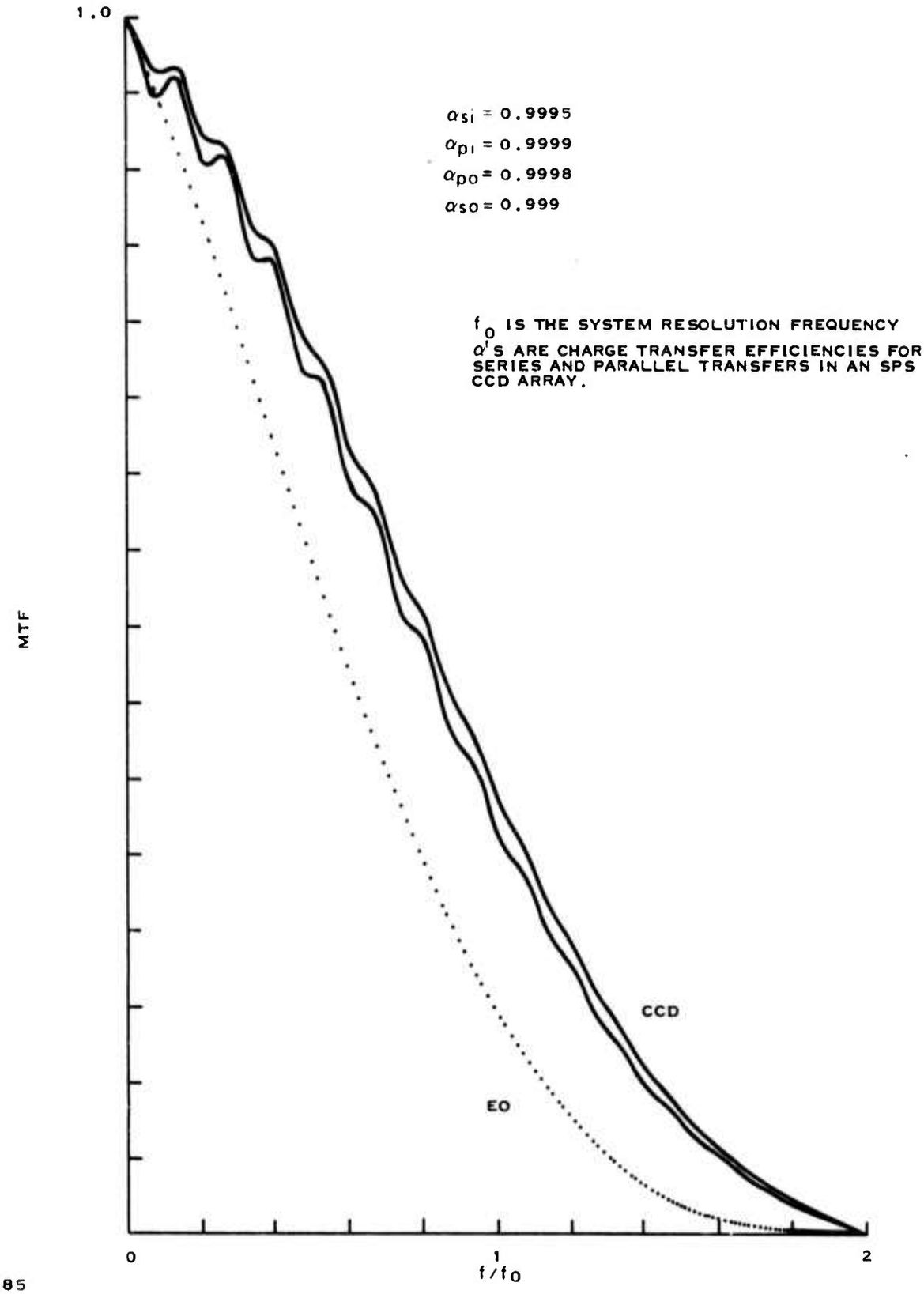

Figure 76. System MTF

(3) Line-to-line Uniformity

One of the persistent problems associated with the present FLIR is variations in brightness from line to line caused by drifting of components, primarily detectors and LEDs. While the worst offenders, the LEDs, are eliminated in the image buffer approach, some drift will still be apparent, in addition, there will be a line-to-line variation caused by differences in dc offset at the output gate of each CCD as a result of nonuniformity of the precharge from MOS transistors. Since the dc variation is on the output of each CCD, it will show on a display as a step at the raster frequency. At the present time, most devices have a dc error which falls within ±200 mV, while the ideal requirement is ±0.2 mV. Most of this factor of 1,000 probably can be gained by modifications on the memory chip, namely a differential sample-and-hold circuit on the output of the CCD. However, to ensure that this is not a problem, a dc restoration network will be introduced in the postconditioner unit of the image buffer module.

An automatic gain normalization technique is also being considered, for ensuring line-to-line uniformity. In this technique the signals from each line, after multiplexing, will pass through a video amplifider with automatically adjustable gain. The gain for each line will be stored in a digital memory that can be updated in a calibration mode by the operator.

(4) Field Registration and Linearity

Any nonuniformity in the scan mirror motion will show up as a shifting of the scene from field to field; in addition, nonlinearity in the scan will distort the image. Such scan nonuniformities were automatically compensated in the modular FLIR by viewing the LEDs from the back side of the scan mirror. Some compensating technique will have to be devised if this proves to be a significant problem.

(5) Scan Efficiency

The scan efficiency of the modular FLIR is relatively high, since both sweeps of the oscillating mirror are used. To be TV-compatible, each field of 180 lines must be read from left to right. To do this for data collected by an oscillating mirror, it would be necessary to use only the left-to-right motion of the mirror, which would automatically cut scan efficiency in half. This could be partially compensated by mechanically decreasing the flyback time, but only at the expense of a somewhat more complex scan mirror drive.

An alternative method would be to read data in on both the forward and reverse scan, as is now done, but to read data entered in the CCD image buffer on the reverse scan with an inverse readout. The first analog sample stored would be the last one read out to the video amplifier. This would aggravate the shading and uniformity problems caused by charge transfer inefficiency, since the first sample would be transferred twice as many times, while the last sample would be stored a shorter time and undergo only two transfers. The magnitude of this problem depends upon the final values of CTE (which will be "state of the art") and the geometry selected. The tradeoffs involved in the display uniformity problem for two-way scan will be the key items in the module concept design in this proposed program.

b. Packaging

Packaging is discussed from the point of view of a high-performance FLIR which contains 180 detectors. The packaging values apply to both options III and IV in Figure 75, that is, the hybrid packages. The only difference between the two hybrid packages is that the standard CMOS bars have been replaced by a custom design and the analog switches have been replaced by on-chip differential sample-and-hold networks. Hence, package size will not be materially affected by this change, and the two hybrid options are equivalent from the point of view of packaging. Preliminary data indicate that satisfactory results can be obtained from state-of-the-art devices. (Refer to Subsection III.C on drive circuitry.)

The three units in the CCD image buffer module are the control, memory, and post conditioner. These units are defined in Figure 73. The three units can be placed on three single-layer and 13 two-layer printed circuit boards. The boards will plug in to a four-layer motherboard. The manner in which the boards may be laid out is outlined for illustration only. All designs and conclusions are tentative.

(1) Control Unit

This unit can be on two of the single-layer PCBs and will provide the signals for the DLM geometry. These are described in Table XIX. Note that the clock lines to the CCD are only in a single unit form, while the actual shift pulses for the CCDs must be in a four-phase format which is the same for all CCDs in a given bank. However, in terms of space, cost, and complexity it is more advantageous to repeat the four-phase formatting in a buffered fashion in the actual memory package.

TABLE XXII. LINE DEFINITION OF CCD CONTROL UNIT

Item	Number of Lines	Function
Field Select	2	Determines which bank of CCDs is being used in the low-speed input mode or high-speed output mode.
Low-speed clock High-speed clock	2 2	Two-phase signals used in the memory unit to generate the four-phase shift pulses, the multiplex pulses, and the precharge pulses. Low speed is for parallel read and high speed is for serial write.
Board address	4	Activates the board in the output bank that is needed at that time.
CCD address	5	Activates the CCD that is needed for serial output at that time.
Sync generator		TV sync signals.

(2) Buffer Storage

The CCD memory units may be packed four per package, eight packages per printed circuit board. A single board layout is shown in Figure 77. The small packages on these two-layer boards are for the board activation and CCD selection (i.e., steering). The larger packages contain the memory elements and are laid out for the two hybrid options as shown in Figure 78. The required spacing of the packages is 2 inches by 1 inch. Each individual package will require 16 pins as given in Table XX . The CMOS chips inside the package will generate the required timing trains from the high- and low-speed clocks. These include: the four-phase clocks for shifting during the readin and readout, the phase multiplex pulses, and the high- and low-speed precharge pulses. The CMOS control gate will route clock signals to the proper device, and the analog switches will multiplex the CCD video output into a single-line video signal. Note that the number of CCDs on the board is 32, which is a power of 2. This simplifies switching or steering on the board and, in addition, simplifies the layout of both the memory boards and the motherboard. If it were desirable to reduce the size of the board, it should be split in half to give 16 CCD memories per board. The number of steering packages would be reduced to three.

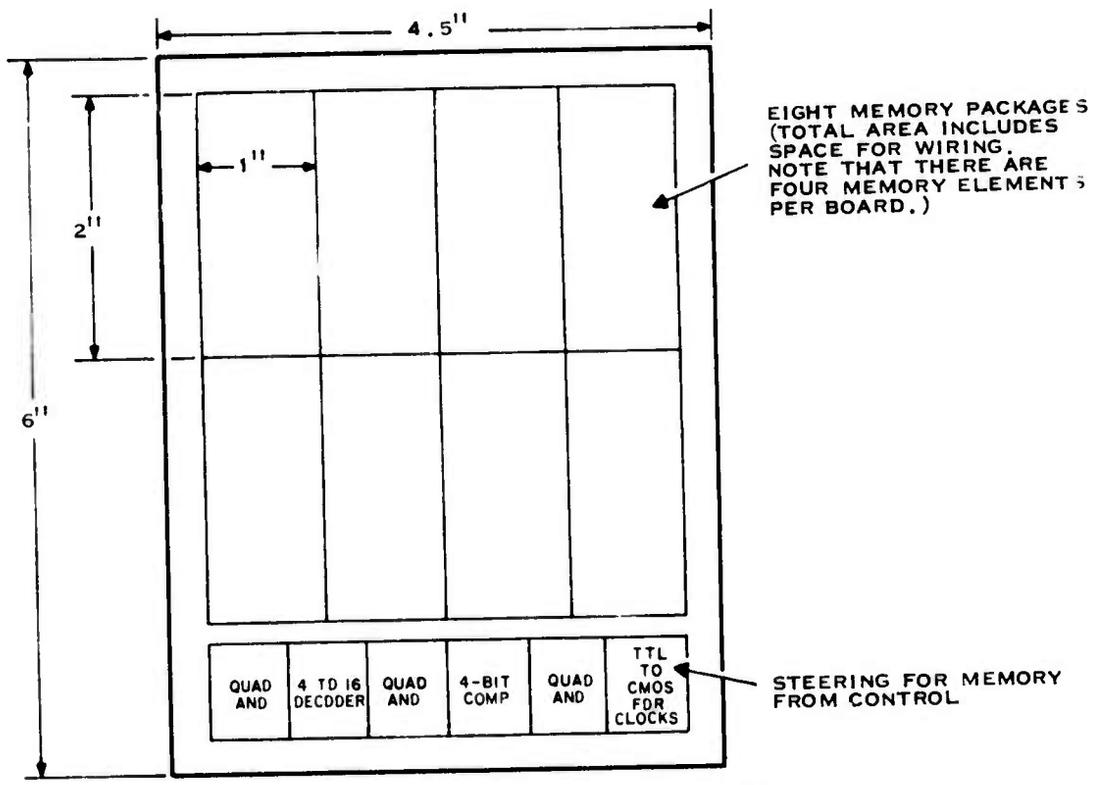

Figure 77. PCB Layout for CCD Memory Unit (32 Elements per Board)

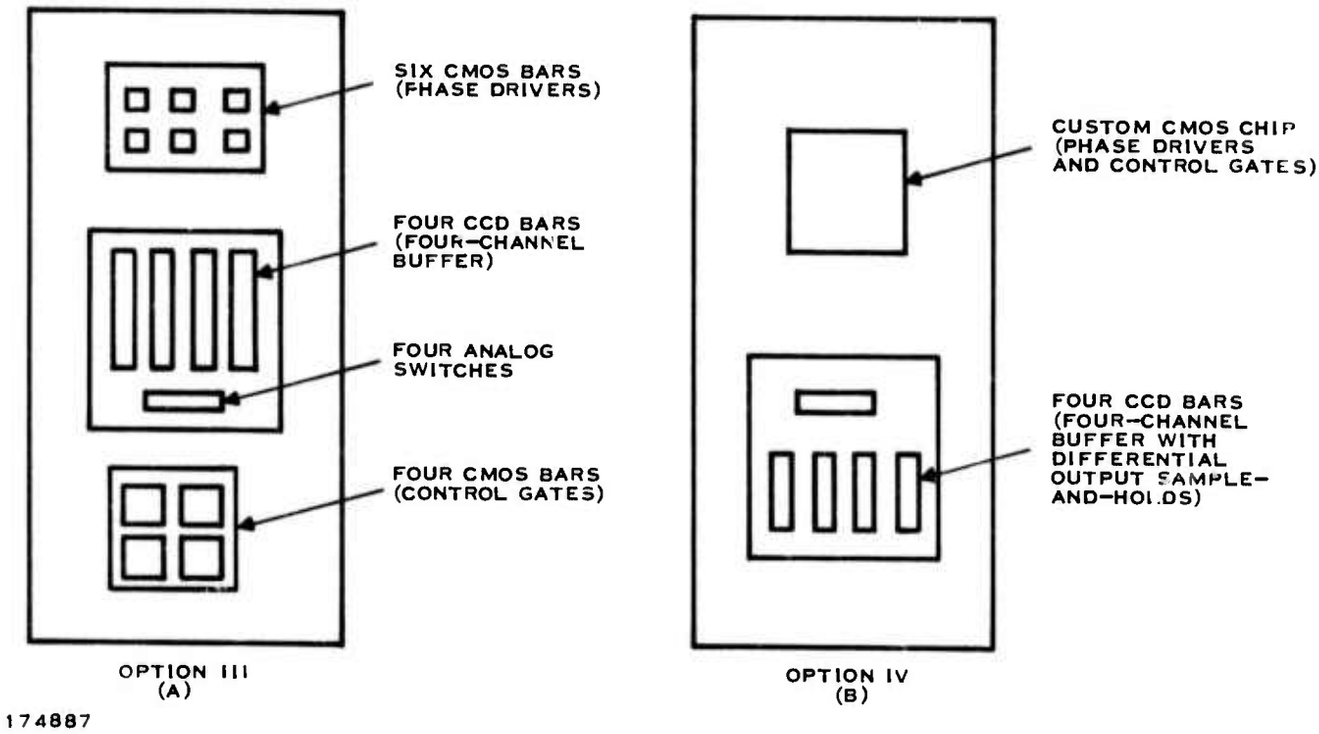

Figure 78. Details of Options III and IV for CCD Memory Units

(3) Post Conditioner

This unit can be on a single two-layer PCB. It should contain the stored values for the gain and offset normalization, a D/A converter, an A/D converter, and a wideband amplifier for controlled gain and offset. This will satisfy the conditions discussed under the topic of line-to-line uniformity.

TABLE XXIII. PIN REQUIREMENTS FOR MEMORY PACKAGE

Item	Number of Pins
Video Input	4
Video Output	1
Sample Clock (High or Low Speed)	2
Device Select	4
DC Bias Voltages	5
Total	16

(4) Volume

The volume of the CCD image buffer is dominated by the memory unit boards. The size of the boards, as discussed previously, has been assumed to be 4.5 by 6 inches. A conservative depth is 0.6 inch. The control unit can be easily placed on two boards, and the post-conditioner unit can be placed on one board of the same size. The total length is therefore:

Length = [2(control) + 1(post conditioner) + 12(Memory)] *0.6 inch

= 9 inches

Note that this gives a potential of 384 infrared lines.

The total volume must include the motherboard. This board will occupy a volume of 4.5 inches by 1.0 inch by the length, giving a total package size of

Volume = (4.5 inches) X (7 inches) X (9 inches) = 283.5 cubic inches.

This is illustrated in Figure 79.

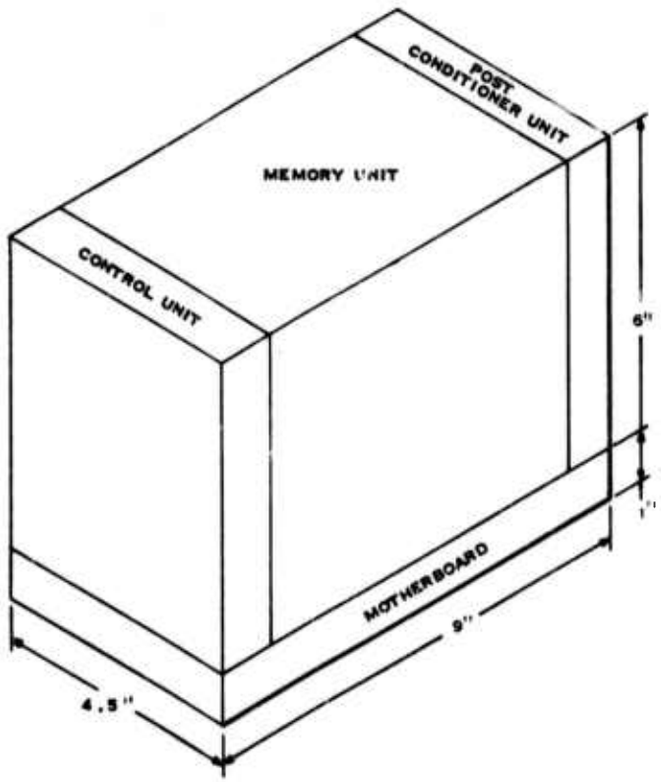

174386

Figure 79. Illustration of CCD Memory Module

c. Power

The power dissipated in the control and the post-conditioner units can be estimated very well, since these units are off-the-shelf devices and, in addition, the actual power consumption has been measured for some of the subassemblies. The ratings are:

Control unit	2.7 watts
Post conditioner	2.8 watts

The key factor for examination here is the memory unit. Only option III has to be considered. There will be a moderate reduction in power for option IV because of reduced stray capacitance, but this will not be significant. In option III the power will be dissipated in the CMOS circuitry and the CCDs which are capacitive loads. Hence, the power can be split into:

Standby power for the CMOS

Dynamic power for the CMOS

Dynamic power for the CCDs.

Using this format, the CMOS dynamic power is based upon a lumped device capacitance. In the case of the CMOS chips, all values are based upon off-the-shelf data values which, in critical cases, have been confirmed by experimentation. The CCD values are worst-case estimates based upon preliminary analytical and experimental results.

The CMOS power includes not only the dynamic and standby components, but also the steering required on each memory unit board and each package on the board. The total power breakout is given in Table XXI. The memory unit is rated at 1.8 watts, giving a total power dissipation rating for the module of 7.7 watts.

d. Cost

The cost of the CCD image buffer module will be estimated on the basis of several key assumptions:

Processes for fabrication of the devices are established

Photomask for the devices and PCB are available

No meaningful learning curve can be applied to the CCD packages until a dedicated pilot line production facility is defined.

With these assumptions as a guideline, preliminary estimates indicate some cost savings over the standard electro-optically multiplexed FLIR.

TABLE XXIV. POWER DISSIPATION IN THE CCD IMAGE BUFFER MODULE

a. Memory Unit

Item	Units	Power/Unit (mW)		Power (W)		Power (W) Total
		Standby	Dynamic	Standby	Dynamic	
On-board steering	No. of units	0	0	0	0.03	0.03
On-board Translator (high-speed)	1 board	10	70	0.06	0.07	0.13
On-board translator (low-speed)	No. of boards/2	10		0.06	0	0.06
Low-speed driver (four-phase)	No. of detectors	0	0.45		0.08	0.73
Low-speed precharge	No. of detectors	-		-		
Low-speed CCD load	No. of detectors	-	0.07	-	0.12	0.12
High-speed driver (four-phase	1	-	500	-	0.50	0.68
High-speed output circuit	1	-	300	-	0.30	0.30
High-speed CCD load	1	-	80	-	0.08	0.08

b. Total for Module (watts)

Control	2.7
Memory	2.2
Post Conditioner	2.8
Total	7.7

e. Compatibility

It is desirable that infrared scanning systems be TV compatible. To a certain extent this is a problem area in the image buffer design, and several options are available. This is true especially for systems with a limited number of detectors (40, for example). The CRT displays with which these systems must interface write in 525-line or 875-line format with a one-way scan and a 2:1 interlace. According to the EIA standards, the buffer must provide data for 92.5 percent of the formatted lines, that is, 485 or 809 lines, respectively. However, it is possible for some of those lines at the edges of the display to be blanked with a uniform signal level corresponding to an average grey shade of the scene.

Since the FLIR module contains a maximum of 180 detectors, resulting in 360 IR lines of video, the buffer must either blank areas of display, and/or write more than one CRT line per IR line of video. To illustrate this situation, a direct approach has been outlined in Figure 80. An examination of this figure reveals that:

There are regions of detector array sizes where rather large areas of the display must be blanked. For example, while the output of 121 detectors can be written twice per field to fill a 525-line CRT, a system with more than 122 detectors can be written only once per field if all of the scene is to be presented. This results in large blank areas on the CRT.

The IR information from the IR scan field B becomes available for CRT display one field period late, yet in every case except the first one, the IR fields are mixed in a CRT field. This means that a delay of at least one field is required to present the IR data on the CRT in the proper position.

For optimum use, the CCD must be completely filled with IR information before it is clocked out. Once it is addressed for high-speed output it is lost for low-speed input until emptied.

In the first case shown, one CCD is required for each CRT line in the frame. This is also true for the other cases unless some technique is developed, such as allowing the output of the CCD to feed its own input during the high-speed write.

In the cases where there are two, three, or four CRT lines per IR line, the number of cells required for storing a single IR line decreases in a corresponding fashion.

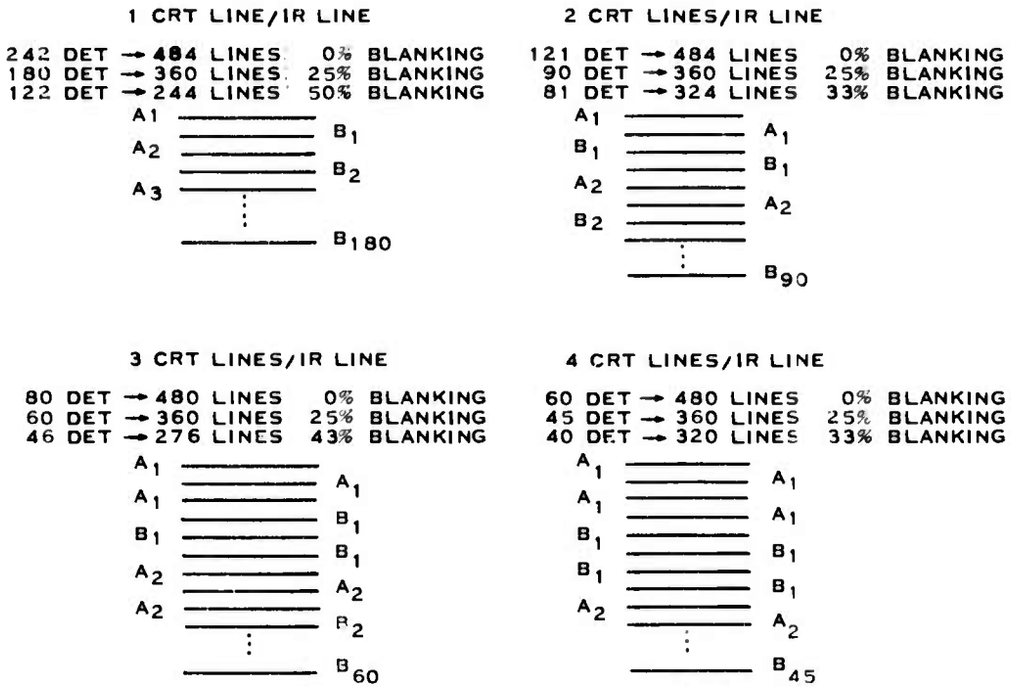

174889 (A AND B STAND FOR IR FIELDS, LEFT AND RIGHT FOR CRT FIELDS AND NUMBER FOR IR DETECTOR)

Figure 80 . Line Sequence for Writing IR Lines on CRT in a 525-Line Format

The latter point means that a smaller memory element could be used in some cases. In the first case of one CRT line per IR line, a minimum of 960 cells is required in each memory element. If a standard cell size of 1,024 is used, then case 2 would require only a 512-cell element, etc. On the other hand, the 1,024-cell element could be filled with information from successive IR frames. For the cases of one and two CRT lines per IR line, the number of memory elements remains the same; the only difference is in the size of the memory element. This can be seen by examining the case of two CRT lines per IR line, as shown in Table XXII. Note that in case 2, four banks of memory elements are required, with each bank containing 90 memory elements. The only difference is that when the optimum cell size of 512 cells per element is used, the information is reloaded into the same CCD memory element. There is no decrease in number of CCDs, compared with the 1,024-cell memory element. However, when three or four CRT lines are required for each IR line, the number of elements, and therefore memory boards, does decrease. This is summarized in Table XXIII. Note that the power does not change very much, since in an optimized control very little of the power is consumed in the CCD itself.

TABLE XXV . TIMING FOR CCD MEMORY BANKS FOR CRT DISPLAY

Case 1: 1 CRT Line/IR Line

IR field number	1	2	3	4	5	6
IR field designation	a	b	a	b	a	b
Load banks (180)	A	B	A	B	A	B
Dump banks		A	B	A	B	A

Case 2: 2 CRT Lines/IR Line With Reload for Second CRT Field

IR Field number	1	2	3	4	5	6
IR field designation	a	b	a	b	a	b
Load banks (90)	A	B	C	D	A	B
Dump banks			(A,B)	(A,B)	(C,D)	(C,D)

Case 2: 2 CRT Lines/IR Line With 2 Fields Loaded in Each Memory Element

IR field number	1	2	3	4	5	6
IR field designation	a	b	a	b	a	b
Load banks (90)	(A/2)	(A/2)	(C/2)	(C/2)	(A/2)	(A/2)
Load banks	(B/2)	(B/2)	(D/2)	(D/2)	(B/2)	(B/2)
Dump banks			A	B	C	D

TABLE XXVI IMAGE BUFFER REQUIREMENTS FOR A CRT IN A 525-LINE FORMAT

Number of Detectors*	CRT Lines per IR Line	Active CRT Lines	Field Delay		Memory Boards		Power (Watts)	
			1,024	Optimum**	1,024	Optimum	1,024	Optimum
243	1	485	1	-	16	-	8.6	-
180	1	260	1	-	12	-	7.7	-
122	2	486	2	2	16	16	7.6	7.4
90	2	360	2	2	12	12	6.8	6.6
81	3	486	-	2	-	11	-	6.8
60	3	360	-	2		8	-	6.2
62	4	486	4	2	16	8	7.1	6.4
45	4	360	4	2	12	6	6.3	6.1

* For each value of the ratio CRT lines/IR line, the two values for number-of-detectors bracket the usable range of values for the number of active CRT lines.

** In this case, optimum means "for the minimum number of cells in the memory element," which here amounts to 1,024, 512, 342, and 256 cells for the various values of the ratio CRT lines/IR line.

It would be very desirable to have a standard package in the image buffer memory which would handle all cases. However, as Table 2-6 shows, this presents problems for the systems which have a small number of detectors. At the same time a high degree of standardization can be achieved. Four element sizes are called out in Table XXIV. These elements have exactly the same architecture, with only the size of the device varying. Also, the same CMOS chip will handle every case presented, as will the PCB itself. Other advantages of using four different CCD sizes is that two-way scan becomes more feasible, and dark current is less restrictive. Hence, these factors must receive the most emphasis in the concept design.

3. Status of CCD and Interface Development

Dark current and charge transfer inefficiency are two CCD parameters that can adversely affect image quality if they are not held within tolerance. Dark current can produce a gradual change in brightness across the display; if the dark current varies markedly from cell to cell within a CCD, it will add noise to the displayed image. Charge transfer inefficiency reduces the MTF of the system and can produce ghosts in parallel channel CCD configuration. In addition, variations of these characteristics from device to device create variations in brightness and contrast between display lines.

The interface to the CCD consists of control circuitry and input/output circuitry. Both of these areas are critical, because of the high frequency of operation required for the CCD in the memory dump mode of operation. If the high-frequency clocks for driving the CCD cannot be maintained at the proper voltage and in proper phase relationships, the device dynamic range and MTF will suffer severely.

a. Dark Current

The effects of dark current on image quality are twofold. A uniform level of dark current in each of the resolution elements of a CCD produces a gradation of brightness from one end of the resulting scan line to the other. In addition, variations of the dark current from one cell to another in the CCD produce smaller-scale variations in brightness and contrast along the scan line and between neighboring scan lines; these variations add to the overall system noise.

The present status of the dark-current effort is indicated by Table XXIV. which shows the average levels of dark current as obtained from each of the 900-element CCD devices on a typical recently processed slice. Note first that two of the 10 devices were lost in the bonding process. One device showed blocked channels and could not be measured further. Of the seven remaining, five showed values of dark current that were closely grouped around 75 to 80 nA/cm^2. This is now a fully typical result of the current processing capability; thus, the present status is that a good and fairly consistent yield can be obtained at the level of 75 to 80 nA/cm^2. The ultimate goal is 2.5 nA/cm^2, which can reasonably be expected to be achieved within a year. The following paragraphs explain the impact of these values.

The maximum density σ_{max} of charge that can be stored on a CCD is about 8×10^{-8} C/cm^2. This corresponds to a full well. Let F be the fraction of a full well that is actually available for use in a reasonably linear range of operation. If a dynamic range capability R is to be maintained, then the worst case integration of dark current must be less than the minimum charge density that is to be resolved. This minimum density corresponds to (1/R) X (the maximum density). Thus, $\dot{\sigma}_{dark} \Delta t \leq \sigma_{min} = \sigma_{max} F/R$.

As charge packets are being loaded into a CCD, dark current is accumulated by each packet already within the CCD. During the load phase, the location of each individual packet is constantly changing. After the loading is complete, at the end of the forward scan, the entire array of packets is held in place during the entire back scan, and during some fraction of the next forward scan, until it is time for the particular CCD to be dumped. Thus, the charge packets are moving through the CCD array for about 1/120 second = 8 milliseconds and, in the extreme case, are being held in place for about 1/60 second = 16 milliseconds.

As long as the charge packets are on the move during the loading phase, it is reasonable to assume that the dark current accumulating in the charge packet is essentially the average value of the dark current for the entire CCD. Thus, by the time the last packet of charge is loaded in, the first packet has accumulated dark current in the amount corresponding to the charge density $\dot{\sigma}_{dark,av}$ X 8 milliseconds. Since increasing charge in the packet corresponds to decreasing brightness in the corresponding CRT picture element, this implies that the left edge of the resulting scan line will be darker by just this much charge density. If this darkening is to be kept to less than the minimum resolvable signal level on the display, then

$$\dot{\sigma}_{dark,\,av} \times (8\ ms) \leq \sigma_{min} = \sigma_{max} F/R$$

The value of the dark current can vary significantly from one cell to another within a CCD. Thus, the charge accumulated by the individual charge packets in a CCD during the hold phase will vary correspondingly, leading to variations in brightness and contrast between neighboring picture elements on the CRT. These variations can occur between picture elements on the same scan line or between neighboring scan lines. If the effect of these variations on the resulting CRT display is to be kept to within the required resolution of the system, then the extreme range of variation, $2\Delta\dot{\sigma}$, of the dark

TABLE XXVII. TYPICAL YIELDS FROM CURRENT CCD PROCESSING

Device No.	Mean Dark Current (nA/cm^2)	Remarks
20-3-1		Lost in bonding
-2		Lost in bonding
-3	72	
-4	40	
-5	75	
-6	80	
-7	85	
-8	160	2 bad current spikes Blocked channels
-9		
-10	77	

current within a single CCD must be kept within the limit given by

$$2\Delta\dot{\sigma}_{dark} \times (16\ ms) \leq \sigma_{min}$$

Let F = 80 percent, then

$$\dot{\sigma}_{dark,\ av} = 8 \times 10^{-6}/R = 8{,}000\ nA/cm^2/R$$

$$\Delta\dot{\sigma}_{dark} = 2 \times 10^{-6}/R = 2{,}000\ nA/cm^2/R$$

These relationships are shown in Figure 81. For the typical average value of dark current (as quoted above) of 80 nA/cm^2, the available dynamic range is nearly 100, or 40 dB. Note, however, that to maintain this level of dynamic range, the extreme variation of the dark current from this average value, considering all the cells of the CCD, must be kept less than $\pm 20\ nA/cm^2$.

As long as the condition on the extreme variation is met for each CCD in the buffer, variations in the average value of the dark current between one CCD and another will be cancelled out by the operation of the dc restorer, since the group of calibration charge packets will integrate the average value of the dark current just as do the following 900 signal packets.

To illustrate the dark-current effects, photographs of some typical CCD outputs are included. These dark current data were obtained for the fixed frequency test unit for SPS devices. This test unit loads the SPS at a fixed frequency, stores the signal for a time interval adjustable from 0.3 to 30 milliseconds and then dumps the signal at the same frequency at which it was loaded. While this test unit is restricted to clock frequencies of less than 2 MHz, it does allow for detailed studies of dark current and nonuniformities in cell transfer efficiency.

In Figure 82(A), the output is shown for a device with an 80 nA/cm^2 dark-current value. The time periods of 16 milliseconds storage are indicated. Note that the signal is a rectangular pulse with a width which is 1/15 of the total 960 SPS storage elements. In this particular test unit, the load and the dump are equivalent, and the small square-wave signal which occurs in the output is a characteristic only of the clock in this particular test unit. To see the effects of the dark current, the voltages at the front and back of the dump cycle should be compared, since dark current will cause a ramp to be generated. A closer examination of a single line is shown in Figure 82 (B). The total ramp effect is less than 3 percent, which is roughly consistent with the above analysis.

A further expansion of the time base allows examination of dark current nonuniformities. An example is shown in Figure 82 (C) where small ripples can be seen in the output. Note that the points indicated as feed-through spikes are caused by parallel-clock pulses; these spikes are to be suppressed by improved circuitry techniques.

It should be noted that the indicated state-of-the-art values for CCD dark current were measured at room temperature, and that dark current values double with each temperature increase of about 8°C. Thus, a dark-current goal

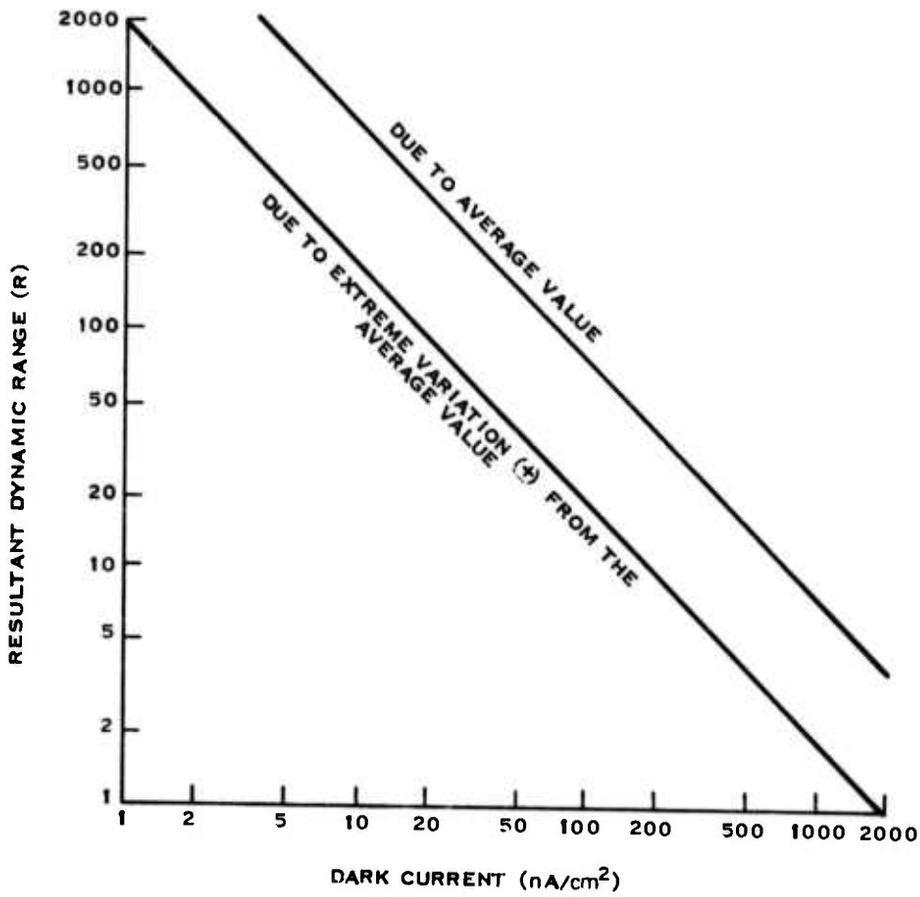

174890

Figure 81. Dark Current in the CCD and the Resulting Dynamic Range Available in the Image Buffer

of 2.5 nA/cm^2 has been set. It is believed that this level can ultimately be obtained.

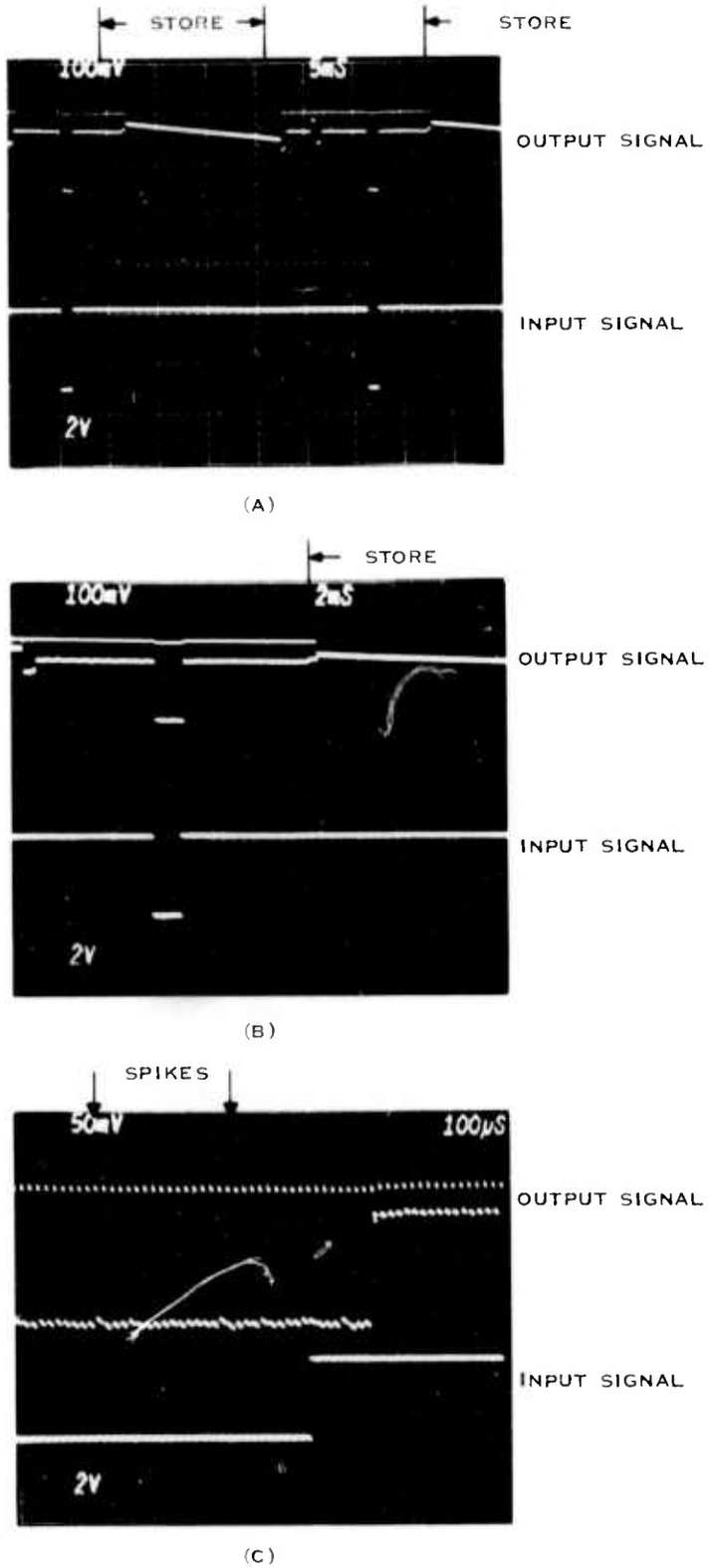

Figure 82. Signal From SPS Device Which Has 80 nA/cm^2 Dark Current

b. Charge Transfer Efficiency

A low value of charge transfer efficiency (CTE) causes a dispersion of the signal as the charge packets of the signal move through the CCD. This lowers the system MTF, especially at the higher spatial frequencies. The CTE is itself a strong function of clock rate frequencies; this means that the critical factor in the SPS device is the CTE for the output serial register. The present status of the CTE is demonstrated in Figure 83 . These data were obtained on the high-frequency serial test unit, which clocks the serial registers at a high frequency. This unit is used for evaluating device CTE and high-frequency clock circuits.

In the example shown in Figure 83 , an SPS is clocked at 12 MHz. The input waveform is a 3-volt square wave, 1 μs long. The 3-volt step level at the input shows at the output as a 0.25-volt step with sharp rise and fall. The constant level voltage in, before and after the pulse, transforms to a constant level of signal voltage out, with no discernible variation in voltage out.

The magnitude of CTE in the serial register can be crudely but quickly estimated from this type of demonstration. For a step function, the loss in the leading pulse, relative to the steady state, is related to the CTE by

$$\Delta V/V = N_S N_p [1 - (CTE)]$$

where N_s = number of cells = 30 for the serial array of the SPS

N_p = number of phases per cell = 4.

Hence for (CTE) ≥ 0.999, $\Delta V/V \leq 0.012$. While this one percent variation is not discernible from the photograph, it has been determined that CTE at 12 MHz is greater than 0.999, which is acceptable for FLIR operation.

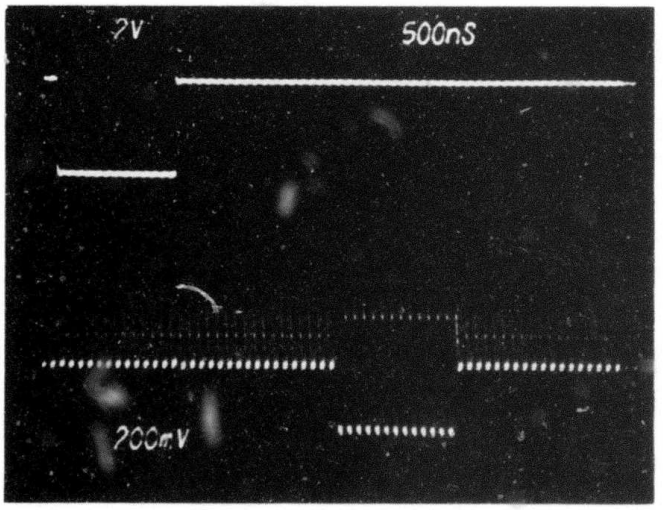

174892

Figure 83 . Output of the Serial Register of SPS at 12 MHz

c. Input-Output Circuitry

The two main functions of the input-output circuitry for use with the CCDs are

> To provide the interfaces between the CCDs and the rest of the system, to allow optimum performance of the entire system.
>
> To provide automatic compensation for variations in characteristics between one CCD and another, so that line-to-line variations are minimized.

Providing the interfaces is relatively easy, since the signal amplitudes and impedance levels seen by the CCDs can readily be adjusted by the existing circuitry in the system. Providing automatic compensation is more difficult, and special circuitry is being added to the image buffer to achieve this purpose.

The best method for injecting the signal into the CCD is to pulse the input diode and to apply the video signal to the input gate. In this way, the amount of charge injected into the CCD is kept independent of the threshold variations. Bias voltage is dc-coupled to the CCD, biasing the CCD into its linear range. The video signal from the last amplifier in the detector chain is capacitively coupled to the same point. This is shown in Figure 84. The maximum amplitude of the video signal is about half of the clock voltage when the CCD is biased to the center of its maximum range. In this way, both the bias voltage and the input signal level are adjusted for optimum performance and are independent of variations from device to device. Thus, both purposes are served for the input circuitry.

The output circuitry is more complex, because it is at the output stage that variations from channel to channel, both in dc offset and in system gain, are to be compensated for. This is achieved by two special circuits: a synchronized dc restorer circuit that cancels the variations in the dc offset and in the average dark current, and a gain normalization circuit that automatically compensates for variations in channel gain. The restorer circuit is shown in Figure 84, while the gain normalization circuit is shown as following directly after it along the signal path.

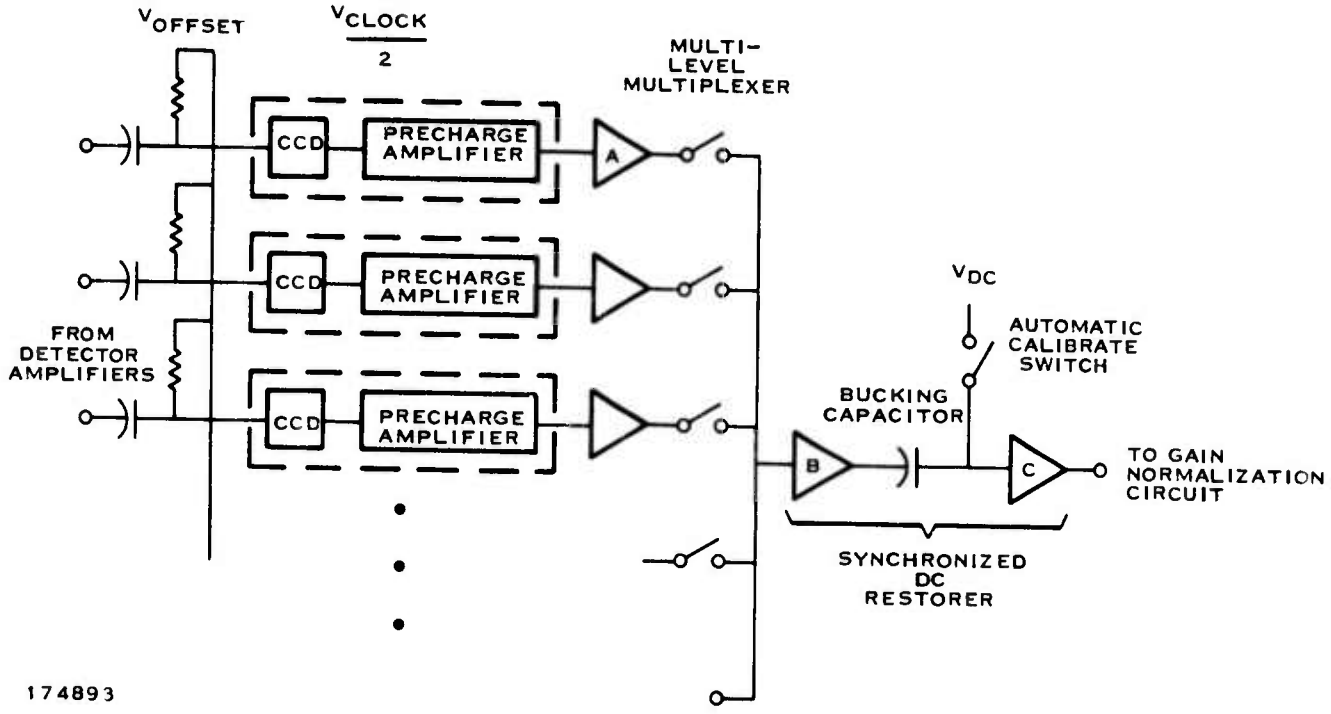

Figure 84. Block Diagram of Input and Output Circuit for the Image Buffer

(1) Precharge Amplifier

The CCD output is fed directly from the output diode to an on-chip precharge amplifier. If the precharge pulse is short enough in duration, then the output signal appears in a sample-and-hold format. Figure 85 shows the present state of achievement in forming the precharge pulse. The signal shown here is the output signal, with the feed through of the 10-volt precharge pulses showing as the 0.5-volt spikes preceding each sample-and-hold interval. The clocking frequency is 12 MHz. It is expected that the voltage decay from the precharge spikes will be substantially faster than shown here, when the output circuitry is put in its final configuration. Of particular interest here is the sharpness of the precharge pulse rise, which is about 5 ns.

From the precharge amplifiers, the signal (still in a sample-and-hold format) goes to the buffer amplifiers A, then to the channel-select multiplexer, which will have a multilevel configuration depending on the number of channels being used. The multilevel approach is needed in order to restrict the capacitive loading on the signal drivers and thus maintain a 10- to 15-MHz signal bandwidth capability at this point. During the dump phase, the channels are multiplexed one after another onto the single video line and then directly to impedance-transforming amplifier B. This has a low input impedance to keep down the noise pickup in the multiplexer.

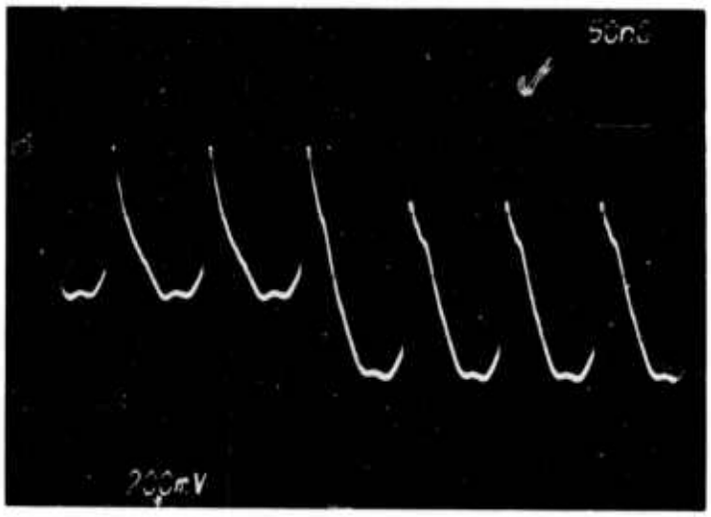

Figure 85. Detailed View of Signal Format at Precharge Amplifier

Another facet of the input-output circuitry is the CCD linearity. Figure 86 shows a bidirectional triangular waveform with a ±2-volt amplitude at the input of a different device. The corresponding waveform at the output shows no more than a 3 to 4 percent deviation from linearity, presumably caused by small variations in dark current with a low spatial frequency. This example of system performance is, of course, at a much lower clock rate and is shown to indicate the degree of linearity currently available over the signal range.

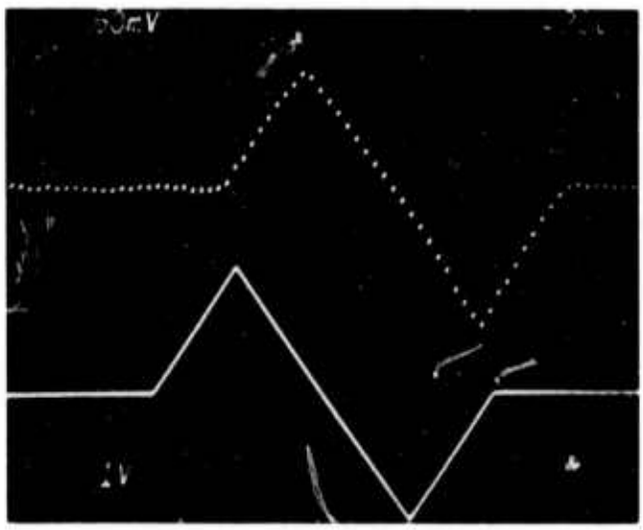

Figure 86. Demonstration of CCD Input-Output Linearity at 3.5-MHz Clock Rate

(2) DC Offset Compensation

Next comes the synchronized dc restorer circuit, which suppresses the channel-to-channel variations in the dc offset level. At the beginning of the process of loading a line of video information into a CCD, the first 30 of the 900 charge packets injected into the CCD are set to a fixed input signal level, V_{ref}. While this group of 30 packets is being clocked out of each CCD, as it is being dumped, the calibrate switch is closed. The series bucking capacitor C_b is charged to a potential that is the difference between V_{dc} and whatever level the signal level V_{ref} corresponds to in the particular CCD being clocked out. At the end of the 30 clock cycles, the switch is opened. Then, as the succeeding packets of video signal-level information are clocked out from this same CCD, the dc level of the signal at voltage follower C is shifted by the voltage across C_b. Thus, whatever level of dc offset and of average dark current is common to both the group of 30 calibrate packets and the succeeding 870 signal packets in a CCD is just cancelled out by C_b; the voltage level at C is independent of the dc characteristics of the individual CCDs, as long as these characteristics do not vary significantly throughout the CCD or during the load and dump times.

The voltage follower C has a very high input impedance, so that the charge built up on C_b during the calibrate interval does not leak off significantly during the rest of the line readout.

The synchronized dc restorer circuit has been tested with typical dc level variations and at the required 12-MHz clock rate. At its present stage of refinement, it has been shown to suppress dc level variations by nearly 40 dB; it is expected that, with further refinements, the suppression level should be significantly greater.

(3) Automatic Gain Normalization

The single-line video signal is then sent to the automatic gain normalization circuit. The function of this circuit is to compensate for channel-to-channel variations in overall signal gain. These variations include not only differences in the gains of both the input and output circuitry of the CCDs but also differences in detector sensitivity and in detector amplifier gain.

For each channel, a value is determined for the incremental gain needed to bring the overall channel gain up to a fixed level. This value is automatically determined during a manually initiated calibration process, and is stored digitally in a random-access memory (RAM). As each CCD is connected in turn to the single-line output, the corresponding value of the gain increment needed is read out of the RAM, reconverted to analog form, and fed to a voltage-controlled variable-gain amplifier.

The circuitry to implement this function has been assembled in an advanced breadboard configuration and has already been tested sufficiently to verify the adequacy of the system concept. Considerably more work remains to be done to complete the advanced development and testing phases for this device.

B. ELECTRONIC MULTIPLEXER

The 80-channel electronic multiplexer scheme was breadboarded uisng several different approaches. The approach selected was optimum in performance and power consumption.

The dual-mode optical system design had to be compatible with the Texas Instruments common module scanner and detector. The final design consisted of two re-imaging telescopes with a common relay system in front of the scanner. The differential mechanism for selecting the optical mode is located ahead of the relay. The differential mechanism design went through several concepts before the final product was selected. One design required the use of non-circular gears to minimize the size of the mirror, but this was rejected because of the power required to operate the mechanism. The present design requires less than 2.5 watts of power, functions extremely accurately, and is small enough to fit within the framework of the sensor. The video processing and enhancement electronics, built into the ground station control, are functional, and evaluation will be made during field testing.

The electronic multiplexer design philosophy called for organizing the multiplexer as a two-level electronic switch. The two-level multiplexer permits the use of conventional analog multiplexers in the first level section operating at a lower speed from the second level. Operating the first level at a lower integral multiple of the second level results in a reduction of total power consumption for the multiplexer. The multiplexer requirements are; the amplitude dynamic range must be at least 40 db, the switching spikes must be consistent with the amplitude dynamic range for an output voltage swing of one volt peak-to-peak, five megahertz operation is easily attained, zero offset, and necessary adjustments can be consistent with ease of interchangeability.

The first device considered for the low level section of the multiplexer was the National Semiconductor AM3705. This device is an eight channel MOS analog multiplex switch, compatible with TTL logic. These switches exhibit channel-to-channel switching times on the order of 600 nanoseconds which require the first level section ot operate below 1.5 megabit. Since the second level multiplexer operates at the five-magabit sampling rate, video inputs to the MOS devices would need to be staggered by 10 video channels, allowing 1.8 microseconds for switching between video inputs. Staggering the video inputs in this manner (10 channels) proved to be undersirable for crosstalk and noise considerations. Any crosstalk between inputs carrying video separated by 10 resolution elements causes contrast reduction, or severe ghosting, on the display. In addition, for minimum component count (for power and weight considerations) the number of devices was not consistent with the common module concept which requires video wiring in groups of five adjacent channels and an associated ground for each group. This approach did not meet system requirements for crosstalk, wiring and power consumption.

The diode switch circuit shown in Figure 87 was designed and evaluated as a first level multiplexer. High speed Shottky diodes were used as the main switching element. This circuit showed excellent switching times and could easily operate at the five-megabit sampling rate. Other characteristics of the diode switch were simplicity, low power and ease of adaptability to the common module video circuits. However, the output voltage swing in this configuration is limited by the output logic swing of the shift register. Also, differences in transistor V_{BE} and diode forward voltage caused offsets at the output that would have required individual offset adjustments for each channel. For these reasons, the diode switch configuration is unacceptable for this application.

Ultimately, the Inselek LO2FT device was chosen as the switching element in the first level multiplexer. The LO2FT is an eight-channel multiplex switch compatible with TTL logic. Its characteristics, which are obtained by forming SOS/MOS transistors on an insulating substrate, are low power (50 mw), fast switching times (100 nanoseconds), zero offset and 50 db channel separation. The fast switching times of the LO2FT permit the video inputs to the devices to be arranged in odd and even channels. In this manner, adjacent inputs are separated by only one resolution element. The arrangement of odd and even video channels, at the inputs of the first level switches, simplifies the second-level multiplexer design to a two-channel to one-channel switch.

Only five inputs are used on each device which allows packaging consistent with the common modular concept discussed previously.

Two different second-level multiplexer designs were built and evaluated - the transistor current switch and the diode bridge switch. The transistor current switch is shown in Figure 88. This design utilizes three high speed transistors in a differential amplifier configuration. The differential pair in this circuit performs current steering during sampling and isolates the clock drive from the output. Switching transients could, therefore, be controlled in this configuration by changing the amplitude of the clock drive signal or bias of a stage slightly. Differences in transistor gain and V_{BE} voltages caused amplitude and offset problems at the output. Adjustments were necessary to compensate for these variations. Further evaluation revealed that the output circuit was extremely sensitive to power supply voltage changes and circuit layout. Therefore, this configuration was unacceptable for the second level multiplexer.

The diode bridge switch shown in Figure 89 was chosen for the second level multiplexer. This multiplexer consists of two high speed diode bridges which are alternately turned on and off through transformers T1 and T2. This switching action alternately samples the odd and even parallel video inputs, thereby converting this information to sequential serial video at the output.

Each diode bridge switch utilizes four high speed Schottky diodes. When driven from the transformer coupling circuit, the bridge is capable of generating switching times of 25 nanoseconds into a 47 picofared load. The matching between the bridge and transformer coupling circuit reduced the channel-to-channel switching spikes to 30 millivolts. Output voltage swing capability of the multiplexer is three volts peak-to-peak giving an amplitude dynamic range of 40 db. The output swing capability will easily provide one volt peak-to-peak of video required

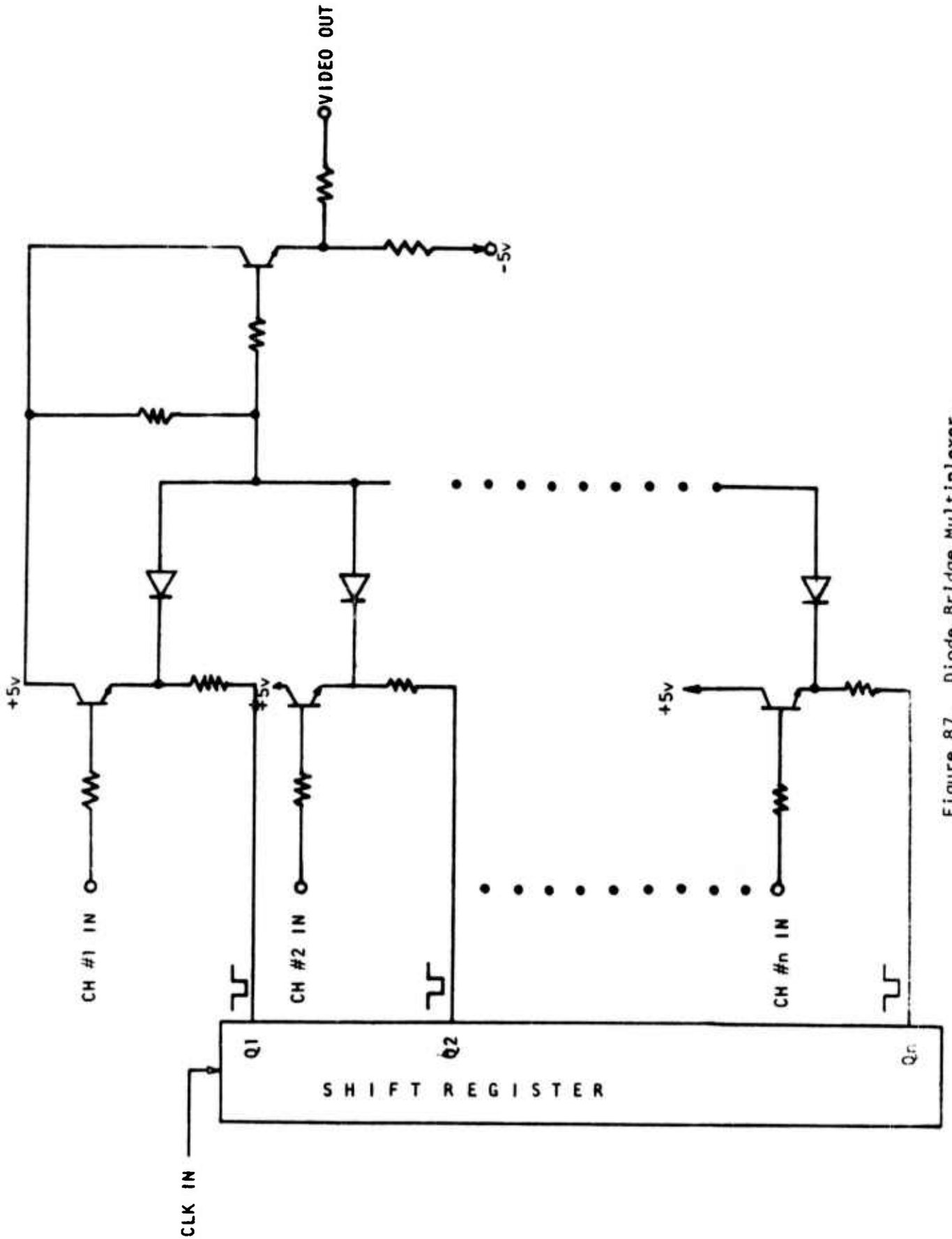

Figure 87. Diode Bridge Multiplexer.

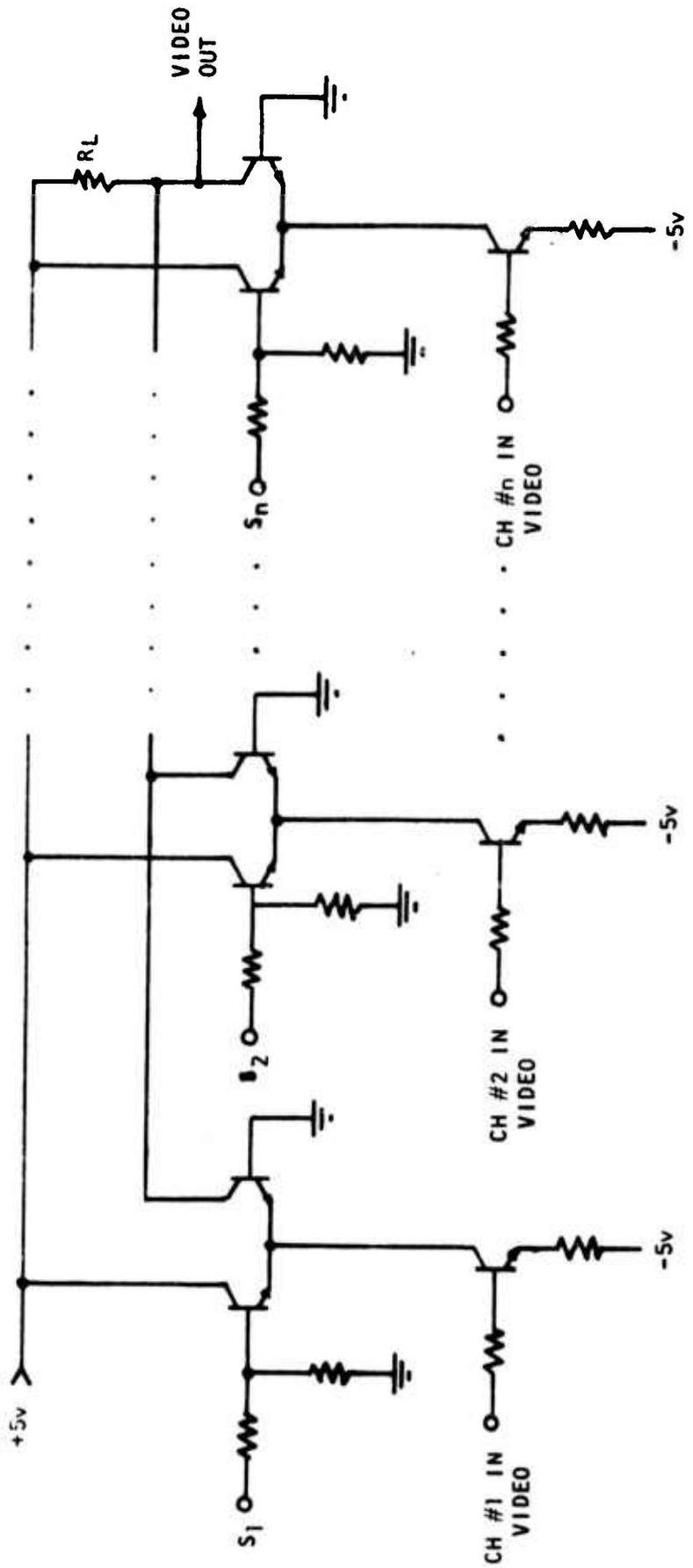

Figure 88. Transistor Current Switch Multiplexer.

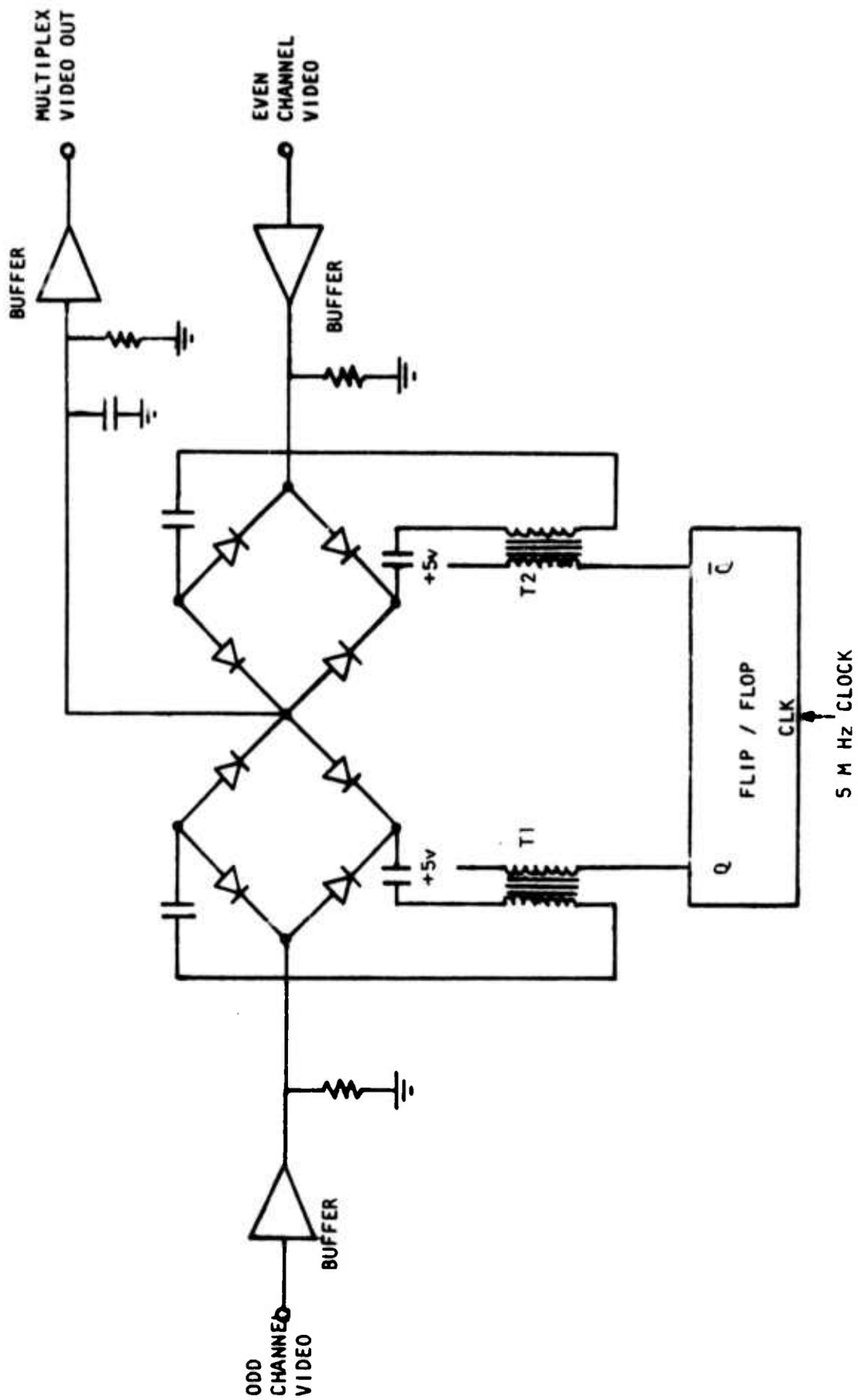

Figure 89. Diode Bridge Multiplexer.

by the data link without distortion or clipping. Offsets, that can be caused by differences in series switch resistance of the LO2FT devices, are eliminated by buffer amplifiers on the odd and even channel video input lines. The high input impedance of the buffer amplifiers eliminates the effects of series resistance variations in the LO2FT used in the first level section. No adjustments are necessary for the mutliplexer because of its low offset, uniform gain, linearity and amplitude dynamic range characteristics. A complete functional block diagram of the electronic multiplexer is shown in Figure 90.

The first level multiplexer switches were relatively free of problems during the system test phase. However, during the early phases of testing, several of the LO2FT devices experienced failures. Failure analysis revealed that system turn-on transients were overstressing the output transistors. Output protection was provided by adding resistors to each board at the odd and even outputs to ground, and the problem did not reappear.

The output of the second level multiplexer showed severe switching transients and offsets during the early stages of system test. Trouble analysis revealed that the even address signal lines had been routed near the odd channel video lines on the postamp carrier board. Capacitive coupling, during the even address switching, was causing the transients and offsets. The postamp and second level multiplexer boards were modified to reroute the odd and even video channels away from the address lines. This modification reduced the offsets and spikes to acceptable levels.

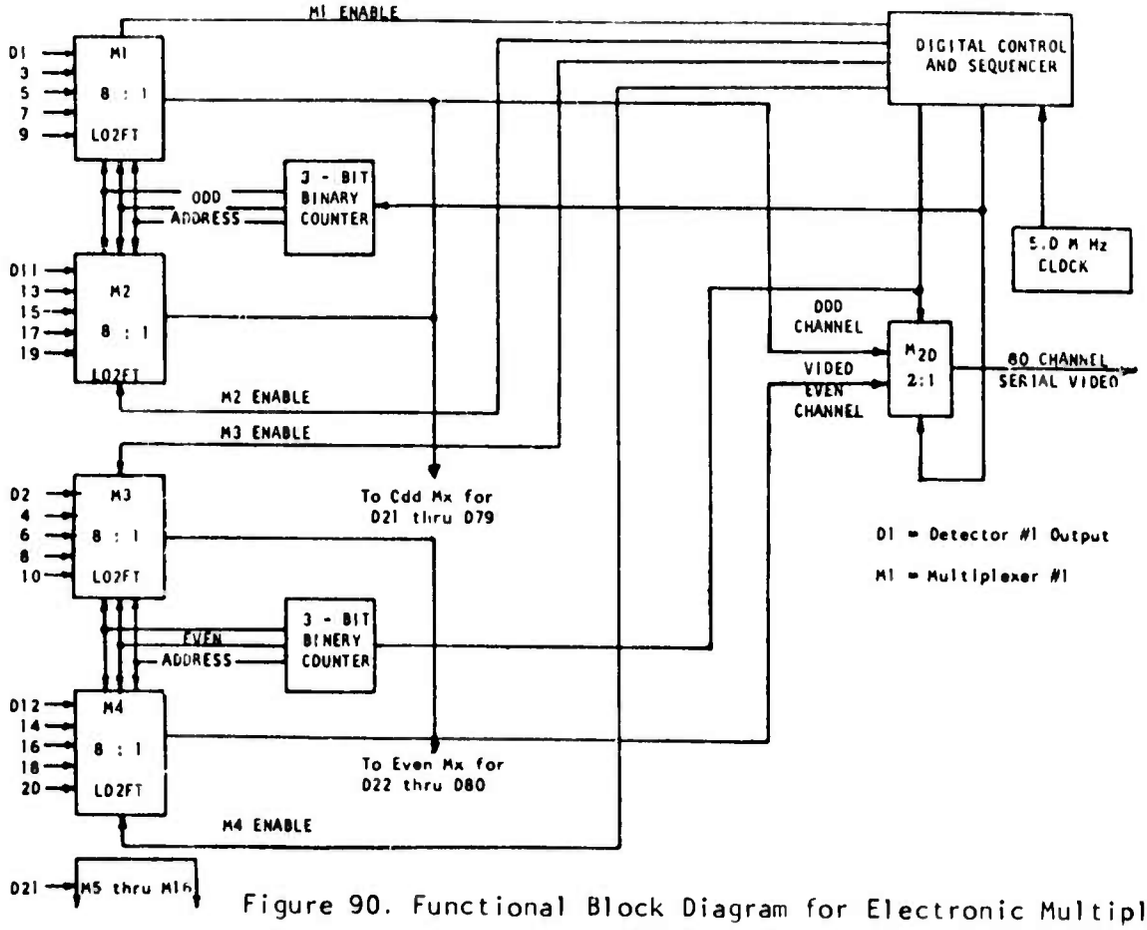

Figure 90. Functional Block Diagram for Electronic Multiplexer

APPENDIX A

AVERAGE PROPERTIES OF PLASTIC MATERIALS

ROOM TEMPERATURE 73°F

MATERIAL	THERMAL EXPANSION 10/10/°F x 10^{-5}	HEAT RESISTANCE °F	TENSILE STRENGTH PSI	TENSILE MODULUS PSI x10^5	IMPACT (NOTCHED) FT-LB/In NOTCH	FLEXURAL MODULUS PSI x10^5	SPECIFIC GRAVITY	WATER ABSORPTION % IN 24 HR	COST/in^3 $/$in^3$	DESIGN & PROCESS ABILITY A=EXCELLENT B=Good C=Fair
URETHANE	7-10	190	4,000	.1-2	Does not break	3.5	1.2	.7-.9	.053	B
20% GLASS	1.5		5,000	3	10	1.5	1.35	.59	.122	B
40% GLASS	1.1		10,000	7.5	10	3.6	1.53	.49	.154	B
POLYESTER THERMOPLASTIC	1.1-6.0	175-250	8,000	13	1.2	3	1.31	.08	.076	B
18% GLASS	3	250	15,000		2.0	12	1.52	.06	.121	B
SAN	3.7	160	9-12,000	4.5	.4	5	1.1	.25	.010	A
20-33% GLASS	1.6-2.3	200-250	14-18,000	8-16	.8-2.0	8-14	1.22-1.35	.15	.022	A
POLYSTYRENE	3.7	140-170	6,000	4	.6	4	1.05	.05	.007	A
20-30% GLASS	1.8-2.5	180-200	11-14,000	10-13	1.4-2.5	10-12	1.20-1.29	.06-.09	.015	A
RIGID VINYL	3-18	160	5-8,000	3.5-6	.5-10	4-5	1.4	.03-.4	.016	B
FLEXIBLE VINYL	7-25	150-220	1-3,500	.01-.03	variable		1.3	.2-1.0	.015	A
PHENYLENE OXIDE	3.8		8,000	4	5	3.6	1.1	.07	.046	B
20-30% GLASS	1.4-2.0		14-17,000	9-13	2 3	7-10	1.21-1.27	.06	.070	B
POLYSULFONE	3.1	340	10,200	3.6	1.3	4	1.24	.22	.045	B
20% GLASS	1.6	350	17,000	11	1.8	12	1.41	.22	.089	B
30% GLASS	1.2	355	19,000	15	2.0	15	1.55	.18	.080	B
POLYPHENYLENE SULFIDE	3	500	10,800	4.8	.3	6	1.34	.2		B
40% GLASS	2.2	500	21,400	11.2	.8	22	1.64	.01		B
EPOXY										
20% GLASS	1.1-3.5	300-500	10-30,000	30.4	.7	14	1.6-2.0	.05-.2	.145	C
PHENOLIC	2	350-550	10,000	30-33	.6	20	1.8	.07	.078	C
NEOPRENE RUBBER	34	240	3-4,000				1.25		.056	C
SILICONE RUBBER	45	600	600-1,300				1.1-1.6		.117	C

Figure A-1. Average Properties of Plastic Materials.

AVERAGE PROPERTIES OF PLASTIC MATERIALS
ROOM TEMPERATURE 73°F

MATERIAL	THERMAL EXPANSION In/In/°F X10-5	HEAT RESISTANCE °F	TENSILE STRENGTH PSI	TENSILE MODULUS PSI X 10^5	IMPACT (NOTCHED) FT-LB/IN NOTCH	FLEXURAL MODULUS PSI X 10^5	SPECIFIC GRAVITY	WATER ABSORPTION %In 24 hr	COST/In^3 $/In^3	DESIGN & PROCESS ABILITY A=Excellent B=Good C=Fair
ALUMINUM	1.3		30,000	10X10^6			2.68		.049	
STAINLESS STEEL	.5		80,000	30X10^6			7.74		.140	
NYLON 6/6	5	200-250	11,000	4	2	1.8	1.15	1.5	.035	A
30% GLASS	1.4	200-250	22,000	17	3.4	1.8	1.37	.9	.061	A
POLYCARBONATE	3.7	250	8,500	3.5	16	3.4	1.20	.15	.056	A
20% GLASS	1.3	260	16,000	9	2	8	1.35	.09	.061	A
40% GLASS	1.0	275	21,000	17	2.3	12	1.51	.08	.081	A
ACETAL COPOLYMER	4.7	220	8,800	4.1	1.3	3.75	1.41	.22	.039	B
25% GLASS	2.2-4.7	220	18,500	12.5	1.8	11	1.61	.29	.074	B
ACETAL HOMOPOLYMER	4.5	195	10,000	5.2	1.4	4.1	1.42	.25	.038	B
20% GLASS	2.0-4.5	195			.8	8.8	1.56	.25	.071	B
POLYPROPYLENE	3.8-5.8	230	5,000	2	2.1	2	.9	.03	.012	A
20-40% GLASS	1.6-2.4	250	7-9,000	5-9	3.5-4.0	4-8	1.04-1.22	.05	.037	A
ACRYLIC	3.0	155-190	10,500	4.5	.3	4.5	1.18	.01	.063	A
HIGH DENSITY POLYETHYLENE	13	250	4,400	1.0	.5-20	1.4	.96	.01	.012	A
ABS	3-3	180	7,000	3.7	3	4	1.05	.3	.018	A
20-40%	1.6-2.5	215	13-16,000	7-10	2	8-12	1.23-1.36	.25	.041	A

Figure A-1 (Continued) Average Properties of Plastic Materials.

REFERENCES

1. GENERAL ELECTRIC PITTSFIELD, MASS. LEXAN POLYCARBONATE RESIN

2. CELANESE PLASTICS CO. P.O. BOX 1000 SUMMIT, NEW JERSEY 07901 CELCON ACETAL COPOLYMER. CELANESE NYLON, FORTIFLEX HIGH DENSITY POLYETHYLENE, CELANEX THERMOPLASTIC POLYESTER

3. MOBAY CHEMICAL CO. PITTSBURGH, PENNA. 15205 TEXIN URETHANE ELASTOMER RESIN

4. FIBERFIL DIV. DART INDUSTRIES INC. EVANSVILLE, INDIANA 47717 FIBER REINFORCED RESINS

5. MODERN PLASTICS ENCYCLOPEDIA 1972

6. MATERIALS SELECTOR 1973

7. DUPONT PLASTICS DEPARTMENT WILMINGTON, DELAWARE 19898 DELRIN ACETAL HOMOPOLYMER, LUCITE ACRYLIC, ZYTEL NYLON

APPENDIX B

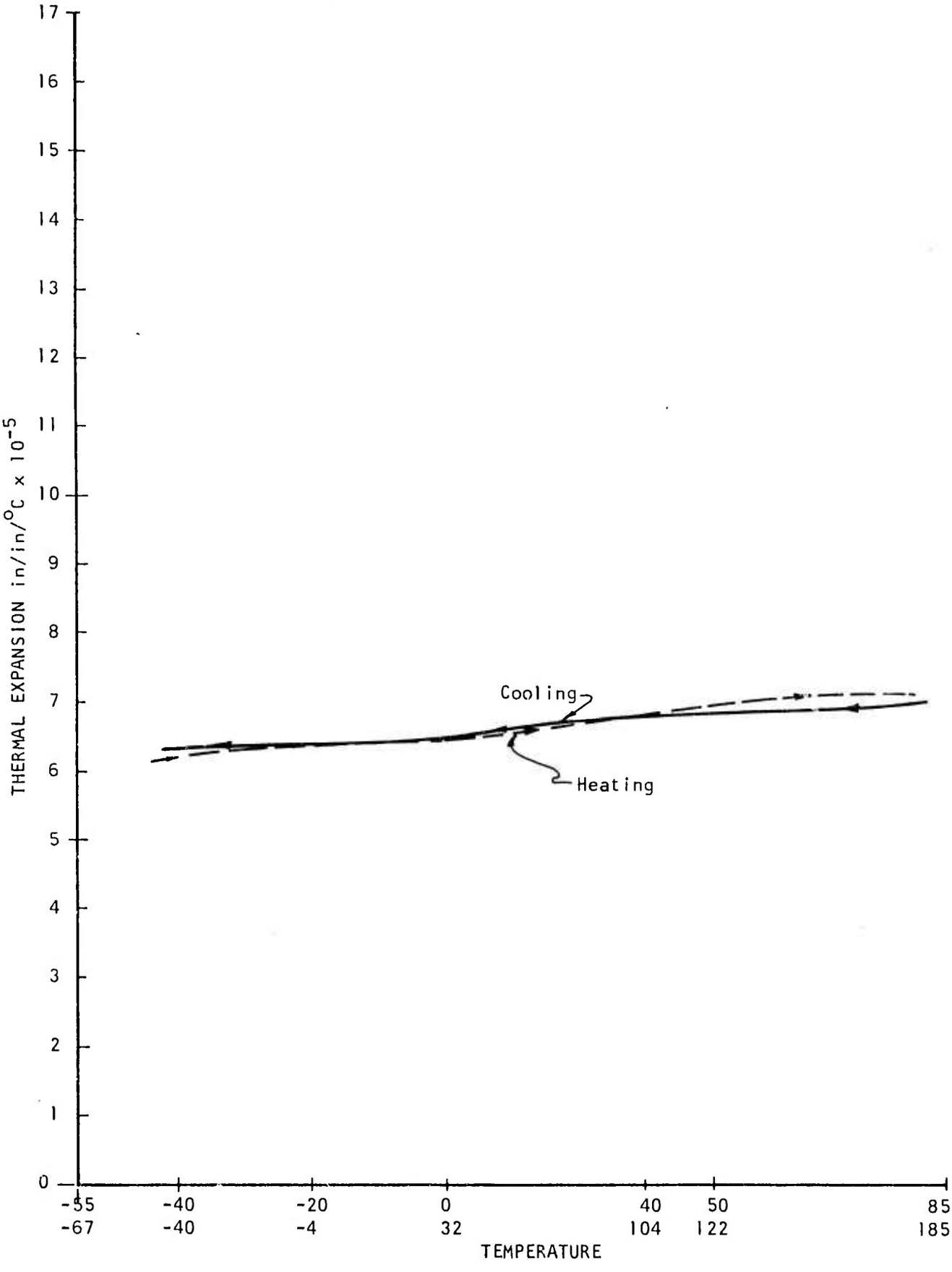

Figure B-1. Thermal Expansion vs Temperature.

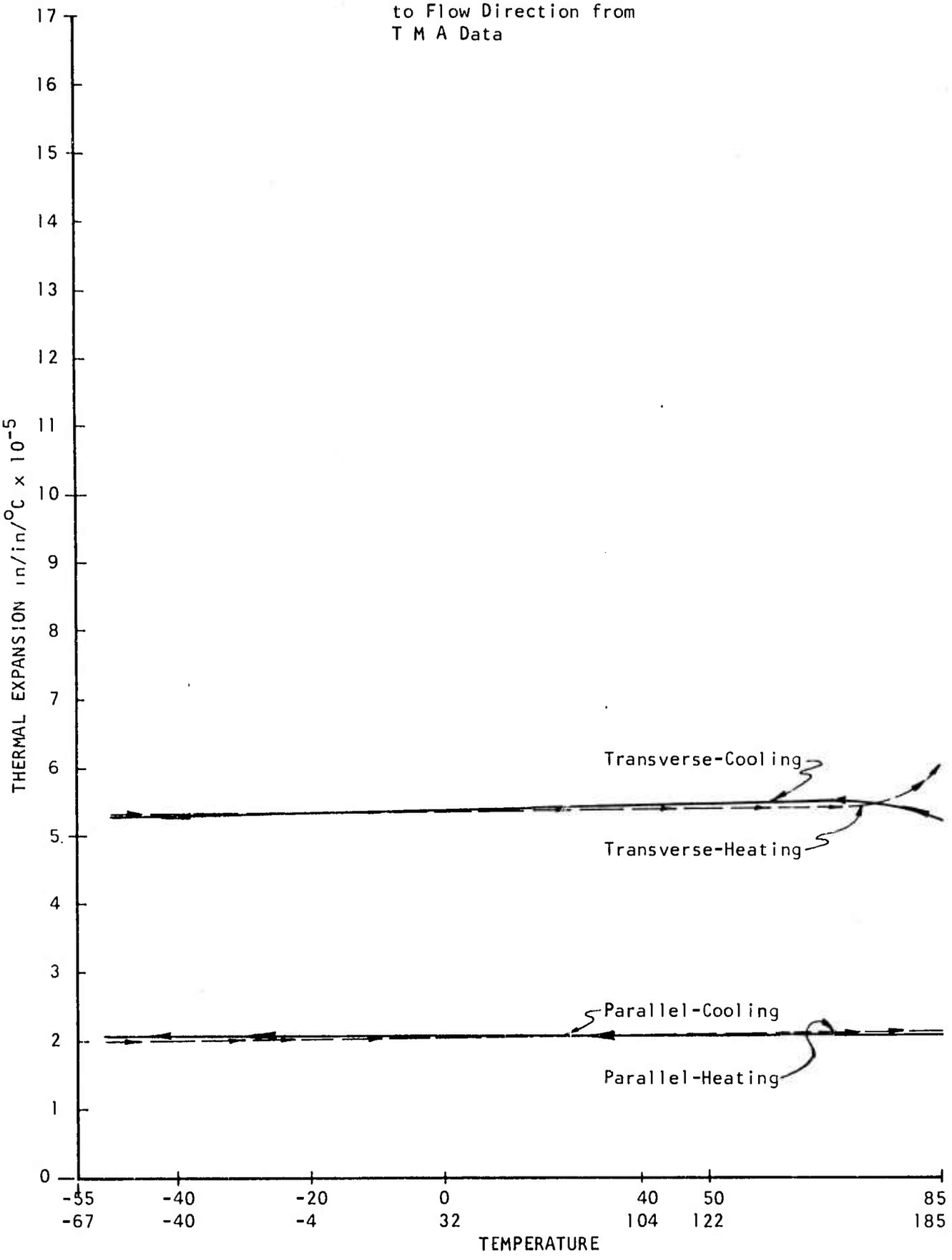

Figure B-2. Thermal Expansion vs Temperature.

Thermal Expansion vs Temperature
SPECIMEN: Acetal Homopolymer

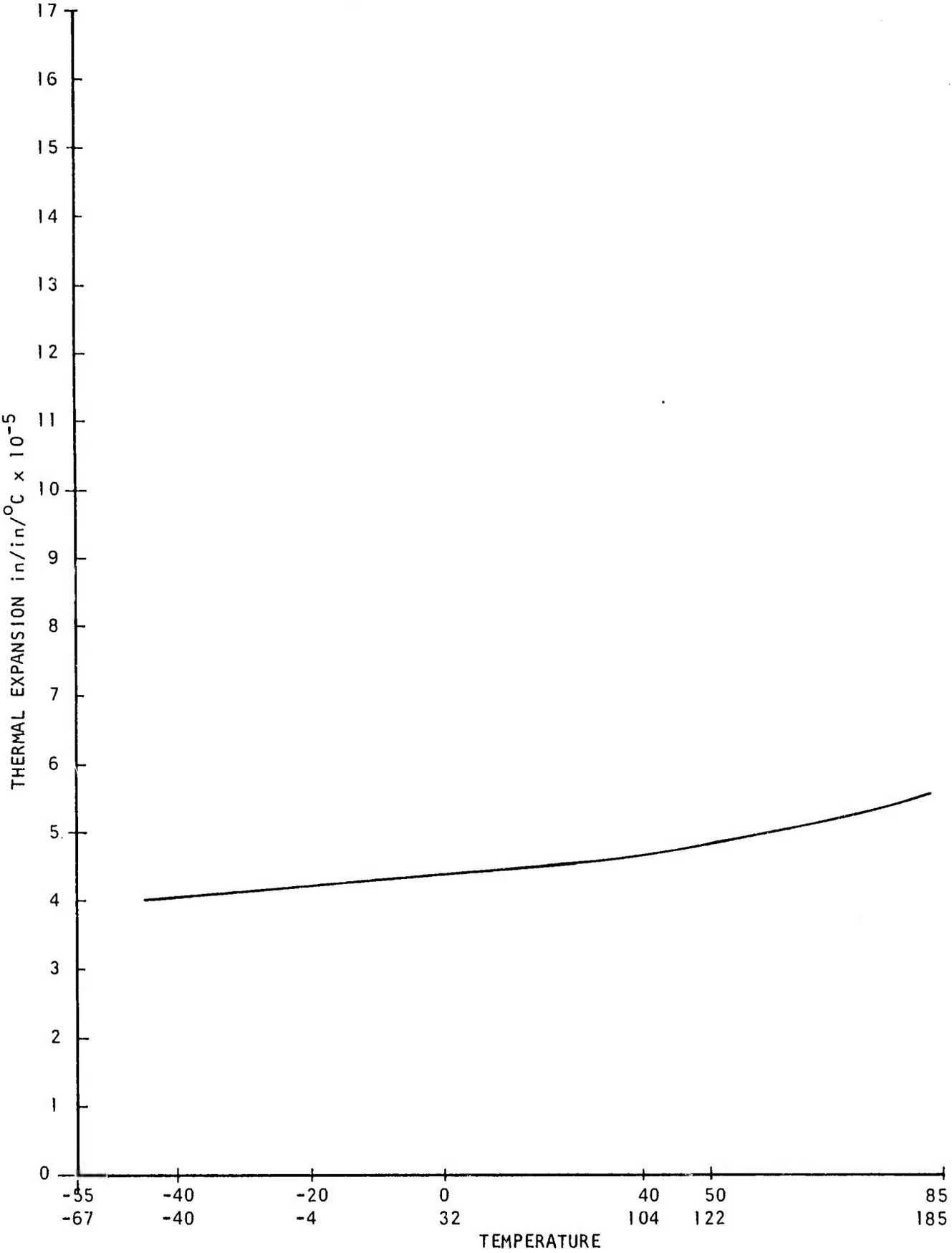

Figure B-3. Thermal Expansion vs Temperature.

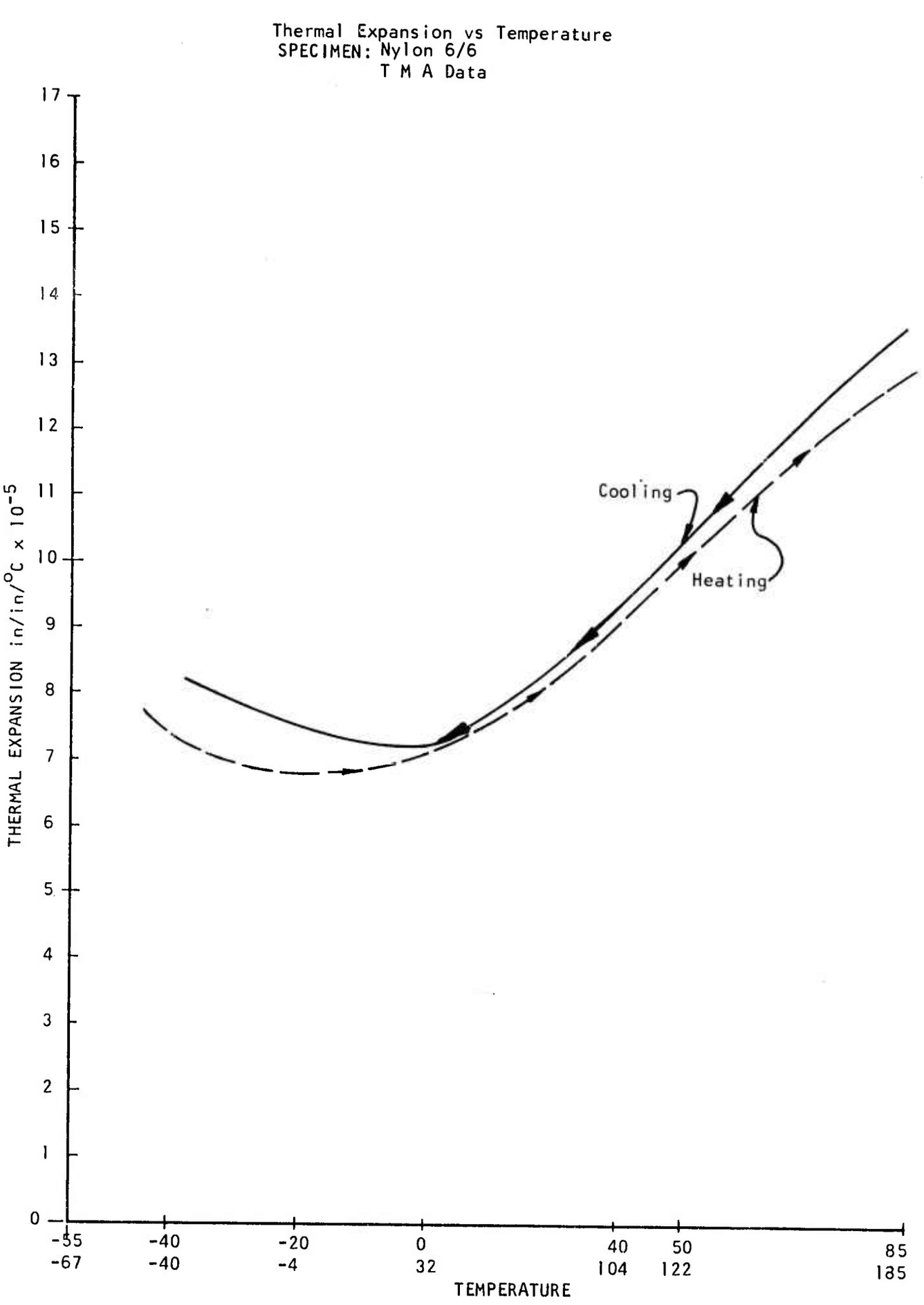

Figure B-4. Thermal Expansion vs Temperature.

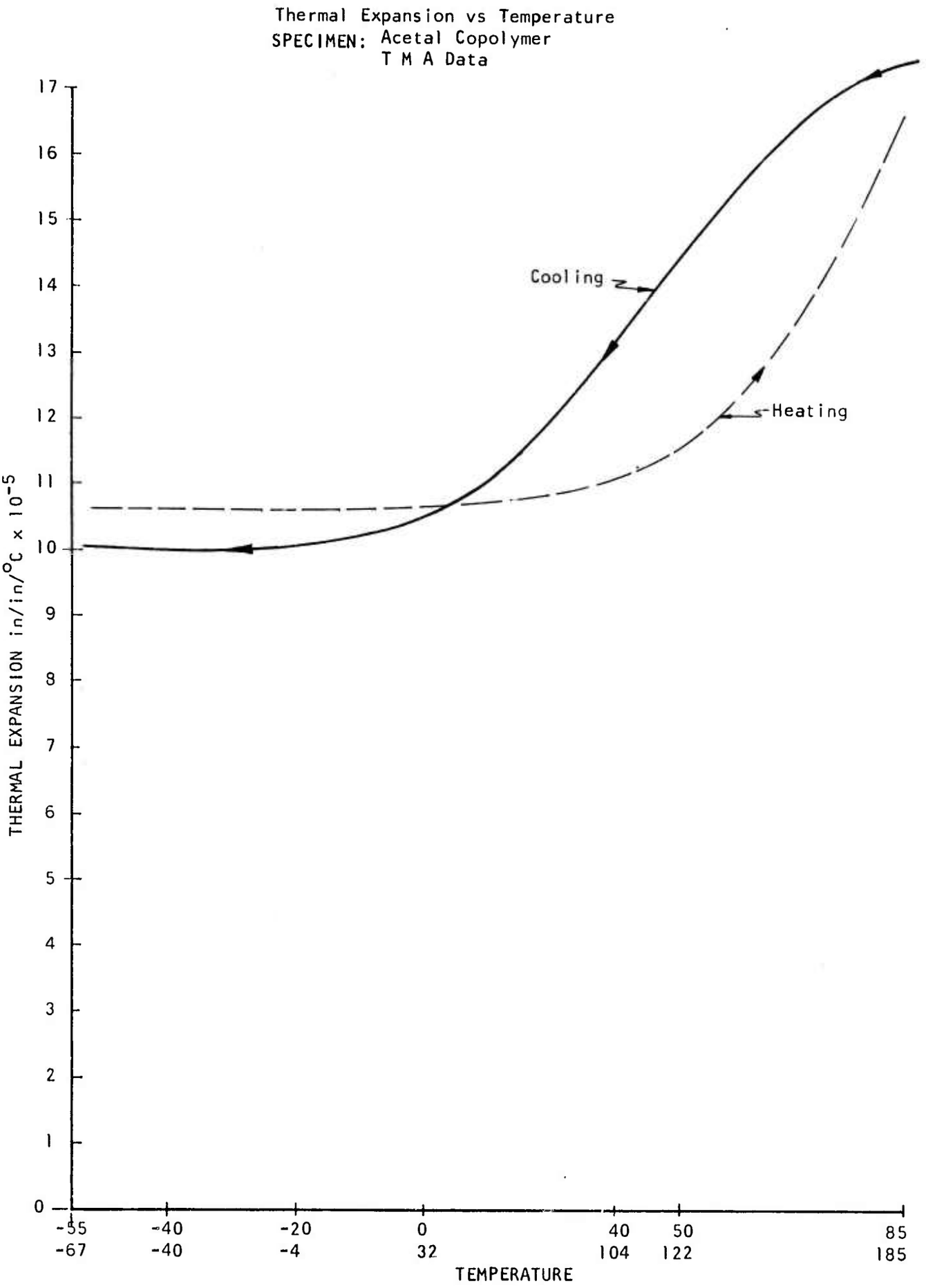

Figure B-5. Thermal Expansion vs Temperature.

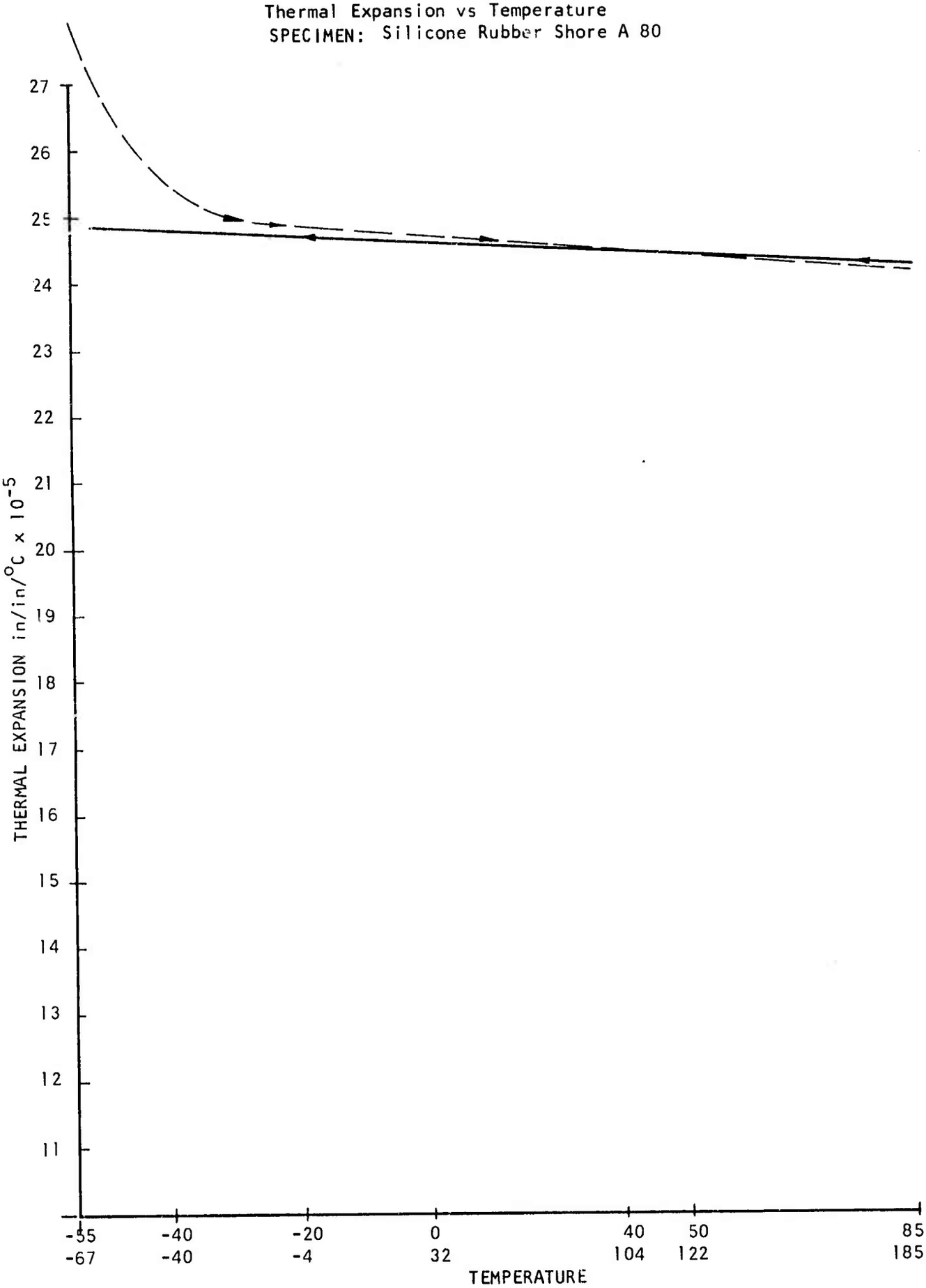

Figure B-6. Thermal Expansion vs Temperature.

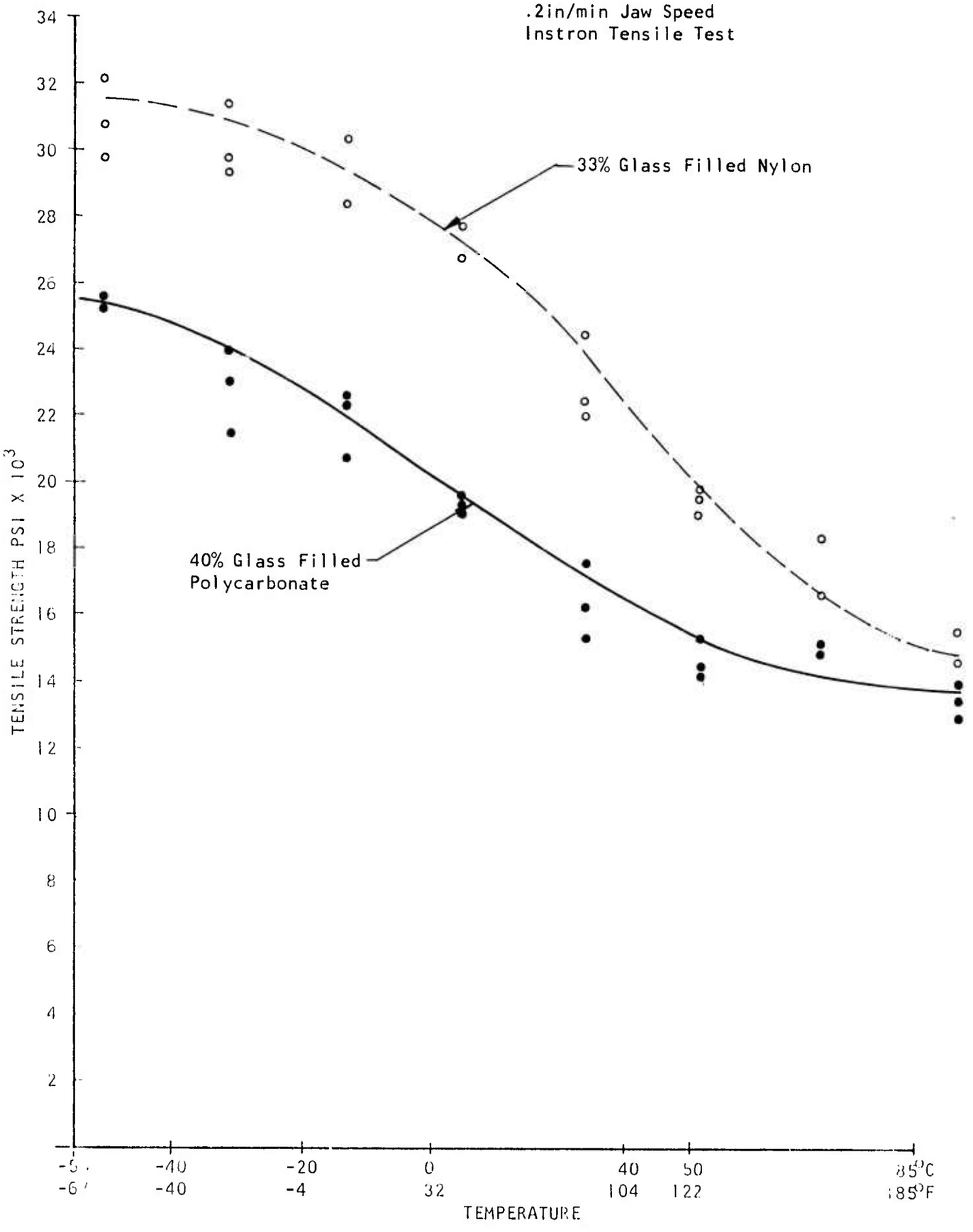

Figure B-7 Thermal Expansion vs Temperature.

Tensile Strength vs Temperature
SPECIMEN: Polycarbonate

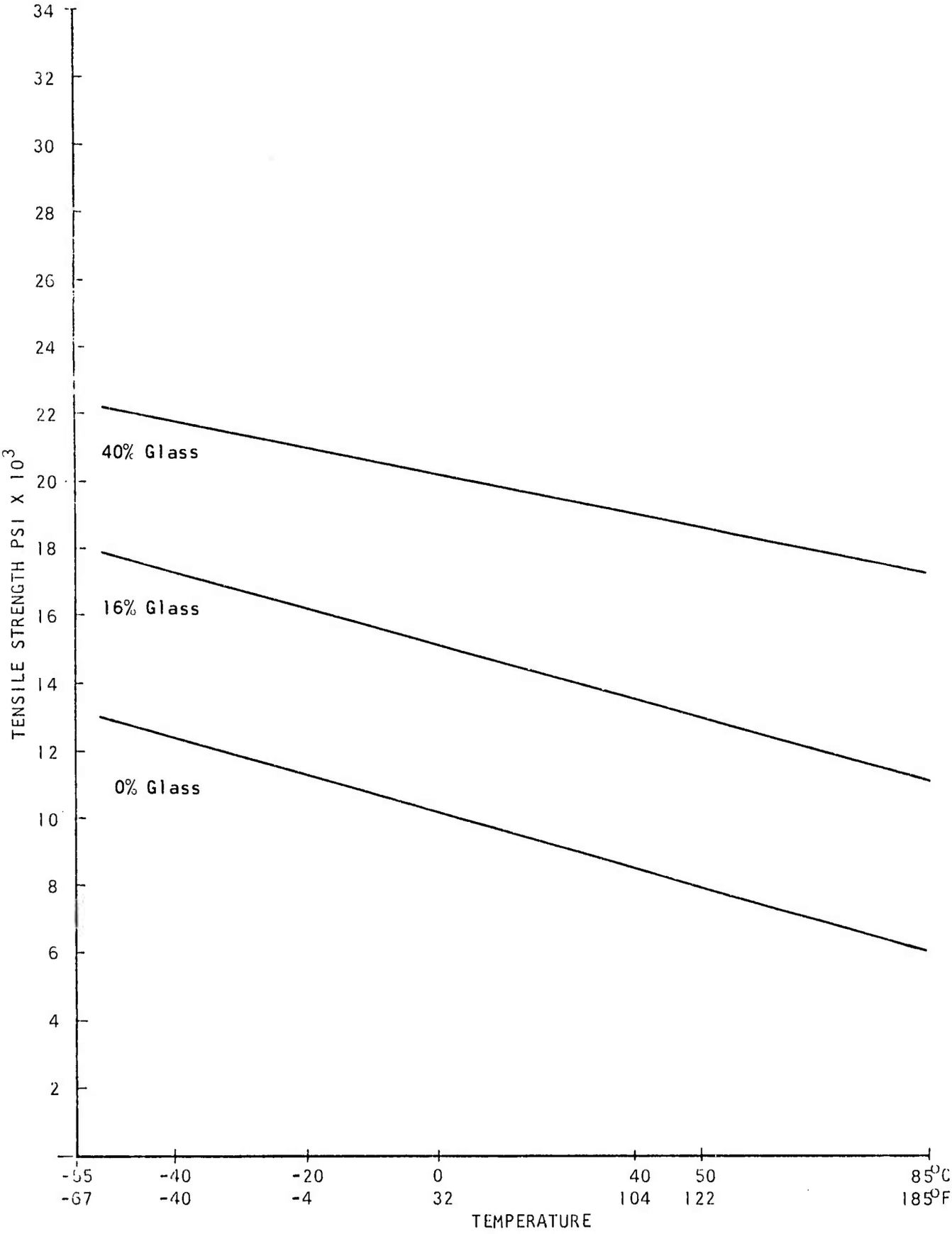

Figure B-8 Thermal Expansion vs Temperature.

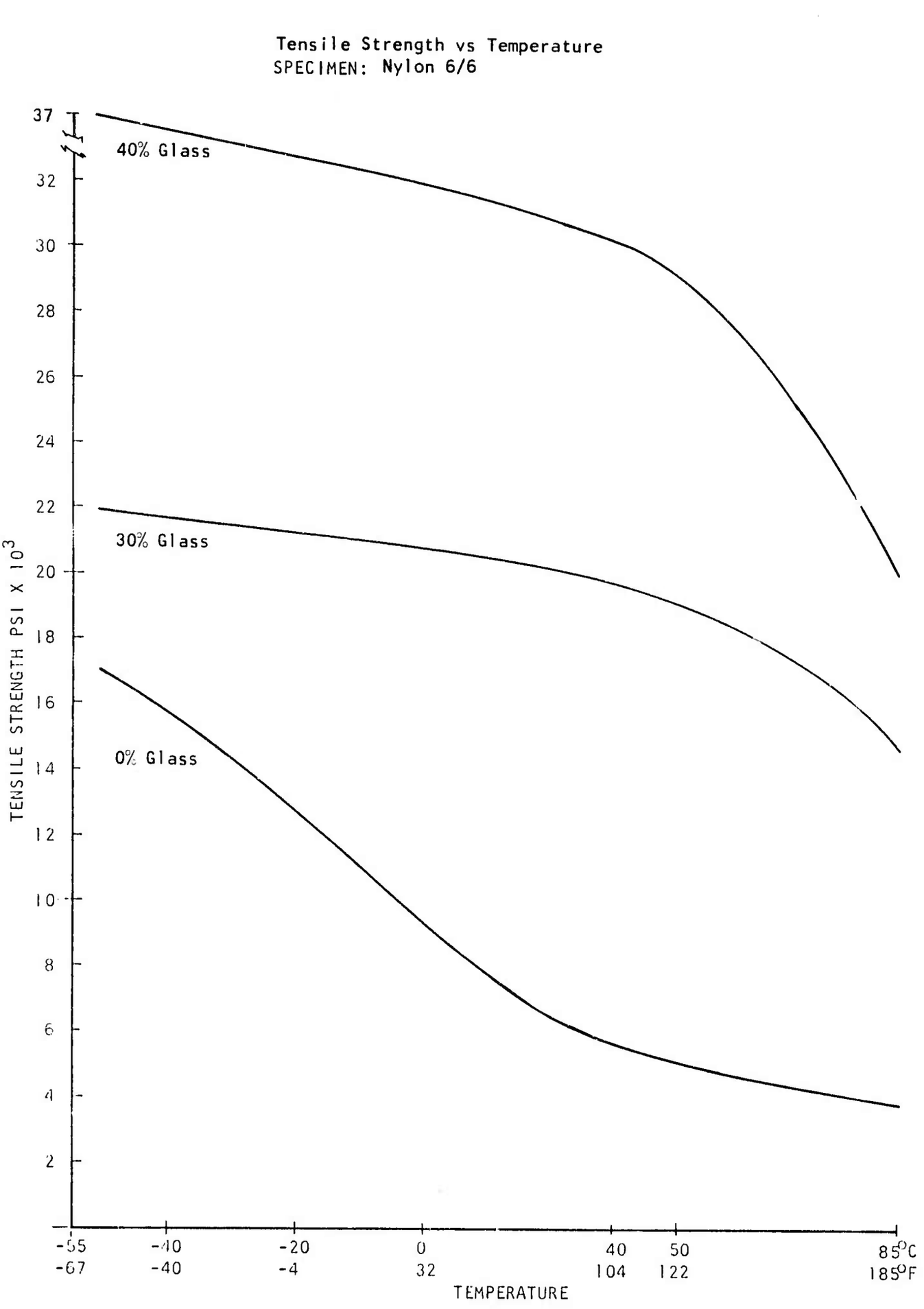

Figure B-9 Thermal Expansion vs Temperature.

Tensile Strength vs Temperature
SPECIMEN: Acrylic

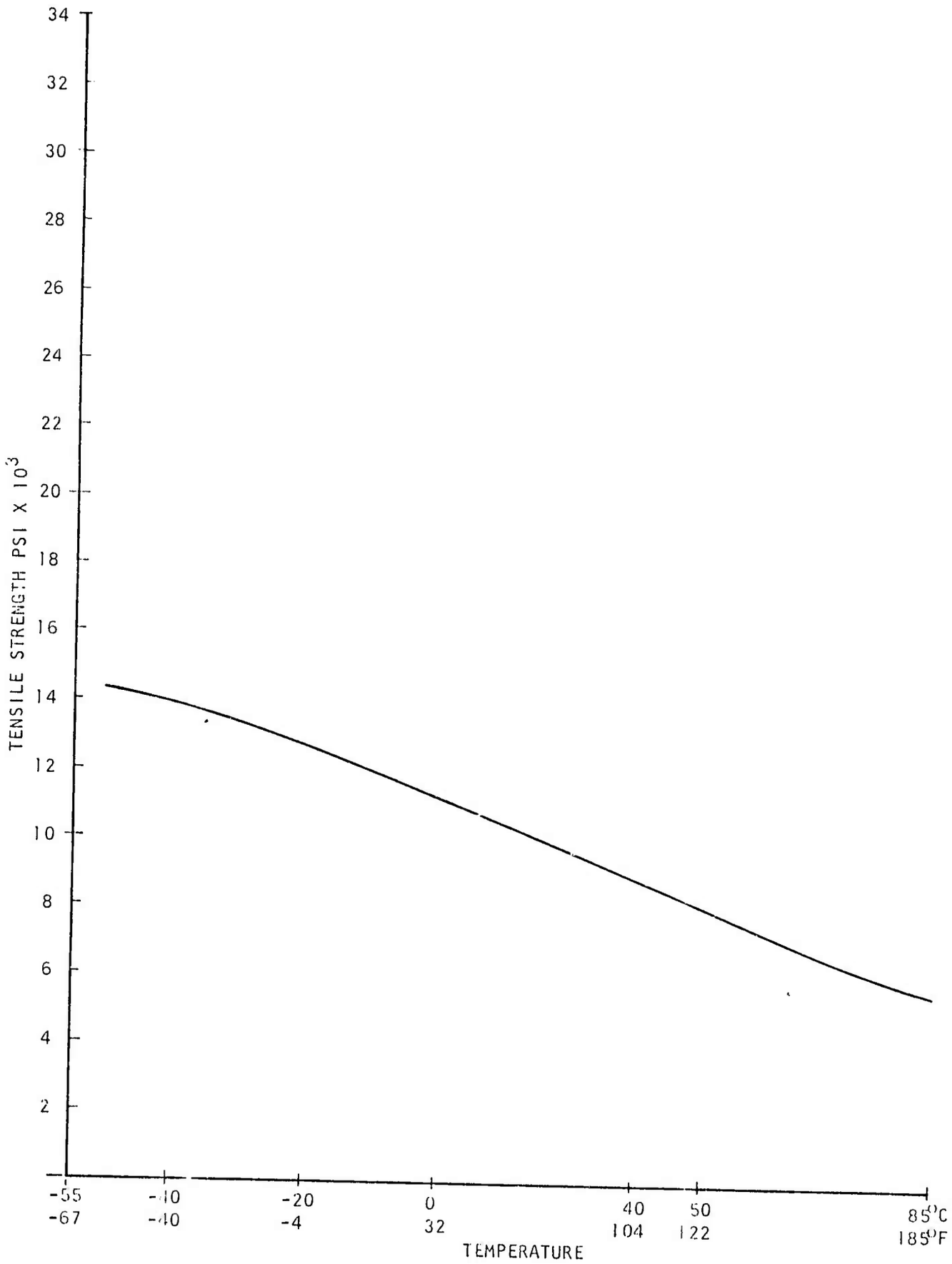

Figure B-10 Thermal Expansion vs Temperature.

Tensile Strength vs Temperature
SPECIMEN: Phenylene Oxide-Noryl

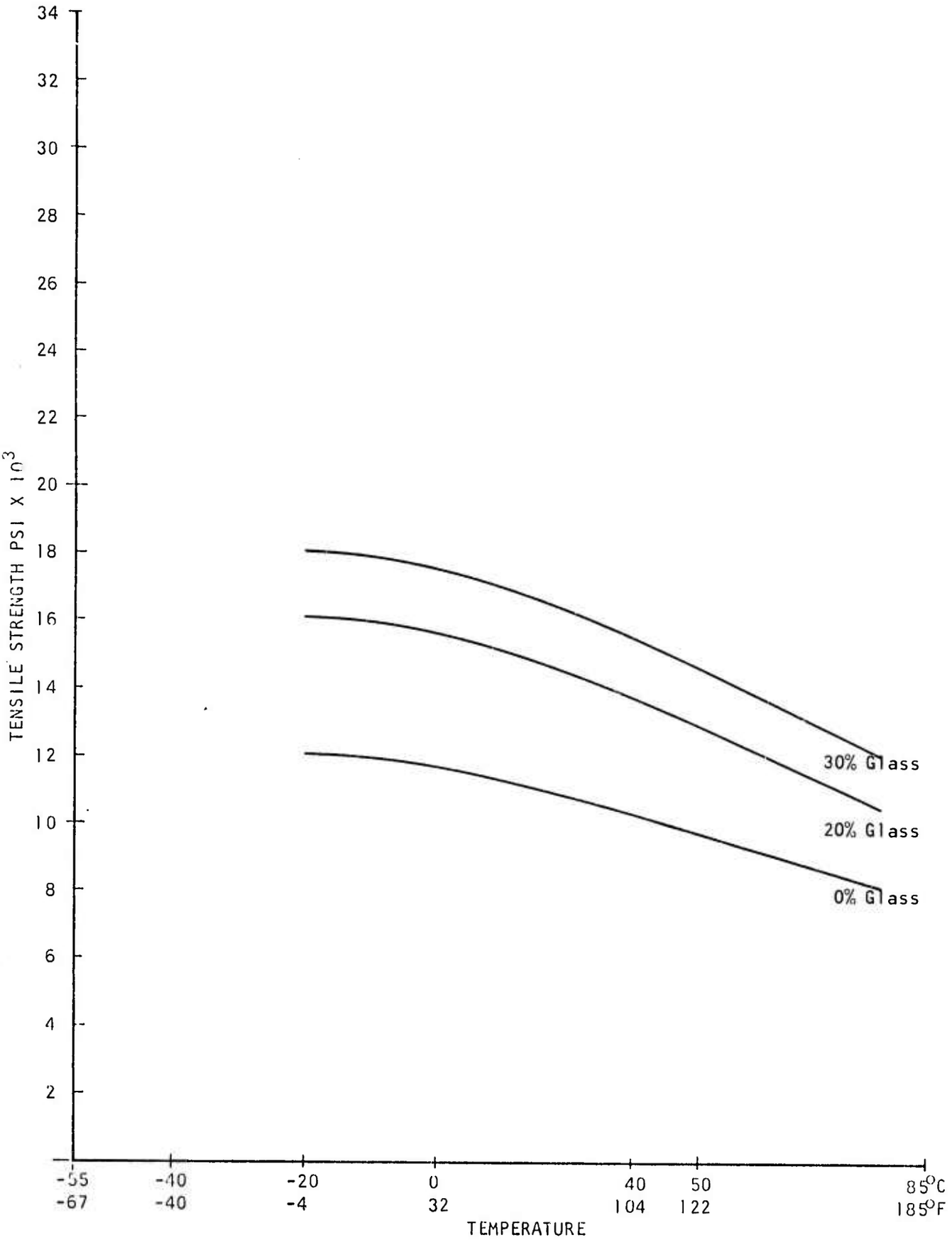

Figure B-11 Thermal Expansion vs Temperature.

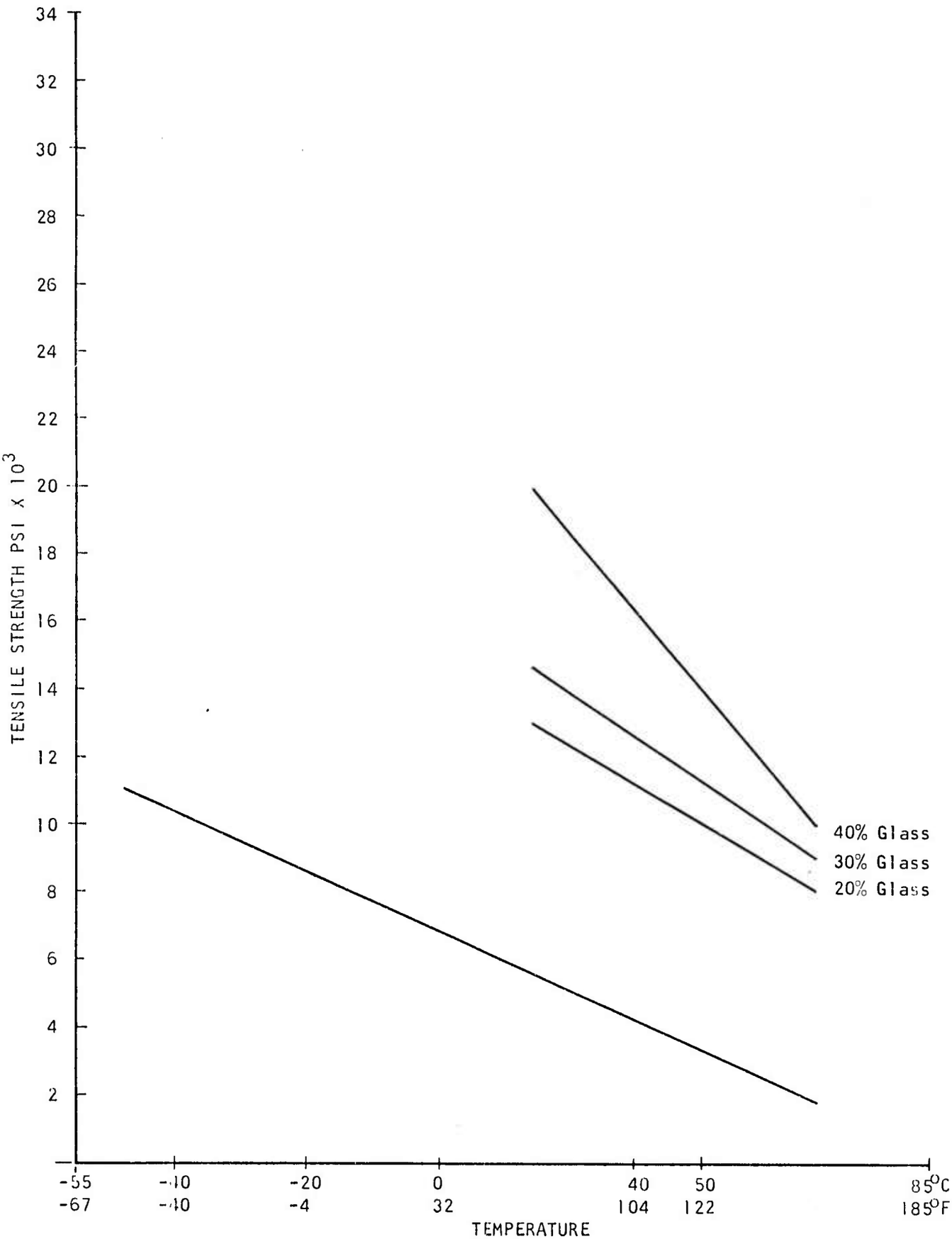

Figure B-12 Thermal Expansion vs Temperature.

Tensile Strength vs Temperature
SPECIMEN: Urethane

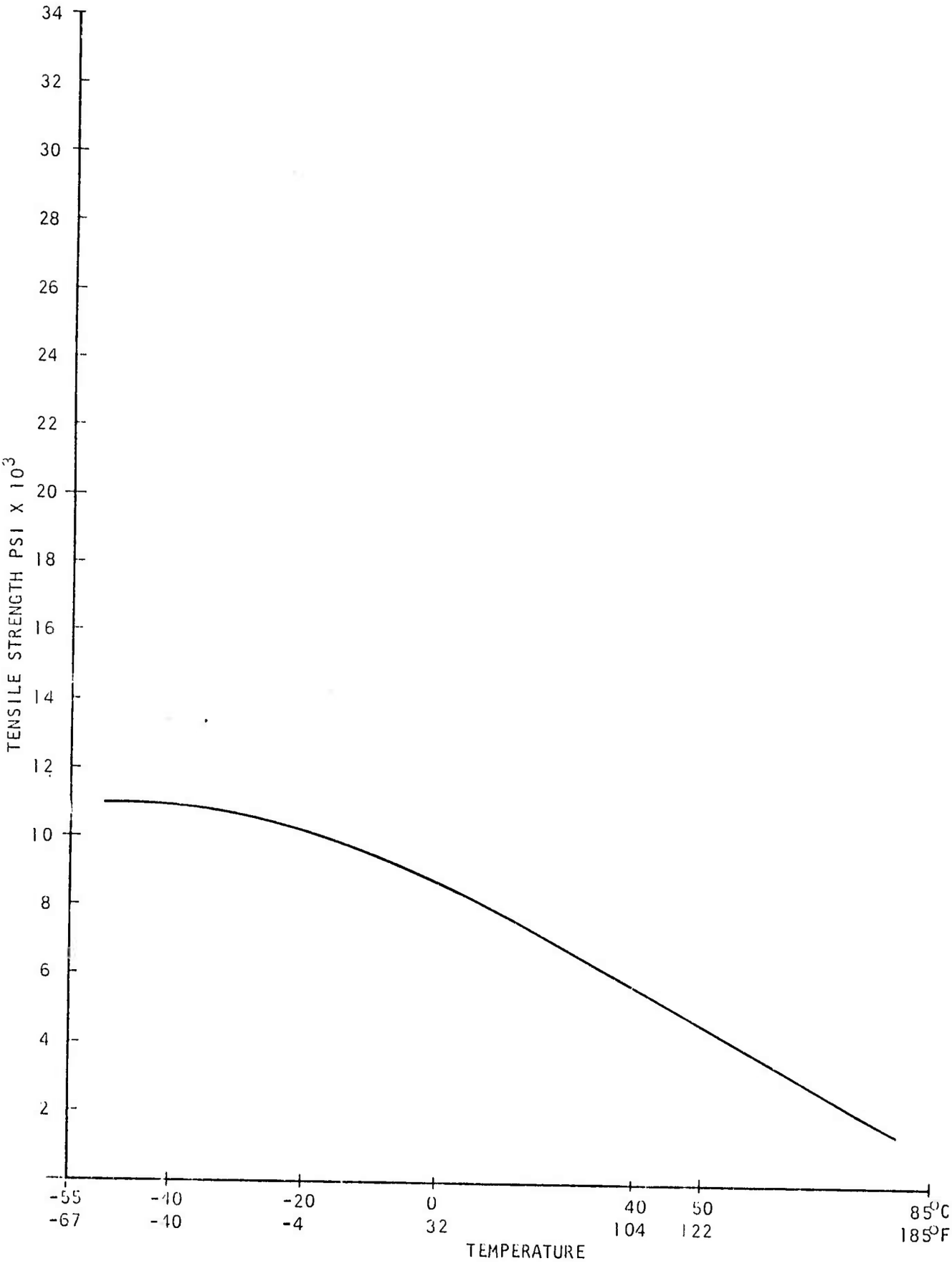

Figure B-13 Thermal Expansion vs Temperature.

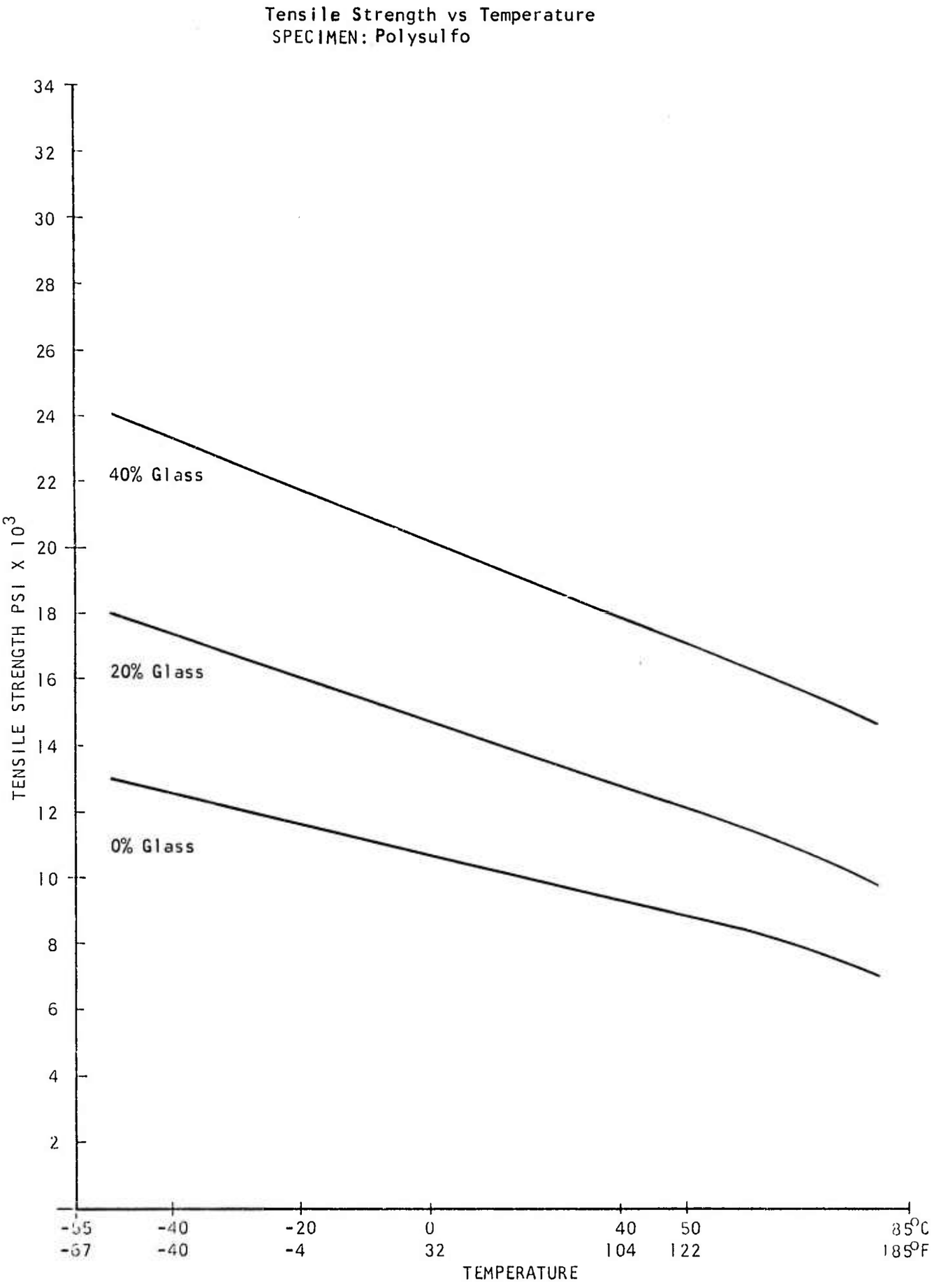

Figure B- 14 Thermal Expansion vs Temperature.

Tensile Strength vs Temperature
SPECIMEN: Acetal Copolymer

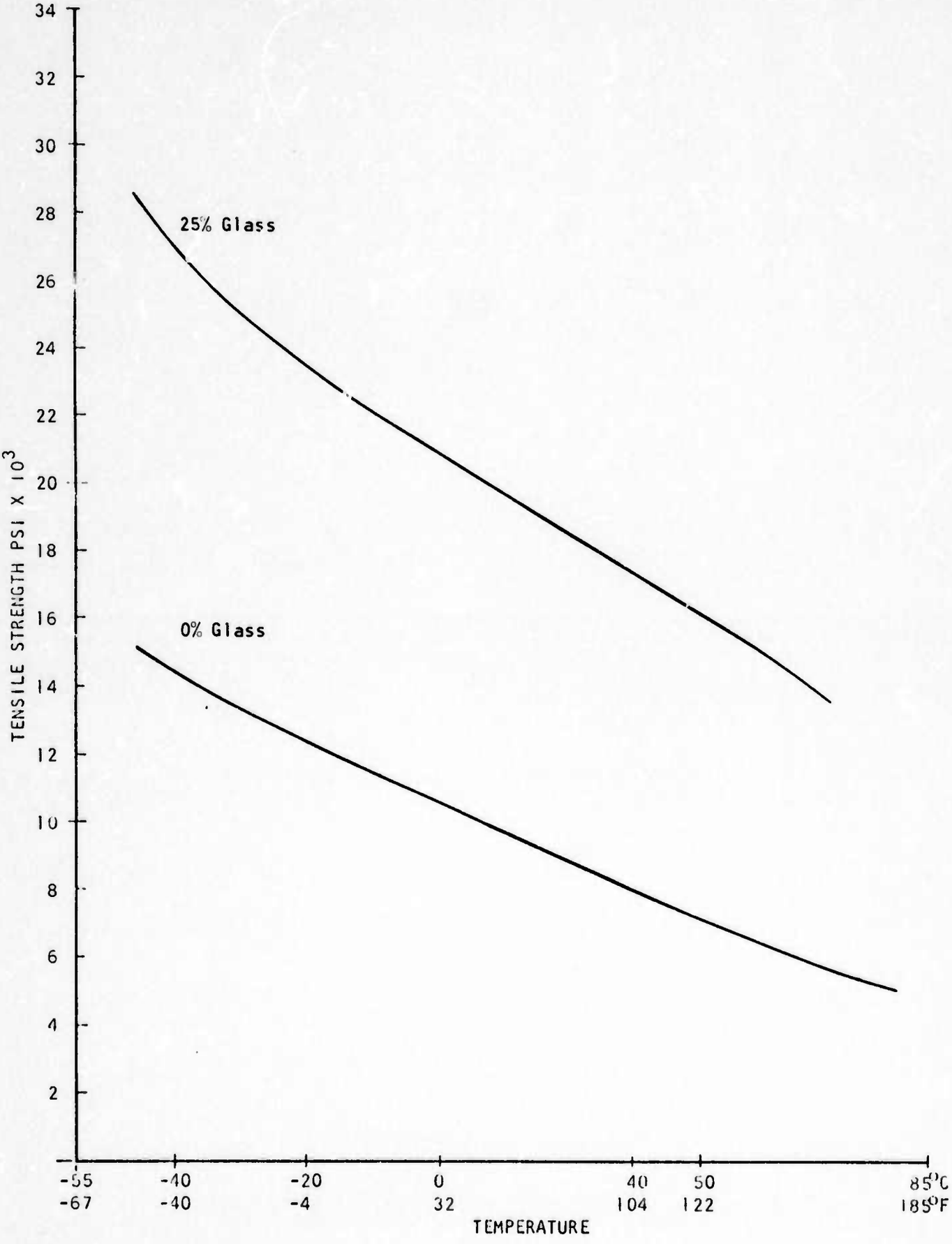

Figure B-15 Thermal Expansion vs Temperature.

Tensile Strength vs Temperature
SPECIMEN: Acetal Homopolymer

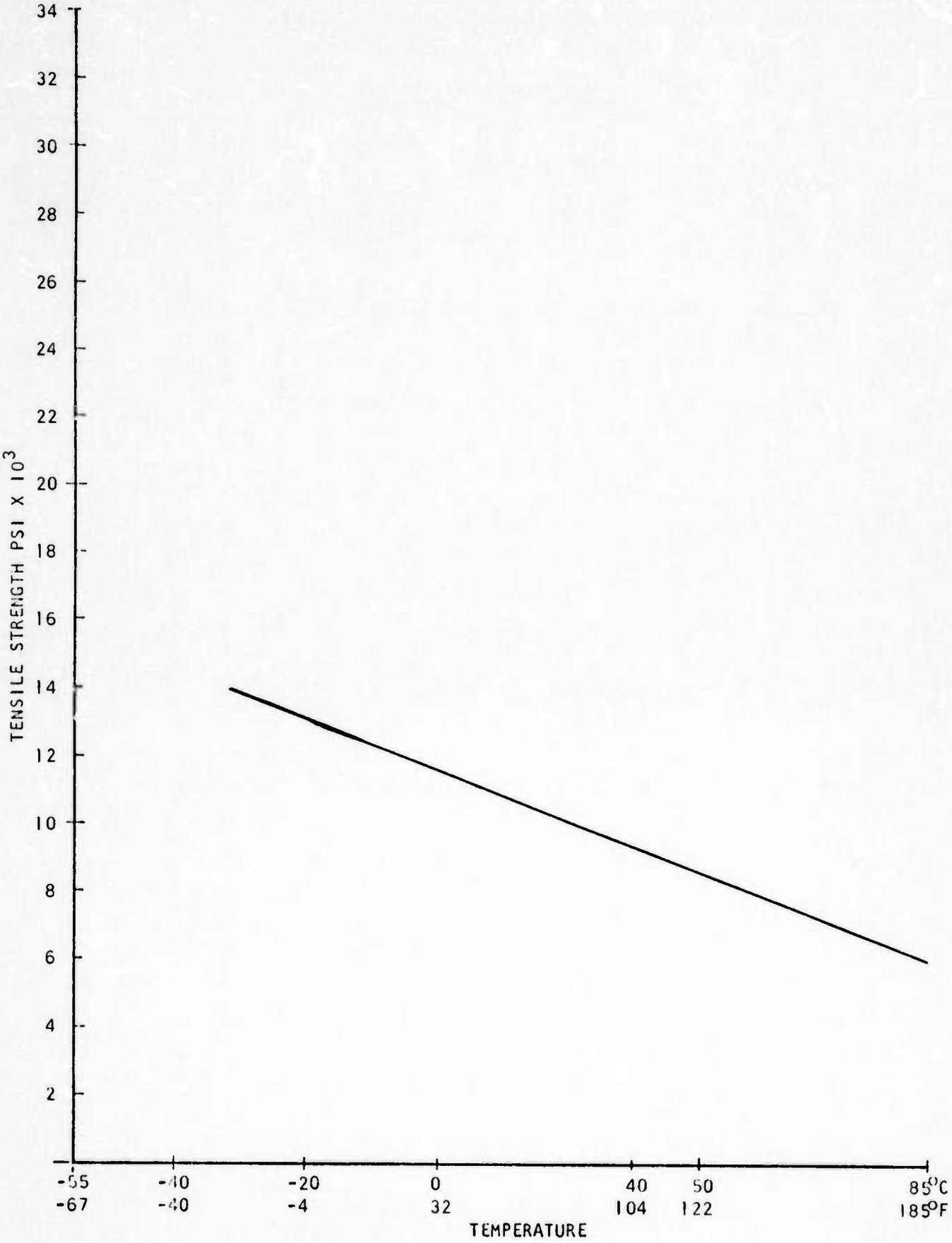

Figure B-16 Thermal Expansion vs Temperature.

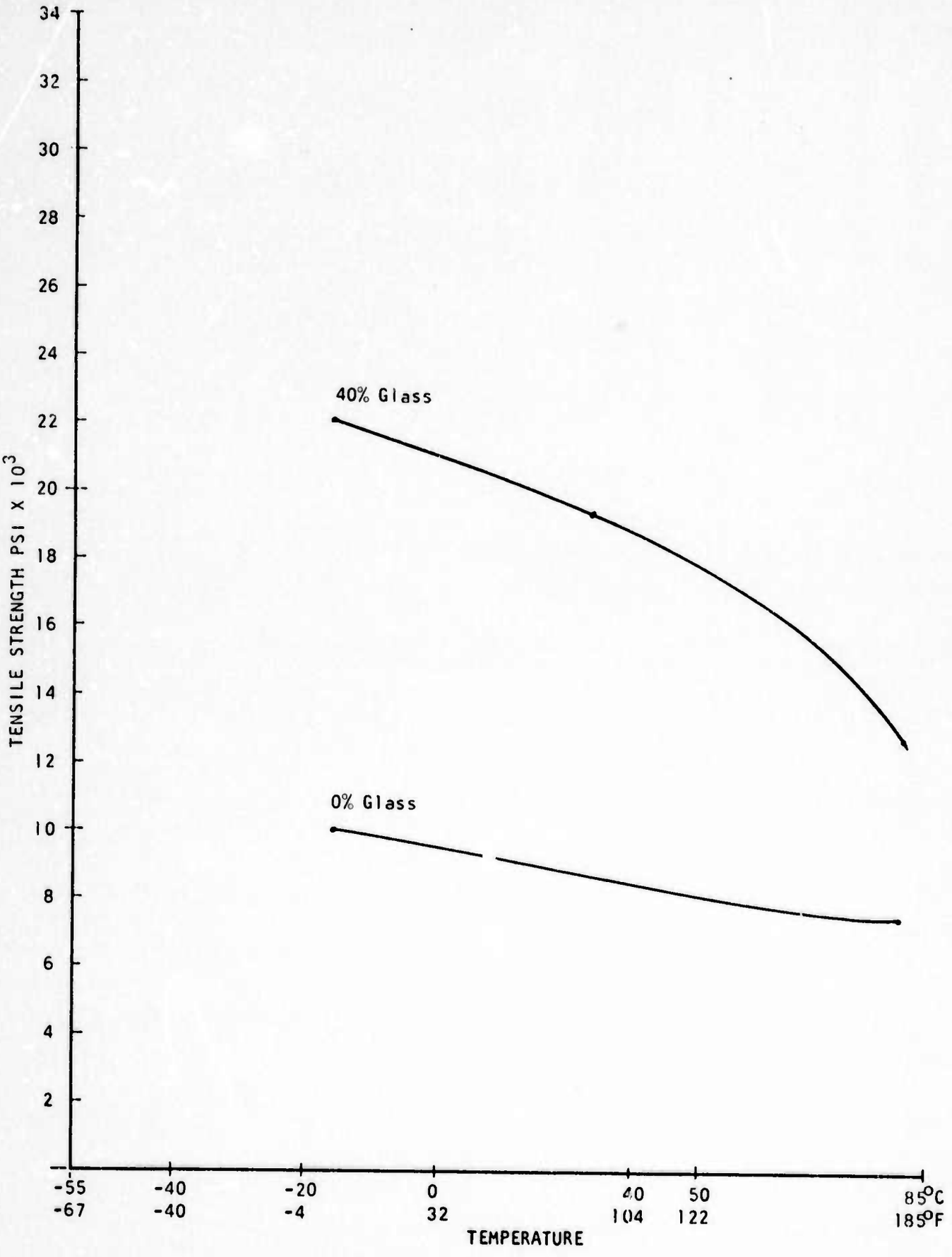

Figure B-17 Thermal Expansion vs Temperature.

Tensile Strength vs Temperature
SPECIMEN: Thermoplastic Polyester

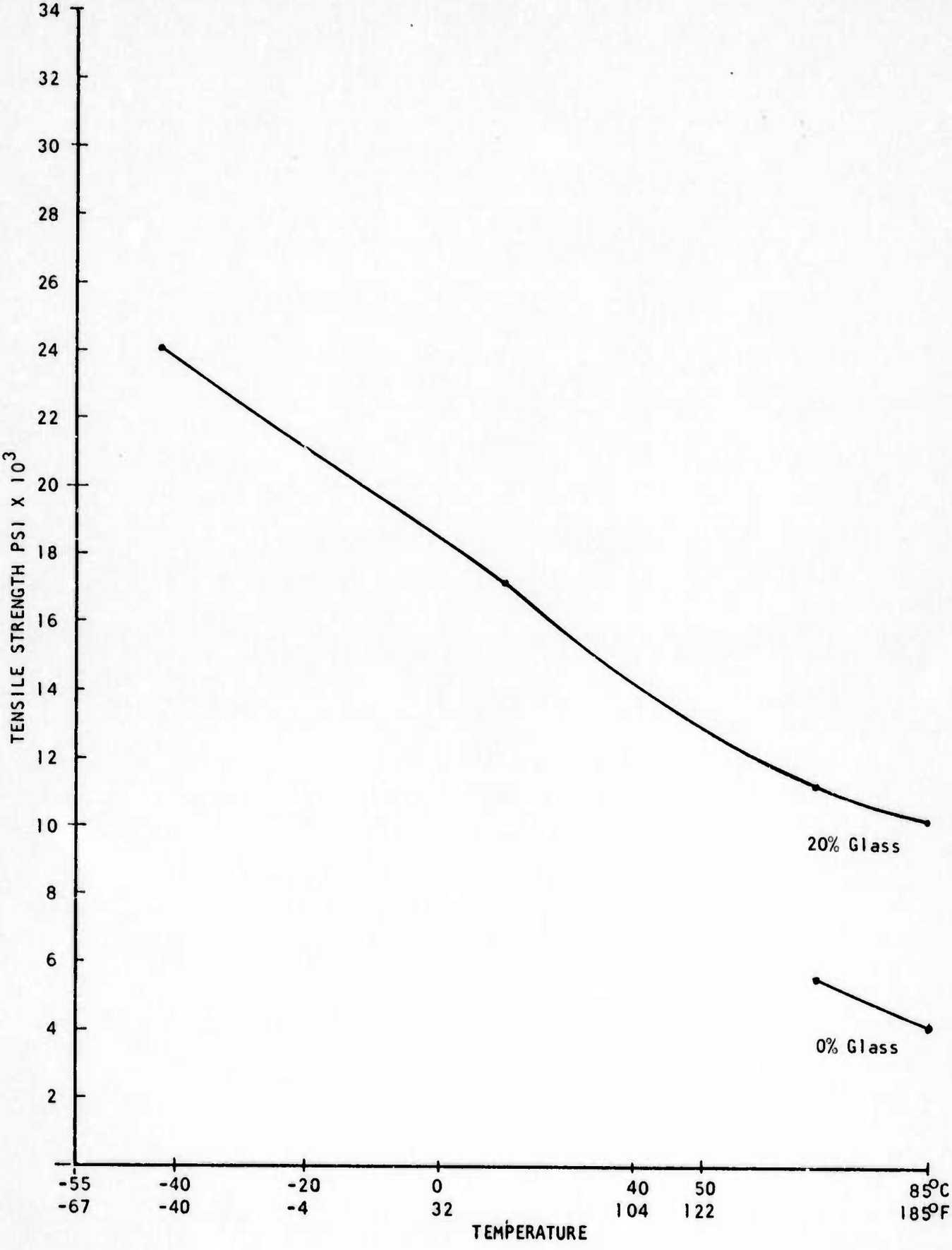

Figure B-18 Thermal Expansion vs Temperature.

Impact Strength vs Temperature
SPECIMEN: Thermoplastic Polyester

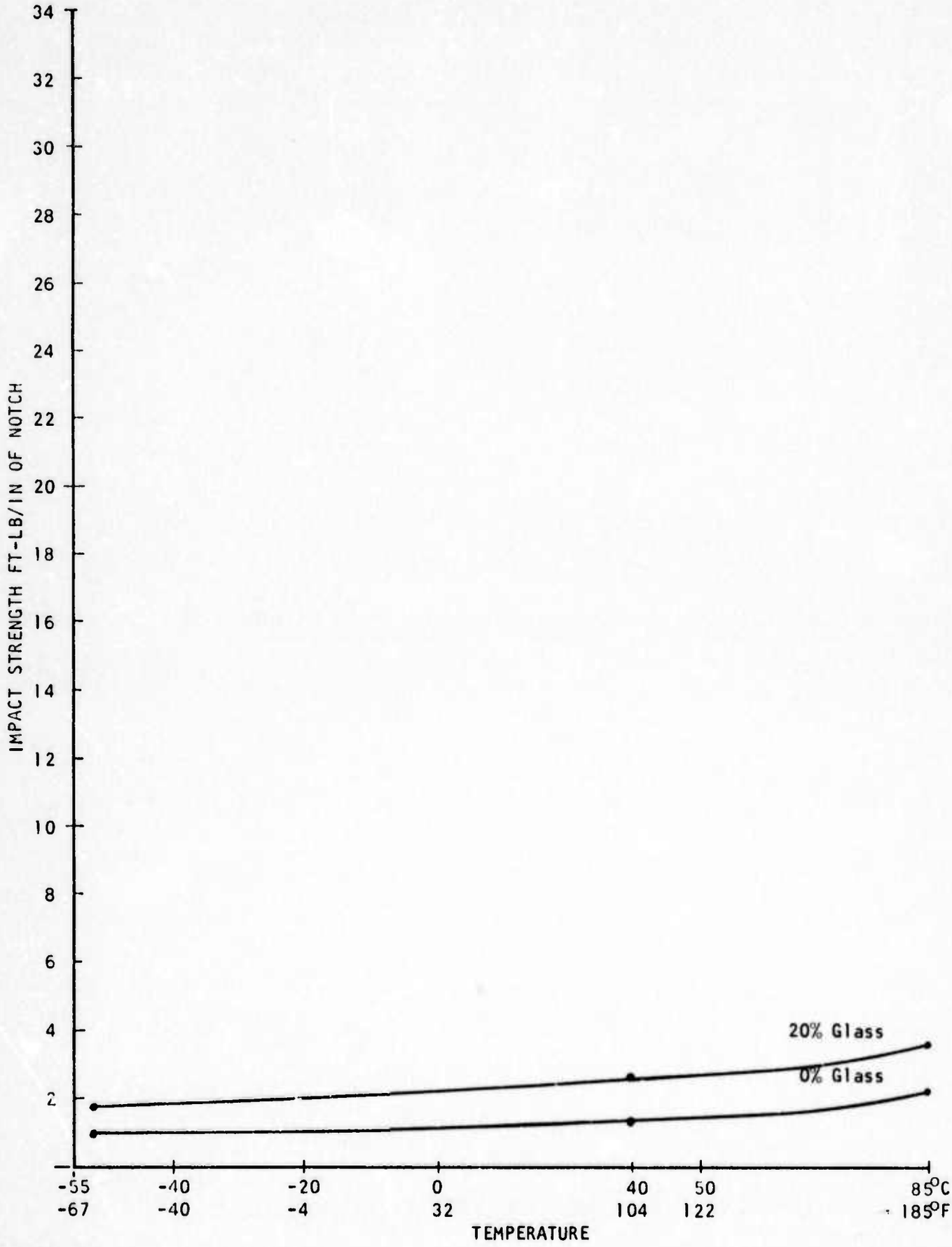

Figure B-19 Thermal Expansion vs Temperature.

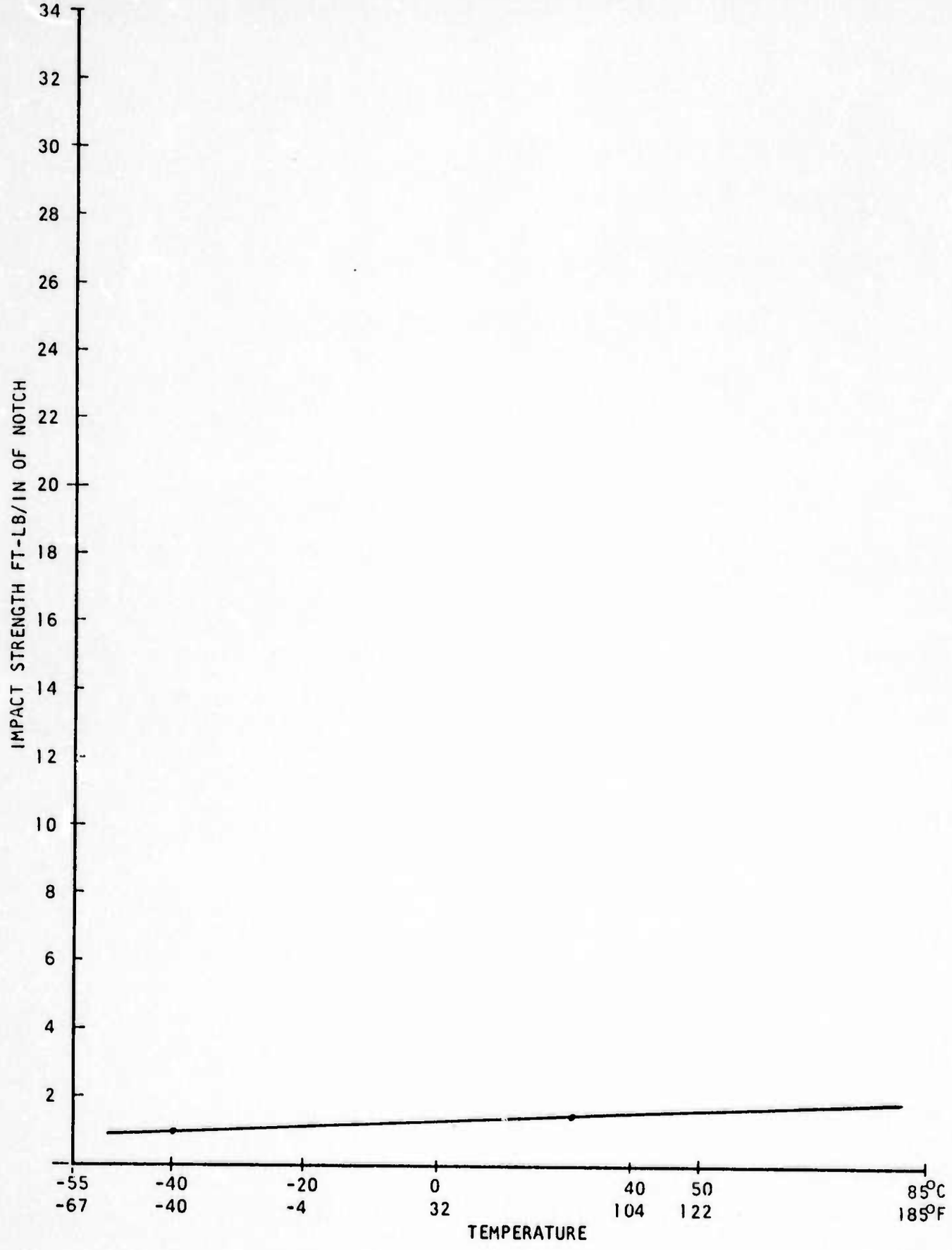

Figure B-20 Thermal Expansion vs Temperature.

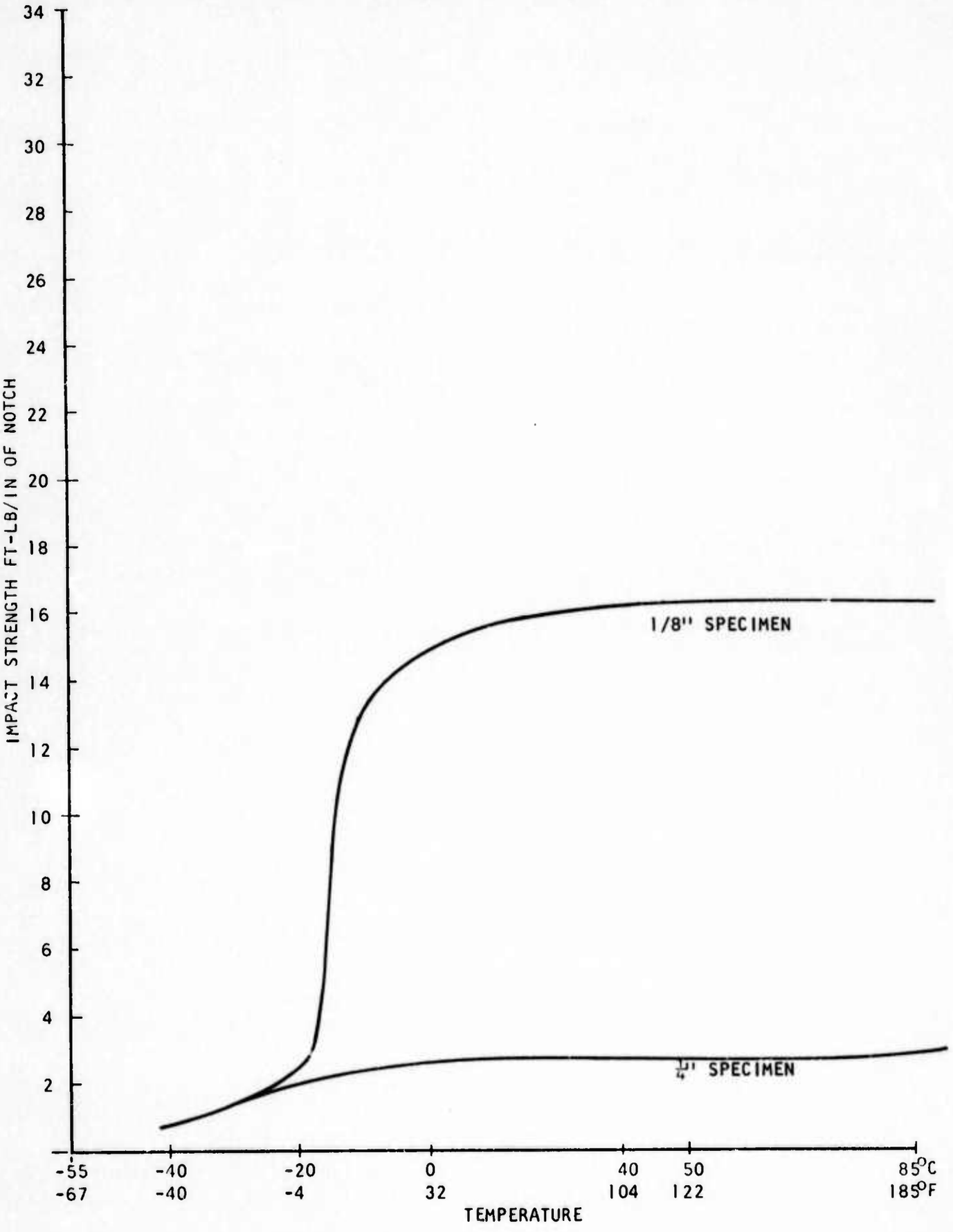

Figure B-21 Thermal Expansion vs Temperature.

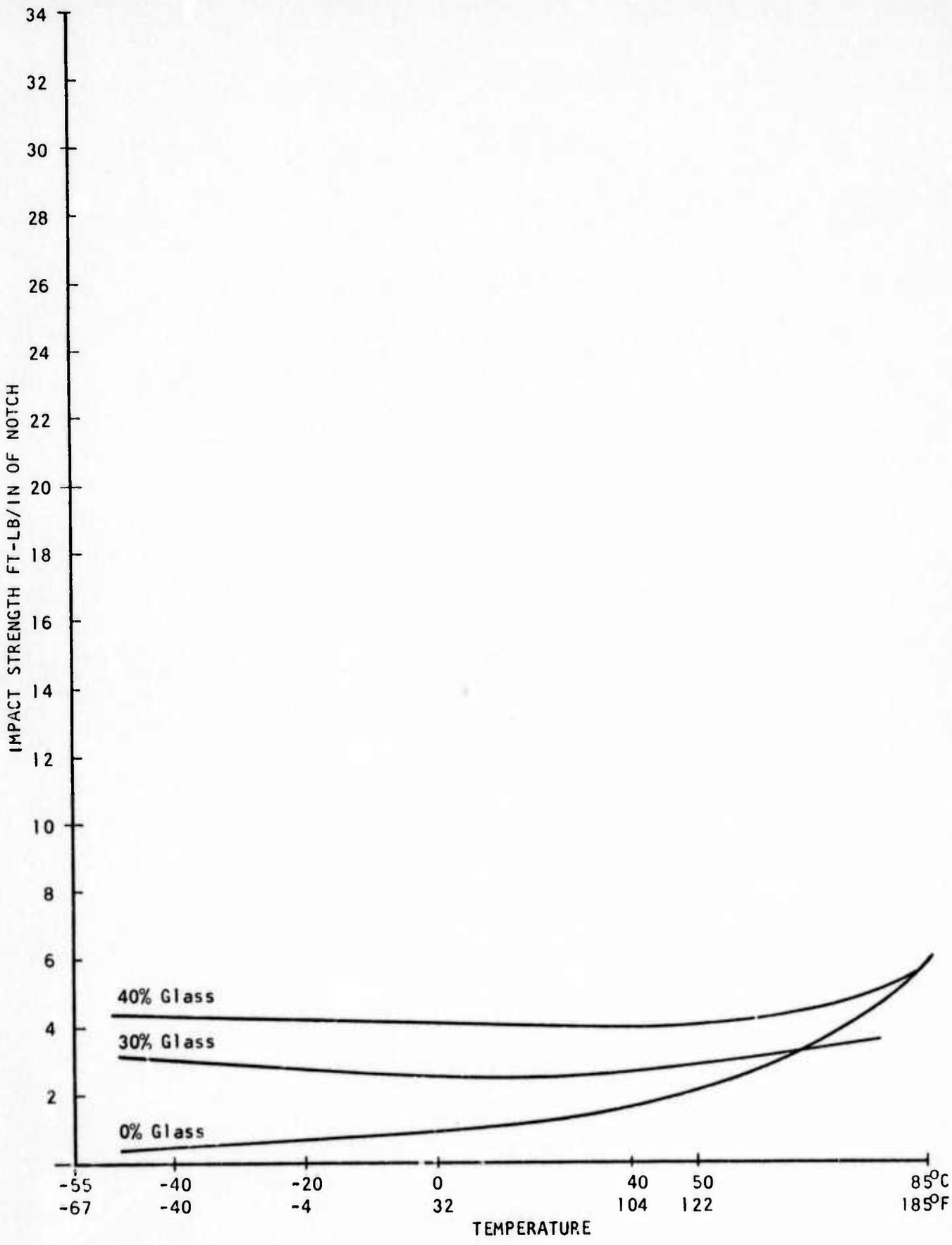

Figure B-22 Thermal Expansion vs Temperature.

Tensile Modulus vs Temperature
SPECIMEN: Acetal Homopolymer

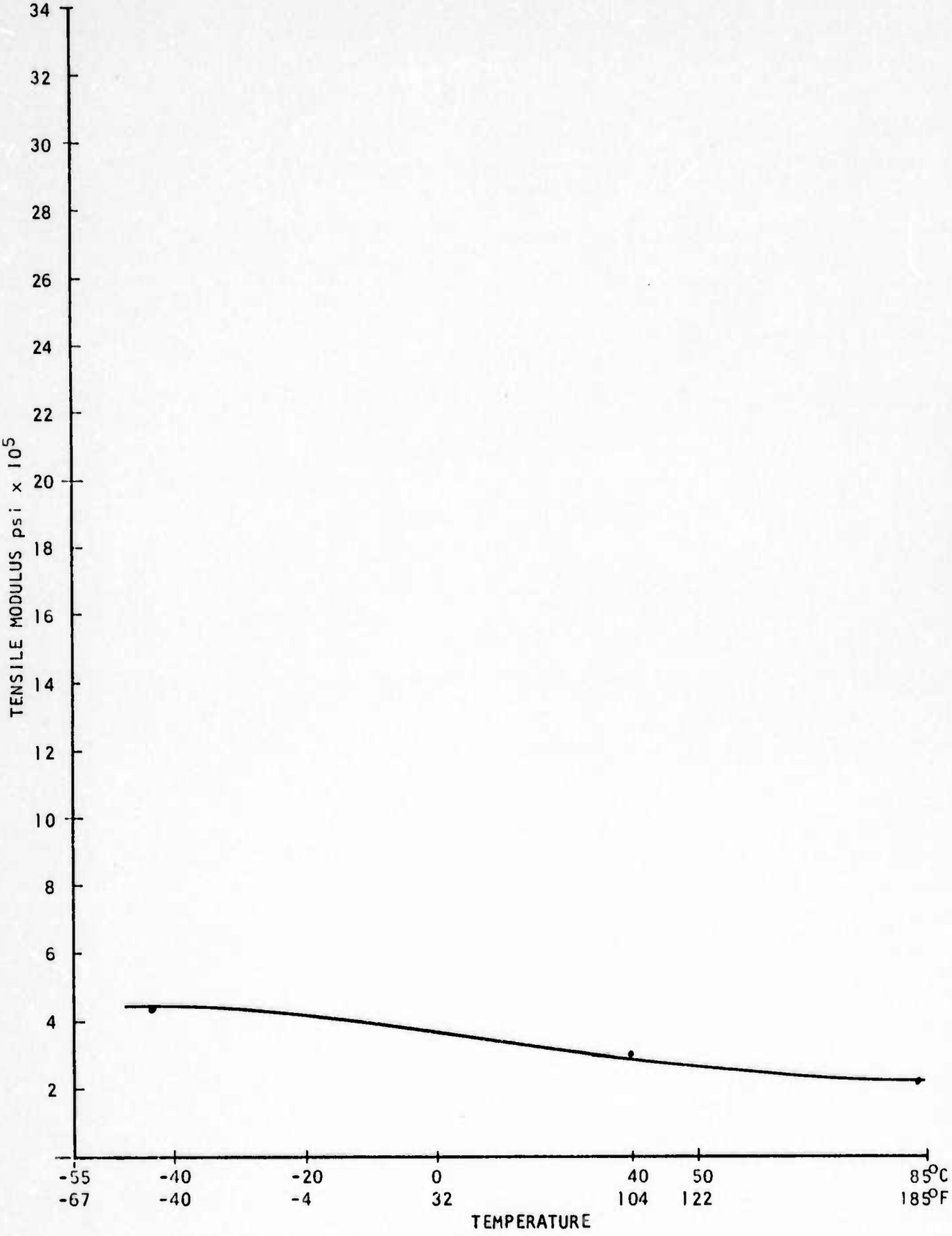

Figure B-23 Thermal Expansion vs Temperature.

Tensile Modulus vs Temperature
SPECIMEN: Nylon 6/6

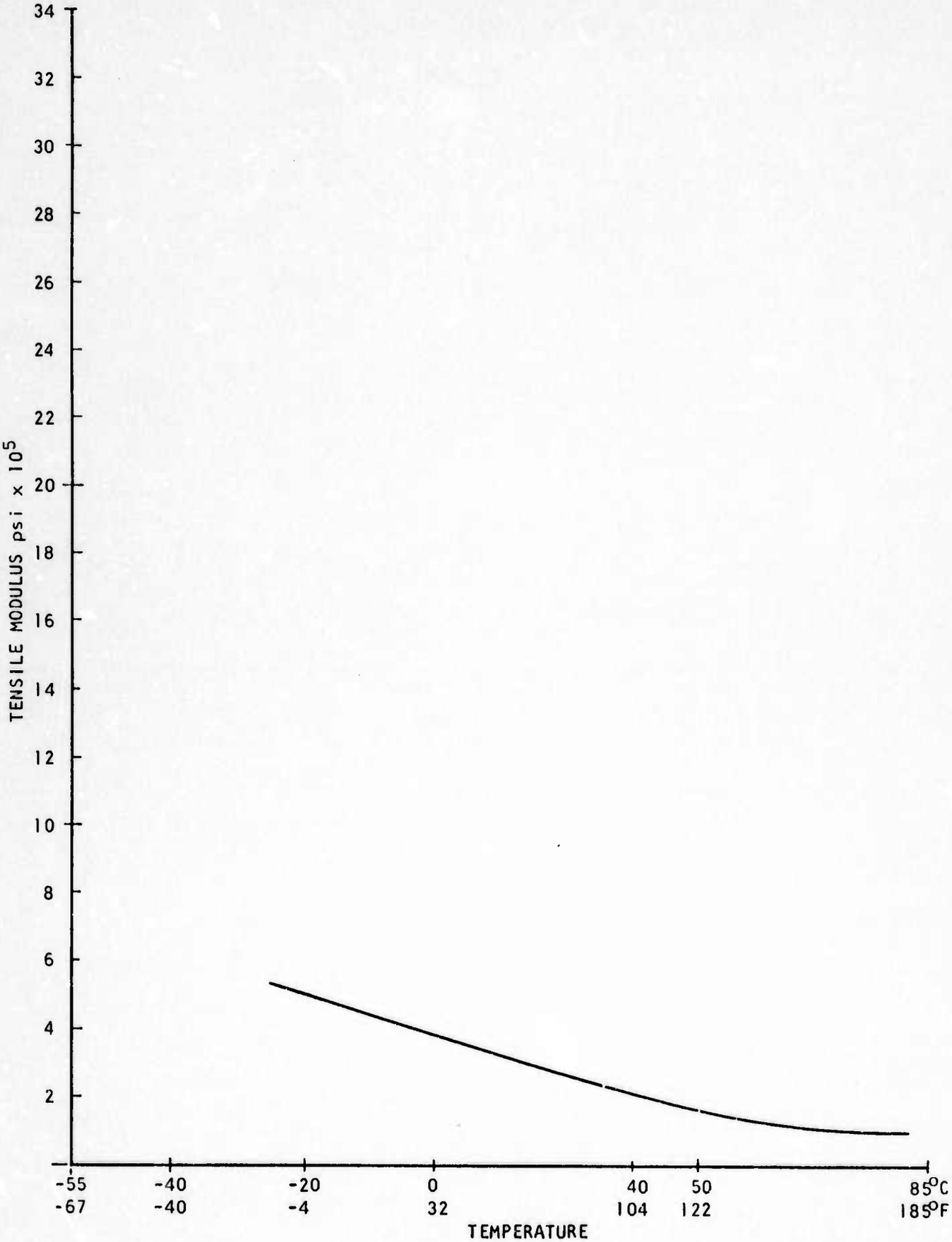

Figure B-24 Thermal Expansion vs Temperature.

Tensile Modulus vs Temperature
SPECIMEN: Polysulfone

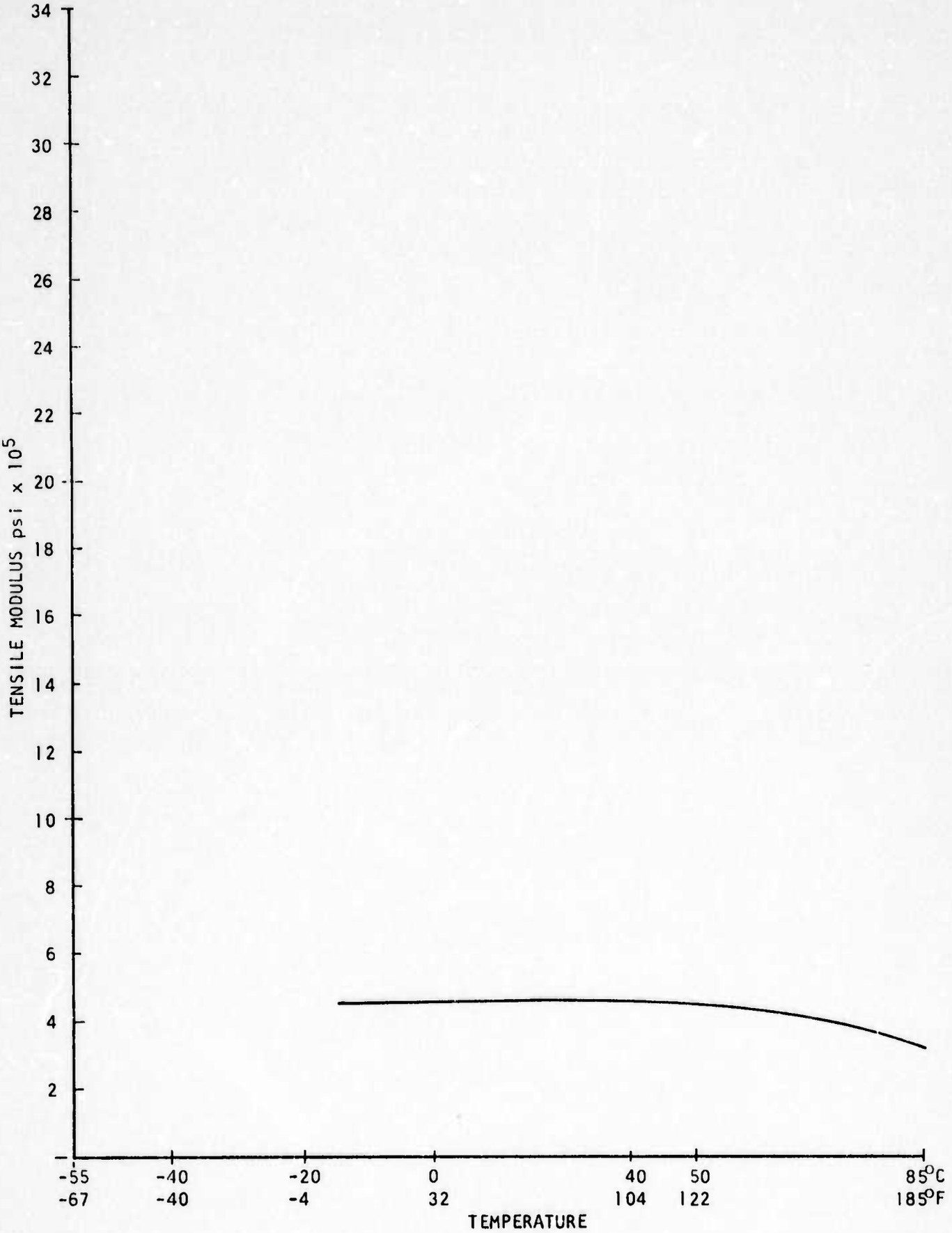

Figure B-25 Thermal Expansion vs Temperature.

Tensile Modulus vs Temperature
SPECIMEN: Phenolic

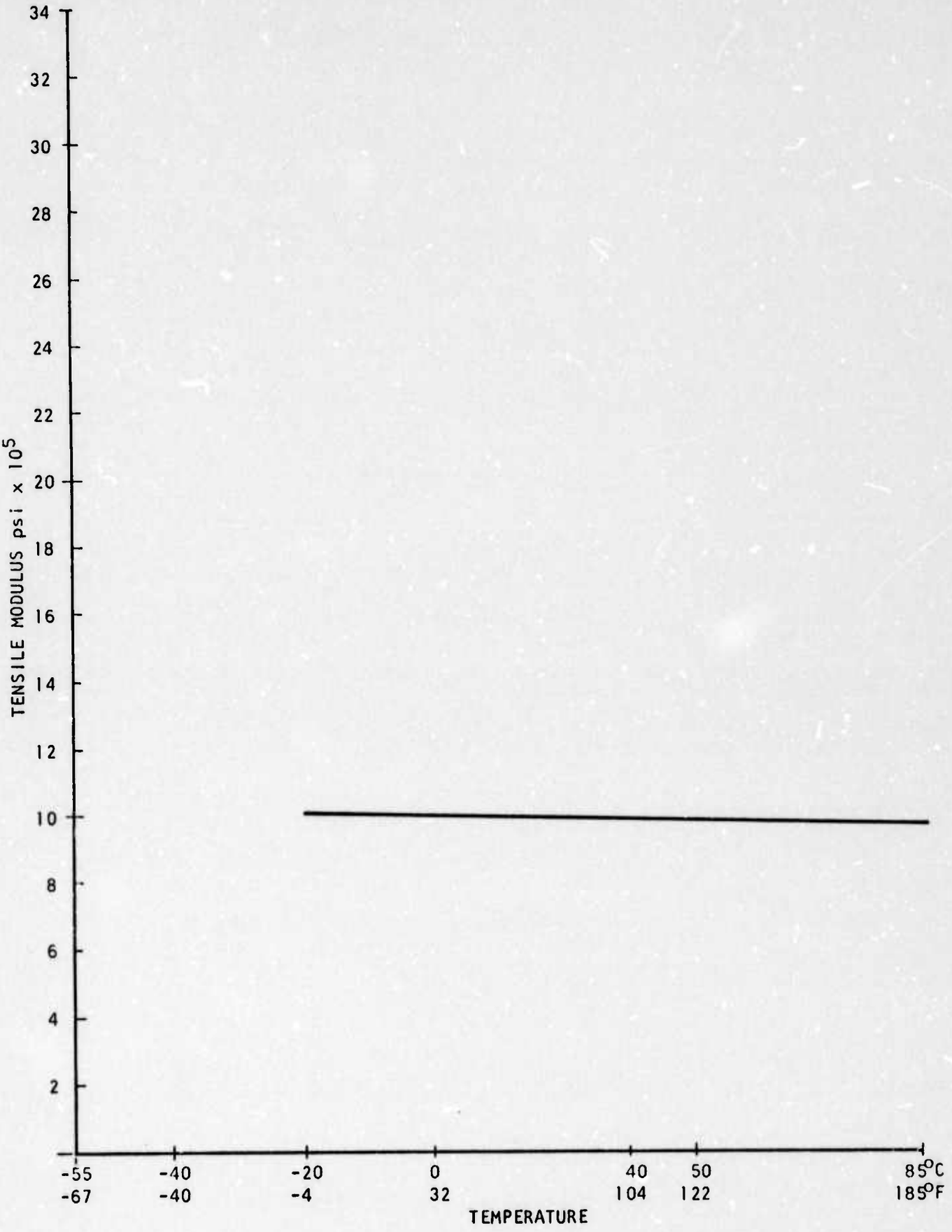

Figure B-26 Thermal Expansion vs Temperature.

Tensile Modulus vs Temperature
SPECIMEN: Polycarbonate

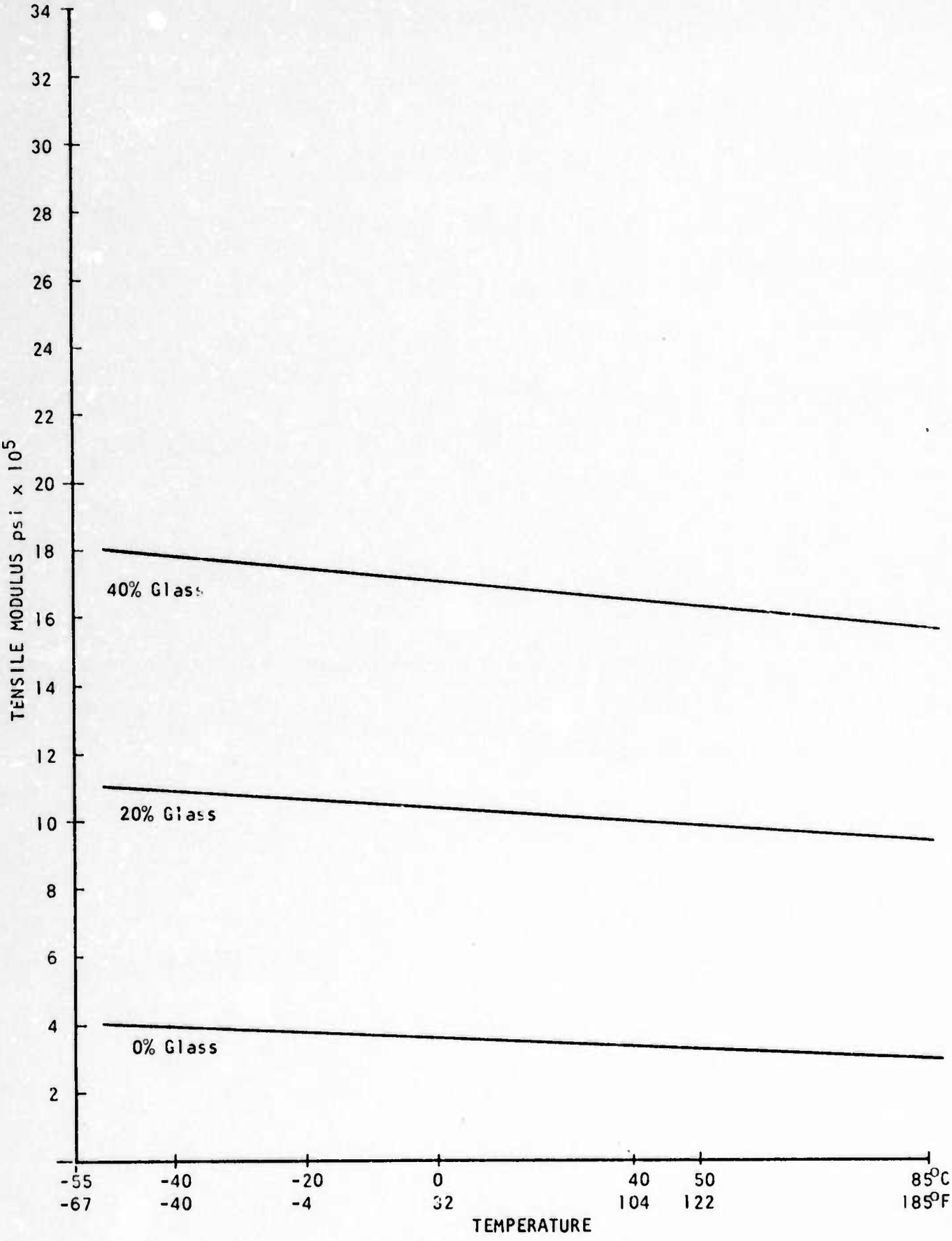

Figure B- 27 Thermal Expansion vs Temperature.

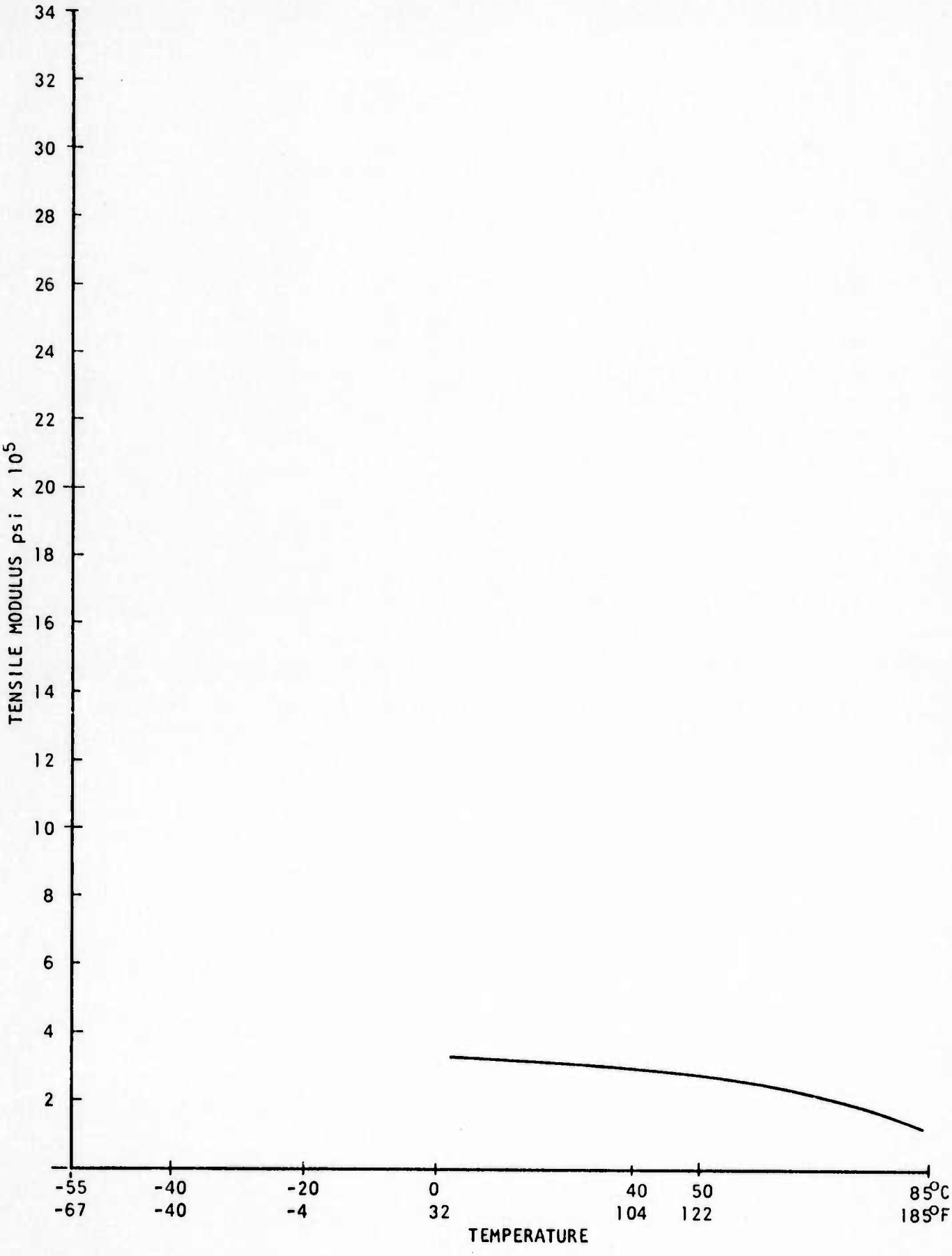

Figure B-28 Thermal Expansion vs Temperature.

Tensile Modulus vs Temperature
SPECIMEN: Phenylene Oxide-Noryl

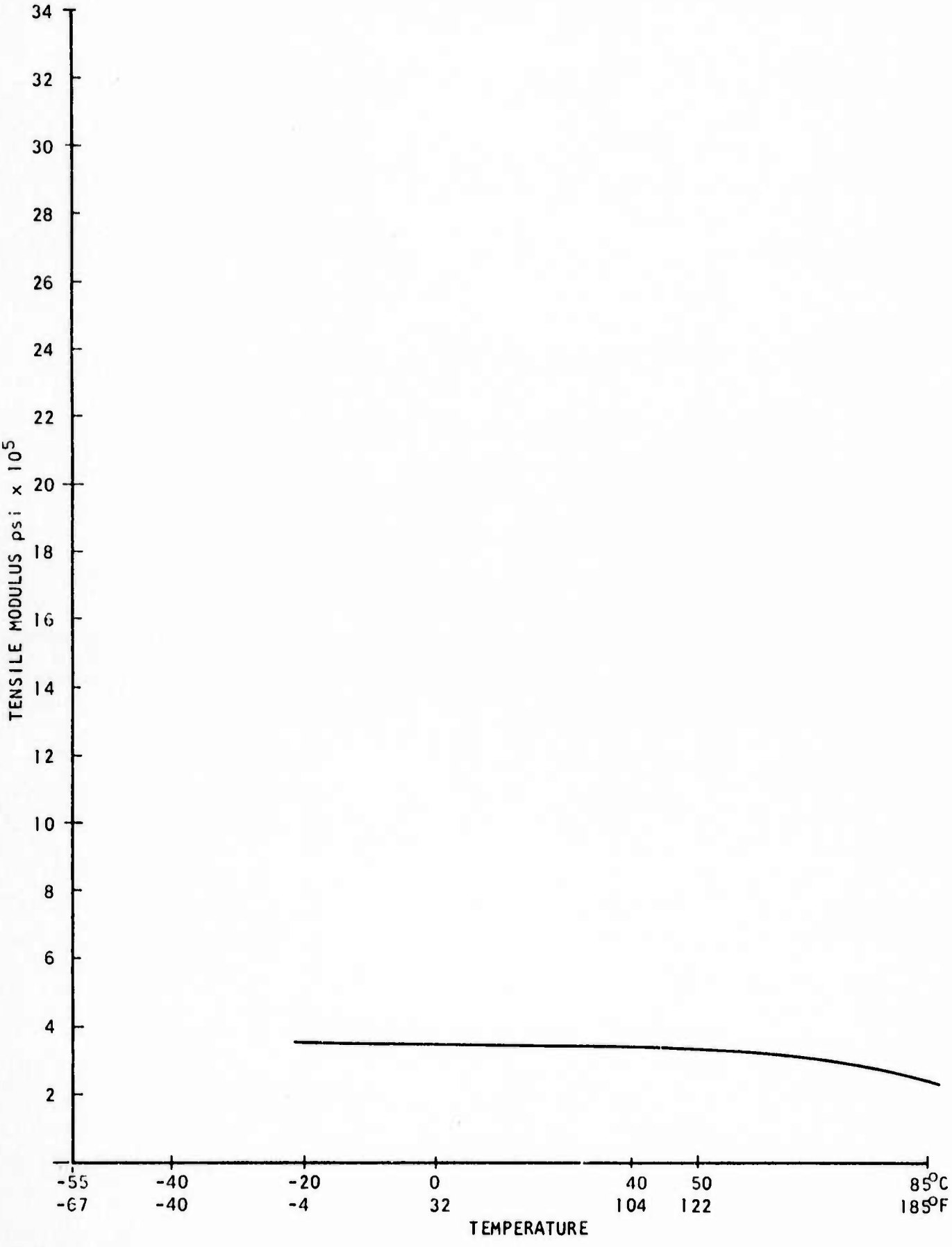

Figure B-29 Thermal Expansion vs Temperature.

Tensile Modulus vs Temperature
SPECIMEN: Acrylic

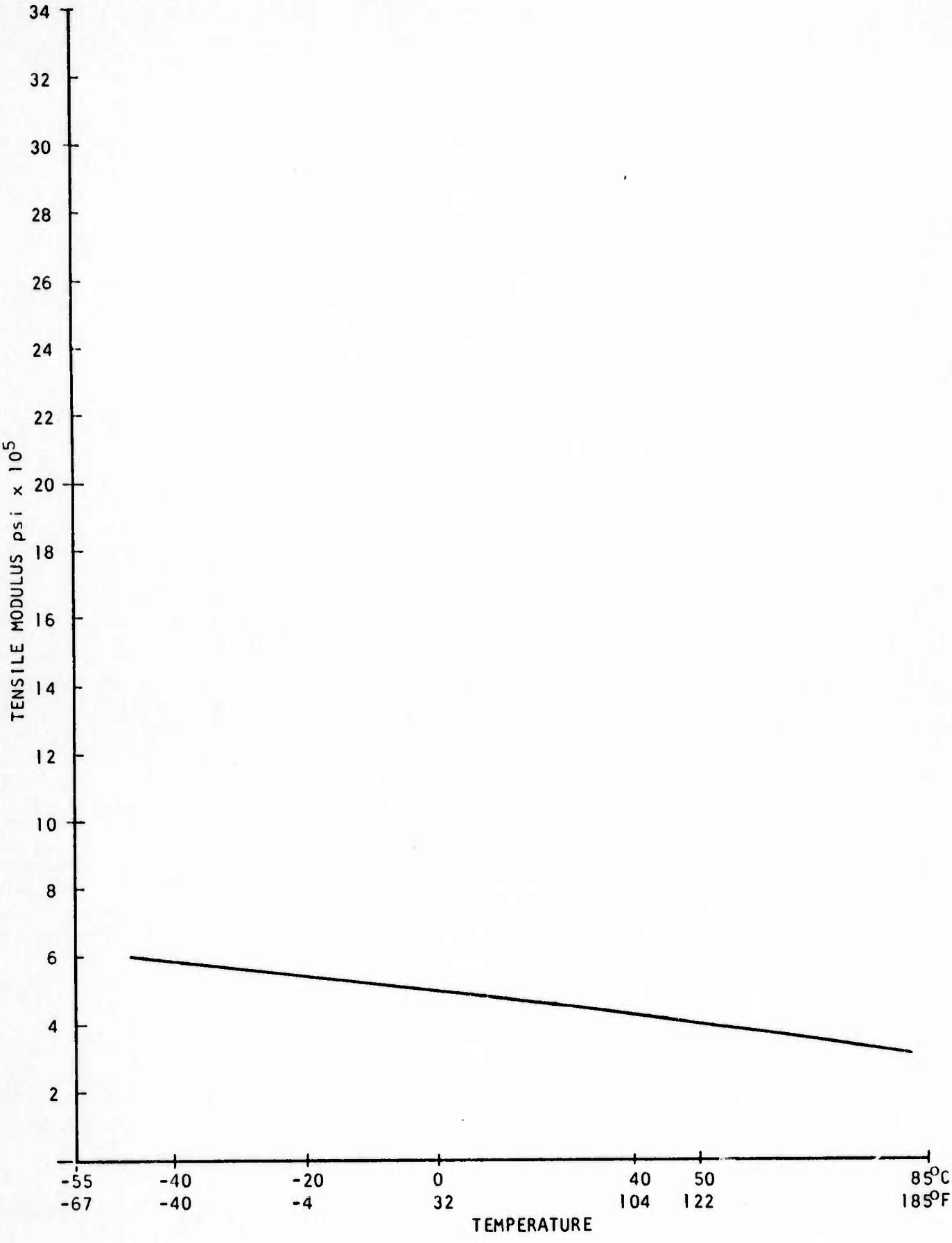

Figure B-30 Thermal Expansion vs Temperature.

Flexural Modulus vs Temperature
SPECiMEN: Thermoplastic Polyester

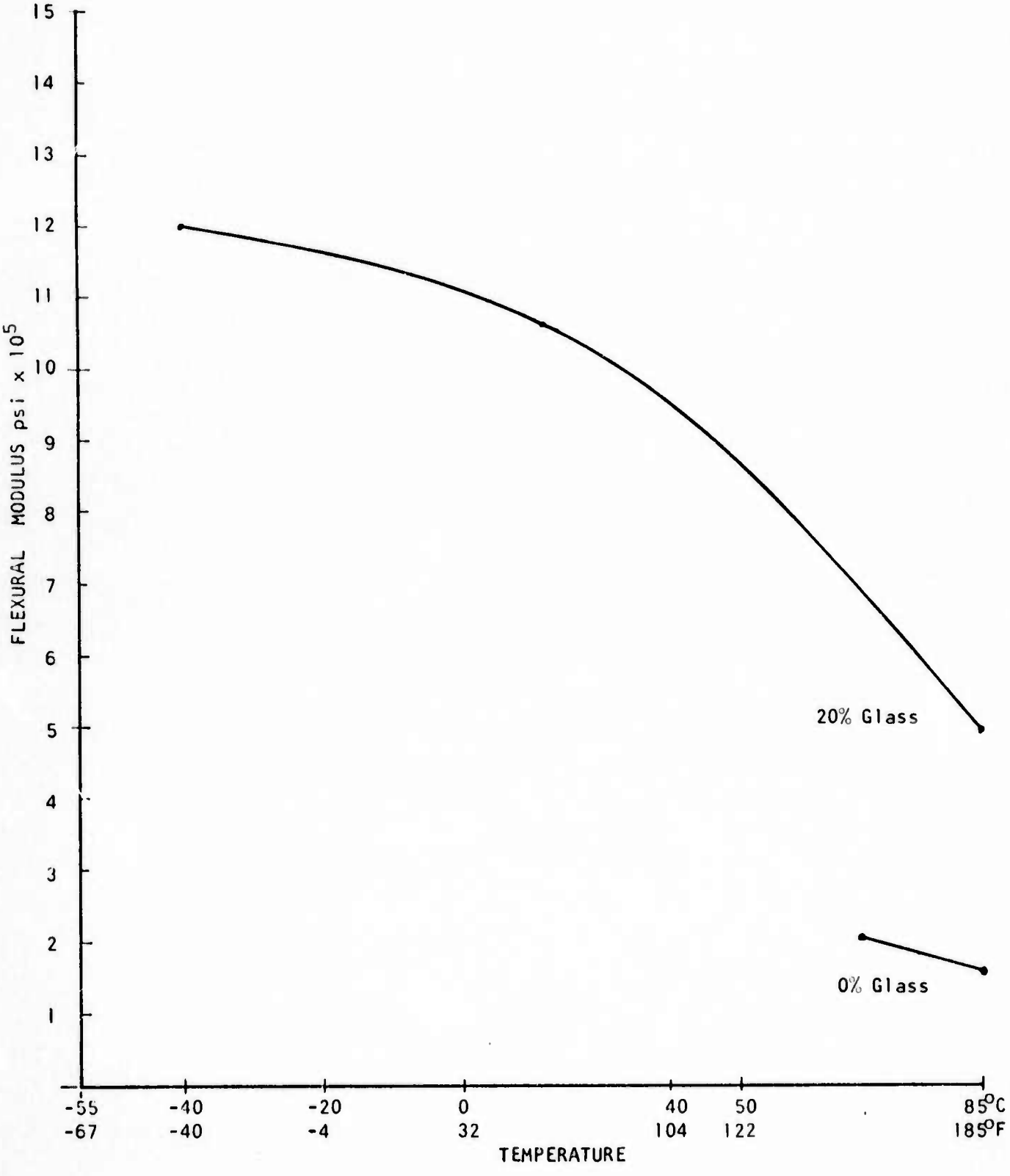

Figure B-31 Thermal Expansion vs Temperature.

Flexural Modulus vs Temperature
SPECIMEN: Phenylene Sulfide

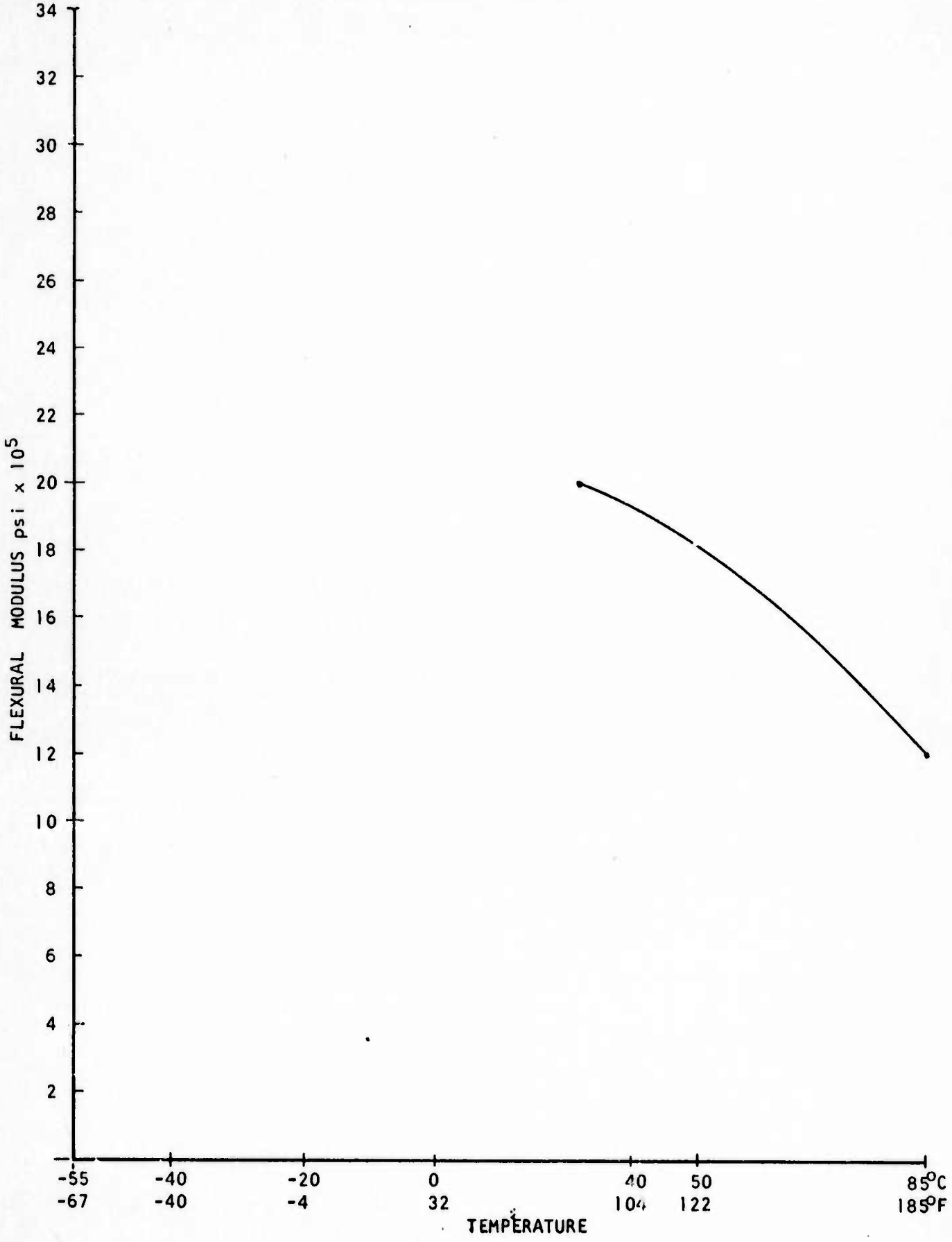

Figure B-32 Thermal Expansion vs Temperature.

Flexural Modulus vs Temperature
SPECIMEN: Acetal Homopolymer

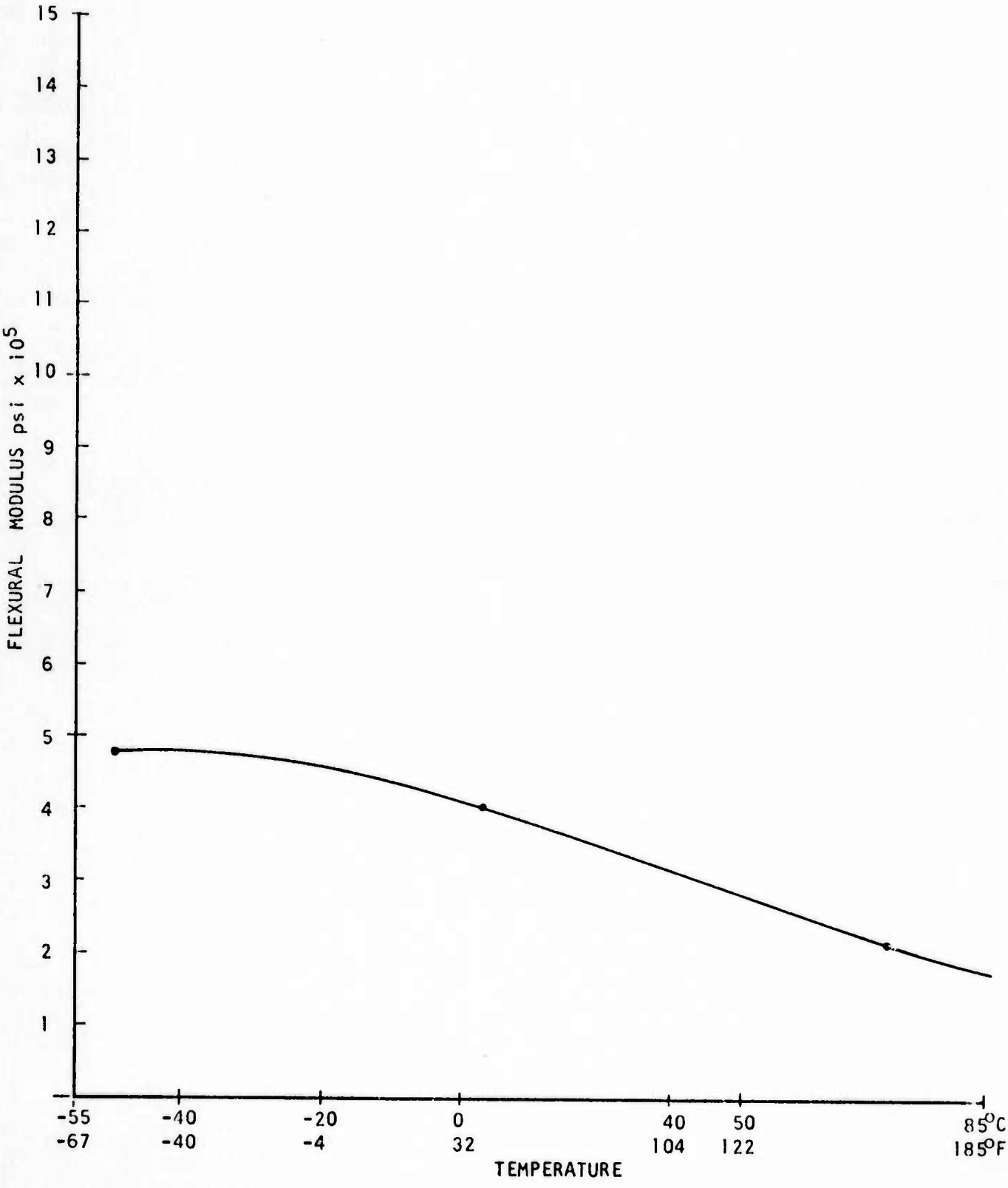

Figure B-33 Thermal Expansion vs Temperature.

Flexural Modulus vs Temperature
SPECIMEN: Acetal Copolymer

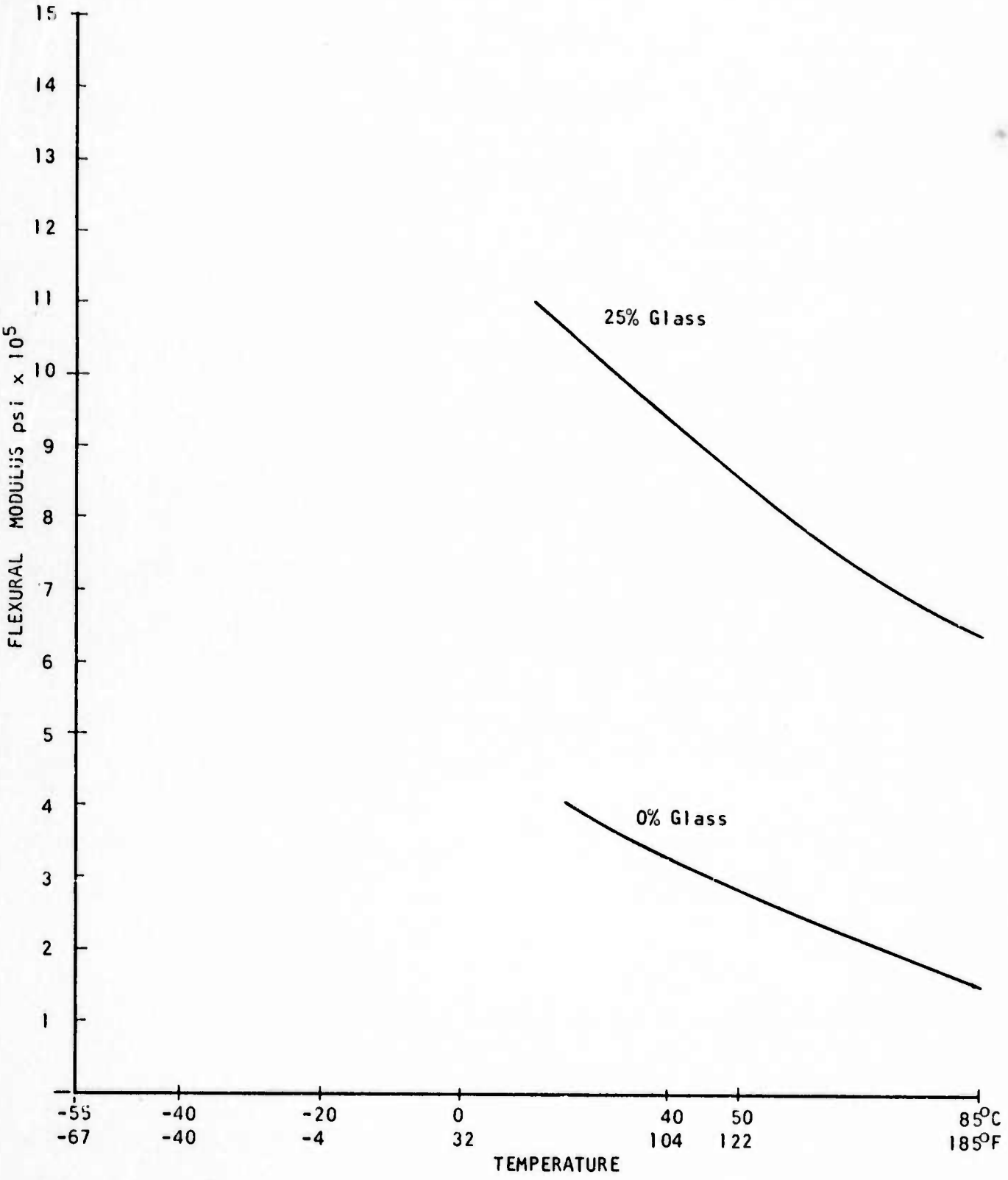

Figure B-34 Thermal Expansion vs Temperature.

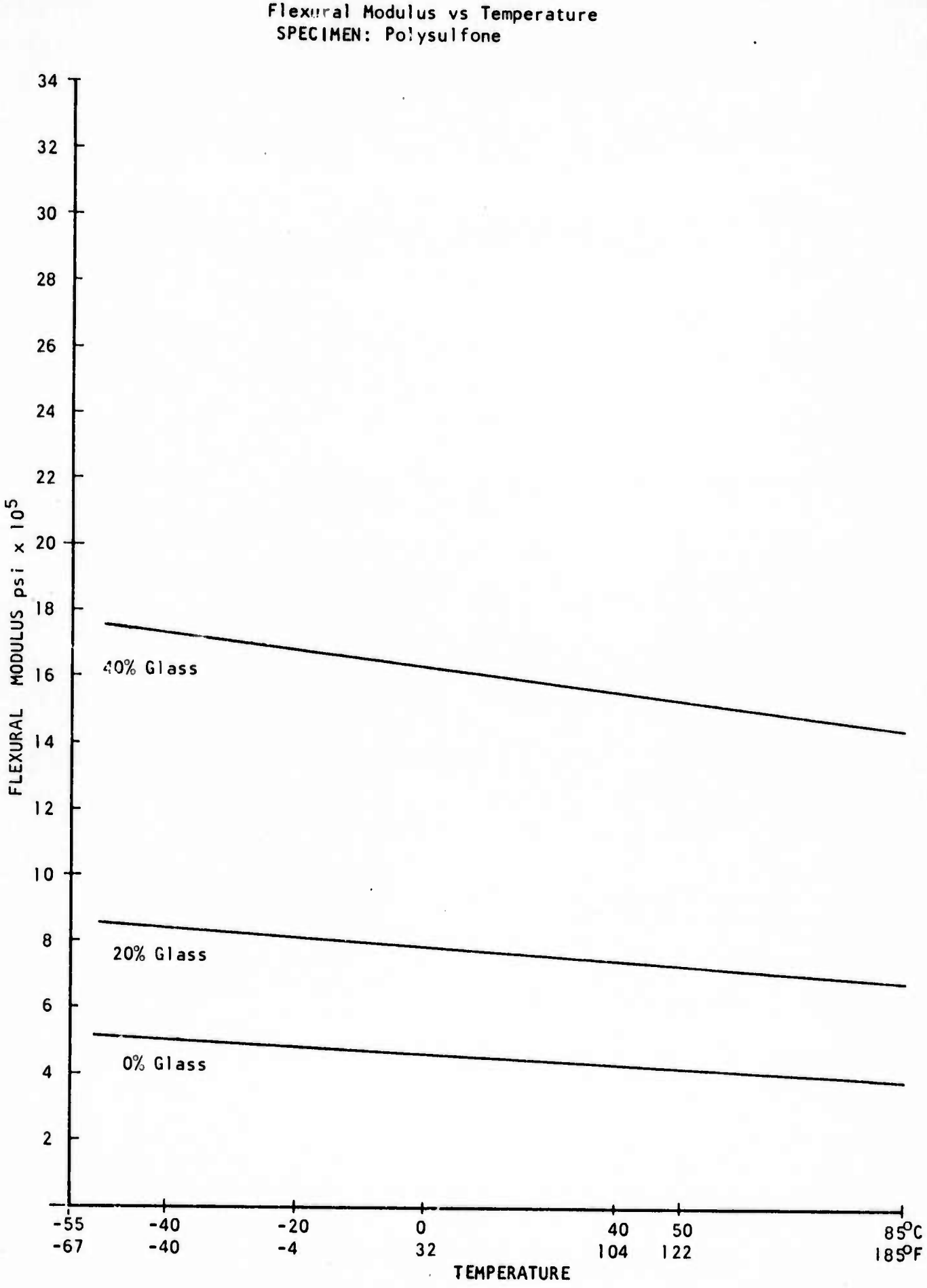

Figure B-35 Thermal Expansion vs Temperature.

Flexural Modulus vs Temperature
SPECIMEN: Nylon 6/6

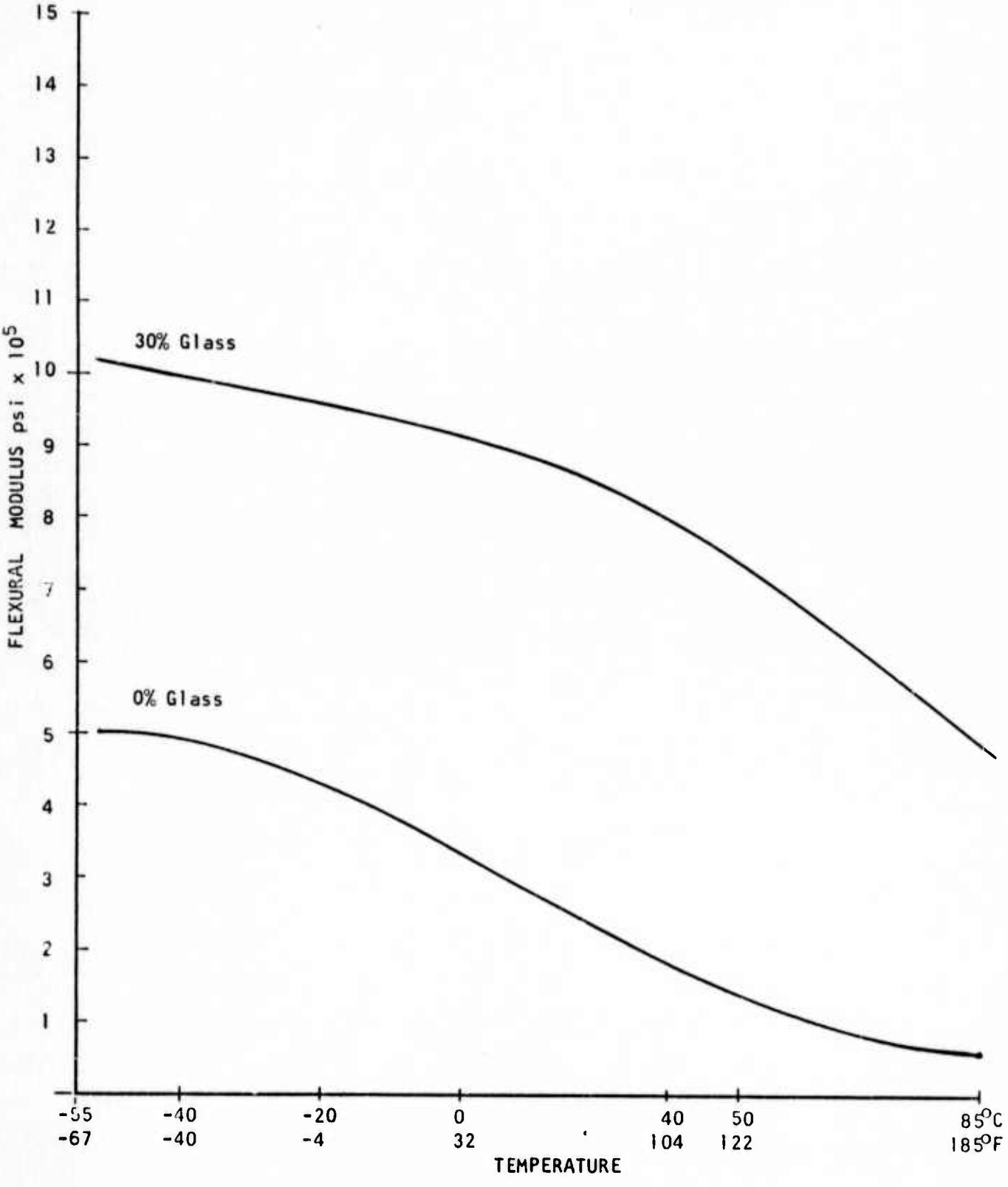

Figure B-36 Thermal Expansion vs Temperature.

Flexural Modulus vs Temperature
SPECIMEN: Phenylene Oxide - Noryl

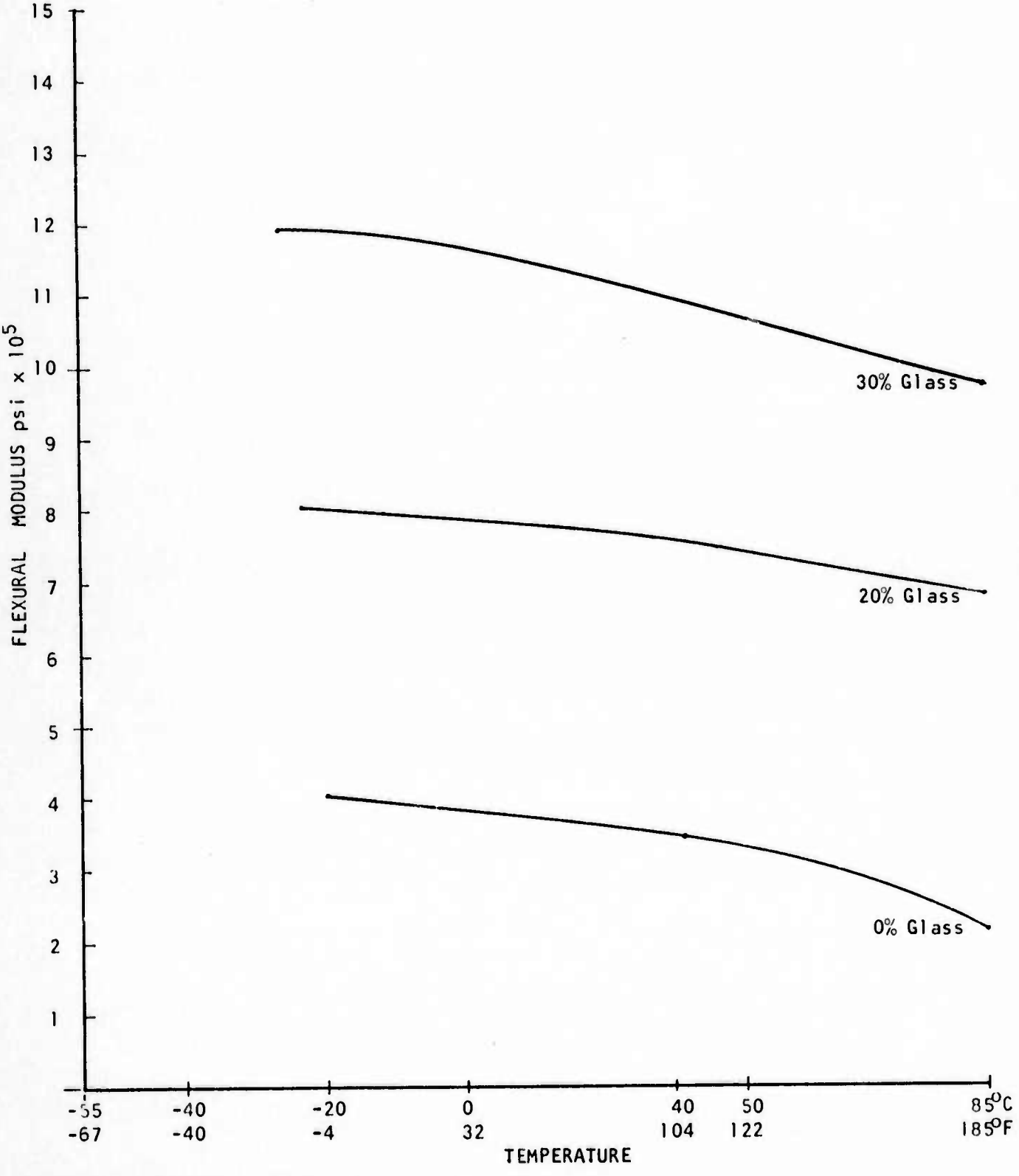

Figure B-37 Thermal Expansion vs Temperature.

APPENDIX C

METHOD 508

FUNGUS

1. **Purpose.** The fungus test is used to determine the resistance of equipment to fungi and to determine if such equipment is adversely affected by fungi under conditions favorable for their development, namely high humidity, warm atmosphere, and presence of inorganic salts.

Typical materials which will support and are damaged by fungi are:

- Cotton
- Wood
- Linen
- Cellulose nitrate
- Regenerated cellulose
- Leather
- Paper and cardboard
- Cork
- Hair and felts
- Natural rubber
- Plastic materials containing linen, cotton or wood flour as a filler
- Vinyl films containing fungus susceptible plasticizers
- Formulations of elastomers containing fungus susceptible catalysts, plasticizers or fillers

2. **Apparatus.** The aparatus required to conduct this test consists of chambers or cabinets together with auxiliary instrumentation capable of maintaining the specified condition of temperature and humidity. Provisions shall be made to prevent condensation from dripping on the test item. There shall be free circulation of air around the test item and the surface area of fixtures supporting the test item shall be kept to a minimum.

3. **Procedures.**

3.1 **Procedure I.**

3.1.1 *Preparation of mineral-salts solution.* The solution shall contain the following:

Potassium dihydrogen orthophosphate (KH_2PO_4)	0.7 g
Potassium monohydrogen orthophosphate (K_2HPO_4)	0.7 g
Magnesium sulfate ($MgSO_4 \cdot 7H_2O$)	0.7 g
Ammonium nitrate (NH_4NO_3)	1.0 g
Sodium chloride (NaCl)	0.005 g
Ferrous sulfate ($FeSO_4 \cdot 7H_2O$)	0.002 g
Zinc sulfate ($ZnSO_4 \cdot 7H_2O$)	0.002 g
Manganous sulfate ($MnSO_4 \cdot 7H_2O$)	0.001 g
Distilled water	1000 ml

Sterilize the mineral salts solution by autoclaving at 121° C (250° F) for 20 minutes. Adjust the pH of the solution by the addition of 0.01 normal solution of NaOH so that after sterilization the pH is between 6.0 and 6.5. Prepare sufficient salts solution for the required tests.

3.1.1.1 *Purity of reagents.* Reagent grade chemicals shall be used in all tests. Unless otherwise specified, it is intended that all reagents shall conform to the specifications of the Committee on Analytical Reagents of the American Chemical Society, where such specifications are available.

3.1.1.2 *Purity of water.* Unless otherwise specified, references to water shall be understood to mean distilled water or water of equal purity.

3.1.2 *Preparation of mixed spore suspension.* The following test fungi shall be used:

Fungi	ATCC No.[1]	NLABS No.[2]
Aspergillus niger	9642	386
Aspergillus flavus	9643	380
Aspergillus versicolor	11730	432
Penicillium funiculosum	9644	391
Chaetomium globosum	6205	459

[1] American Type Culture Collection, 12301 Parklawn Drive, Rockville, Maryland 20852

[2] Pioneering Research Division, U.S. Army Natick Laboratories, Natick, Massachusetts 01760

Maintain cultures of these fungi separately on an appropriate medium such as potato dextrose agar. However, the culture of *Chaetomium globosum* shall be cultured on strips of filter paper on the surface of mineral — salts agar. (Mineral salts agar is identical to mineral salts solution described in 3.1.1, but contains in addition 15.0 g of agar per liter.) The stock cultures may be kept for not more than 4 months at 6 ±4° C (43° F). Use subcultures incubated at 29° C (84° F) for 7 to 20 days in preparing the spore suspension.

Prepare a spore suspension of each of the five fungi by pouring into one subculture of each fungus a sterile 10-ml portion of water or of a sterile solution containing 0.05 g per liter of a nontoxic wetting agent such as sodium dioctyl sulfosuccinate. Use a sterile platinum or nichrome inoculating wire to scrape gently the surface growth from the culture of the test organism. Pour the spore charge into a sterile 125-ml glass-stoppered Erlenmeyer flask containing 45 ml. of sterile water and 10 to 15 solid glass beads, 5 mm. in diameter. Shake the flask vigorously to liberate the spores from the fruiting bodies and to break the spore clumps.

Filter the shaken suspension through a thin layer of sterile glass wool in a glass funnel into a sterile flask in order to remove mycelial fragments.

Centrifuge the filtered spore suspension aseptically, and discard the supernatant liquid. Resuspend the residue in 50 ml. of sterile water and centrifuge.

Wash the spores obtained from each of the fungi in this manner three times. Dilute the final washed residue with sterile mineral-salts solution in such a manner that the resultant spore suspension shall contain 1,000,000 ±200,000 spores per ml. as determined with a counting chamber.

Repeat this operation for each organism used in the test and blend equal volumes of the resultant spore suspension to obtain the final mixed spore suspension.

The spore suspension may be prepared fresh each day or may be held at 6° ±4° C (43° F) for not more than 4 days.

3.1.3 *Viability of inoculum control.* With each daily group of tests place each of three pieces of sterilized filter paper, 1 in. square, on hardened mineral-salts agar in separate Petri dishes. Inoculate these with the spore suspension by spraying the suspension from a sterilized atomizer[1] so that the entire surface is moistened with the spore suspension. Incubate these at 29° C (84° F) at a relative humidity not less than 85 percent and examine them after 14 days' incubation. There shall be copious growth on all three of the filter paper control specimens. Absence of such growth requires repetition of the test.

[1] DeVilbiss No. 154 atomizer or equivalent has been found satisfactory for this purpose.

3.1.4 *Control items.* In addition to the viability of inoculum control, a number of known susceptible substrates shall be inoculated along with the test item to insure that proper conditions are present in the incubation chamber to promote fungus growth. The control items shall include three pieces each of preservative free vegetable tanned leather and protein-glue bonded cork.

3.1.5 *Inoculation of test and control items.* (a) Mount the test and control items on

suitable fixtures or suspended from hangers.

(b) Precondition the chamber and its contents at 29° C (81° F) and 95 percent R.H. for at least 4 hours.

(c) Inoculate the test and control items with the mixed fungus spore suspension (3.1.2) by spraying it on the test and control items in the form of a fine mist from a previously sterilized atomizer or nebulizer until they are thoroughly wet with the spray. Incubation is to be started immediately following the inoculation.

3.1.6 *Incubation.*

(a) Maintain the test chamber at 29° C (84° F) and 95 percent R.H. (minimum) during the life of the test. Keep the test chamber closed during the incubation period except during inspection or for addition of other test items.

(b) After 14 days, inspect the control items. They should show an abundant growth of fungus. If the control items do not show an abundant growth, the entire test shall be repeated.

(c) If the control items show satisfactory fungus growth, continue the test for a period of 28 days from the time of innoculation or as specified in the equipment specification.

3.7 Criteria for passing test. At the end of the incubation period, the test item shall be removed from the test chamber and inspected in accordance with section 3, paragraph 3.2.4. If so specified in the equipment specification, the test item shall be operated and the results compared with those obtained in accordance with section 3, paragraph 3.2.1.

4. Summary. The following details shall be designated in the equipment specification:

(a) Pretest data required (section 3, paragraph 3.2.1).

(b) Test period if other than 28 days (see 3.1.6 (c)).

(c) Whether test item shall be operated (see 3.1.7).

APPENDIX D

REQUIREMENT 3

FLAMMABLE MATERIALS

1. Purpose. The purpose of this requirement is to establish the tests for the determination of the flammability of materials and the limitations on their use.

2. Documents applicable to Requirement 3.

ASTM D-568	Test for Flammability of Plastics 0.127 cm (0.050 in.) and Under in Thickness
ASTM D-635	Test for Flammability of Rigid Plastics over 0.127 cm (0.050 in.) in Thickness
ASTM D-1000	Pressure-Sensitive Adhesive Coated Tapes Used for Electrical Insulation

3. Characteristics. In the design and construction of electrical or electronic circuits, materials used for electrical insulation or mechanical purposes which will support combustion or which are capable of causing an explosion when the equipment is subjected to the environmental conditions specified in the detail equipment specification, shall not be used unless specifically approved by the procuring activity.

3.1 The test used to determine the fire retardant feature shall be the test specified in the material specification. If the specification does not have such a test, materials shall be tested and classified as nonburning or self extinguishing in accordance with ASTM D-568 or ASTM D-635, as applicable. Tapes shall be tested in accordance with the flammability test in ASTM D-1000. Additives shall not adversely affect the specified performance requirements of the basic materials. Fire retardance shall not be achieved by virtue of nonpermanent additives to the basic resin.

This method is a part of Fed. Test Method Std. No. 406
(formerly Fed. Spec. L-P-406b)

FLAMMABILITY OF PLASTICS OVER 0.050 INCH IN THICKNESS

1. SCOPE

1.1 This method is designed as a laboratory procedure in determining the relative flammability of rigid plastics in the form of sheets or molded bars over 0.050 inch in thickness. The rate of burning will vary with thickness.

2. TEST SPECIMENS

2.1 **Dimensions.** At least 10 specimens, 5 inches in length by 0.5 inch in width by the thickness of the material as normally supplied shall be cut from sheet or molded from each of the samples to be tested. Injection-molded bars may be 0.25 by 0.5 by 5.0 inches and compression-molded bars may be 0.5 by 0.5 by 5.0 inches.

2.2 **Marking of specimens.** Each specimen shall be marked by scribing two lines, 1 inch and 4 inches from one end of the specimen. The specimens shall have smooth edges; machined edges shall be sanded to a smooth finish.

3. APPARATUS

3.1 **Test chamber.** A laboratory hood, totally enclosed with a heat-resistant glass window for observing the test, shall be used. The exhaust fan shall be turned off during the test and turned on periodically to clear out the fumes between tests.

3.2 **Testing equipment.** The testing equipment shall consist of a laboratory ring stand, a bunsen burner, a 20-mesh wire gauze, 4 inches square, a stop watch, and a pan of water.

4. PROCEDURE

4.1 **Positioning of specimen.** The specimen shall be clamped in a support at the end farthest from the 1-inch mark with its longitudinal axis horizontal and its transverse axis inclined at 45 degrees to the horizontal. Under the specimen there shall be clamped a piece of bunsen burner gauze about four inches square in a horizontal position $\frac{3}{4}$ inch below the edge of the specimen and with about $\frac{1}{2}$ inch of the specimen extending beyond the edge of the gauze as shown in figure 2021.

4.2 **Ignition.** A standard $\frac{3}{8}$-inch bunsen burner with air ports open to produce a blue flame approximately one inch high shall be placed under the free end of the specimen and adjusted so that the flame tip is just in contact with the specimen. At the end of 30 seconds the flame shall be removed and the specimen allowed to burn. In case the specimen does not continue to burn after the first ignition, the burner shall be placed under the free end for a second period of 30 seconds immediately after the specimen ceases to burn. The burner flame shall be extinguished after the second application and the hood window shall be closed for the remainder of the test. A stop watch shall be started when the flame along the lower edge of the specimen reaches the first mark, one inch from the end and the time t observed when the flame reaches the four inch mark.

4.3 **Evaluation of test.**

4.3.1 *Nonburning by this test.* If the specimen does not ignite on two attempts, it is judged as "nonburning by this test". The sample shall be judged as "nonburning by this test" when all 10 specimens do not burn.

4.3.2 *Burning by this test.* If a specimen burns to the four-inch mark, it is judged as "burning by this test" and its burning rate

This method is a part of Fed. Test Method Std. No. 406
(formerly Fed. Spec. L-P-406b)

METHOD 2022
OCTOBER 5, 1961

FLAMMABILITY OF PLASTICS 0.050 INCH AND UNDER IN THICKNESS

1. SCOPE

1.1 This method is designed for use in determining the flammability of plastics in the form of thin sheets or films 0.050 inch and under in thickness.

2. TEST SPECIMENS

2.1 Dimensions. The test specimen shall be 18 inches in length, 1 inch in width, and the thickness of the sheet.

2.2 Marking. The test specimen shall be marked into squares ½ inch on a side before the test is started. This marking may be done by any convenient means, provided the markings are still visible on the unburned portion of the specimen after the test is completed.

3. APPARATUS

3.1 Shield. A shield constructed from sheet metal or other fire-resistant material, 12 inches in width, 12 inches in depth, and 30 inches in height, and open at the top shall be used. The shield shall be so constructed as to provide a ventilating opening approximately 1 inch in height around the bottom and shall have a viewing window in one side of sufficient size and in such a position that the entire length of the specimen under test may be observed. Because of danger due to breaking glass, it may be necessary to use heat-resistant glass for the viewing window. One side of the shield shall be hinged (or some other suitable form of construction used) so that the shield may be readily opened and closed to facilitate the mounting and ignition of the test specimen.

3.2 Clamp. A spring-type of paper clamp for holding the test specimen in position shall be used. The holding clamp shall be attached rigidly to the shield in such a manner that when the specimen is clamped therein, it is centered within the shield facing the viewing window.

4. PROCEDURE

4.1 Fusee method of ignition.

4.1.1 *Fusee.* A pyroxylin plastic fusee material 0.010 ± 0.001 inch in thickness shall be used for ignition. The fusee material shall be made from pyroxylin having a nitrogen content of 11 ± 0.10 percent and containing 25 percent camphor. This material shall be cut into 1-inch squares for purpose of test.

4.1.2 *Positioning and ignition.* The 1-inch square piece of fusee material shall be affixed by means of acetone to one end of the test specimen, with an overlap of ½ inch. In some cases it may be necessary to dry under slight pressure or to use a stapling device to fasten the fusee to the test specimen. After drying for 2 hours while exposed to air at 23° ± 3°C, the specimen shall be hung vertically by means of the supporting clamp in approximately the center of the shield. The fusee shall be at the lower end of the test specimen. The specimen shall be clamped in such a manner that 12 inches of it is exposed below the clamp. The shield shall be placed in a hood with the ventilating fan turned off at the time of test. The square of fusee material shall be ignited by means of a safety match, and the door of the shield shall be closed immediately.

4.1.3 *Measurements.* The time required for the flame to either extinguish itself or to completely burn the test specimen shall be determined by means of a stop watch or

is 180/t inch per minute. The sample shall be judged as "burning by this test" if more than two of the ten specimens tested have been found burning to the four-inch mark. The burning rate of the sample is the average burning rate of the actually burning specimens.

4.3.3 *Self-extinguishing by this test.* If a specimen does not burn to the four-inch mark after the first or second ignition, it is judged as "self-extinguishing by this test", and four inches minus the unburned length in inches from the clamped end, measured along the lower edge, is its "extent of burning". The sample shall be judged as "self-extinguishing by this test" if more than two of the test specimens tested are found to be self extinguishing with the rest nonburning. The "extent of burning" of the sample shall be equal to the average extent of burning of the self-extinguishing specimens.

5. REPORT

5.1 The report shall include the da specified under section 4, paragraph 4.6 this standard (General Requirements), a the following:

(1) Thickness of the specimens, any trea ment to which the specimens we subjected prior to testing, such as r laxation of a stretched material, co ditioning, etc., and method preparation of specimens.

(2) The length burned from the one-in mark when a material is reported "self-extinguishing by this test".

(3) The burning rate in inches per mi ute when a material is reported "burning by this test".

(4) The number of ignitions.

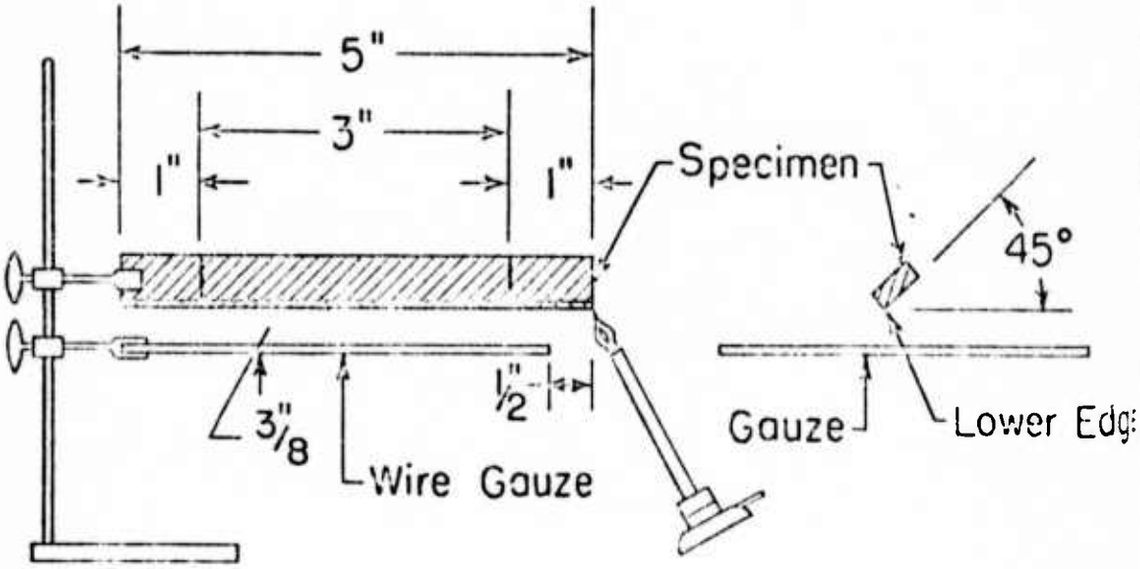

FIGURE 2021.— *Apparatus for flammability test.*

timer started at the instant of ignition of the fusee. The area of the specimen that is burned or charred shall be measured to the nearest ¼ square inch. The markings on the specimen may be used for estimating the amount of material burned. If material melts and drops from the specimen, the area melted shall be included in the burned area. The charred portion which drops off when touched with the fingers or in handling shall also be included in the burned area.

4.1.3.1 *Alternate method of measurement.* Another convenient method, which may be used for measuring the burned area in the case of materials that do not stretch under test, is to use a scale 12 inches in length by 1 inch in width ruled with lines into squares ½ inch on a side. The partially burned test specimen may be laid over this scale, and the amount of burned material estimated by means of the area of the scale left exposed.

4.2 Benzene drop method of ignition.

4.2.1 *Benzene.* Ordinary laboratory grade benzene (C_6H_6) shall be used for ignition.

4.2.2. *Positioning and ignition.* A drop of benzene shall be placed on the test specimen approximately ¼ inch above the lower edge of the specimen and allowed to run down to form a large drop on the blunt end without dripping off. This drop shall be ignited within 7 seconds after application to the test specimen with either of the following means: (a) A high potential, low energy spark such as delivered by an automobile ignition coil, or (b) a safety match. After ignition, the door of the shield shall be closed immediately.

4.2.3 *Measurements.* The time required for burning and the area burned shall be observed in accordance with the procedure described in paragraphs 4.1.3 and 4.1.3.1.

5. REPORT

5.1 The report shall include the data specified under section 4, paragraph 4.6 of this standard (General Requirements), and the following:

(1) Length of time in seconds that the material continues to burn.
(2) Area in square inches of the burned portion of the test specimen.
(3) Method of ignition.

FLAME RESISTANCE

1. SCOPE

1.1 This method is designed for use in determining the flammability of plastics that are difficult to ignite. It is used primarily for materials that are found to be self-extinguishing when tested by methods 2021 and 2022.

2. TEST SPECIMENS

2.1 Dimensions. The test specimen shall be 5 by 0.5 by 0.5 inch.

3. APPARATUS

3.1 Enclosure. An enclosure of sufficient size to contain the specimen, supports, heater coil, spark plugs, flame travel gage and their associated accessories shall be arranged to eliminate air drafts and permit a clear view of the interior through shatterproof glass windows. Vent holes distributed around the sides adjacent to the base shall be provided to admit fresh air when an exhaust fan, connected to the top of the enclosure, is operated at a minimum suction just sufficient to carry off smoke and gases.

3.2 Supports. Supports shall be suitable for holding the specimens in a vertical position with an unsupported span not less than 4 inches in length. The lower end of the specimen shall be wrapped in such a manner that gases released through this end are diverted toward the spark plugs.

3.3 Heating coils. Heating coils shall consist of seven turns of No. 10 (0.102-inch diameter) resistance wire, grade E, Federal Specification QQ-R-175, space wound to 0.25-inch per turn. The nominal inside diameter of the coil used shall be $1^{3}/_{16}$ inches. The lower end of the heater coil shall be located 1.5 inches above the top of the lower specimen support.

3.4 Spark plugs. Two spark plugs, with extended electrodes spaced $1/8$ inch from the surface of the specimen, located on diametrically opposit sides of the specimen, shall be placed with their longitudinal center lines in a horizontal plane $1/2$ inch above the top of the heater coil to ignite the gases emitted from the heated specimen. A suitable electric circuit shall be provided to maintain continuous sparking at the electrodes during the specified time. The spark plugs shall be mounted in such a manner that they may be moved away from the specimen after ignition takes place so as not to impede the travel of the flame and to prevent their electrodes from becoming fouled by soot.

3.5 Gage. A suitable flame travel gage shall be positioned near the specimen to judge the distance of flame travel without appreciably impeding the progress of the flame.

4. PROCEDURE

4.1 Ignition time. With the enclosure closed and ventilated, the specimen centered in the heater coil, and the spark plugs and flame gage properly located, a stop watch shall be started simultaneously with the energizing of the heater coil and spark plugs. A constant current of 55 amperes shall be supplied from a suitable transformer source to the heater coil. Ignition shall be considered as occurring when the flame transfers from the escaping gases to the surface of the specimen and continues there, disregarding the flashes which may occur in the gassing space prior to the sustained flame.

4.2 Time of heating. Heating shall be discontinued 30 seconds after ignition occurs. If ignition does not occur within 600 seconds, the test shall be discontinued.

4.3 Flame travel. Immediately after ignition occurs, as defined in 4.1, the electrical supply to the spark plugs shall be cut off and the plugs shifted away from the flame. The maximum distance to which the flame travels along the surface of the specimen measured from the top of the heater coil before extinction shall be observed.

4.4 Burning time. The number of seconds that the specimen continues to burn, until the cessation of all flaming, after the current in the heater coil has been cut off shall be recorded as the time required for self-extinction.

5. REPORT

5.1 The report shall include the data specified under section 4, paragraph 4.6 of this standard (General Requirements) and the following:

(1) The time required to ignite the specimen in seconds.
(2) The maximum distance of flame travel in inches.
(3) The burning time in seconds.

APPENDIX E

ANALYSIS REQUEST TI-12292

MEMO CHARGE 70,720-02

REQUESTED BY	COST CENTER	PHONE NO	MAIL STATION	DIVISION P.O. NUMBER	TO BE COMPLETED BY LABORATORY	
RYAN PROVENZANO	628	SH 774	371		DATE STARTED	LAB E.O. NO
DEPARTMENT: PLASTICS GROUP SHERMAN	DATE INITIATED			DATA FORMAT: ☐ RAW DATA ☐ PROCESSED DATA ☐ REPORT ☐	DATE COMPLETED: 9-19-73	JOB NUMBER: 3[illegible]37
PROGRAM OR ACTIVITY: FLIR	IDENTIFICATION/LOT NUMBER					

DESCRIPTION OF SAMPLE OR DEVICE

PLEASE RUN TMA THERMAL EXPANSION ON THESE 3 SAMPLES AS BEFORE IN PREVIOUS TEST. -55°C TO +80°C. OBTAIN DATA IN 2 DIRECTIONS ON EACH PART. UNIT THICKNESS DIRECTION.
CYCLE EACH SAMPLE AT LEAST 3 TIMES

INFORMATION REQUESTED

TO BE COMPLETED BY LABORATORY	METHOD OF ANALYSIS
ANALYSIS REPORT	TMA

1. Urethane - too thin and ■ not flat
2. Valox - valox expansion non linear; i.e., constantly curving over this temp. range

#1 direction -	1st cycle heat	-55-80°	α =	75.3 X 10^{-6}	in/in/°C
	cool	80-(-55)°	α =	82.8 X 10^{-6}	in/in/°C
	2nd cycle heat	-55-80°	α =	77.1 X 10^{-6}	in/in/°C
	cool	80-(-55)°	α =	79.7 X 10^{-6}	in/in/°C
	3rd cycle heat	-55-80°	α =	76.5 X 10^{-6}	in/in/°C
	cool	80(-55)°	α =	78.8 X 10^{-6}	in/in/°C
#2 direction	1st cycle heat	-55-80°	α =	35.2 X 10^{-6}	in/in/°C
	cool	80-(-55)°	α =	35.8 X 10^{-6}	in/in/°C
	2nd cycle heat	-55-80°	α =	34.7 X 10^{-6}	in/in/°C
	cool	80-(-55)°	α =	36.0 X 10^{-6}	in/in/°C
	3rd cycle heat	-55-80°	α =	34.8 X 10^{-6}	in/in/°C
	cool	80-(-55)°	α =	36.1 X 10^{-6}	in/in/°C

ANALYST - ENGINEER	PHONE NO	DATE REPORTED	LOCATION OF ORIGINAL DATA	APPROVED BY
G.Heinen				C.Baker

COPY DISTRIBUTION ORIGINAL - REQUESTER COPY PART 2 - LAB PERMANENT FILE PART 3 - SPECIAL FILES

ADDITIONAL RESULTS ON JOB REQUEST 63438

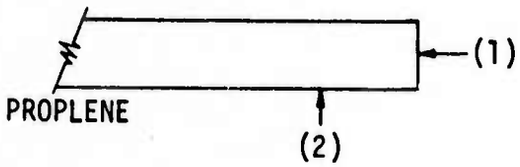

1 - 1st cycle	heat	-55-80°	=	74.2×10^{-6} in/in/°C
	cool	80-(-55°)	=	90.3×10^{-6} in/in/°C
2nd cycle	heat	-55-80°	=	85.5×10^{-6} in/in/°C
	cool	80-(-55)	=	89.5×10^{-6} in/in/°C
3rd cycle	heat	-55-80°	=	83.8×10^{-6} in/in/°C
	cool	80-(-55	=	88.6×10^{-6} in/in/°C
2 - 1st cycle	heat	-55-80°C	=	113.9×10^{-6} in/in/°C
	cool	80-(-55°C)	=	124.3×10^{-6} in/in/°C
2nd cycle	heat	-55-80°C	=	121.7×10^{-6} in/in/°C
	cool	80-(-55)	=	125.9×10^{-6} in/in/°C
3rd cycle	heat	-55-80°C	=	120.2×10^{-6} in/in/°C
	cool	80-(-55°C	=	123.0×10^{-6} in/in/°C

GAIL HEINEN

ANALYSIS REQUEST TI-12292

REQUESTED BY	COST CENTER	PHONE NO	MAIL STATION	DIVISION P.O. NUMBER	TO BE COMPLETED BY LABORATORY	
[illegible]				731425-9	DATE STARTED: 8-3-73	LAB E.O. NO
DEPARTMENT		DATE INITIATED		DATA FORMAT: ☐ RAW DATA ☐ PROCESSED DATA ☐ REPORT ☐	DATE COMPLETED: 8-30-73	JOB NUMBER: 63271
PROGRAM OR ACTIVITY	IDENTIFICATION/LOT NUMBER					

Memo Chg.

DESCRIPTION OF SAMPLE OR DEVICE

polycarbonate 40% filled

INFORMATION REQUESTED

[illegible] 3 directions [illegible] #1-[illegible]

#2

↑

#3

←

TO BE COMPLETED BY LABORATORY

METHOD OF ANALYSIS: TMA

ANALYSIS REPORT

Material is glass fiber filled - 41.75%

	#1 (and #62896)	#2	#3
first cycle heating	46.2×10^{-6}	56.3×10^{-6}	21.8×10^{-6}
first cycle cooling	58.3×10^{-6} (80°-(-35°)	59.7×10^{-6}	22.9×10^{-6}
second cycle heating	53.7×10^{-6}	57.9×10^{-6}	22.6×10^{-6}
cooling	57.8×10^{-6}	59.6×10^{-6}	22.7×10^{-6}
third cycle heating	56.4×10^{-6}	58.6×10^{-6}	22.3×10^{-6}
cooling	56.1×10^{-6}	58.3×10^{-6}	22.6×10^{-6}

all measurements -55° to 80°C
units = in/in/°C

Scans attached.

ANALYST - ENGINEER	PHONE NO	DATE REPORTED	LOCATION OF ORIGINAL DATA	APPROVED BY
Gail Heinen				CWB C.Baker

COPY DISTRIBUTION ORIGINAL - REQUESTER COPY PART 2 - LAB PERMANENT FILE PART 3 - SPECIAL FILES

JOB NO. 62896 - POLYCARBONATE, ETC.

ACETAL COPOLYMER - NON LINEAR EXPANSION - 1st CYCLE HAS BREAK

ALL SCANS SHOW 3 MM CORRECTION FOR PEN LOG

1st cycle	heating	α (-55-(75)	=	101.8×10^{-6} in/in/°C
	cooling	α (70-(-45)	=	122.6×10^{-6} in/in/°C
2nd cycle	heating	α (-55-(+60)	=	115.1×10^{-6} in/in/°C
	cooling	α (55-(-55)	=	116.8×10^{-6} in/in/°C
3rd cycle	heating	α (-55-(80)	=	119.1×10^{-6} in/in/°C
	heating	α (-55-(90)	=	124×10^{-6} in/in/°C
	cooling	α (80-(-55)	=	123.7×10^{-6} in/in/°C

Al Std -55-(80°) = 21.9 & 22.0×10^{-6} in/in/°C

Lit values -50° - +20° = 21.8×10^{-6} in/in/°C

20° -100 = 23.6×10^{-6} in/in/°C

NYLON 6/6 UNFILLED

1st cycle	heating	α -55-(80)	=	70.6×10^{-6} in/in/°C
	cooling	α 80-(-40)	=	99.2×10^{-6} in/in/°C
2nd cycle	heating	α -55-(80)	=	90.6×10^{-6} in/in/°C
	cooling	α 80-(-55)	=	93.2×10^{-6} in/in/°C
3rd cycle	heating	α -55-(80)	=	90.3×10^{-6} in/in/°C
	cooling	α 80-(-55)	=	92.3×10^{-6} in/in/°C

POLYCARBONATE - NON-FILLED

1st cycle	heating	α -55-(80)	=	54.1×10^{-6} in/in/°C (non linear)
	cooling	α 80-(-55)	=	66.4×10^{-6} in/in/°C
2nd cycle	heating	α -55-(80)	=	66.9×10^{-6} in/in/°C
	cooling	α 80-(-55)	=	67.1×10^{-6} in/in/°C
3rd cycle	heating	α -55-(80)	=	67.6×10^{-6} in/in/°C
	cooling	α (80)-(-55)	=	67.1×10^{-6} in/in/°C

POLYCARBONATE 40% GLASS

1st cycle	heating	α -55°-(+80°)	=	46.2×10^{-6} in/in/°C
	cooling	α 80°-(-35°)	=	58.3×10^{-6} in/in/°C
2nd cycle	heating	α -55-(+80)	=	53.7×10^{-6} in/in/°C
	cooling	α 80-(-55)	=	57.8×10^{-6} in/in/°C
3rd cycle	heating	α -55-(+80)	=	56.4×10^{-6} in/in/°C
	cooling	α 80-(-55)	=	56.1×10^{-6} in/in/°C

ABS 20 GLASS

1st cycle rapid cool	heating	α -55-(+80)	99.6
2nd cycle rapid cool	heating	α -(55-(+80)	91.4
3rd cycle	heating	α -55-(+80)	88.4
	cool	α +80-(-45)	91.1
4th cycle	heating	α -55-(+80)	87.4
	cooling	α 80-(-55)	87.1
4th cycle	heating	α -55-(+80)	83.2
	cooling	α 80-(-55)	85.3

Ed Gillis

Dave Rodgers

Keith Ely

Mike VanDeWalle

Bulldog Transformer

Epoxy - thermal shock (low temp end) problems

Silastic 50 - passed thermally

breaks or bends transformer due to molding pressures

Silastic 30 - only limited improvement over filastic 50 problems

721815 - terminal ship not secure in cpd

adhesion - change coating

100°C

Moisture Mil 202 Method 106

Flammability

721809 Get TP urethane lit info to Ely

APPENDIX F

REFRACTORY OXIDES

Type	Alumina (Al_2O_3)	Beryilia (BeO)	Calcla (CaO)	Magnesia (MgO)	Thoria (ThO_2)	Zirconia (Stabilized ZrO_2)	Silica Vitreous SiO_2)
Melting Point, F	3700	4620	4710	5070	6000	4710	-
Ther Cond (st spec temp and porosity), Btu/hr/sq ft/^{o}F/ft	10.7 (200F, 0%)	9.52 (2190F, 5-10%)	4.12 (1830F, 9%)	1.47 (2190F, 22%)	0.0 (2190F, 17%)	0.53 (2190F, 28%)	0.80 (0.9%)
Coef of Ther Exp, per ^{o}F	43 X 10^{-7} (77-1830F)	52.8 X 10^{-7} (68-2550F)	75.5 X 10^{-7} (68-2190F)	77.8 X 10^{-7} (68-2550F)	52.8 X 10^{-7} (68-2550F)	30.6 X 10^{-7}[a] (68-2190F)	2.8 X 10^{-7} (68-2280F)
Max Use Temp in Oxidizing Atmosphere, F	3540	4350	4350	4350	4890	4530	-
Hardness (Molis)	9	9	4.5	6	7	7-8	-
Thermal Shock Resistance	Good	Excellent	Fair	Fair	Poor	Fair	Excellent
Stability in -							
Reducing Atmosphere	Excellent	Excellent	Poor	Poor	Good	Good	Fair
Carbon	Excellent	Excellent	Poor	Good	Fair	Fair	Good
Acid Slags	Excellent[b]	-	Poor	Poor	Poor	Good	Good
Basic Slags	Excellent	Fair	Fair	Good	Good	Poor	-
Metals	Good	Good	Fair	Fair	Excellent	Good	-

[a]Depends on degree of stabilization. [b]Except HF.

CARBIDE-BASE CERMETS

Type (base)	Titanium Carbide (TiC)[a]	Tungsten-Titantum Carbide ($WTiC_2$)[b]	Tungsten Carbide (WC)	Chromium Carbide (Cr_4C, Cr_7C_3, Cr_3C_2)[c]
Density, lb/cu in	0.20-0.26	0.38-0.47	0.47-0.55	0.25-0.29
Ther Cond (68F), Btu/hr/sq ft/^{o}F/ft	-	16.5-32.9	25.7-50.1	-
Coef of Ther Exp (68-1200 F), per ^{o}F	4.3-7.5 X 10^{-6}	3.5-4.0 X 10^{-6}	2.5-3.9 X 10^{-6}	5.8-6.3 X 10^{-6} [f]
Electrical Conductivity, % IACS	1.34-6.0	4.3-5.8	5.0-10.1	2.58-2.78
Mod of Elast in Tension, psi				
70 F	42-57 X 10^{6}	65.5-80.6 X 10^{6}	61.6-94.3 X 10^{6}	-
1600-1800 F	33-48 X 10^{6}	-	-	-
Tensile Strength, 1000 psi[d]				
75 F	26-134 (0-61)	118-145	130[e]	36-37 (0)
1500 F	45-94 (0-2.7)	-	-	20-42 (0.2)
1800 F	35-72 (0-2.4)	-	-	-
Hardness (Rockwell)	A73-A91	A90-A93	A90-A93	A86.5-A89
Impact Strength (unnotched Charpy), ft-lb				
75 F	1.5-16	5.3-8.9	-	-
1800 F	2.5-16	-	-	-
Transverse Rupture Strength, 1000 psi	122-236	125-350	175-460	100-120
Stress-Rupture Strength (100 hr, 1800 F), 1000 psi	8-28	-	-	-
Compressive Strength, 1000 psi	265-450	585-705	518-800	422-480

[a]Property range covers grades ranging from 17.5% to 90% TiC with different binder metal contents.
[b]Property range covers various grades of different carbide-metal proportions.
[c]The type of chromium carbide and the type of binder metal affects properties.
[d]Elongation (%) in parenthesis. [e]Typical of one grade. [f]68-576 F.

ALUMINA CERMETS

Type	Chromium-Alumina	Molybdenum-Chromium-Alumina[a]
PHYSICAL PROPERTIES		
Density, lb/cu.in.	0.21	0.22
Porosity, %	0.25	0.25
Melting Point (approx.) F	336	-
Ther Cond, But/hr/sq ft/^{o}F/ft	29[a]	-
Coef of Ther Exp, per ^{o}F	4.7 X 10^{-6}[b]	5.2 X 10^{-6}[c]
Spec Ht (calc), Btu/lb/^{o}F	0.16	0.16
Poisson's Ratio	0.22	0.25-0.27
MECHANICAL PROPERTIES		
Mod of Elast in Tension, 10^{6} psi	41 X 10^{6}	37-39 X 10^{6}
Ult Ten Str, 1000 psi		
Rm Temp	21	-
800 F	20.5	-
1200 F	20	-
1500 F	19.7	-
1800 F	16.8	-
2000 F	11.7	-
Hardness (Rockwell)	C37	C45-55
Mod of Rupture, 1000 psi		
Rm Temp	45	55[d]
1800 F	27	55
2100 F	18	29
2400 F	4.6	12
Compr Str, 1000 psi	110	240
Mod of Rigidity, psi	17 X 10^{6}	15 X 10^{6}
Shear Str, 1000 psi	40	-
Bulk Modulus, psi	21 X 10^{6}	26 X 10^{6}

[a]At 500 F. [b]At 32-1832 F. [c]At 68-1472 F. [d]Addition of tungsten raises room temperature modulus of rupture to about 70,000 psi.

TABLE PHYSICAL PROPERTIES OF $70Al_2O_3$-30Cr CERMETS

Firing shrinkage		13.0=14.5%
Apparent porosity		<0.5%
Apparent specific gravity		4.60-4.65
True specific gravity		4.68-4.72
Thermal expansion		77°-1472°F, 4.8×10^{-6}
		72°-2400°F, 5.25×10^{-6}
		25°-800°C, 8.65×10^{-6}
		25°-1315°C, 9.25×10^{-6}
Heat Transfer		Slightly <sintered alumina
		*66.5-20% $Btu \cdot in \cdot hr^{-1} \cdot ft^{-2} \cdot {}^{\circ}F^{-1}$
Resistance to thermal shock		Good
10 cycles 2400 to 75°F		15 to 50% strength gain
Resistance to oxidation		Excellent up to 2750°F
Hardness		1100-1200 VPN (Vickers pyramid number)
Modulus of elasticity at 75°F		5.23×10^7 psi
Impact resistance at 75°F		<1 ft-lb standard Charpy unnotched
Compressive strength at 75°F		320,000 psi
Bending strength, 75°F (bars)		55,000 psi
	1600°F	43,125 psi
	2000°F	32,800 psi
	2400°F	24,400 psi
Tensile strength, 75°F (rods)		35,000 psi
	1600°F	21,560 psi
	2000°F	18,490 psi
	2400°F	14,120 psi
Stress rupture in tension		
Temp, °F	Stress, psi	Life, hr
1800	16,700	10
	16,300	100
	16,000	1000
2000	14,000	10
	13,300	100
	13,000	1000
2200	12,900	10
	12,400	100
	11,600	1000

*Determined in laboratories of the AC Spark Plug Company, Flint Michigan

ALUMINA-METAL CERMETS

The determined properties or behavior characteristics of 28 w/o Al_2O_3 72 w/o CR cermets are given in Table 5.2

TABLE PHYSICAL PROPERTIES OF $28Al_2O_3$-72Cr Cermets

Firing shrinkage	$15 \pm 1\%$	
Apparent porosity	0.000	
Apparent specific gravity	5.92	
Thermal expansion		
	77-1472°F	4.79×10^{-6}
	72-2400°F	5.75×10^{-6}
	25-800°C	8.04×10^{-6}
	25-1315°C	10.35×10^{-6}
Resistance to thermal shock	Very good -20 to 600 cycles of simulated jet engine burner blow-out as nozzle diaphragm blades, i.e., instantaneous 1900°F to 75°F air blast.	
Resistance to oxidation	Excellent to above 2000°F	
Modulus of elasticity, 75°F	4.7×10^7 psi	
Impact resistance at 75°F	<1 ft-lb standard Charpy unnotched	
Bending strength at 75°F (bars)		
1600°F	80,000 psi	
2000°F	62,000 psi	
2400°F	58,000 psi	
Tensile strength 75°F (rods)		
1600°F	35,000 psi	
2000°F	39,000 psi	
2200°F	25,000 psi	
	22,000 psi	
	19,000 psi	
Stress rupture in tension		
Temp., °F	Stress, psi	Life, hr
1800	19,000	10
	16,700	100
	14,500	1000
2000	10,800	10
	8,700	100
	7,000	1000

TABLE PHYSICAL PROPERTIES OF $34Al_2O_3$-66DrMo CERMETS

Firing shirnkage	$14 \pm 1\%$ (approximately 18% for items pressed from dry granulated powder)	
Apparent porosity	0.00 to 0.33%	
Apparent specific gravity	5.82	
Thermal expansion	75-1475°F	4.42×10^{-6}
	75-2400°F	5.82×10^{-6}
	25-800°C	7.95×10^{-6}
	25-1315°C	10.47×10^{-6}
Resistance to thermal shock	Excellent; 1000 cycles of simulated jet engines burner blow-out as nozzle diaphram blades, i.e., instantaneous 1900°F to 75°F air blast.	
Resistance to oxidation	Excellent to above 2000°F	
Modules of elasticity	4.51×10^7 psi	
Bending strength at 75°F (bars)		
1600	87,000 psi	
2000	62,000 psi	
2400	52,000 psi	
Tensile strength 75°F (rods)	39,000 psi	
1600	53,000 psi	
2000	46,000 psi	
2400	27,000 psi	
	10,000 psi	

Stress rupture in tension

Temp., °F	Stress, psi	Life, hr
1800	25,000	10
	22,000	100
	20,000	1000
2000	11,000	10
	7,000	100
	4,000	1000

CHROMIUM-ALUMINA BASE CERMETS

TABLE PHYSICAL PROPERTIES

	$Cr\text{-}Al_2O_3$	$Cr\text{-}Mo\text{-}Al_2O_3\text{-}TiO_2$	$W\text{-}Cr\text{-}Al_2O_3$
Density			
g/cm^3 @ 22°C	5.9	6.0	8.8
lb/in^3 @ 72°F	0.21	0.22	0.32
Sintering temp., °F	2850	2900	3100
Maximum service temp., °F	2400[a] 3000[b]	2800	3100[c]
Oxidation resistance at 2200°F, 100 Hr:			
continuous, ipy	0.105	0.095	37.5
Intermittent, ipy	0.131	0.159	231.0
Electrical resistivity			
microhm-cm @ 21°C	87	64.8	46.2
microhm-in. @ 70°F	84.3	25.5	18.2
ohms/cir.mil. ft. @ 70°F	522	390	278
microhm-cm @ 300°C	164	115	81
microhm-in. @ 572°F	64.5	45.3	31.8
ohms/cir.mil. ft. @ 572°C	980	693	487
microhm-cm @ 500°C	223	158	105
microhm-in. @ 932°C	87.9	62.2	41.3
ohms/cir.mil. ft. @ 932°F	1344	952	682
microhm-cm @ 900°C	320	300	184
microhm-in. @ 1472°F	126	121.5	72.5
ohms/cir.mil. ft. @ 1472°F	1930	1859	1109
Coefficient of themral expansion			
μ/in/°C (25-1000°C)	8.93	8.48	8.36
μ-in/in/°F (77-1832°F)	4.95	4.71	4.64
Thermal conductivity			
watt-cm/cm^2-°C, 260°C (av. temp.)	0.500		
Btu-in/ft^2-hr-°F 500°F(av. temp.)	348		
Specific heat (calculated)			
cal./g-°C	0.16	0.14	
Btu/lb-°F	0.16	0.14	

[a]Continuous service.

[b]Short time service.

[c]Reducing atmosphere.

TABLE TYPICAL MECHANICAL PROPERTIES

	$Cr\text{-}Al_2O_3$	$Cr\text{-}Mo\text{-}Al_2O_3\text{-}TiO_2$	$W\text{-}Cr\text{-}Al_2O_3$
Hardness (Rockwell)	C-37	C-50	C-52
Modulus of rupture (psi)			
room temp.	45,000	56,000	73,000
1800°F	27,000	54,000	67,000
2100°F	18,000	29,000	45,000
2400°F	4,600	11,800	25,000
Modulus of elasticity (psi)			
room temp.	37.5×10^6	38×10^6	38×10^6
1832°F	32.6×10^6	31.4×10^6	32.6×10^6
Compressive strength (psi)			
room temp.	110,000	240,000	-
Ultimate tensile strength (psi)			
room temp.	21,000		
800°F	20,500		
1200°F	20,000		
1500°F	19,700		
1800°F	16,800		
2000°F	11,700		
Shear modulus (psi) (modulus of rigidity) room temp.	17×10^6	15×10^6	
Shear strength (psi)			
room temp.	40,000		
Bulk modulus (psi)	21×10^6	25×10^6	
Poisson's ratio (flexure)	0.20-0.22	25 to 27	

TABLE CHEMICAL COMPOSITION OF SELECTED TiC-METAL ALLOYS [1,5]

Trade Designation	Weight per cent before sintering							
	Metal	TiC*	Ni	Co	Cr	Mo	Al	W
K152B	30.0	70.0	30.0					
K162B	30	70	25			5		
WZ1b	40	60	32		8			
WZ12B	40	60	24	8	8			
K163B1	40	60	33			7		
K183A	40	60	32		2.5	3	2.5	
WZ1c	50	50	40		10			
WZ12c	50	50	30	10	10			
K164B	50	50	42.5			7.5		
K184B	50	50	40		3	4	3	
WZ1d	65	35	52	13	13			
WZ12d	65	35	52	13	13			
K196	72	28	60					

* Kennametal materials include 6 per cent (Cb, Ta, TiC)

Properties of Titanium Carbide-Metal Compositions

TABLE PHYSICAL PROPERTIES OF SELECTED TiC-METAL COMPOSITION

Trade Designation	% Binder	Hardness-R_A		Density lb/in^3	Coef. of Exp. X 10^{-6} 70-1800°F	Young's Mod. 10	
		70°F	1400F°			70°F	1600F°
K152B	30	85	69	0.217	5.3	55	46
K162B	30	89	74	0.217	5.3	57	48
WZ1b	40	85	N.D.	0.224	5.6	55	47
WZ12b	40	85	N.D.	0.226	5.1	56	48
K163B1	40	86	74	0.228	5.4	55	N.D.
K183A	40	87	76	0.224	5.6	50	N.D.
WZ1c	50	84	N.D.	0.235	N.D.	N.D.	N.D.
WZ12c	50	84	N.D.	0.237	5.9	51	N.D.
K164B	50	84	69	0.238	5.6	50	40
K184B	50	85	70	0.228	6.0	50	41
WZ1d	65	78	N.D.	0.249	7.0	N.D.	N.D.
WZ12d	65	79	N.D.	0.251	6.6	46	N.D.
K196	72	73	62	0.257	7.5	42	33

N.D. = No Data

TABLE SHORT TIME MECHANICAL PROPERTIES OF SELECTED TiC-METAL COMPOSITIONS

Trade Designation	% Binder	Ultimate Tensile Strength 1000 psi 70°F	1600°F	1800°F	% Elongation 70°F	1600°F	1800°F	Compressive Yield Strength 1000 psi 70°F	1200°F	1400°F	1600°F	Impact Strength (11-lb)[a] 70°F	1600°F	Modulus of Rupture 1000 psi 70°F
K152B	30	125	59	31	0.30	0.37	0.32	400	307	173	118	11	7	194
K162B	30	112	93	50	0.21	0.33	0.31	450	296	207	147	11	9	185
WZ1b	40	107	75	42	- no data -							4	4	190
WZ12b	40	120	75	52	- no data -							4	N.D.	200
K163B1	40	113	78	46	0.23	0.62	0.70	420	306	172	93	13	9	236
K183A	40	104	N.D.	72	-no data-			461	266	200	133	N.D.	N.D.	184
WZ1c	50	155	80	40	- no data -							4	7	230
WZ12c	50	142	78	42	- no data -							5	6	245
K164B	50	126	74	42	0.28	0.99	1.18	425	260	148	79	16	8	212
K184B	50	134	94	54	0.32	0.62	0.74	449	230	179	112	11	N.D.	193
WZ1d	65	142	65	38	- no data -							7	N.D.	250
WZ12d	65	148	65	40	- no data -							7	9	258
K196	72	128	50	29	0.61	2.70	2.08	264	117	91	63	8	8	203

[a] Unnotched Charpy tests.

APPENDIX G

TEST DATA FOR "KELVAR" 49
PLASTIC COMPOSITES

MECHANICAL PROPERTIES	UNIDIRECTIONAL*	FABRIC**
DENSITY	.050 lbs/cu. in	.045 lbs/cu. in.
TENSILE STRENGTH	240,000 psi	75,000 psi
TENSILE MODULUS	11.0×10^6 psi	4.5×10^6 psi
COMPRESSIVE STRENGTH	40,000 psi	30,000 psi
COMPRESSIVE MODULUS	11.0×10^6 psi	4.5×10^6 psi
INTERLAMINAR SHEAR STRENGTH	10,000 psi	7,500 psi
IMPACT STRENGTH (Charpy Unnotched)	150 ft. lbs/in^2	75 ft. lbs/in^2
COEFFICIENT OF THERMAL EXPANSION	-2×10^{-6} in/in°C	~0
ELECTRICAL PROPERTIES		
DIELECTRIC CONSTANT (10^{10} Hz)		3.36
LOSS TANGENT (10^{10} Hz)		0.016
VOLUME RESISTIVITY		1.5×10^{15} ohms-cm
DIELECTRIC STRENGTH (125 mil)		500 V/mil

*Filament wound, continuous aligned fiber reinforced epoxy resin, v/o = 65. (Autoclave cured)

**8-Harness satin weave fabric (~5 oz/yd^2), epoxy resin, v/o ~55. (autoclave cured)

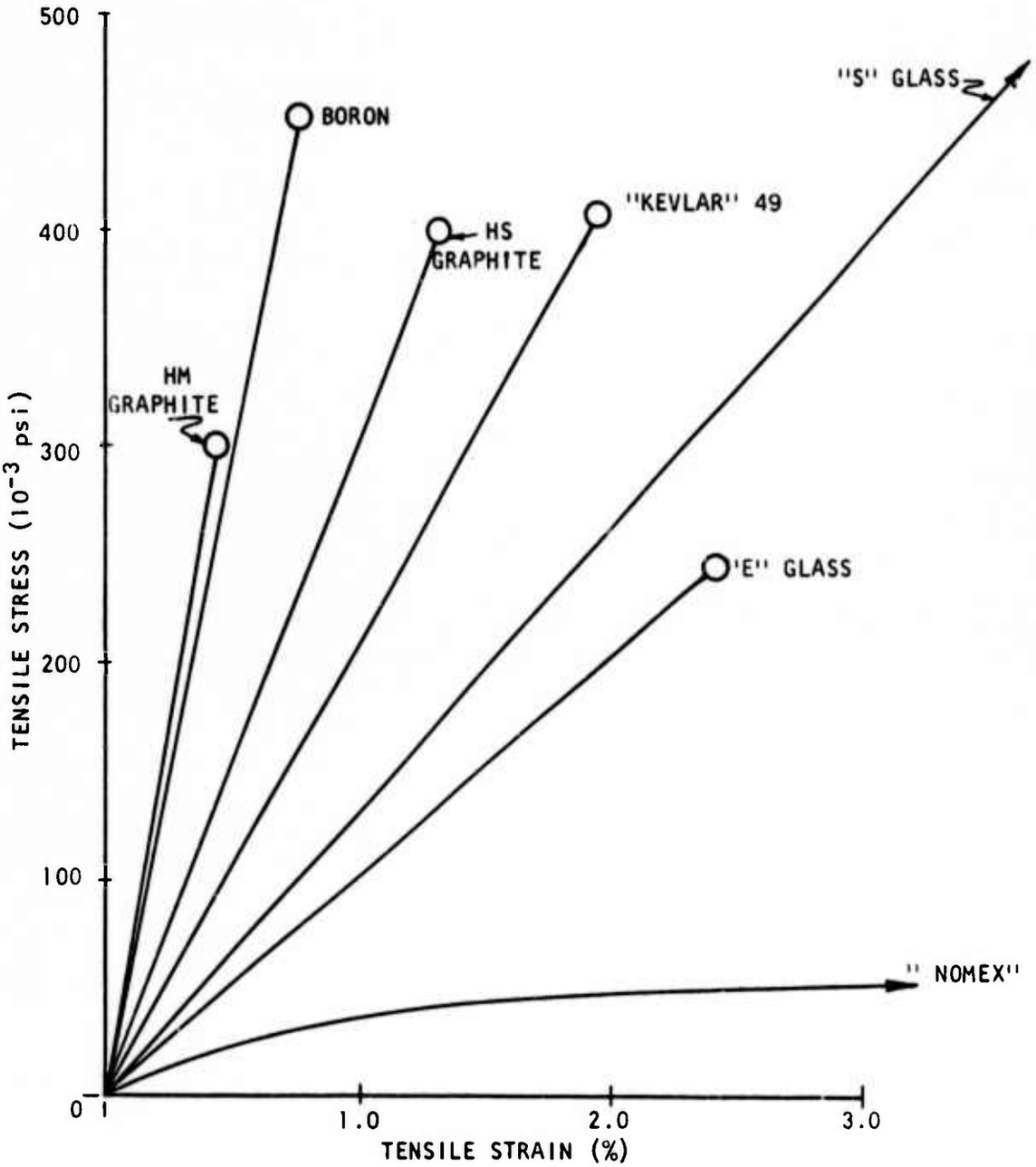

Figure G-1. Stress/Strain Curves (Fibers).

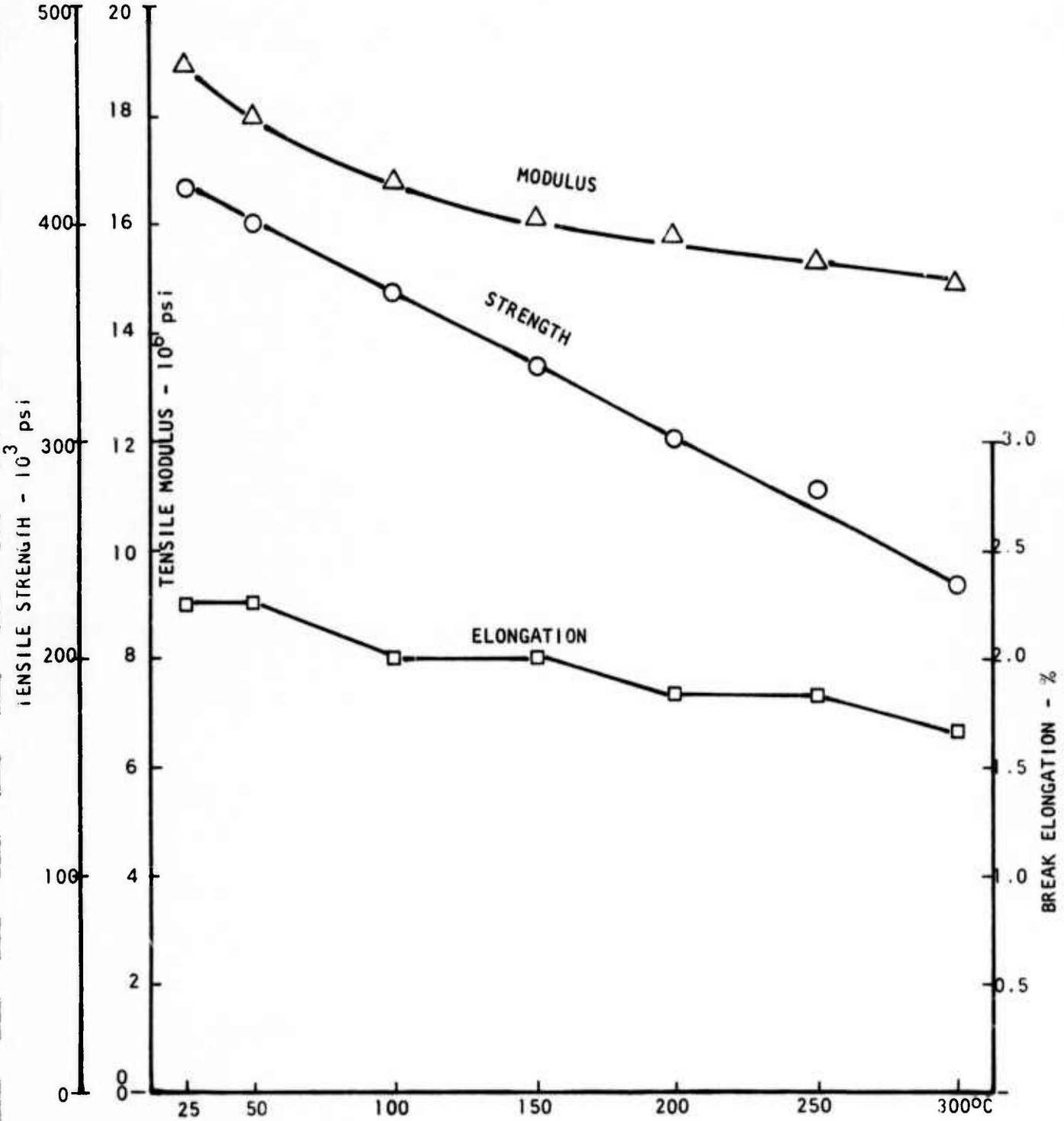

Data Points are Averages of 6 Determinations on 10 in. Gage Lengths Measured at Temperature after $\frac{1}{2}$ Hour Exposure in Air.

Figure G-2. "Kevlar" -49 Yarn Performance vs Temperature.

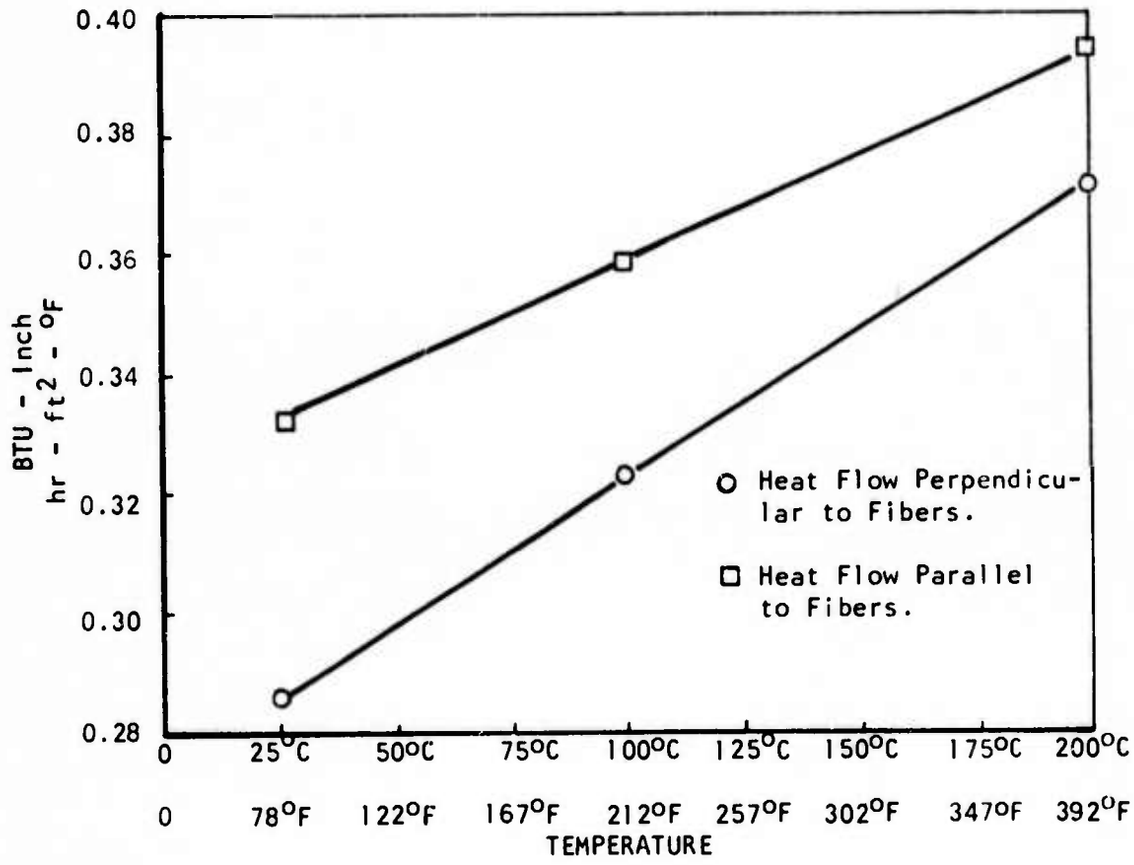

Figure G-3. Thermal Conductivity vs Temperature "Kevlar" 49 Yarn.

APPENDIX H

APPENDIX H

ANALYSIS OF PRE-SAMPLING FILTERS ON MULTIPLEXER PERFORMANCE

I. INTRODUCTION

A low pass filter preceding the sampling is required on each of the input channels of a multiplexer to avoid signal-to-noise degradation. Several types of filters are analyzed in the following paragraphs.

II. REQUIREMENTS

Figure H1a shows the response of a typical infrared channel. The scene spectrum, modified by the system optical modulation transfer function (MTF) and the amplifier channel response gives the signal spectrum. The infrared detector is a wide band device, and it is usually desirable to maintain the amplifier chain high frequency response, to obtain a high system MTF. The display response or the eye response effectively removes the excess high frequency noise.

Electronic multiplexing because of the sampling characteristics, however, introduces another requirement (Figures H1b and H1c). The detector and preamplifier noise spectra are essentially not band-limited and a signal-to-noise degradation can result from the sampling process due to the foldback of high frequency noise into the signal spectrum. To minimize these effects some band-limiting must be performed in each infrared channel. The filter requirements are as follows:

1. A high response must be maintained at the resolution frequency.

2. The filter must be sharp enough to prevent aliasing and signal-to-noise degradation. The filter must be easy to implement because one is required for each channel. The problem is therefore one of arriving at an overall satisfactory compromise between the number of samples, the filter complexity, and system performance. The effects of the following types of filters and samples/element are considered.

   a. Single RC low pass filter at 1.5 and 2 samples per element. (3 dB down at resolution frequency.)

   b. Double RC section at 1.5 and 2.0 samples per element (3 dB down @ resolution frequency).

   c. Sin x/x aperture filter at 1.5 and 2.0 samples per element (3 dB down @ resolution frequency).

   d. Sin x/x aperture filter with cutoff at 3 times resolution frequency (1.5 samples per element).

   e. Sin x/x aperture filter with cutoff at 4 times resolution frequency (2.0 samples/element).

   f. Double RC section at 2.0 samples per element (10% down at resolution frequency).

   g. Double RC section at 2.0 samples per element (20% down at resolution frequency).

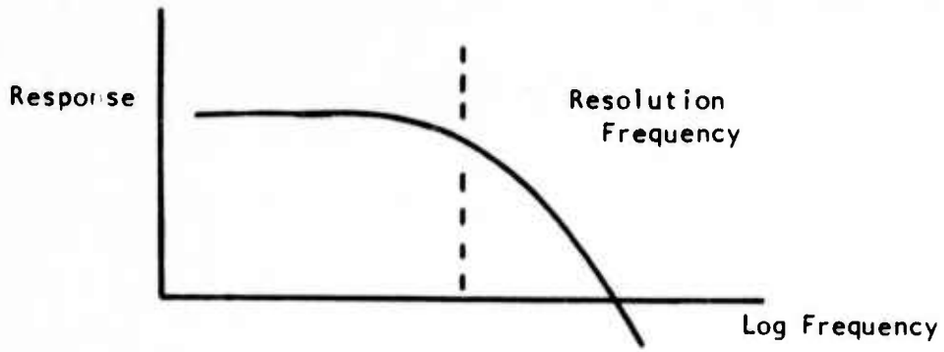

a. Typical Infrared Channel Frequency Response

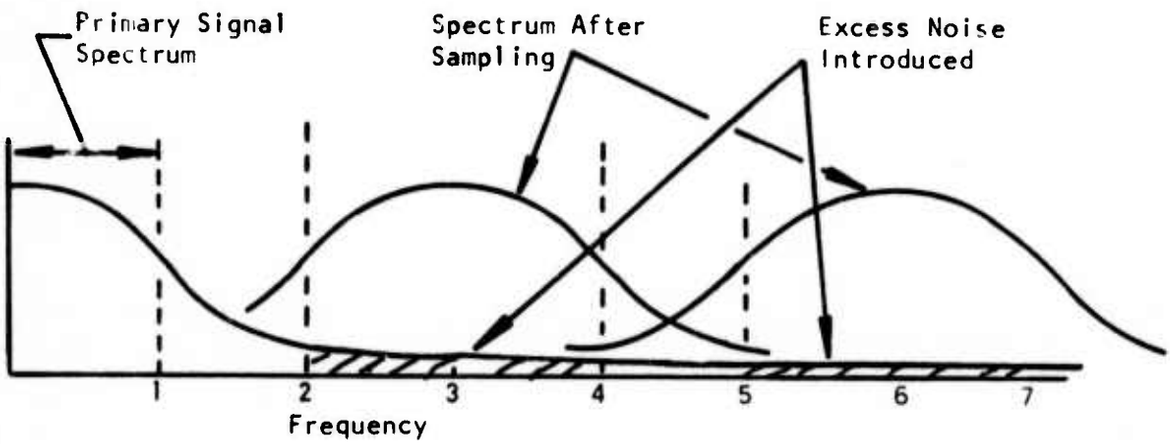

b. The Sampling Process at 3 Samples/Cycle (1.5/element)

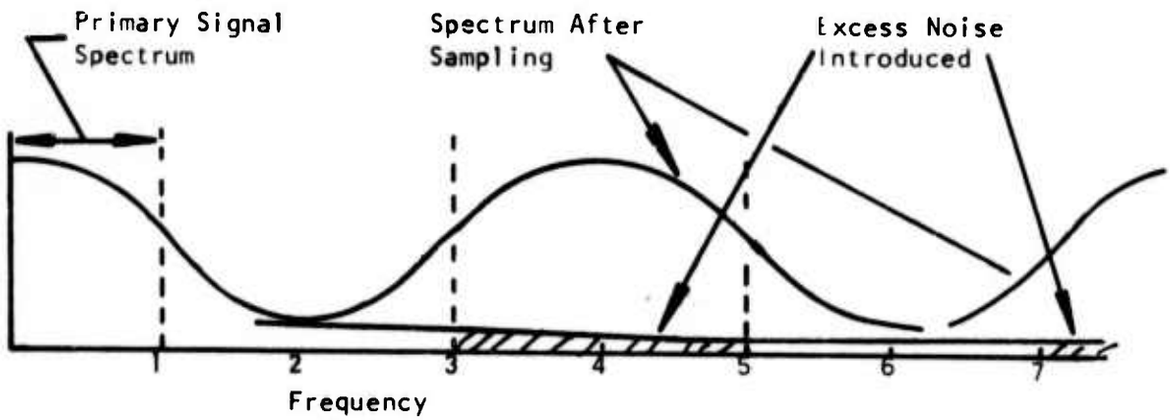

c. The Sampling Process at 4 Samples/Cycle (2.0/element)

Figure H1. Infrared Channel Response and Sampling

These filters were chosen for the following reasons. Filters a. and b. are easy to construct. Filter c. was chosen for comparison purposes. Filters d. and e. are relatively easy to implement by integrating charge on a capacitor and resetting the capacitor voltage to zero at the sampling rate. Filters f. and g. were chosen because they represent a good compromise between signal response at the resolution frequency and minimizing the degradation of system performance by unnecessary noise components.

Each of the selected filter equations are:

FILTER a. Single RC low pass filter at 1.5 samples/element. The frequency response of this filter is given by

$$A(f) = \frac{1}{1 + f^2} \qquad (-3db \text{ at } f=1)$$

The signal power in the passband is given by

$$P_L = \qquad A^2(f)df$$

The additional signal power (outside of the desired passband) which also appears in the output at 1.5 samples/element.

$$P_u = \quad A^7(f)df + \quad A^2(f)df + \qquad +$$

For 2.0 samples/element

$$P_u = \quad A^7(f)df + \quad A^2(f)df + \qquad +$$

These integrals were evaluated by numerical techniques although it would have been just as easy to obtain an analytical solution for this simple case. The results for 1.5 samples/element are

$$P_L = .79$$

$$P_u = .31$$

$$P_t = 1.10 \text{ (total power)}$$

The noise power is therefore increased by 1.10/.79 = 1.39. The signal-to-noise ratio is degraded by the square root of this number = 1.18 (an 18% degradation due to noise).

The response at the resolution frequency is given by

$$A_1 = \frac{1}{1 + f^2} \qquad = .707 \quad (-3db)$$

$$f = 1$$

The results for this filter (case a.) are given in Table H1 together with the results for other filters. The equation for filters b. through g. are as follows:

FILTER b. (DUAL RC)

$$A(f) = 1/[1 + (f/1.55)^2]$$

FILTER c. $A(f) = (\text{Sin } x)/x, \quad x = (\ f)/2.26$

FILTER d. $A(f) = (\text{Sin } x)/x, \quad x = (\ f)/3.0$

FILTER e. $A(f) = (\text{Sin } x)/x, \quad x = (\ f)/9.0$

FILTER f. (DUAL RC, 10% down at f=1)

$$A(f) = 1/[1 + (f/3)^2]$$

FILTER g. (DUAL RC, 20% down at f=1)

$$A(f) = 1/[1 + (f/2)^2]$$

Figures H2, H3 and H4 show the frequency response of each of the filters.

III. IMPLEMENTATION

All the filters considered (except the sin x/x which is 3 dB down at the resolution frequency) are easy to implement. The RC low pass and the double RC low pass consist of only two or four components. The sin x/x filters can be implemented with an integrating capacitor, or current source, and a periodic "dump" or reset to zero at the sampling rate.

The RC type filters do not introduce gain or level offsets into the channels. If one of the component values is slightly different on an individual channel, it will not affect the low frequency channel gain or the level. The only effect will be a modification of the high frequency response.

The sin x/x filter implemented with a charging capacitor is another matter. Offsets in the current sources or variation in the value of the capacitor between channels will produce dc offsets and also variations in the low frequency gain.

Other simple filters implemented with an operational amplifier and a few components can also be used so long as the complexity does not get out of hand.

IV. FILTER COMPARISONS

Reference to Table H1 gives the following results. A single RC low pass filter (filter a.) introduces too much additional noise at 3 samples/cycle (18%) and 4 samples/cycle (11%).

Filter	a.		b.		c.		d.	e.	f.	g.
Type	RC		RCRC		Sin x/x		Sin x/x	Sin x/x	RCRC	RCRC
Response @f=1	.707		.707		.707		.83	.90	.90	.80
Cut off frequency	-		-		2.26		3.0	4.0	-	-
Samples/element	1.5	2.0	1.5	2.0	1.5	2.0	1.5	2.0	2.0	2.0
Noise in Passband (P_L)	.790	.790	.802	.802	.820	.820	.891	.939	.933	.870
Undesired noise (Pu)	.350	.178	.124	.044	.079	.056	.103	.059	.32	.10
Signal/Noise degradation	18%	11%	7.5%	2.7%	4.7%	3.3%	5.6%	3.1%	16%	5.6%

TABLE H1. FILTER PERFORMANCE

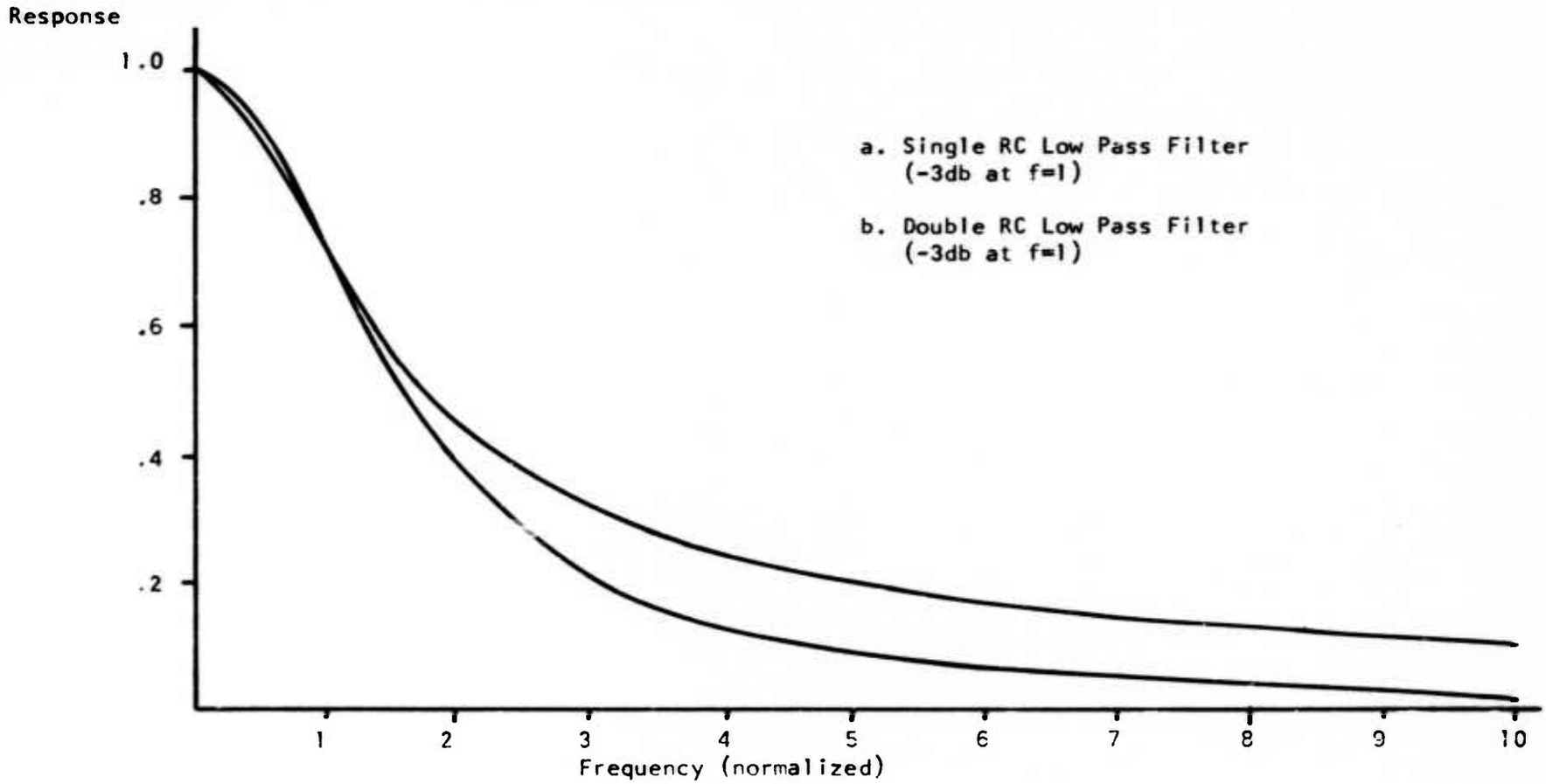

Figure H2. Frequency Pesponse of Filters a. and b.

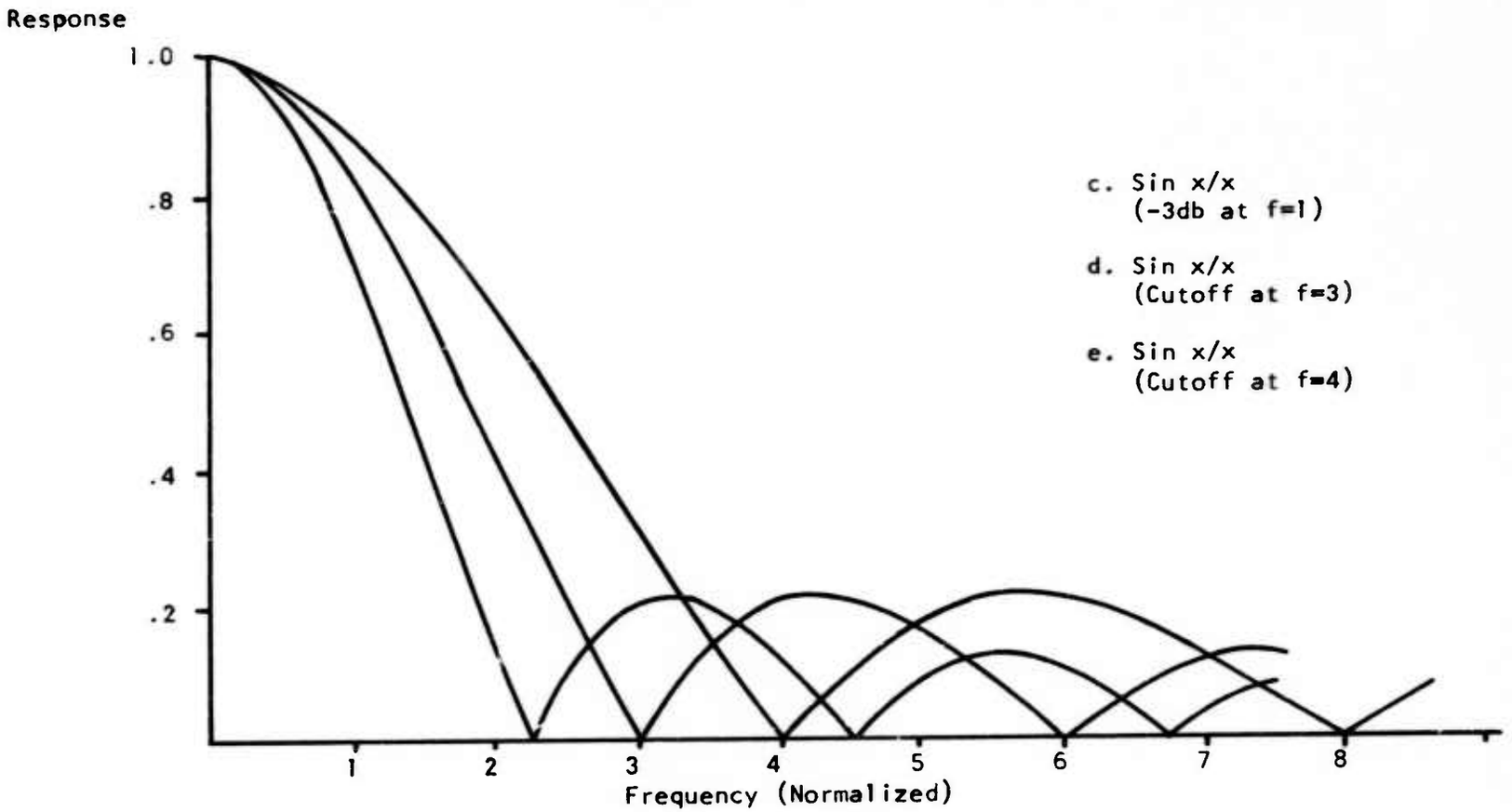

Figure H3. Frequency Respomse of Filters c., d. and e.

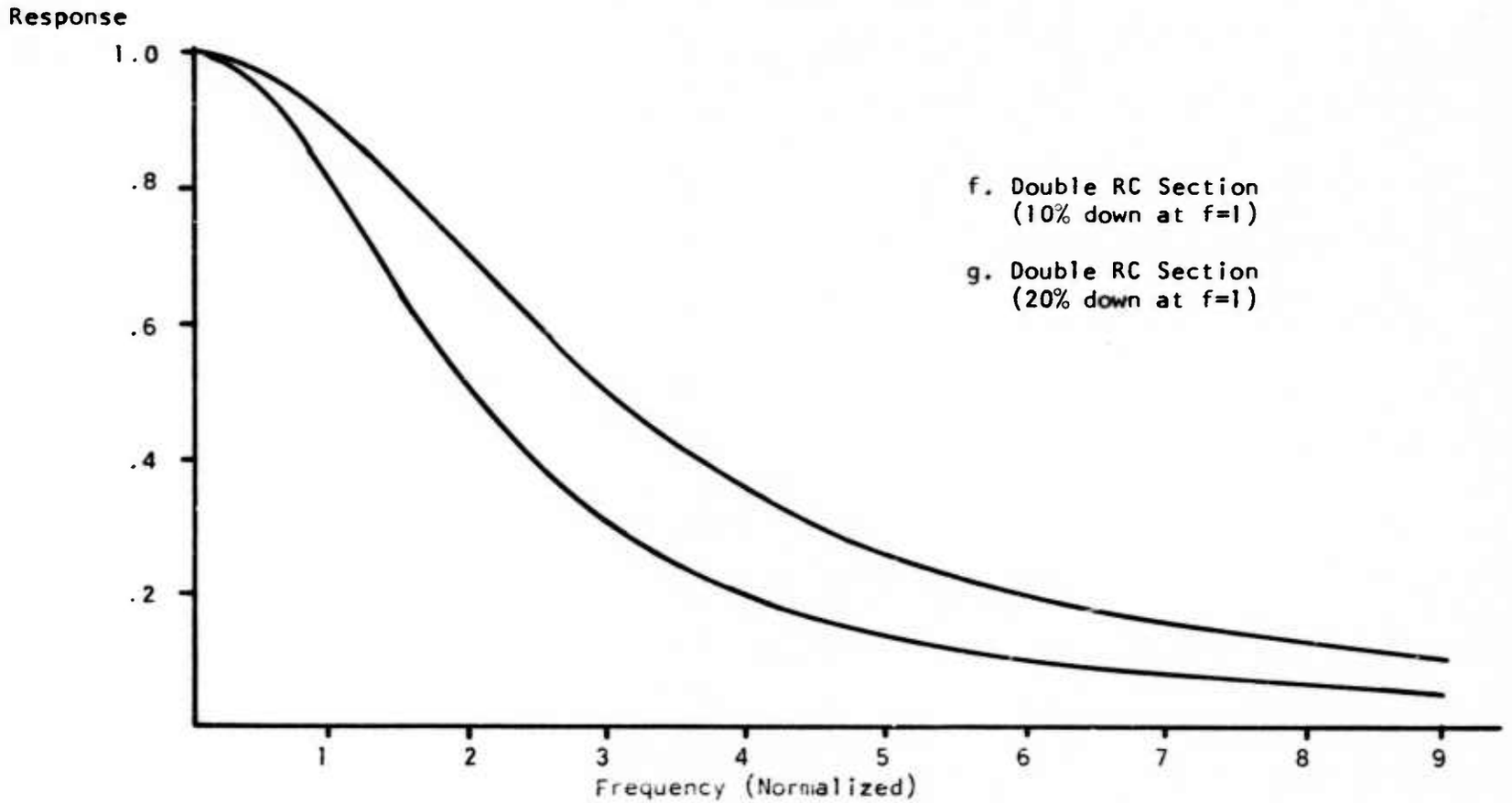

Figure H4. Frequency Response of Filters f. and g.

The Dual RC low pass (filter b.) introduces less additional noise at 3 samples/cycle (7.5%) and negligible additional noise at 4 samples/cycle (2.7%). The figures for filters a. and b. are with the breakpoint chosen as -3 dB at the resolution frequency which represents a slightly low MTF.

Filters of the sin x/x type (filters d. and e.) give good MTF at the resolution frequency (89% and 93%) and low noise degradation (5.6% and 3.1%). The implementation of these filters can, however, introduce gain and level offsets into the channels.

Filters of the double RC type with appropriately chosen breakpoints such as filter f. and g. represent a good compromise. Filter g. has an 80% response at the resolution frequency and introduces only 5.6% additional noise.

V. CONCLUSIONS

It was determined that low pass filters of the double RC type with appropriately chosen breakpoints give excellent results and are easy to implement. It is therefore suggested that this type of filter be utilized.

APPENDIX I

APPENDIX I

SYSTEM-OPERATOR PERFORMANCE

The results of the work of Rose, Coltman, Coltman and Anderson, Rozelle, and others have indicated that one can make the following assumptions regarding the human operating-display interface:

- The eye integrates displayed noise over an integration time is generally believed to be about 0.2 second.

- The eye integrates displayed noise, spatially, over the displayed subtense of the target.

- The probability of operator perception of any displayed target is a monotonically increasing function of the signal-to-noise ratio resulting after the above two integrations.

As stated, the above assumptions are tacitly assumed in all current performance predictions and will be assumed here.

Scanning array type FLIR systems and all TV systems are basically spatial intensity sampled data systems. That is, each point in the object plane (the target scene) is sampled once per frame time and the corresponding point in the output plane (the display) is illuminated for a very short time. The level of the illumination is proportional to the level of the object point intensity. Thus, when we examine the display, we find it is made up of a series of light impulses, each point receiving a new impulse once per frame. If a target scene were stationary and if there were no noise, each impulse would be the same magnitude. The effect of system noise is to cause the amplitude of the impluses to vary. The average value of the impulses will be the same as the no-noise case, and the standard deviation of the values about this mean is proportional to the rms noise.

In the actual case, each output point is "on" at different times. For the purposes of this analysis we can imagine that each point is illuminated at the same time.

If we assume, then, that the eye acts as a perfect temperal and spatial integrator, the perceived noise at the eye will be proportional to

$$N_E^2 \sim \frac{t_E}{f_F} \frac{\alpha}{\ell} \int_0^\infty G(f)\, a^2(f)\, S^2 \frac{\pi}{2} \frac{f}{f_T}\, df \qquad \text{(A-1)}$$

where

α = approximate noise correlation length in the vertical direction (the detector angular subtense)

ℓ = target extent in the vertical direction in milliradians

$G(f)$ = detector noise spectrum, volts^2/Hz

$a^2(f)$ = frequency response of all components following the detector, normalized to unity at zero frequency

f_τ = target fundamental frequency expressed in terms of Hz in the electrical channel

$S(z)$ = sin Z/Z.

The first term in Equation (A-1) accounts for all eye integration in time and is just equal to the number of independent samples of the noise in time. The second term times the integral expression accounts for the spatial integration. The sin x/x term is characteristic of a perfect integrator with integration period equal to 1/2 f_T.

The signal is proportional to

$$S \sim (t_E/t_F)\,\Delta T_o \quad TF \tag{A-2}$$

where $\Delta T_o = \Delta T$ [illegible] and TF is the system amplitude response to the target, and is derivable from the system MTF. The operator-perceived signal-to-noise ratio, SNRD or signal-to-noise ratio at the display, is thus

$$SNRD = \Delta T_o \left(\frac{t_E}{t_p}\right)^{\frac{1}{2}} \left(\frac{\ell}{\alpha}\right)^{\frac{1}{2}} \left[\int_0^\infty G(f)a^2(f)\, S^2\left(\frac{\pi}{2}\,\frac{f}{f_T}\right)df\right]^{-\frac{1}{2}} TF \tag{A-3}$$

Now, the system NET^2 is proportional to the detector noise spectrum at some reference frequency times the reference electrical bandwidth or,

$$NET^2 \sim G(f_R) \cdot \left(\frac{1}{2\tau}\right) \tag{A-4}$$

Thus, we can write

$$SNRD = \left(\frac{T_o}{NET}\right)\left(\frac{t_E}{t_F}\right)^{\frac{1}{2}} \left(\frac{\ell}{\alpha}\right)^{\frac{1}{2}} \left(\frac{\omega}{\alpha}\right)^{\frac{1}{2}} \left[\left(\frac{\omega}{\alpha}\right)(2\tau)\int_0^\infty g(f)a^2(f)S^2\left(\frac{\pi}{2}\,\frac{f}{f_T}\right)df\right]^{\frac{1}{2}} \tag{A-5}$$

where $g(f) = G(f)/G(f_R)$ and we have multiplexed and divided by target width, ω and α. .

We now note that the terms multiplying the integral in the bracketed term above is just the reciprocal of the target fundamental frequency in the electrical channel, for

$\frac{1}{2\omega}$ = target spatial frequency

$\frac{\alpha}{\tau}$ = scan velocity in mrad/s

and

$$f_{ELECTRICAL} = f_{SPATIAL} \times V_{SCAN\ VELOCITY} \tag{A-6}$$

Now, defining a quantity

$$Q = \left[\frac{1}{f_T} \int_0^{\infty} g(f)\ a^2(f)\ S^2\ \frac{\pi}{2}\ \frac{f}{f_T}\ df\right] \tag{A-7}$$

we have

$$SNRD = \left(\frac{t_E}{t_F}\right)^{\frac{1}{2}} \left(\frac{\Omega}{\alpha_x \alpha_y}\right)^{\frac{1}{2}} Q^{-\frac{1}{2}} \left(\frac{\Delta T_o}{NET}\right) TF \tag{A-8}$$

Equation (A-8) is the central result.

A target of particular significance is the standard eight-bar, 7:1 aspect ratio MRT target. For the MRT target of bar width Δx we have

$$\begin{aligned} f &= \frac{1}{2\Delta x} \\ w &= \Delta x = 1/2f \\ &= 7\Delta x = 7/2f \end{aligned} \tag{A-9}$$

$$SNRD = \left(\frac{t_E}{t_F}\right)^{\frac{1}{2}} \left[\frac{7}{4\alpha^2}\right]^{\frac{1}{2}} \left(Q^{-\frac{1}{2}}\right) \frac{\Delta T}{NET}\ \frac{TF(f)}{f} \tag{A-10}$$

MRT is equal to the temperature required to produce a high probability of perceiving the presence of the target. Letting this value be K, we have

$$MRT = \left[K\left(\frac{t_E}{t_F}\right)^{\frac{1}{2}} \left(\frac{2\alpha}{7^{\frac{1}{2}}}\right) Q^{\frac{1}{2}}\right] f\ \frac{NET}{TF} \tag{A-11}$$

Assuming now, the following values

t_F = 1/30 seconds

t_E = 0.2 seconds

Q = 1

K = 6

TF = $4/\pi$ MTF.

and defining a system critical frequency f_o by

$$f_o = \frac{1}{2\alpha} \tag{A-12}$$

we have for MRT

$$MRT \cong 0.75 \left(\frac{f}{f_o} \right) \frac{NET}{MTF(f)} \tag{A-13}$$

Equation (A-13) is a central result. The assumption that Q is approximately one (1) is saying that the detector noise spectrum is essentially flat (no 1/f noise) and that the effective frequency transfer of all elements following the detector is essentially flat. If this is not the case, Q must be computed directly and the MRT equation accordingly modified. The approximation is, however, generally good.

APPENDIX J

APPENDIX J

FREQUENCY FOCUS DATA

The following original data was collected during the feasibility study using video frequency information as an IR focus device.

The first test was the analyzation of frequency content of the video information. The graphs are presented with an index to position, time and scene.

The S-3A video chain 3db point is at 200 KHz. The limiting spatial frequency varies from top to bottom to the soup bowl scan of the channels selected for this study. The corresponding spatial frequencies are:

Channel	Spatial Frequency
21	43KHz
83 85 89	50KHz
151	57.3KHz

This information is of importance in interpreting the following data.

FOCUS VS. VIDEO INFORMATION

This test (#2) had the FLIR Video filtered by a Kronkite Filter and read out on an RMS voltmeter. The filter bandwidths were changed in order to enhance the information content to determine when changes in information occurred and at what frequency.

RUN 2

FOCUS KNOB POSITION	20-40 KHz	20-30 KHz	20-60 KHz	25-35 KHz	25-40 KHz
1	2.3	2.1	2.65	1.9	2.1
3	2.55	2.25	2.92	2.05	2.25
4	2.6	2.35	3.1	2.15	2.32
5	2.8	2.25	3.1	2.1	2.35
6	2.6	2.1	2.9	2.0	2.15
7	2.3	2.0	2.66	1.9	2.05
8	2.2	2.0	2.6	1.85	2.02
9	2.15	2.0	2.6	1.85	2.0
11	2.15	2.0	2.55	1.85	2.0

FOCUS KNOB POSITION	30-50 KHz	30-40 KHz	30-60 KHz	30-35 KHz	40-60 KHz
1	2.4	1.91	2.45	1.95	2.3
3	2.55	2.05	2.65	2.1	2.4
4	2.6	2.12	2.68	2.15	2.45
5	2.56	2.25	2.6	2.15	2.45
6	2.4	2.15	2.5	2.1	2.35
7	2.3	2.1	2.45	2.0	2.35
8	2.3	2.1	2.45	2.0	2.35
9	2.3	2.1	2.45	2.0	2.35
11	2.28	2.05	2.45	2.0	2.35

INDEX TO SCENE CONTENT OF GRAPHS

CHANNELS	83	Probe 2	
	85	Probe 3	Footage and Time
	89	Probe 4	vs.
	Sync	Probe 5	Scene Content

Gain in all preamps were upped by 2.

Tape Footage	Description
200 ft - 500 ft	Stationary Scene in Parking Lot TI Track.
500 ft - 800 ft	Stationary Scene in Parking Lot Track Defocused 2 Marks Closer.
800 ft -1100 ft	Stationary Scene in Parking Lot Track Defocused Far all way.
1100 ft -1400 ft	Stationary Scene in Parking Lot Search
1400 ft - 1710 ft	Stationary Scene in Parking Lot at Corner of S-C building. Track in Focus.
1710 ft - 2010 ft	Stationary Scene of SC Building Track Out of Focus 2 marks near. (A noticeable amount)
2010 ft - 2300 ft	Stationary Scene of SC Building Track Out of Focus Far.
2300 ft - 2600 ft	Stationary Scene of SC Building Track - Out of Focus All Way Near
2600 ft - 2900 ft 1352:26 - 1354:20	Stationary Scene SC Building Search - In Focus

TAPE FOOTAGE	DESCRIPTION
2900 ft - 3230 ft 1345:20 - 1356:58	Start of Slew Left to Right Parking Lot to S-C Building Track - In Focus
3230 ft - 3550 ft 1356:58 - 1359:00	Ref. Slew Right to Left SC Building to Parking Lot Track - In Focus
3550 ft - 4069 ft 1359:00 - 1402:10	Start of Slew Left to Right Parking Lot to S-C Building Track - Out of Focus Near (2 Units)
4069 ft - 4507 ft 1402:10 - 1405:07	Ref. Slew Right ot Left SC Building to Parking Lot Track Out of Focus Near (2 mks)
4507 ft - 4820 ft 1405:07 - 1407:08	Start Slew Left to Right Parking Lot to S-C Track Out of Focus Far
4820 ft - 5042 ft 1407:08 - 1408:37	Ref Slew Right to Left. SC to Parking Lot Track out of focus. Far
0	
5048 ft - 5320 ft 1408:37 - 1410:30	Pan Ch. 85, 21, 151 In Focus L to R
5320 ft - 5610 ft 1410:30 - 1412:20	Return Above R to L In Focus
5610 ft - 5820 ft 1412:20 - 1413:52	Pan Out of Focus Near by 2 Marks L to R
5820 ft - 6080 ft 1413:52 - 1415:30	Return Above R to L Out of Focus
6080 ft - 6350 ft 1415:30 - 1417:19	Pan Out of Focus Far L to R
6350 ft - 6505 ft 1417:19 - 1418:24	Return Out of Focus Far R & L

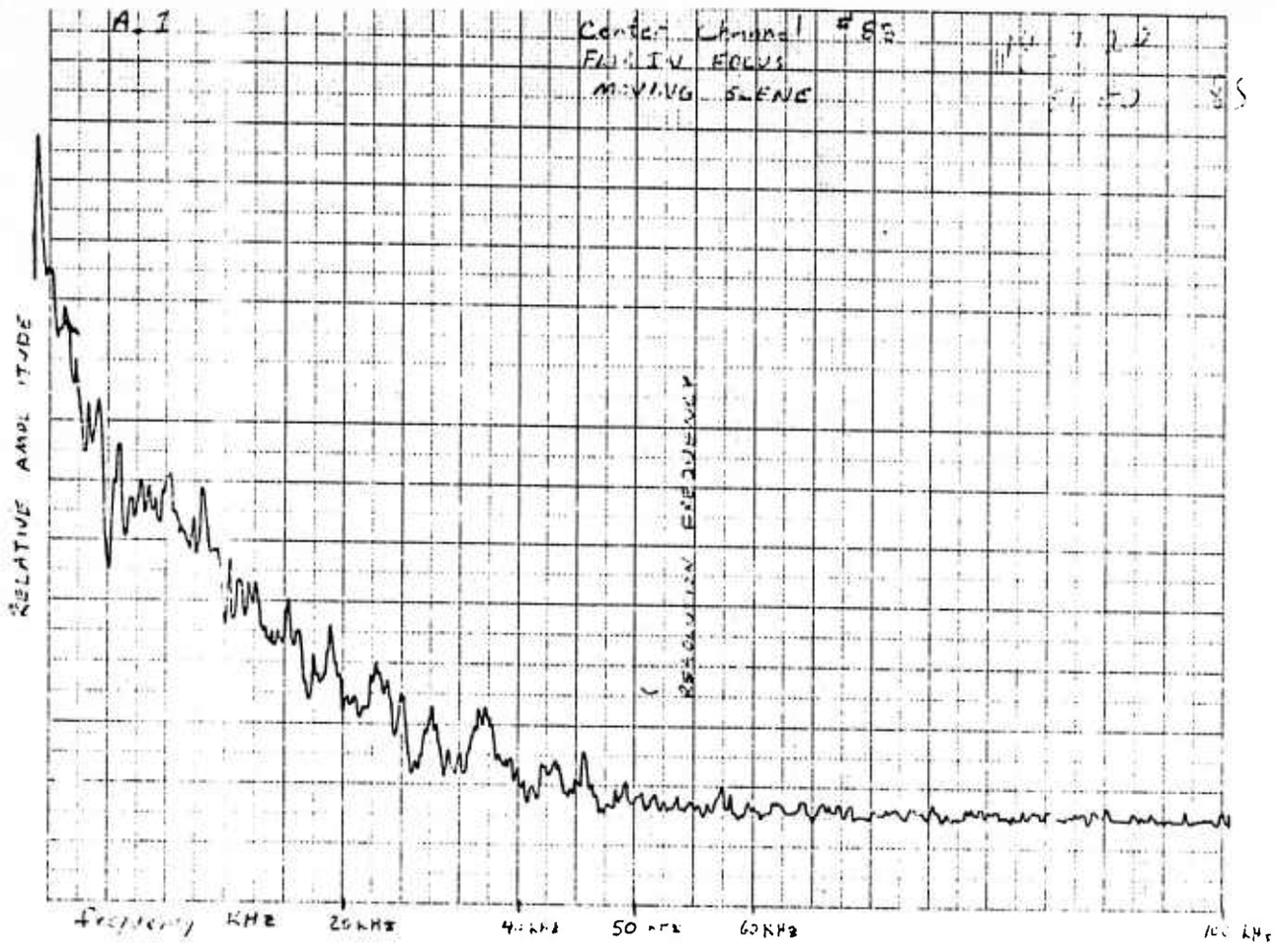

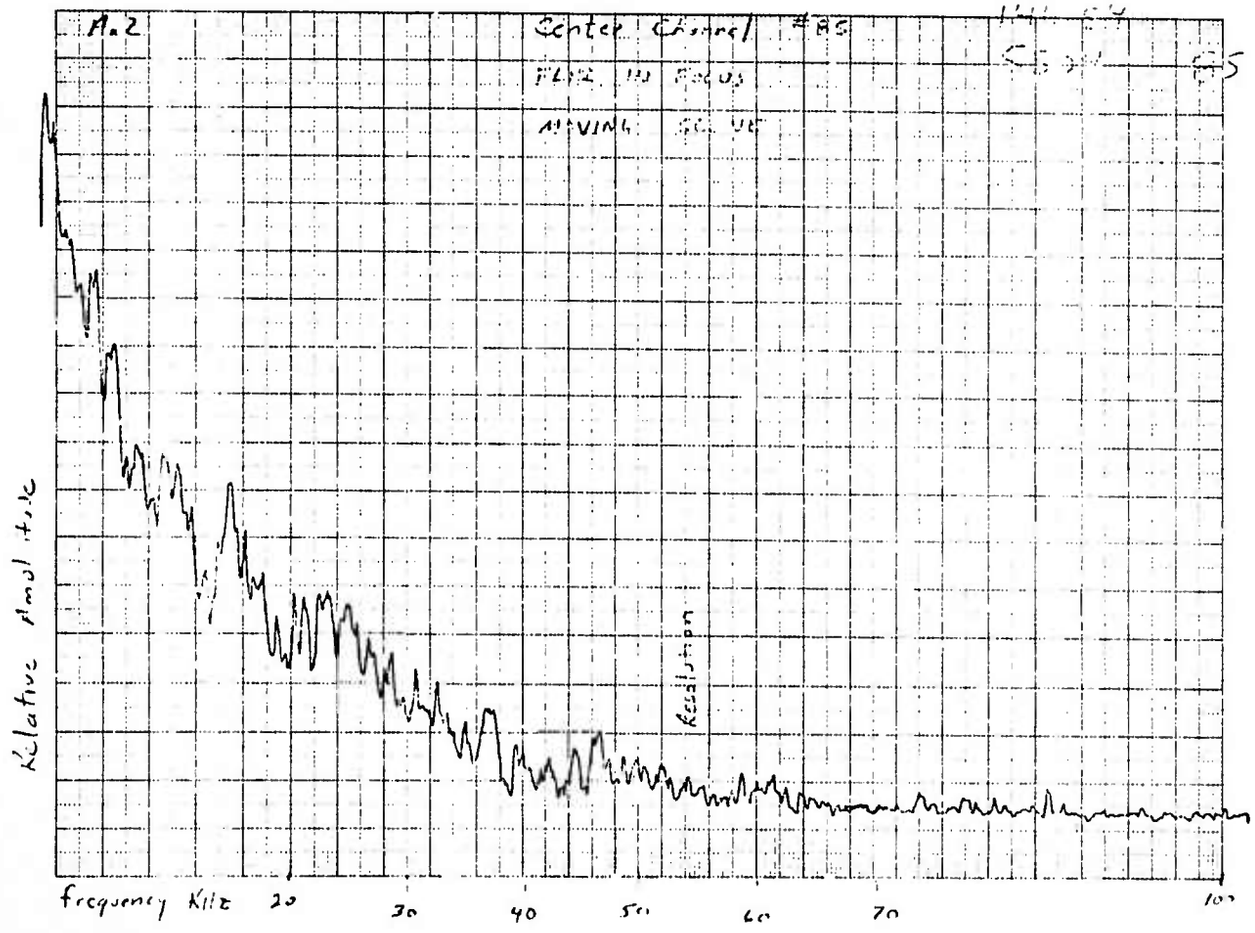

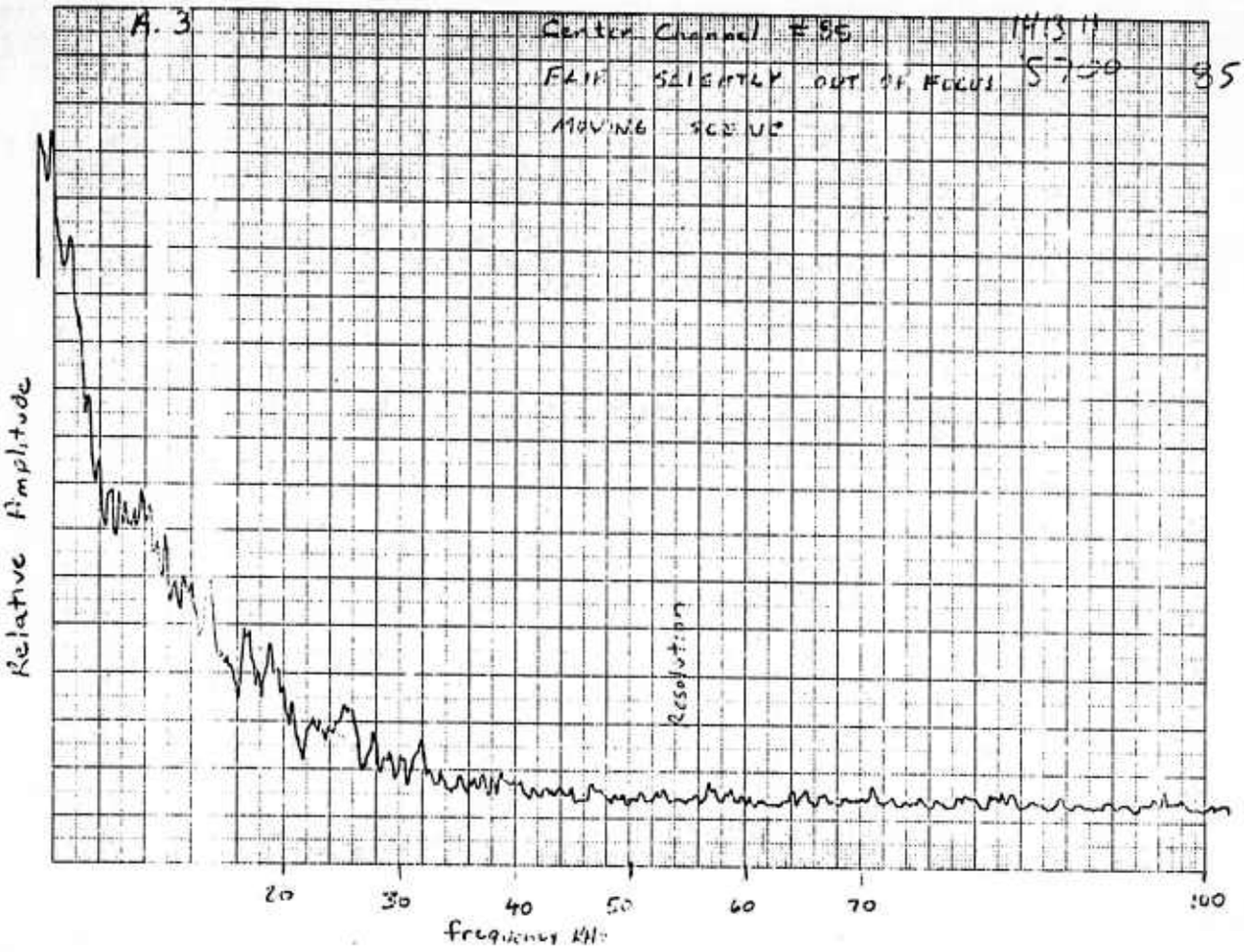
A. 3
Center Channel #55
FLAT SLIGHTLY OUT OF FOCUS
MOVING SCENE
Relative Amplitude
Resolution
20
30
40
50
60
70
100
Frequency KHz

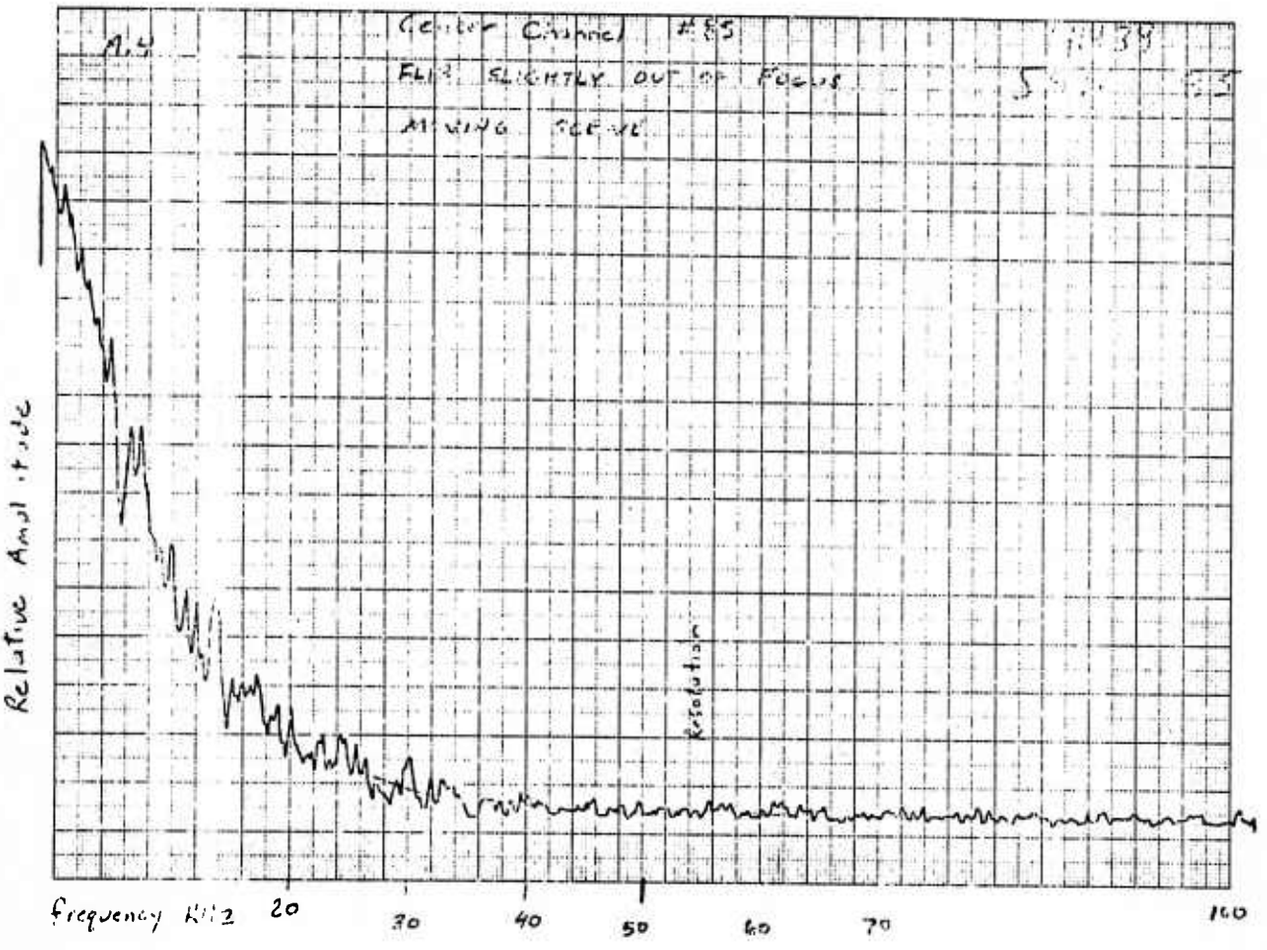
A.4
Center Channel #55
FLAT SLIGHTLY OUT OF FOCUS
MOVING SCENE
Relative Amplitude
Resolution
Frequency KHz
20
30
40
50
60
70
100

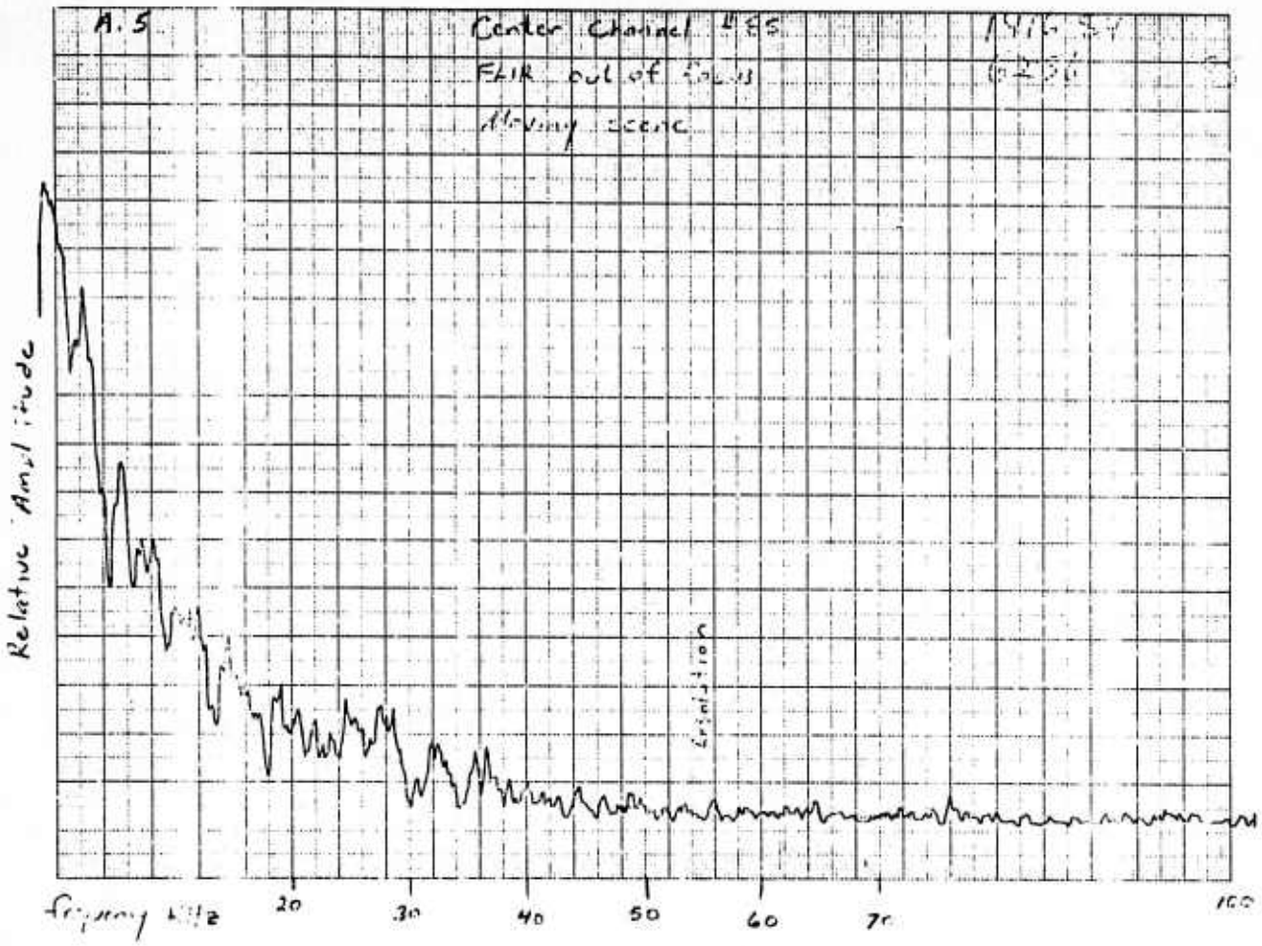
A.5
Center Channel #85
FLIR out of focus
Moving scene
Relative Amplitude
frequency KHz
20
30
40
50
60
70
100

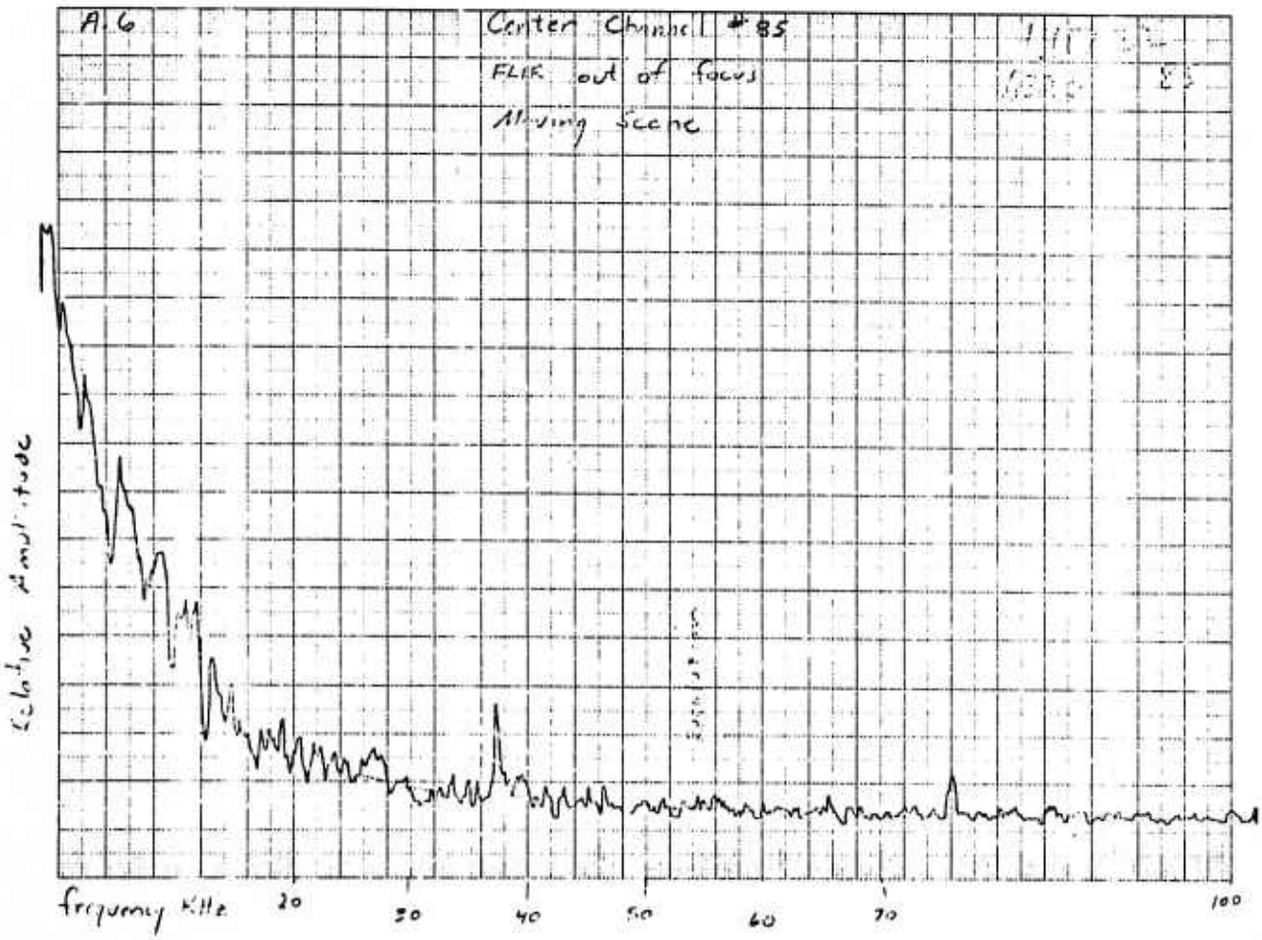
A.6
Center Channel #85
FLIR out of focus
Moving Scene
Relative Amplitude
frequency KHz
20
30
40
50
60
70
100

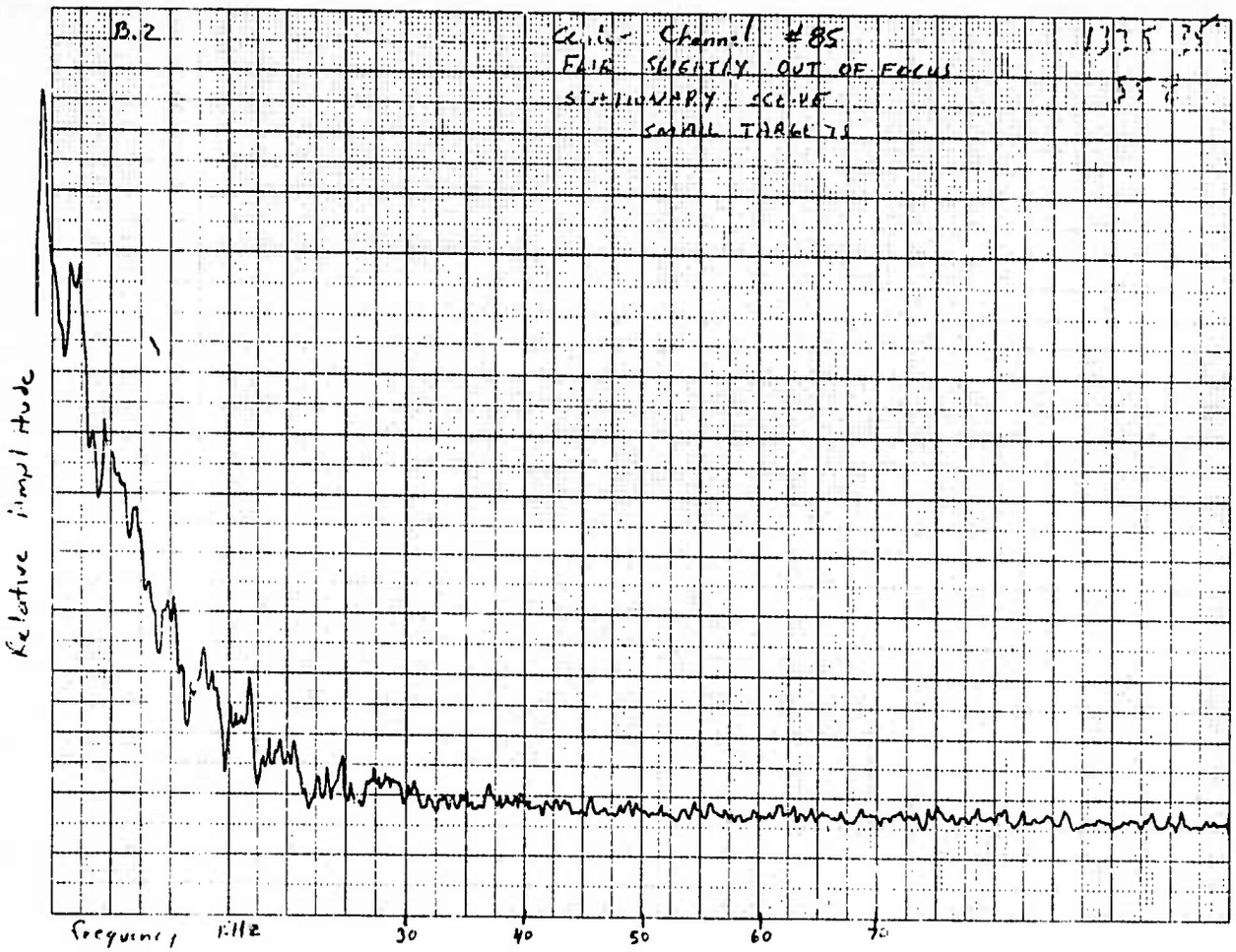
B.2
Relative Impl Hude
Frequency KHz
30
40
50
60
70

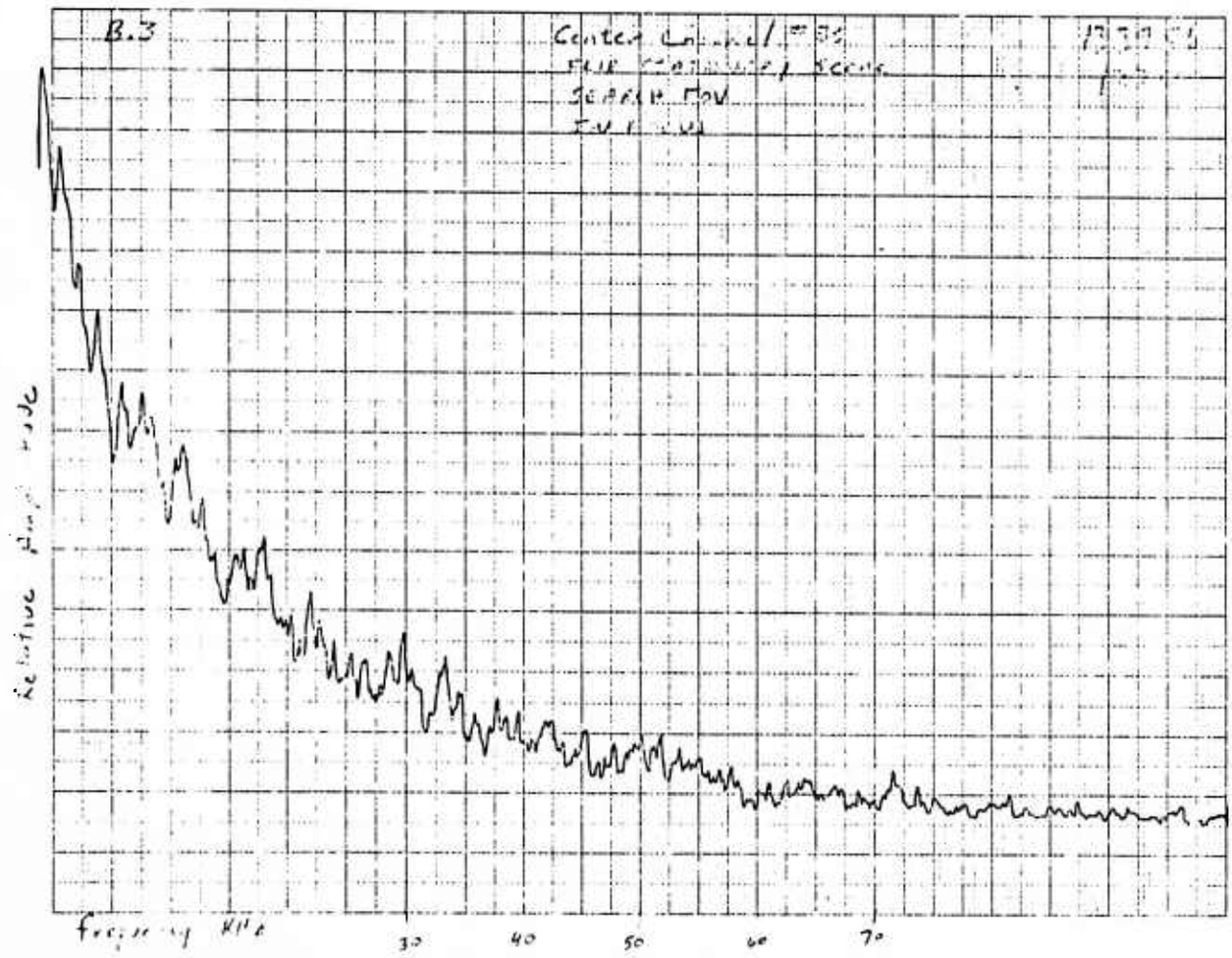
B.3
Relative Impl Hude
30
40
50
60
70

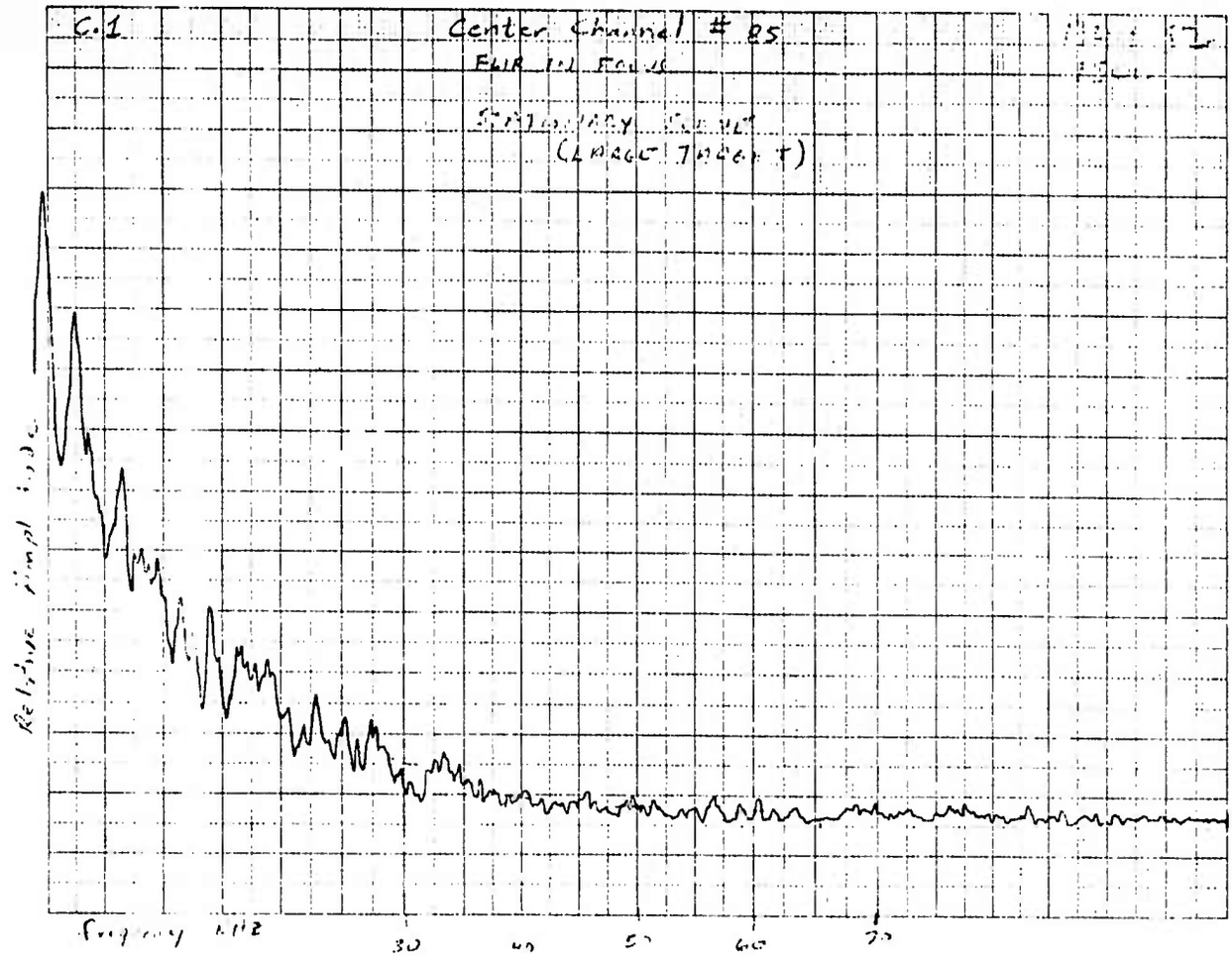

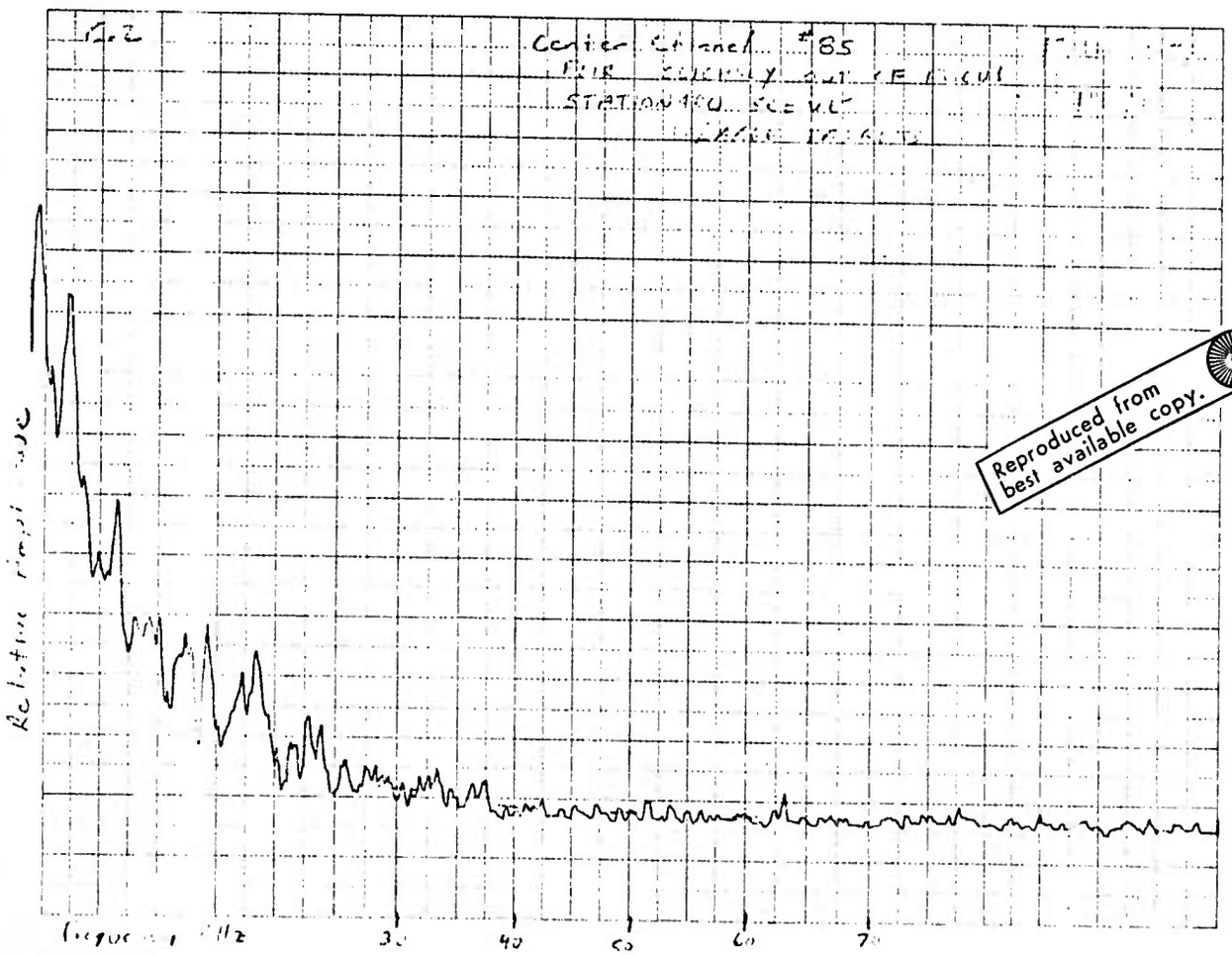

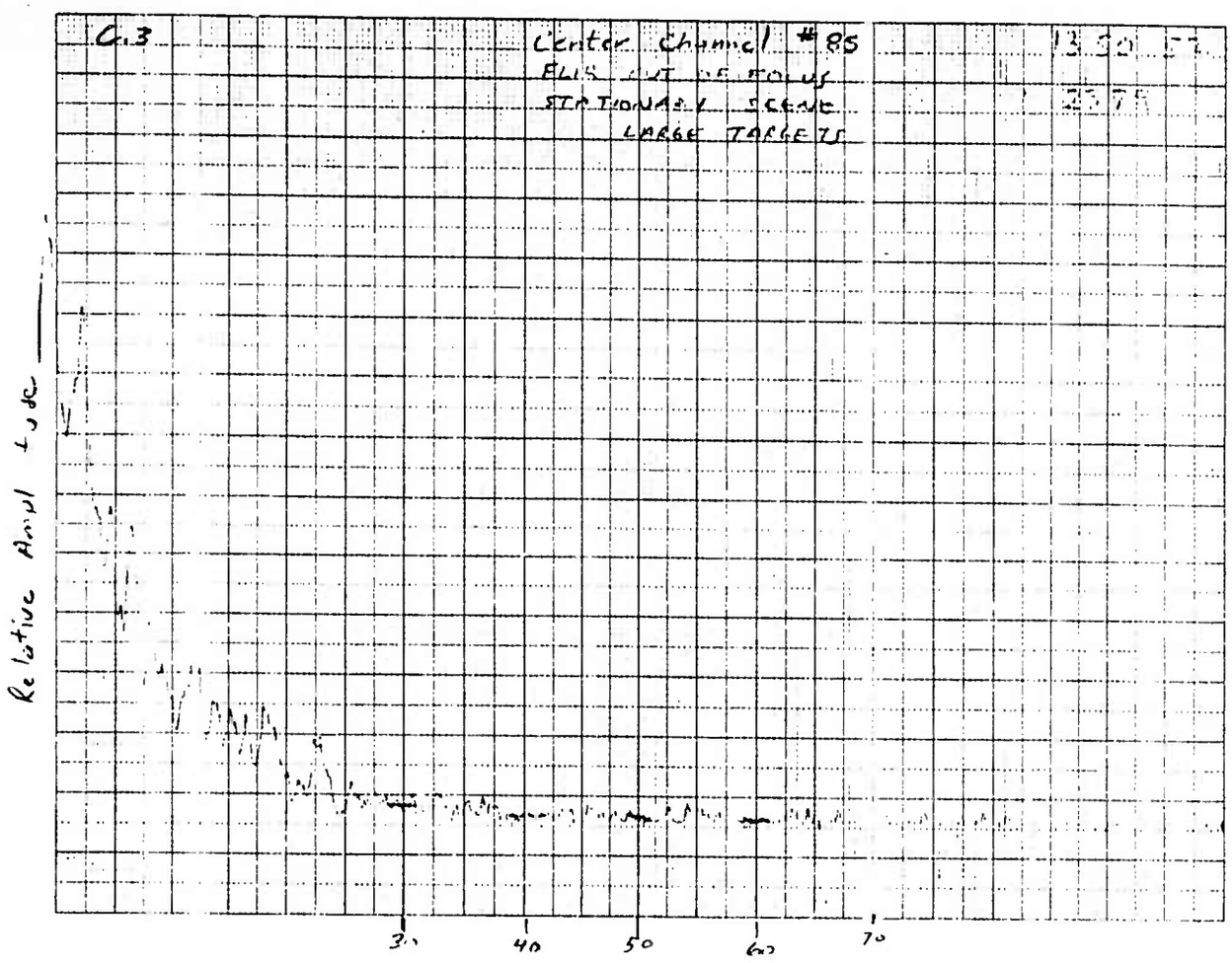
C.3
Center Channel #85
FLIR OUT OF FOCUS
STATIONARY SCENE
LARGE TARGETS
Relative Ampl Scale
30
40
50
60
70

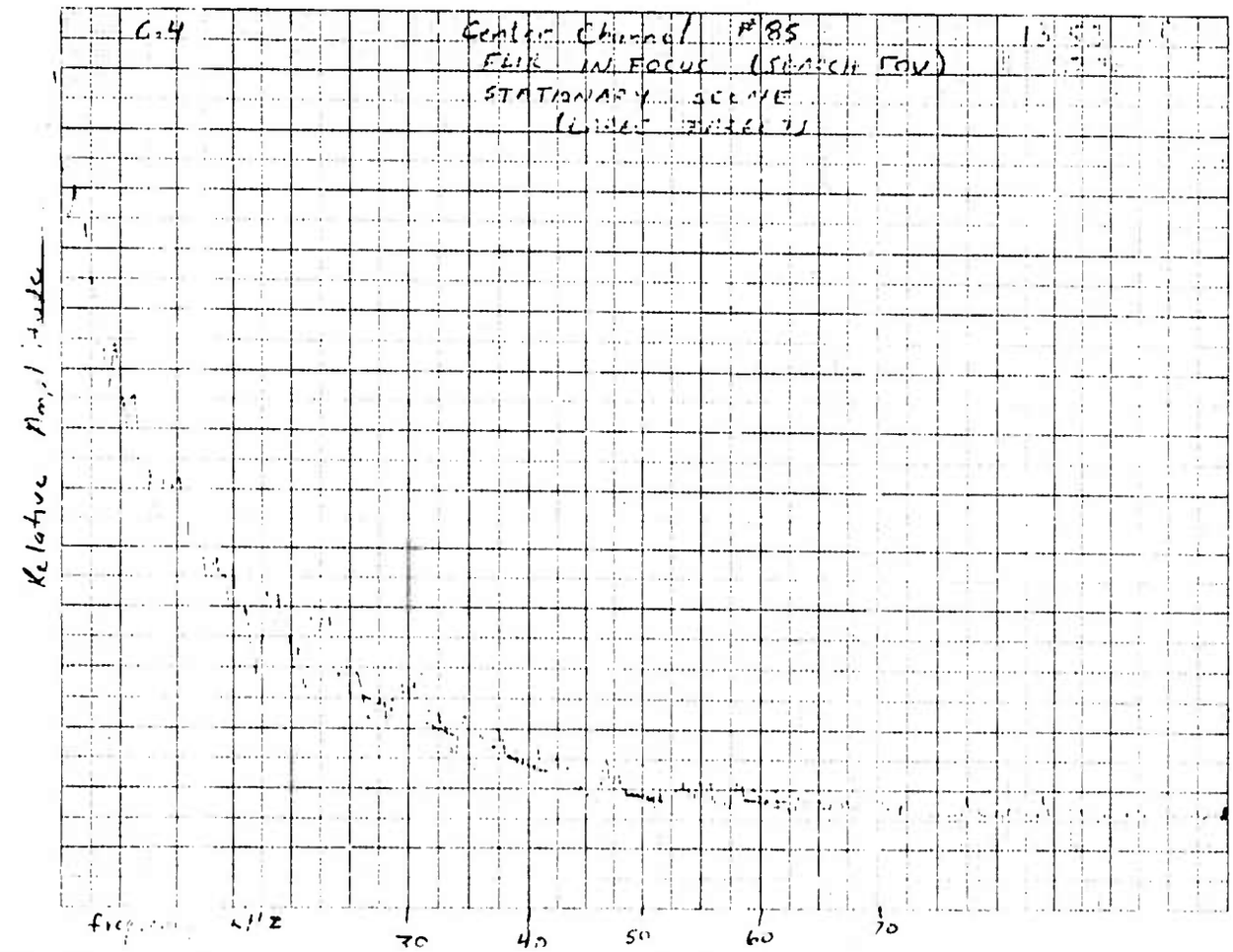
C.4
Center Channel #85
FLIR IN FOCUS (SEARCH FOV)
STATIONARY SCENE
Relative Ampl Scale
70
40
50
60
70

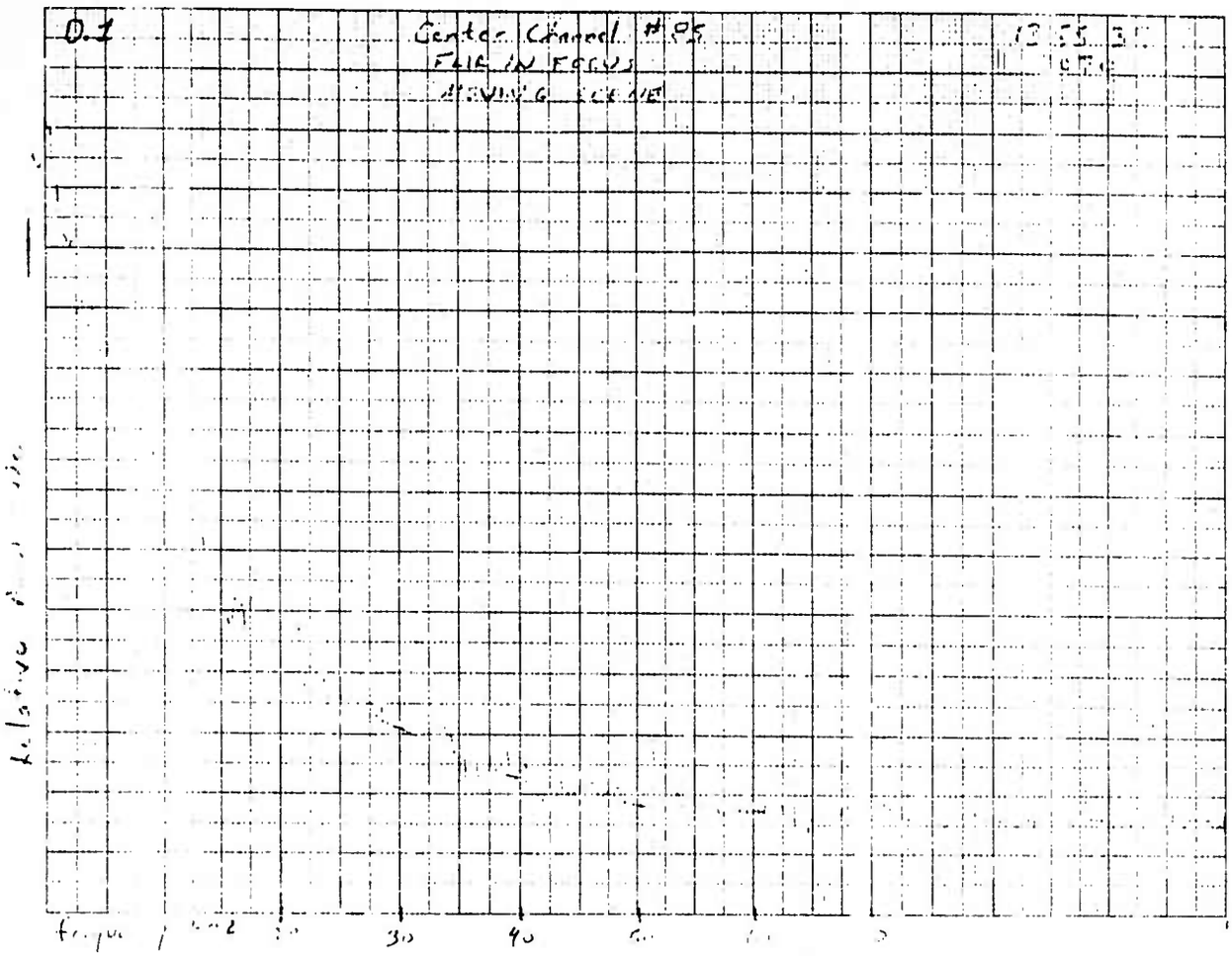
0.1
Center Channel #05
FLIR IN FOCUS
MOVING SCENE

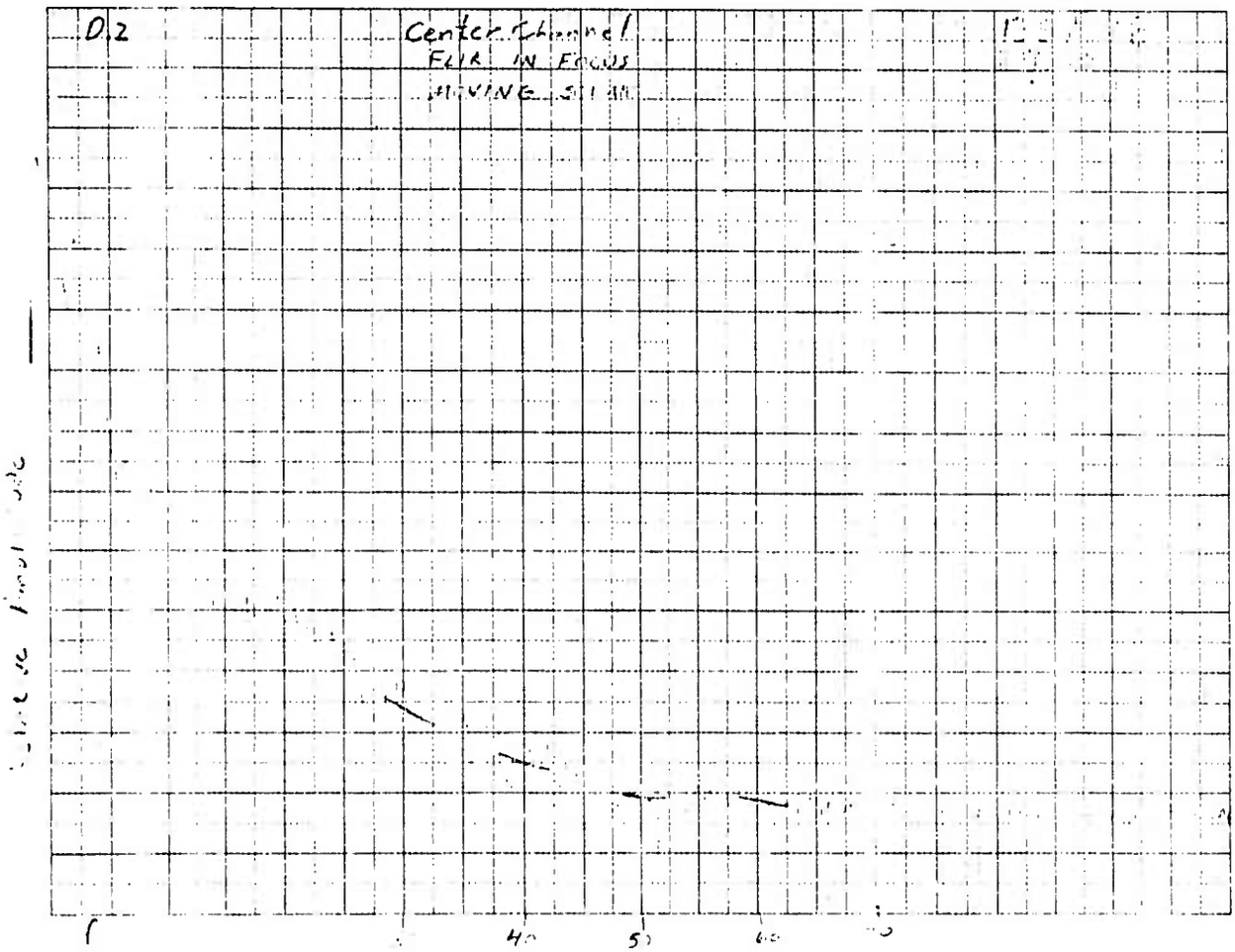
0.2
Center Channel
FLIR IN FOCUS
MOVING SCENE